Chapter I. General Introduction

I-1. Gastrointestinal immunity

I-1-1. Introduction

Mucosal tissues of the human body (i.e., respiratory, gastro-intestinal, and uro-genital tracts) are covered by mucus layers and are linked directly with various exogeneous antigens and symbiotic microorganisms (i.e., commensal bacteria) (*1*). Mucosal membrane consists of epithelial cells connected by tight junction, so that works as first physical defense barrier. The mucosal immune systems play critical roles for development of innate immune responses that protect the host within a few minutes and hours after infection of pathogens (*2*). Therefore, the study of the cross-talk mechanism between host and symbiotic/pathogenic microorganisms will be able to reveal the pathogenesis of diverse diseases and contribute to the development of new therapies.

I-1-2. Gastrointestinal defense mechanism

I-1-2-1. Secretory immunoglobulin A (sIgA)

IgA is a secretory antibody that mainly found in mucus secretions such as tears, saliva, and vaginal secretion, and that plays an essential role in mucosal immunity as humoral defense factors. The numerous IgA-producing cells in the gut can secrete IgA into lumen area between two and

five grams per day and play an important role on the host defense (*3*). Secretory IgA (sIgA) can exist in a dimeric form, which is connected by J chain, and can exist intact form in the gut because sIgA is resistant to proteolysis (*4*). The primary defense mechanism of sIgA against pathogens is to prevent attachment to mucosal surfaces and penetration into the gut (*5*).

I-1-2-2. Intestinal epithelial cells (IECs)

The mucosal surfaces are formed by layers of epithelial cells covered with complex of glycoproteins. Of note, the IECs are maintained on a network of interconnected enterocytes, goblet cells, enteroendocrine cells (L cells), and paneth cells. Mucosal barrier function of IECs is closely related with nervous system, which can increase tight junction between adjacent cells (*6*). Secretory bioactive factors produced by commensal bacteria can also elevate epithelial barrier function (*7*). Further, various types of epithelial cells involve in mucosal defense function. The most frequent cells are conventional enterocytes which construct mechanic barrier. Both goblet cells producing mucin and Paneth cells secreting antibiotic peptides-defensins preclude the invasion of exogenous pathogens (*8, 9*). Enteroendocrine cells produce gut hormones such as glucagon-like peptides (GLPs) and peptide YY (PYY) (*10*). Of the many important roles of IECs, it

is the distinct responsibility to discriminate between harmful and beneficial antigens (*6*).

I-2. Autophagy

I-2-1. Introduction

Autophagy is a ìkey òmachinery to maintain homeostatic condition of human body. Autophagy is essential to degrade cellular proteins and organelles, to recycle them for cell survival. This mechanism is active at a basal level in most cells and contributes to the routine turnover of cytoplasmic components (*11*).

I-2-2. The autophagic pathway

There are four stages of autophagy and many proteins (autophagy protein, ATG) involved in each step of autophagic responses, respectively. First, autophagy can be induced by diverse situations such as starvation, depletion of growth factor and immune signals (*12*). Autophagy is inhibited under nutrient-rich conditions and therefore simulated by starvation mediated by Tor/mTOR signal. Inactivation of mTOR under starvation is leading to induction of autophagy. In addition, Tor inactivation leads to downstream dephosphorylation resulting in transcriptional activation of autophagy genes, like *Atg1* and *Atg13* (*13*). Secondly, a double membrane vesicle forms autophagosome in the cytosol, and sequester those cytoplasmic components for degradation. Although the mechanism of

formation of double membrane is not fully defined, the *ATG* genes involved in vesicle formation are well identified. The *Atg5-Atg12* conjugate induces both the recruitment of LC3 and the conversion of LC3 to its phosphatidylethanolamine-conjugated LC3-II form. Formation of large complex with Atg16L1 also requires the *Atg5-Atg12* conjugate (*14*). Of note, *Atg7* is required for two ubiquitin-like conjugation pathways as mentioned before, indicating that *Atg7* is a key regulator in the generation of the autophagosome (*15*). Thirdly, the autophagosome meet with the lysosome, and thus the contents of the autophagosome are exposed to the lysosome for degradation by lysosomal proteases (*16*). Finally, following fusion of these two vesicle bodies, the membrane of autophagosome is broken down by the lysosomal proteases (*17*).

I-3. Gut microbiota

I-3-1. Introduction

Commensal bacteria means beneficial bacteria to host that reside on host barrier surfaces covered by epithelial cells. It is well established that five bacterial phyla (i.e. *Firmicutes*, *Bacteroidetes*, *Actinobacteria*, *Proteobacteria* and *Verruco-microbia*) are dominant gut microbiota in human (*18*). The duodenum and jejunum of the small intestine have only a few bacteria because of low pH conditions. However, numerous microbes in ileum (about 10^7 ml^{-1}) and colon (about 10^{14} ml^{-1}) inhabit the gut lumen and contents (*19*). The gut microbiota is heavily diverse and varies between individulas. More than 90% of the bacterial populations are Gram negative anaerobes and predominant species can list as follow; *Bacteroides*, *Eubacterium*, *Bifidobacterium*, *Fusobacterium*, and others (*20*). Over 100 trillions of gut microbiota plays indispensable roles in carbohydrate fermentation and nutrient absorption (*21*), protection of pathogenic bacteria (*22*, *23*), stimulation of innate/adaptive immunity (*24*, *25*), and regulation of metabolic disorders including obesity (*26*). However, under specific conditions like the treatment of antibiotics or medicines, some commensal bacteria are prone to change its characteristic to pathogenic bacteria to provoke inflammation or cancer (*27*).

I-3-2. The role of intestinal commensal microbes

The host intestinal area has a unique and complex circumstance which is exposed to numerous antigens like a daily food and exogenous bacteria. Resident gut microbiota contains a number of components able to activate innate and adaptive immunity. For examples, the majority of the intestinal bacteria are Gram-negative anaerobes having diverse structural agents, such as lipopolysaccharide (LPS) and flagella, give continuously signals to intestinal epithelial cells (IECs) through toll-like receptors (TLRs) (*28*, *29*). Segmented filamentous bacteria (SFB) embedded in the ileum can also stimulate to induce T helper 17 cell (T_H17) responses and induce the production of mucosal IgA (*30*). In addition, innate lymphoid cells (ILCs) directly regulate specific commensal bacteria (*31*) or indirectly modulate $CD4^+$ T cells that promoted intestinal inflammation (*32*).

Commensal bacteria have enzymes which does not produced by human cells, thus can help for human to digest and absorb some carbohydrates (*33*). Gut microbiome, meanwhile, can be changed by dietary habits. For instances, *Bacteroides* genus is predominantly detected in people who usally eat diet including high fat and protein, whereas *Prevotella* genus is mainly found in people who have diatary patterns based on carbohydrates (*34*).

I-4. Obesity

I-4-1. Introduction

Obesity represents the situation that body mass index (BMI) is more than 30 kg / m^2, and provoke secondary complications which may be caused from excessive body fat such as cardiovascular diseases, diabetes, and osteoarthritis (*35*). In world health organization (WHO) reports, obesity is not only considered as a simple risk factor for other diseases, but also classified as a disease to be managed and treated (*36*). According to the 2012 national health statistics, the prevalence of obesity was 32.8% in Korea, and person who has 30 kg / m^2 or more in BMI is increasing with 4.8 % in the population 19 years old or elder. Direct or indirect costs due to overweight and obesity accounted for 3.7% of national health care spending by 1.8 trillion won, suggesting that the time required aggressive weight management at the national level (*37*).

I-4-2. Commensal microbiota in host metabolism

Gut microbiota has also been implicated in obesity and metabolic syndrome. In support, altering composition of gut microbiota using antibiotic treatment increased host adiposity (*38*). Moreover, gnotobiotic mice transplanted with fecal microbiota from obese or lean volunteers

provide representing donorś phenotypes (*39*). Dietary habits influence numbers and diversity of gut microbes. Several studies suggest that dietary consumption patterns might cause changes in the microbiota with consequences for host nutritional status and immune responses (*40*). For instance, rural African children revealed higher bacterial richness and a lower proportion of *Bacteroides* than European children (*41*). Inversely, the commensal microbiota involve in synthesizing a variety of vitamins and the absorption of minerals, which can adversely impact immune system (*42*).

I-4-3. Application of commensal microbiota: Bacteriotherapy

Many groups have tried to develop ñBacteriotherapy ò by fecal microbiota transplantation (FMT) which commensal bacteria taken from a healthy donor transfer its beneficial function to recipients. *Enterobacter cloacae* B29 which were expanded in obese mice can induce obesity after feces transplantation to germ-free mice (*43*). In addition, infusion of fecal microbiota harvested from lean donor can increase insulin sensitivity and alter butyrate-producing commensal bacteria (*44*), indicating that commensal bacteria is the potential as therapeutic agents to metabolic diseases.

I-5. Objectives

Commensal bacteria play pivotal roles to regulate gut homeostasis by competing with pathogenic bacteria and to control host metabolisms by regulating food digestion. In this respect, I was tried to figure out these basal questions and performed several experiments with the objectives below.

1. **Identification of commensal bacteria regulated by host autophagic reaction in species levels and investigation of phenotypes can be modulated by microflora.**
2. **Investigation of the correlation between single commensal bacteria and host lipid metabolism, and mechanism how they modulate.**

I-6. References

1. **J. Mestecky, H. Nguyen, C. Czerkinsky, H. Kiyono.** 2008. Oral immunization: an update. *Current Opinion in Gastroenterology* 24, 713-719.
2. **C. A. Janeway, Jr., R. Medzhitov.** 2002. Innate immune recognition. *Annual Review of Immunology* 20, 197-216.
3. **P. Brandtzaeg, R. Pabst.** 2004. Let's go mucosal: communication on slippery ground. *Trends in Immunology* 25, 570-577.
4. **E. E. Max, S. J. Korsmeyer.** 1985. Human J chain gene. Structure and expression in B lymphoid cells. *The Journal of Experimental Medicine* 161, 832-849.
5. **S. Fagarasan, T. Honjo.** 2003. Intestinal IgA synthesis: regulation of front-line body defences. *Nature Reviews Immunology* 3, 63-72.
6. **D. C. Baumgart, A. U. Dignass.** 2002. Intestinal barrier function. *Current Opinion in Clinical Nutrition and Metabolic Care* 5, 685-694.
7. **B. Sanchez, M. C. Urdaci, A. Margolles.** 2010. Extracellular proteins secreted by probiotic bacteria as mediators of effects that promote mucosa-bacteria interactions. *Microbiology* 156, 3232-3242.
8. **M. E. Johansson, G. C. Hansson.** 2013. Mucus and the goblet cell. *Digestive Diseases* 31, 305-309.
9. **N. H. Salzman, D. Ghosh, K. M. Huttner, Y. Paterson, C. L. Bevins.** 2003. Protection against enteric salmonellosis in transgenic mice expressing a human intestinal defensin. *Nature* 422, 522-526.
10. **D. J. Drucker, M. A. Nauck.** 2006. The incretin system: glucagon-like peptide-1 receptor agonists and dipeptidyl peptidase-4 inhibitors in type 2 diabetes. *Lancet* 368, 1696-1705.
11. **B. Levine, N. Mizushima, H. W. Virgin.** 2011. Autophagy in immunity and inflammation. *Nature* 469, 323-335.
12. **S. T. Shibutani, T. Yoshimori.** 2014. A current perspective of autophagosome biogenesis. *Cell Research* 24, 58-68.
13. **C. H. Jung, S. H. Ro, J. Cao, N. M. Otto, D. H. Kim.** 2010. mTOR regulation of autophagy. *FEBS Letters* 584, 1287-1295.
14. **N. Mizushima, T. Noda, T. Yoshimori, Y. Tanaka, T. Ishii, M. D. George, D. J. Klionsky, M. Ohsumi, Y. Ohsumi.** 1998. A protein conjugation system essential for autophagy. *Nature* 395, 395-398.
15. **A. M. Taherbhoy, S. W. Tait, S. E. Kaiser, A. H. Williams, A.**

Deng, A. Nourse, M. Hammel, I. Kurinov, C. O. Rock, D. R. Green, B. A. Schulman. 2011. Atg8 transfer from Atg7 to Atg3: a distinctive E1-E2 architecture and mechanism in the autophagy pathway. *Molecular Cell* 44, 451-461.

16. **I. G. Ganley, P. M. Wong, N. Gammoh, X. Jiang.** 2011. Distinct autophagosomal-lysosomal fusion mechanism revealed by thapsigargin-induced autophagy arrest. *Molecular Cell* 42, 731-743.
17. **I. Tanida, N. Minematsu-Ikeguchi, T. Ueno, E. Kominami.** 2005. Lysosomal turnover, but not a cellular level, of endogenous LC3 is a marker for autophagy. *Autophagy* 1, 84-91.
18. **G. Vedantam, D. W. Hecht.** 2003. Antibiotics and anaerobes of gut origin. *Current Opinion in Microbiology* 6, 457-461.
19. **R. D. Berg.** 1996. The indigenous gastrointestinal microflora. *Trends in Microbiology* 4, 430-435.
20. **F. Guarner, J. R. Malagelada.** 2003. Gut flora in health and disease. *Lancet* 361, 512-519.
21. **J. Qin, R. Li, J. Raes, M. Arumugam, K. S. Burgdorf, C. Manichanh, T. Nielsen, N. Pons, F. Levenez, T. Yamada, D. R. Mende, J. Li, J. Xu, S. Li, D. Li, J. Cao, B. Wang, H. Liang, H. Zheng, Y. Xie, J. Tap, P. Lepage, M. Bertalan, J. M. Batto, T. Hansen, D. Le Paslier, A. Linneberg, H. B. Nielsen, E. Pelletier, P. Renault, T. Sicheritz-Ponten, K. Turner, H. Zhu, C. Yu, S. Li, M. Jian, Y. Zhou, Y. Li, X. Zhang, S. Li, N. Qin, H. Yang, J. Wang, S. Brunak, J. Dore, F. Guarner, K. Kristiansen, O. Pedersen, J. Parkhill, J. Weissenbach, H. I. T. C. Meta, P. Bork, S. D. Ehrlich, J. Wang.** 2010. A human gut microbial gene catalogue established by metagenomic sequencing. *Nature* 464, 59-65.
22. **N. Kamada, Y. G. Kim, H. P. Sham, B. A. Vallance, J. L. Puente, E. C. Martens, G. Nunez.** 2012. Regulated virulence controls the ability of a pathogen to compete with the gut microbiota. *Science* 336, 1325-1329.
23. **J. Behnsen, S. Jellbauer, C. P. Wong, R. A. Edwards, M. D. George, W. Ouyang, M. Raffatellu.** 2014. The cytokine IL-22 promotes pathogen colonization by suppressing related commensal bacteria. *Immunity* 40, 262-273.
24. **T. Karrasch, J. S. Kim, M. Muhlbauer, S. T. Magness, C. Jobin.** 2007. Gnotobiotic IL-$10^{-/-}$;NF-kappa B (EGFP) mice reveal the critical role of TLR/NF-kappa B signaling in commensal bacteria-induced colitis. *Journal of Immunology* 178, 6522-6532.

25. **I. Jarchum, E. G. Pamer.** 2011. Regulation of innate and adaptive immunity by the commensal microbiota. *Current Opinion in Immunology* 23, 353-360.
26. **L. Trasande, J. Blustein, M. Liu, E. Corwin, L. M. Cox, M. J. Blaser.** 2013. Infant antibiotic exposures and early-life body mass. *International Journal of Obesity* 37, 16-23.
27. **M. V. Pirotta, S. M. Garland.** 2006. Genital Candida species detected in samples from women in Melbourne, Australia, before and after treatment with antibiotics. *Journal of Clinical Microbiology* 44, 3213-3217.
28. **J. L. Round, S. M. Lee, J. Li, G. Tran, B. Jabri, T. A. Chatila, S. K. Mazmanian.** 2011. The Toll-like receptor 2 pathway establishes colonization by a commensal of the human microbiota. *Science* 332, 974-977.
28. **M. M. Heimesaat, A. Fischer, H. K. Jahn, J. Niebergall, M. Freudenberg, M. Blaut, O. Liesenfeld, R. R. Schumann, U. B. Gobel, S. Bereswill.** 2007. Exacerbation of murine ileitis by Toll-like receptor 4 mediated sensing of lipopolysaccharide from commensal Escherichia coli. *Gut* 56, 941-948.
30. **Ivanov, II, K. Atarashi, N. Manel, E. L. Brodie, T. Shima, U. Karaoz, D. Wei, K. C. Goldfarb, C. A. Santee, S. V. Lynch, T. Tanoue, A. Imaoka, K. Itoh, K. Takeda, Y. Umesaki, K. Honda, D. R. Littman.** 2009. Induction of intestinal Th17 cells by segmented filamentous bacteria. *Cell* 139, 485-498.
31. **G. F. Sonnenberg, L. A. Monticelli, T. Alenghat, T. C. Fung, N. A. Hutnick, J. Kunisawa, N. Shibata, S. Grunberg, R. Sinha, A. M. Zahm, M. R. Tardif, T. Sathaliyawala, M. Kubota, D. L. Farber, R. G. Collman, A. Shaked, L. A. Fouser, D. B. Weiner, P. A. Tessier, J. R. Friedman, H. Kiyono, F. D. Bushman, K. M. Chang, D. Artis.** 2012. Innate lymphoid cells promote anatomical containment of lymphoid-resident commensal bacteria. *Science* 336, 1321-1325.
32. **M. R. Hepworth, L. A. Monticelli, T. C. Fung, C. G. Ziegler, S. Grunberg, R. Sinha, A. R. Mantegazza, H. L. Ma, A. Crawford, J. M. Angelosanto, E. J. Wherry, P. A. Koni, F. D. Bushman, C. O. Elson, G. Eberl, D. Artis, G. F. Sonnenberg.** 2013. Innate lymphoid cells regulate $CD4^+$ T-cell responses to intestinal commensal bacteria. *Nature* 498, 113-117.
33. **S. C. Resta.** 2009. Effects of probiotics and commensals on intestinal epithelial physiology: implications for nutrient handling.

The Journal of Physiology 587, 4169-4174.

34. **G. D. Wu, J. Chen, C. Hoffmann, K. Bittinger, Y. Y. Chen, S. A. Keilbaugh, M. Bewtra, D. Knights, W. A. Walters, R. Knight, R. Sinha, E. Gilroy, K. Gupta, R. Baldassano, L. Nessel, H. Li, F. D. Bushman, J. D. Lewis.** 2011. Linking long-term dietary patterns with gut microbial enterotypes. *Science* 334, 105-108.
35. **D. W. Haslam, W. P. James.** 2005. Obesity. *Lancet* 366, 1197-1209.
36. **W. P. James.** 2008. WHO recognition of the global obesity epidemic. *International Journal of Obesity* 32 Suppl 7, S120-126.
37. **M. K. Kim, W. Y. Lee, J. H. Kang, J. H. Kang, B. T. Kim, S. M. Kim, E. M. Kim, S. H. Suh, H. J. Shin, K. R. Lee, K. Y. Lee, S. Y. Lee, S. Y. Lee, S. K. Lee, C. B. Lee, S. Chung, I. K. Jeong, K. Y. Hur, S. S. Kim, J. T. Woo, G.** 2014. 2014 clinical practice guidelines for overweight and obesity in Korea. *Endocrinology and Metabolism* 29, 405-409.
38. **I. Cho, S. Yamanishi, L. Cox, B. A. Methe, J. Zavadil, K. Li, Z. Gao, D. Mahana, K. Raju, I. Teitler, H. Li, A. V. Alekseyenko, M. J. Blaser.** 2012. Antibiotics in early life alter the murine colonic microbiome and adiposity. *Nature* 488, 621-626.
39. **V. K. Ridaura, J. J. Faith, F. E. Rey, J. Cheng, A. E. Duncan, A. L. Kau, N. W. Griffin, V. Lombard, B. Henrissat, J. R. Bain, M. J. Muehlbauer, O. Ilkayeva, C. F. Semenkovich, K. Funai, D. K. Hayashi, B. J. Lyle, M. C. Martini, L. K. Ursell, J. C. Clemente, W. Van Treuren, W. A. Walters, R. Knight, C. B. Newgard, A. C. Heath, J. I. Gordon.** 2013. Gut microbiota from twins discordant for obesity modulate metabolism in mice. *Science* 341, 1241214.
40. **P. J. Turnbaugh, F. Backhed, L. Fulton, J. I. Gordon. 2008.** Diet-induced obesity is linked to marked but reversible alterations in the mouse distal gut microbiome. *Cell Host & Microbe* 3, 213-223.
41. **J. Ou, F. Carbonero, E. G. Zoetendal, J. P. DeLany, M. Wang, K. Newton, H. R. Gaskins, S. J. O'Keefe.** 2013. Diet, microbiota, and microbial metabolites in colon cancer risk in rural Africans and African Americans. *The American Journal of Clinical Nutrition* 98, 111-120.
42. **S. C. Resta.** 2009. Effects of probiotics and commensals on intestinal epithelial physiology: implications for nutrient handling. *The Journal of Physiology* 587, 4169-4174.
43. **N. Fei, L. Zhao.** 2013. An opportunistic pathogen isolated from the gut of an obese human causes obesity in germfree mice. *The ISME Journal* 7, 880-884.

44. **A. Vrieze, E. Van Nood, F. Holleman, J. Salojarvi, R. S. Kootte, J. F. Bartelsman, G. M. Dallinga-Thie, M. T. Ackermans, M. J. Serlie, R. Oozeer, M. Derrien, A. Druesne, J. E. Van Hylckama Vlieg, V. W. Bloks, A. K. Groen, H. G. Heilig, E. G. Zoetendal, E. S. Stroes, W. M. de Vos, J. B. Hoekstra, M. Nieuwdorp.** 2012. Transfer of intestinal microbiota from lean donors increases insulin sensitivity in individuals with metabolic syndrome. *Gastroenterology* 143, 913-916 e917.

Chapter II. Specific deletion of autophagy-related gene *(atg7)* in $CD11c^+$ cells alter murine gut microbiota

II-1. Introduction

Autophagy, self-eating pathway, has been firstly known as an innate adaptation to starvation (*1*, *2*). Autophagy machinery play indispensable roles in the maintain host homeostasis due to their ability for removing misfolded proteins and damaged organelles (*3*). Over recent years, autophagy has been implicated in several pathological and physiological conditions such as infectious diseases, cancer, autoimmune diseases, and metabolic disorders including obesity (*4*). Previous studies demonstrated that inhibition of autophagy with 3-methylademine (3MA) in vitro lead to increased triglycerides and lipid droplets accumulation in hepatocytes (*5*) and defective hepatic autophagy-related gene 7 (*Atg*7) in obesity causes insulin resistance (*6*). On the other hand, adipose-specific *Atg*7 deleted mice exhibited lower body weight, decreased white adipose tissues (WATs), and increased insulin sensitivity which contributing resistant to diet-induced obesity (*7*, *8*). In addition, skeletal muscle-specific *Atg*7 deleted mice showed ţlean Ř phenotypes supported by decreased fat mass and amelioration of insulin resistance (*9*), indicating that autophagy is one of key mechanisms to regulate host lipid metabolism. However, it is still unveiled whether controlling autophagy pathway could be one of

environmental factors for regulating energy balance.

Obesity is associated with substantial changes in the composition and metabolic function of the gut microbiota which has emerged for therapeutic potential (*10*). In initial studies, data from mice models and human volunteers with lean and obese phenotypes revealed that change of relative abundance of specific phyla such as *Firmicutes* and *Bacteroidetes* are associated with obesity (*11, 12*). It has been hypothesized that these distinct abundances in the gut microbiota resulted in different yield to harvest energy from the diet (*13*). Mice deficient in TLR5 developed metabolic syndrome including insulin resistance and increased adiposity which closely related with changes in the composition of their gut microbiota (*14*). In support, altering composition of gut microbiota using antibiotic treatment increased host adiposity (*15*). Moreover, gnotobiotic mice transplanted with fecal microbiota from obese or lean volunteers provide representing donor Ś phenotypes (*16*). In terms of energy expenditure, commensal microbes can contribute to obesity by providing digestive enzymes, by regulating fat storage (*17*), and by producing short-chain fatty acids (SCFAs) (*18, 19*).

Here, I unexpectedly identified lean phenotypes in *Atg7*^{qCD11c} mice including lower levels of body weight / fat mass and glucose in serum,

which were associated with increased production of insulin. Interestingly, I got the clues that commensal bacteria are closely related in these phenomenons using co-housing and fecal extracts transplantation. In depth, pyrosequencing analysis revealed that specific commensal bacteria, especially *Bacteroides acidifaciens*, were expanded in feces and colon epithelial cells of *Atg7*^{qCD11c} mice. My results suggest that single strain of commensal bacteria can be regulated by autophagy of CD11c positive cells and those bacteria might be related with host lipid metabolism.

II-2. Materials and Methods

II-2-1. Ethics statement

All animal experiments were approved by the Institutional Animal Care and Use Committee of the Asan biomedical research center (Approval No: PN 2014-13-069). All experiment was performed under anesthesia with a mixture of ketamine (100 mg/kg) and xylazine (20 mg/kg), and all efforts were made to minimize suffering.

II-2-2. Mice and bacteria strains

C57BL/6 (B6) and *CD11c*^{cre} mice were purchased from Charles River Laboratories (Orient Bio Inc., Sungnam, Korea) and Jackson Laboratory (Bar Harbor, ME), respectively. *ATG7*$^{flox/flox}$ mice were kindly provided by Dr. Masaaki Komatsu (Tokyo Metroplitan Institue of Medical Science, Japan). All mice were maintained under specific pathogen-free conditions in the animal facility at the Asan biomedical research center (Seoul, Korea) where they received sterilized food and water *ad libitum*. *Bacteroides* (*B.*) *acidifaciens* (JCM10556) and *B. sartorii* (JCM17136) used in this study were purchased from Japan Collection of Microorganisms (JCM) at RIKEN BioResource Center.

II-2-3. Bacteria culture

B. acidifaciens and *B. sartorii* were grown in peptone-yeast-glucose (PYG) broth at 37 ^{o}C for 48 hours anaerobically with BBL^{TM} GasPak 100^{TM} EZ gas generating container (Becton Dickinson, Sparks, MD). The bacteria were concentrated by centrifuging for 15 minutes at 5,000 g and resuspended with sterile PBS. The actual bacterial dose given was confirmed by plating serial dilutions onto Eggerth-Gangon (EG) blood agar plates.

II-2-4. Glucose tolerance test (GTT) and insulin tolerance test (ITT)

GTT and ITT were done as previously described (*20*). For GTT, in brief, 16 hours-fasted mice were injected 2 mg of glucose per gram of body weight through intraperitoneal (i.p.) route. For ITT, 6 hours-fasted mice were injected 0.75 Unit of insulin through i.p. route. The concentration of plasma glucose was monitored at 0, 30, 60, 90 and 120 min after injection of glucose or insulin, respectively.

II-2-5. Fecal microbiota transplantation

Transfer of feces was done as previously described (*21*). In brief, fresh feces were harvested and thoroughly mashed up with sterile PBS containing 0.05 % cysteine HCl (Sigma-Aldrich) on 100 μm cell strainers. The resulting suspension after passing through strainers was briefly centrifuged at 100 g to remove large aggregates and then administrated daily for 18 weeks to mice by needleless intubation tools.

II-2-6. Magnetic resonance imaging (MRI) analysis

All MRI experiments were performed at 9.4 T / 160 mm by Agilent MRI scanner (Agilent Technologies, Santa Clara, CA) using a millipede-shaped volume radiofrequency coil. All animals were anesthetized through a mask by spontaneous inhalation of 1.5 ~ 2% isoflurane. Shimming was performed to minimize B0 inhomogeneity prior to MR scanning both automatically and manually. The axial T1-weighted (T1-WI) fast spin echo (FSE) images was used to cover both kidneys completely. The parameters of T1-WI image were TR = 1100 msec, kzero = 1, echo spacing (ESP) = 9.82 msec (effective TE = 48 msec), 48 segments, echo train length (ETL) =

4, 4 averages, matrix = 192 × 192, the field of view (FOV) = 25 × 30 mm, slice thickness = 1.0 mm; and total scan time = 3 min 33 sec, respectively. During MR scanning, external triggering was used to eliminate respiratory motion artifacts.

II-2-7. Gas chromatography mass spectrometry (GC-MS) measurement

Organic acid concentrations of feces were determined by gas chromatography–mass spectrometer (*22*). In brief, aliquots (80 ml) of ether extracts of feces were mixed with 16 ml N-tert-butyldimethylsilyl-Nmethyltrifluoroacet amide (MTBSTFA). The vials were sealed tightly, heated at 80 ^{o}C for 20 min in a water bath, and then left at room temperature for 48 h for derivatization. The derivatized samples were run through a 6890N Network GC System (Agilent Technologies, *Santa Clara*, CA) equipped with an HP-5MS column (0.25 mm × 30 m × 0.25 mm) and a 5973 Network Mass Selective Detector (Agilent Technologies). Pure helium (99.9999%) was used as carrier gas and delivered at a flow rate of 1.2 ml min^{-1}. The head pressure was set at 97 kPa with split 20:1. The inlet and transfer line temperatures were 250 and 260 ^{o}C, respectively. The following temperature program was used: 60 ^{o}C (3 min), 60-120 ^{o}C (5^{o}C /min), 120-

300 °C (20°C /min). Then, 1 ㎕ of each sample was injected with a runtime of 30 min. Organic acid concentrations were quantified by comparing their peak areas with standards.

II-2-8. Fluorescence *in situ* hybridization (*FISH*) analysis

Localization of *B. acidifaciens* in the gut mucosa was detected by *FISH* method as previously described (*23*). In brief, the large intestines were isolated and fixed with 4 % formaldehyde and dehydrated with 15 % - and 30 % - sucrose in PBS consecutively. Then dehydrated tissues were embedded in OCT compound (Sakura Finetek, Tokyo, Japan), frozen, sliced into 5-μm sections, and dried thoroughly. Hybridization buffer containing 5 ng of oligonucleotide probe μl^{-1} [Bacid2 (5′-AACATGTTTCCACATTATT CAGG-3′)] was applied to the slide and incubated at 50 °C for 2 hours. Oligonucleotide probes labeled with fluorescein were synthesized by Bioneer Corporation (Daejeon, Korea). The slides were rinsed with washing buffer at 50 °C for 10 min. After mounting with PermaFluor (Thermo scientific, Fremont, CA), slides were viewed under a confocal laser microscope (Zeiss, Göttingen, Germany).

II-2-9. Cytokine levels in serum

Cytokine levels in serum measured using the Cytometric Bead Array-mouse inflammation kit (BD Biosciences, San Jose, CA) according to the manufacturers Śnstructions.

II-2-10. Histology

The visceral adipose tissues were washed with PBS and fixed in 4 % formaldehyde for 1 hour at 4 ^{o}C. Tissues were dehydrated by gradually soaking in alcohol and xylene and then embedded in paraffin. The paraffin-embedded specimens were cut into 5-μm sections, stained with H&E, and viewed with a digital light microscope (Olympus, Tokyo, Japan).

II-2-11. Bacterial antigen preparation and *B. acidifaciens*-specific ELISA

The commensal bacteria specific ELISA was performed as previously described (*24*). In brief, bacteria cultured in mass volume for 48 hours were centrifuged at 5,000 g for 15 min and washed in sterile PBS twice by centrifuging for 1 minute at 8,000 rpm. On the last wash bacteria were resuspended in 2 ml ice-cold PBS and sonicated on ice (0.2 mV pulse,

20 seconds). After spin-down with 20,000 g for 10 min at 4 ^{o}C, and recovered supernatants used for *B. acidifaciens*-specific ELISA as antigen. 5 μg/ml of *B. acidifaciens* antigen in 50 mM sodium bicarbonate was coated for overnight at 4 ^{o}C. After a blocking step, two-fold serially diluted samples (serums and feces) were applied onto plates and incubated for 2 hours at 37 ^{o}C. HRP-conjugated goat anti-mouse IgG and IgA antibody (Southern Biotechnology Associates, Birmingham, AL) (1:3000 in 0.1 % BSA in PBS plus 0.1 % Tween 20) was added. Plates were developed with TMB substrate solution (Moss, INC), stopped by adding 0.5 N HCl, and measured at 450 nm on an ELISA reader (Microplate spectrophotometer; Molecular Devices).

II-2-12. 454 pyrosequencing analysis

cDNA was extracted from the feces using QIAamp DNA stool mini kits (QIAGEN, Venlo, Netherlands). PCR amplification was performed using primers targeting from V1 to V3 regions of the 16S rRNA gene with extracted cDNA. For bacterial amplification, barcoded primers of 9F (5′-CCTATCCCCTGTGTGCCTTGGCAGTC-TCAG-AC-AGAGTTTGATCMTGGCTCAG-3′, underlining sequence indicates the target region primer) and 541R (5′-CCATCTCATCCCTGCGTGTCTCCGAC-TCAG-X-AC-

ATTACCGCGGCTGCTGG-3ŚXXŚindicates the unique barcode for each subject) (http://oklbb.ezbiocloud.net/content/1001). The amplifications was carried out under the following conditions: initial denaturation at 95 ^{o}C for 5 min, followed by 30 cycles of denaturation at 95 ^{o}C for 30 sec, primer annealing at 55 ^{o}C for 30 sec, and extension at 72 ^{o}C for 30 sec, with a final elongation at 72 ^{o}C for 5 min. The amplified products were purified with the QIAquick PCR purification kit (Qiagen, Valencia, CA). Equal concentrations of purified products were pooled together and short fragments (non-target products) were removed with an AMPure bead kit (Agencourt Bioscience, Beverly, MA). The quality and product size were assessed on a Bioanalyzer 2100 (Agilent, Palo Alto, CA) using a DNA 7500 chip. Mixed amplicons were conducted by using emulsion PCR and then deposited on picotiter plates. The sequencing was carried out at Chunlab, Inc. (Seoul, Korea) by GS Junior Sequencing System (Roche, Branford, CT) according to the manufacturerŚs instructions. Pyrosequencing data analysis was performed as previously described (*25*).

II-2-13. Real-time PCR for tissues

Tissue RNA was extracted using TRIzol^{È} (Invitrogen), and total RNA (0.5 µg) was reverse-transcribed into cDNA according to the

manufacturer's instructions. All signal mRNAs were normalized to GAPDH mRNA. The following primers were used to determine the relative gene expression. *F4/80*: FP, 5'-GCCTGGACGAATCCTGTGAA-3'; RP, 5'-GCTAGATGCAAAGCCAGGGT-3' *TNF-α* FP, 5'-GGCAGGTCTACTTTGGAGTC-3'; RP, 5'-TCGAGGCTCCAGTGAATTCG-3' All reactions were performed in the same manner: 95 °C for 10 seconds, followed by 45 cycles of 95 °C for 15 seconds and 60 °C for 1 minute. The results were analyzed with real-time system AB 7900HT software (Life Technologies), and all values were normalized to the levels of GAPDH.

II-2-14. Analysis of metabolic parameters

Serum glucose, total cholesterol and triglyceride concentrations were determined using commercially available enzymatic assay kits (Asan Pharmacology, Seoul, Korea). Serum insulin levels were measured with an ultra-sensitive mouse insulin ELISA kit (Shibayagi, Gunma, Japan).

II-2-15. Statistics

GraphPad Prism software (GraphPad, La Jolla, CA) was used for statistical analysis. Significant differences between two groups were analyzed with two-tailed paired *t*-test or Mann-Whitney *t*-test. Multiple

groups were analyzed by two-way ANOVA followed by Bonferroni *post-hoc* test (*, $P < 0.05$; **, $P < 0.01$; ***, $P < 0.001$).

II-3. Results

II-3-1. *Atg7*$^{\varphi CD11c}$ mice showed lean phenotypes with reduced body weight and fat mass.

In order to address a role of autophagy on the development of metabolic disorders, I carefully monitored the body weight and behavior of three different kinds of *Atg7* conditional knockout mice in dendritic cells (*Atg7*$^{\varphi CD11c}$), gut epithelial cells (*Atg7*$^{\varphi villin}$), or macrophages (*Atg7*$^{\varphi M\wedge}$) with normal chow diet (NCD) feeding. As mice aged, I unexpectedly found that *Atg7*$^{\varphi CD11c}$ mice of 24 weeks old showed significantly lower body weight and fat mass than those of control littermates (*Atg7*$^{flox/flox\ (f/f)}$) (Fig. 1A-C). No significant body weight changes were found in *Atg7*$^{\varphi villin}$ and *Atg7*$^{\varphi M\check{k}}$ mice of same ages (Fig. 1D-E). The difference of body weight between *Atg7*$^{\varphi CD11c}$ and *Atg7*$^{f/f}$ mice were gradually increased with age (Fig. 1F). Those lean phenotypes of *Atg7*$^{\varphi CD11c}$ mice were detected both male and female (Fig. 1G). When *Atg7*$^{\varphi CD11c}$ and *Atg7*$^{f/f}$ mice of 9 weeks old were fed high fat diet (HFD) for four weeks, body weight loss were also found in the *Atg7*$^{\varphi CD11c}$ mice (Fig. 1H). Magnetic resonance imaging (MRI) analysis further revealed that mass of the abdominal adipose tissues both in axial and colonal derection were significantly reduced in the *Atg7*$^{\varphi CD11c}$ mice when

compared with those of littermate *Atg7*$^{f/f}$ mice (Fig. 1I). In addition, the size of a single adipocyte in visceral adipose tissues obtained from *Atg7*$^{\Delta CD11c}$ mice was significantly smaller than that of *Atg7*$^{f/f}$ mice (Fig. 1J).

A.

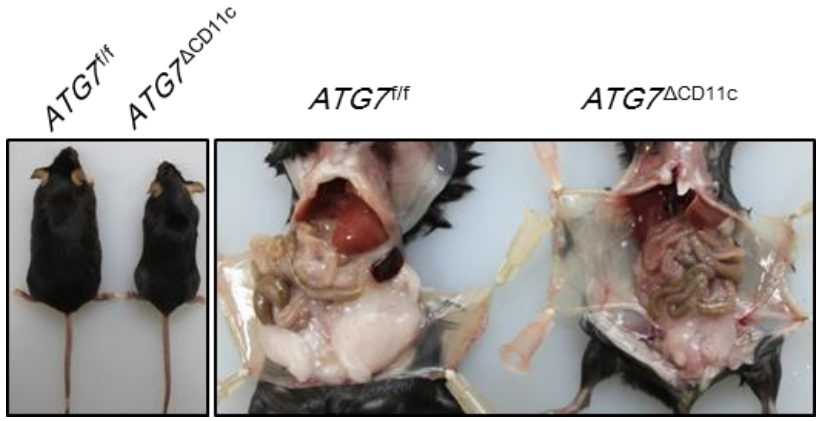
ATG7f/f
ATG7ΔCD11c
ATG7f/f
ATG7ΔCD11c

B.

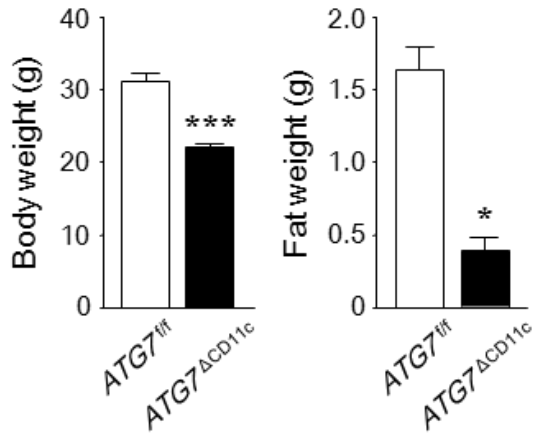
Body weight (g)
40
30
20
10
0
***
ATG7f/f
ATG7ΔCD11c
Fat weight (g)
2.0
1.5
1.0
0.5
0
*
ATG7f/f
ATG7ΔCD11c

C.

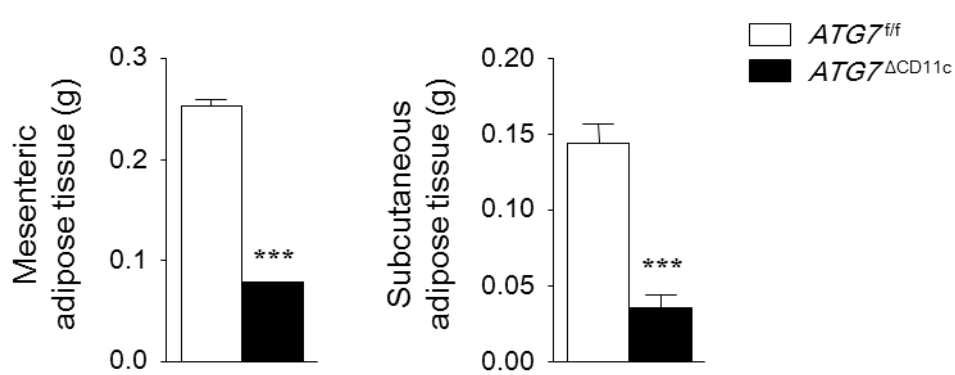
ATG7f/f
ATG7ΔCD11c
Mesenteric adipose tissue (g)
0.3
0.2
0.1
0.0
***
Subcutaneous adipose tissue (g)
0.20
0.15
0.10
0.05
0.00
***

D.

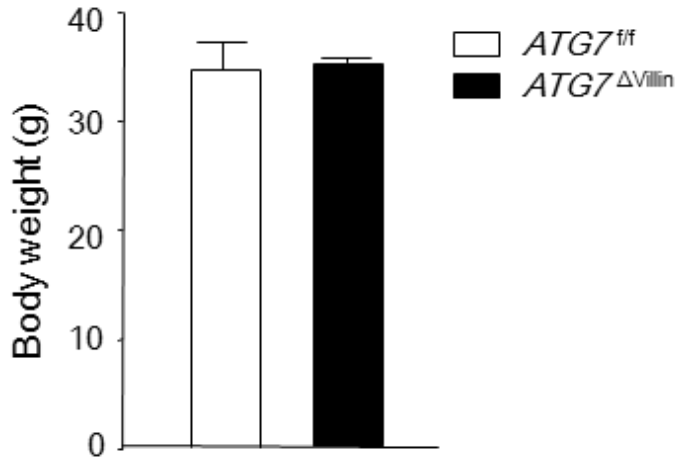
40
30
20
10
0
Body weight (g)
ATG7 f/f
ATG7 ΔVillin

E.

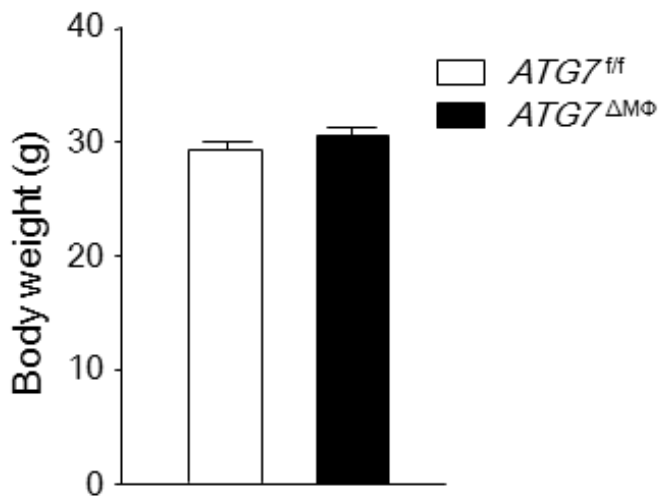
40
30
20
10
0
Body weight (g)
ATG7 f/f
ATG7 ΔMΦ

F.

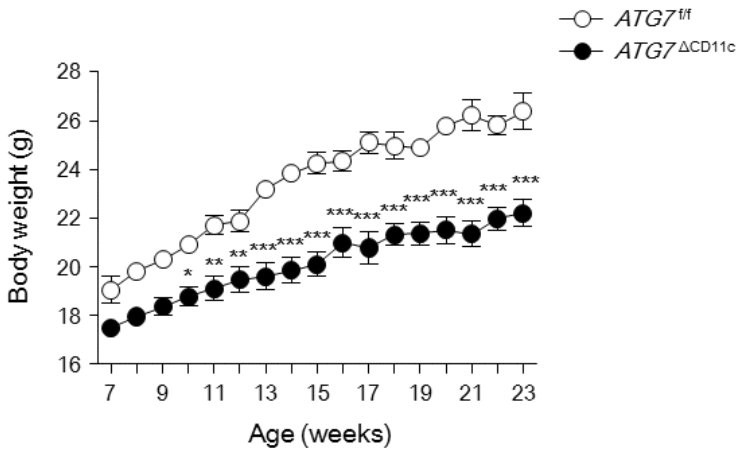
ATG7f/f
ATG7ΔCD11c
Body weight (g)
28
26
24
22
20
18
16
7
9
11
13
15
17
19
21
23
Age (weeks)
*
**
**
***
***
***
***
***
***
***
***
***
***

G.

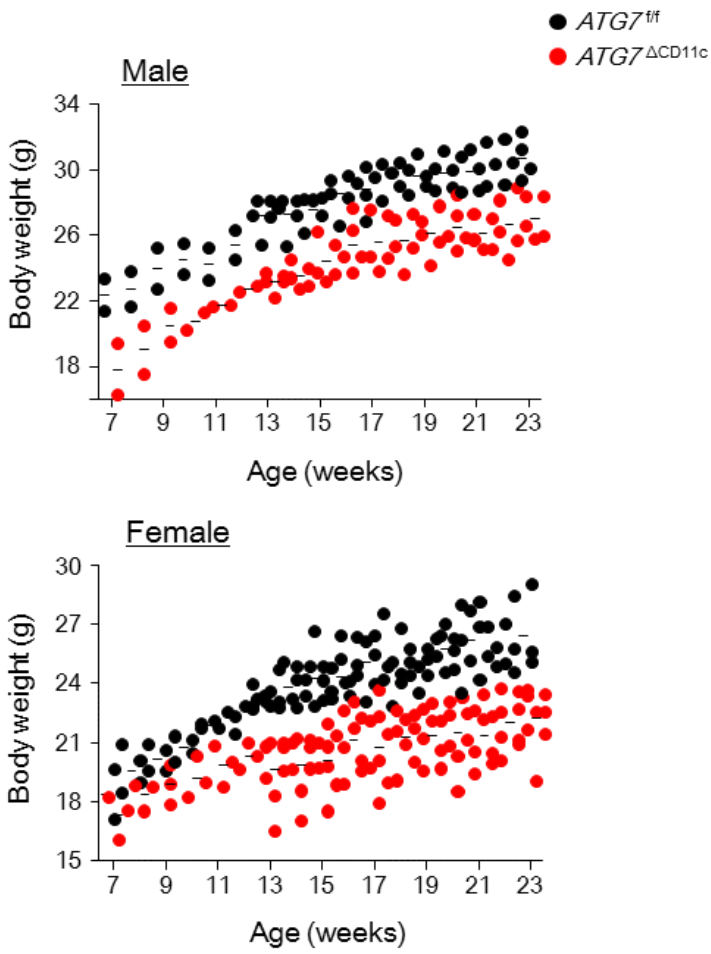
ATG7f/f
ATG7ΔCD11c
Male
Body weight (g)
34
30
26
22
18
7
9
11
13
15
17
19
21
23
Age (weeks)
Female
Body weight (g)
30
27
24
21
18
15
7
9
11
13
15
17
19
21
23
Age (weeks)

H.

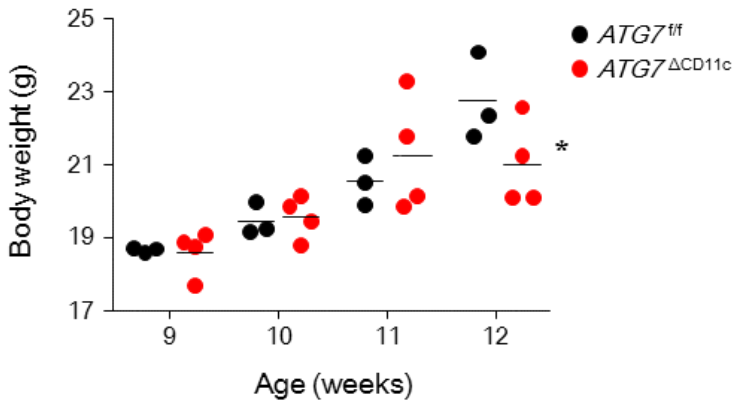
25
23
21
19
17
Body weight (g)
9
10
11
12
Age (weeks)
ATG7 f/f
ATG7 ΔCD11c
*

I.

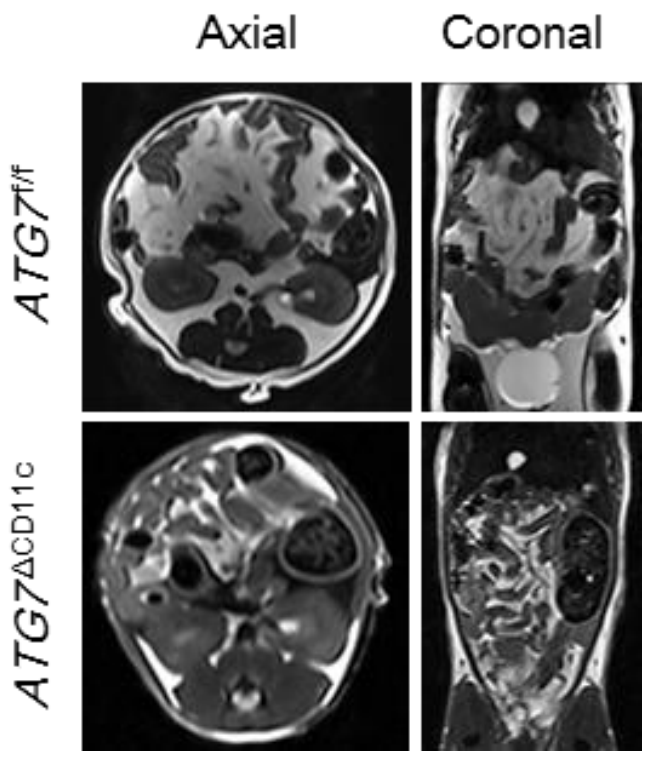
Axial
Coronal
ATG7f/f
ATG7ΔCD11c

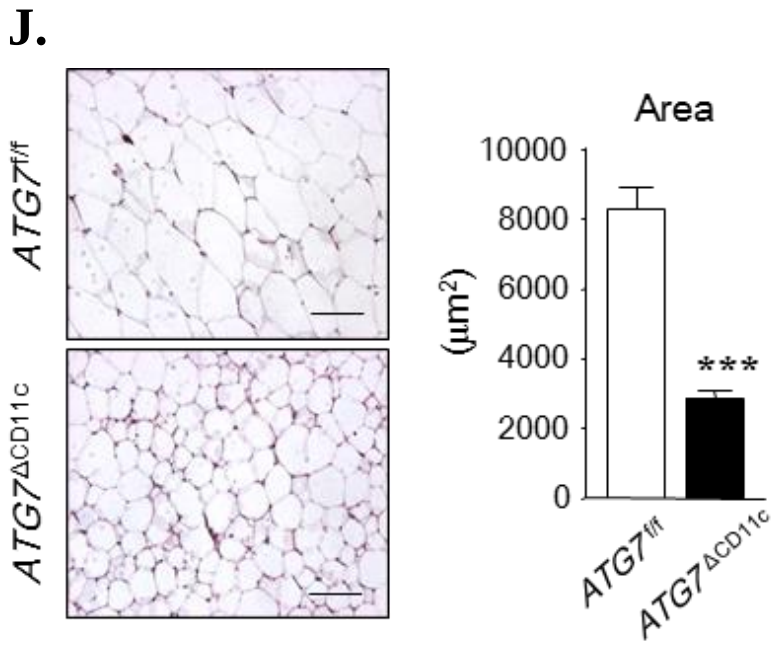

Figure 2.1. Morphological characteristics of *Atg7*$^{\varphi CD11c}$ mice.

Lean phenotypes were discovered in *Atg7*$^{\varphi CD11c}$ mice. **(A).** Representative photos of 24-week-old *Atg7*$^{f/f}$ and *Atg7*$^{\varphi CD11c}$ mice. **(B).** Body weight (left panel) and fat mass (right panel) of 24-week-old male *Atg7*$^{f/f}$ and *Atg7*$^{\varphi CD11c}$ mice fed normal chow diet (NCD; n = 5-8). **(C).** The specific fat depot were further analysed. The comparison of body weight between littermate control and conditional KO mice (n = 3) having an impaired autophagy function in intestinal villi **(D**; male, n = 3**)** and macrophages **(E**; female, n = 5**)**. **(F).** Body weight changes of *Atg7*$^{f/f}$ and *Atg7*$^{\varphi CD11c}$ mice (n = 8) were monitored for 23 weeks. **(G).** Monitoring of body weight for 23 weeks in male (upper) and female (bottom) *Atg7*$^{f/f}$ and *Atg7*$^{\varphi CD11c}$ mice fed NCD. **(H).** Monitoring

of body weight for 12 weeks in male *Atg7*$^{f/f}$ (n = 3) and *Atg7*$^{\Delta CD11c}$ (n = 4) mice fed HFD. **(I).** The abdominal adipose tissues from 24-week-old male *Atg7*$^{f/f}$ and *Atg7*$^{\Delta CD11c}$ mice fed NCD were analyzed by magnetic resonance imaging (MRI). **(J).** Histological changes of adipose tissues (left panel) and size of adipocytes (right panel) of *Atg7*$^{f/f}$ and *Atg7*$^{\Delta CD11c}$ mice. Scale bars=50 ㎛. All data are presented as mean ± s.e.m. Statistical analyses were done with two-tailed paired *t*-test (**B**-**E** and **J**) and two-way ANOVA with Bonferroni *post-hoc* test (**F** and **H**). *P<0.05, **P<0.01, and ***P<0.001.

II-3-2. *Atg7*$^{\Delta CD11c}$ mice shown lean phenotypes were not related with inflammation.

To clarify involvement of systemic and mucosal inflammation on the lean phenotype of *Atg7*$^{\Delta CD11c}$ mice, I have measured proinflammatory cytokine levels in serum, mRNA expression of F4/80 and TNFŬin visceral adipose tissues, and did histological analysis of small and large intestines. I found similar or even decreased levels of several indicators for systemic and mucosal inflammation in the *Atg7*$^{\Delta CD11c}$ mice, indicating lean phenotype chronically shown in *Atg7*$^{\Delta CD11c}$ mice is not associated with inflammation issues (Fig. 2A-C).

A.

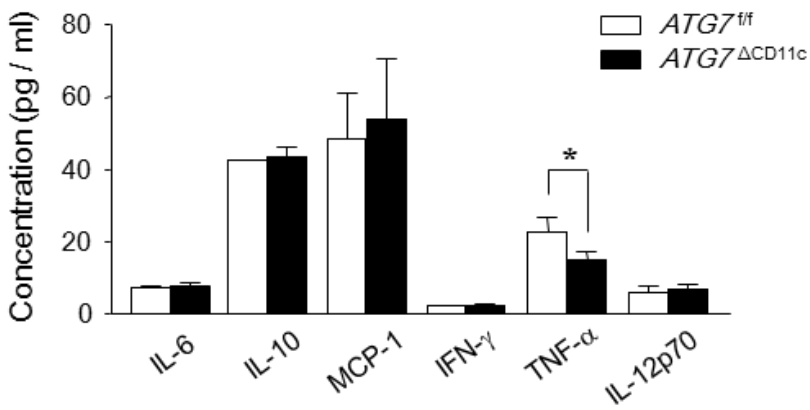
Concentration (pg / ml)
80
60
40
20
0
ATG7 f/f
ATG7 ΔCD11c
*
IL-6
IL-10
MCP-1
IFN-γ
TNF-α
IL-12p70

B.

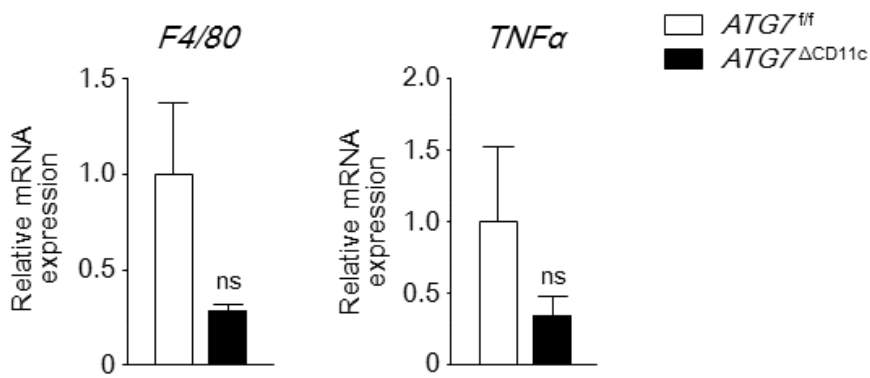
F4/80
TNFα
ATG7 f/f
ATG7 ΔCD11c
Relative mRNA expression
1.5
1.0
0.5
0
ns
Relative mRNA expression
2.0
1.5
1.0
0.5
0
ns

C.

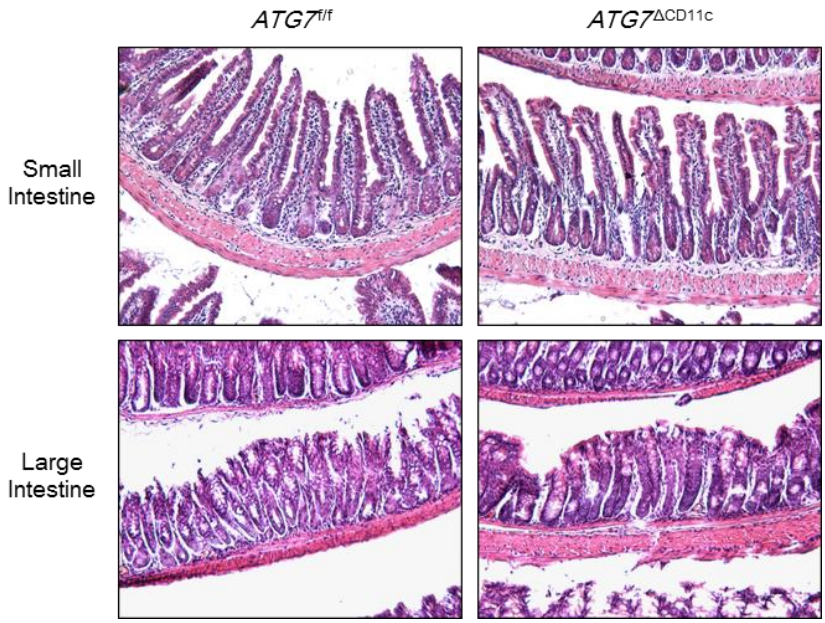

Figure 2.2. No inflammatory phenomenons in serum, adipose tissue, and intestinal area of *Atg7*$^{\Phi CD11c}$ mice.

(A). Proinflammatory cytokine levels in serum taken from 24-week-old *Atg7*$^{f/f}$ and *Atg7*$^{\Phi CD11c}$ mice (n = 7) by CBA mouse-inflammatory kit (BD Biosciences). (**B).** The mRNA expression levels of *F4/80* (left) and *TNF Ŭ* (right) in adipose tissue by real-time PCR. **(C).** Hematoxylin-eosin (H&E) staining of small intestine and large intestine taken from 24-week-old *Atg7*$^{f/f}$ and *Atg7*$^{\Phi CD11c}$ mice. Scale bar = 100 ɞm. All data are presented as mean ± s.e.m. Statistical analyses were done with one-way ANOVA with Bonferroni *post-hoc* test (**A**) and two-tailed paired *t*-test (**B**). *P<0.05. ns, not significant.

II-3-3. Insulin sensitivity was improved in *Atg7*^{qCD11c} mice.

Of note, higher insulin and subsequent lower glucose levels were detected in the serum of *Atg7*^{qCD11c} mice then those of *Atg7*$^{f/f}$ mice under the non-fasting condition. (Fig. 3A). Moreover, insulin resistance as determined by glucose tolerance test (GTT) and insulin tolerance test (ITT) was significantly improved in *Atg7*^{qCD11c} mice when compared with littermate *Atg7*$^{f/f}$ mice (Fig. 3B). Taken together, these data indicate that aged *Atg7*^{qCD11c} mice showed the improved glucose homeostasis with lean phenotypes of reduced body weight and fat mass.

A.

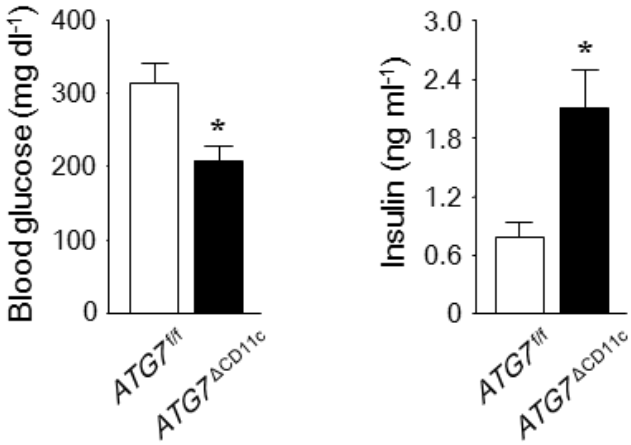
Blood glucose (mg dl-1)
400
300
200
100
0
*
ATG7f/f
ATG7ΔCD11c
Insulin (ng ml-1)
3.0
2.4
1.8
1.2
0.6
0
*
ATG7f/f
ATG7ΔCD11c

B.

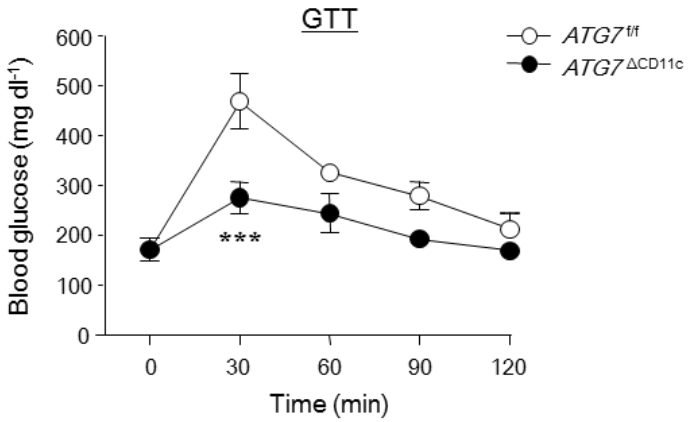
GTT
ATG7f/f
ATG7ΔCD11c
Blood glucose (mg dl-1)
600
500
400
300
200
100
0
***
0
30
60
90
120
Time (min)

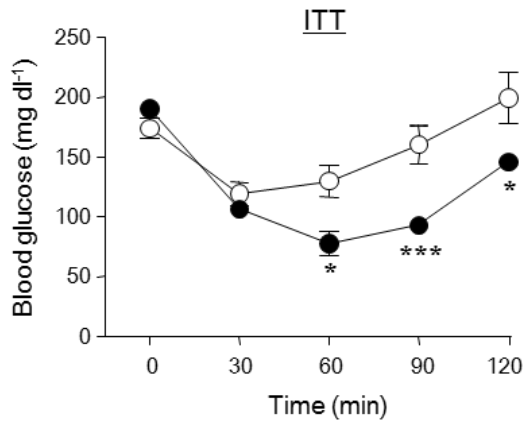
ITT
Blood glucose (mg dl-1)
250
200
150
100
50
0
*
***
*
0
30
60
90
120
Time (min)

Figure 2.3. Glucose / insulin levels in serum of *Atg7*$^{\varphi CD11c}$ mice

(A). Non-fasting glucose and insulin concentration in NCD-fed *Atg7*$^{f/f}$ and *Atg7*$^{\varphi CD11c}$ mice (n = 3). **(B).** Concentrations of serum triglycerides and total cholesterol were analyzed using enzymatic assay kits in *Atg7*$^{f/f}$ and *Atg7*$^{\varphi CD11c}$ mice (n = 3). **(C).** Glucose tolerance test (GTT) and insulin tolerance test (ITT) in male *Atg7*$^{f/f}$ and *Atg7*$^{\varphi CD11c}$ mice (n = 7). All data are presented as mean ± s.e.m. Statistical analyses were done with two-tailed paired *t*-test (**A** and **B**) and two-way ANOVA with Bonferroni *post-hoc* test (**C**). *P<0.05, and ***P<0.001.

II-3-4. Low levels of short-chain fatty acids (SCFAs) in the feces of *Atg7*^{qCD11c} mice.

Because aged *Atg7*^{qCD11c} mice had shown a decreased body weight and fat mass, I next assessed metabolome analysis in the feces to investigate the correlation between lean phenotypes and energy utilization. Although principal component analysis (PCA) revealed a weak correlation (data not shown), individual spots of *Atg7*^{qCD11c} mice in orthogonal partial least squares discriminate analysis (OPLS-DA) were clearly segregated from those of *Atg7*$^{f/f}$ mice (Fig. 4A). Moreover, some of short-chain fatty acids (SCFAs) such as acetate, propionate, butyrate and lactate, were located at remote spots from the axis (Fig. 4B), indicating that those factors contribute to separate the class between *Atg7*$^{f/f}$ and *Atg7*^{qCD11c} mice. I then further investigated the concentration of SCFAs and all sorts of compounds in feces using gas chromatography-mass spectrometry (GC-MS). While the level of lactate in *Atg7*^{qCD11c} mice was higher than that of *Atg7*$^{f/f}$ mice, the amounts of acetate, butyrate and propionate in *Atg7*^{qCD11c} mice were significantly decreased (Fig. 4C).

A.

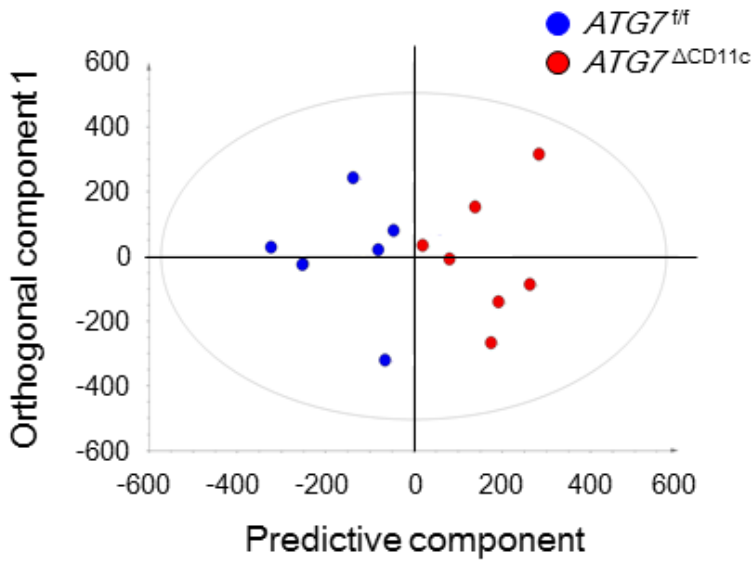
ATG7 f/f
ATG7 ΔCD11c
Orthogonal component 1
600
400
200
0
-200
-400
-600
-600
-400
-200
0
200
400
600
Predictive component

B.

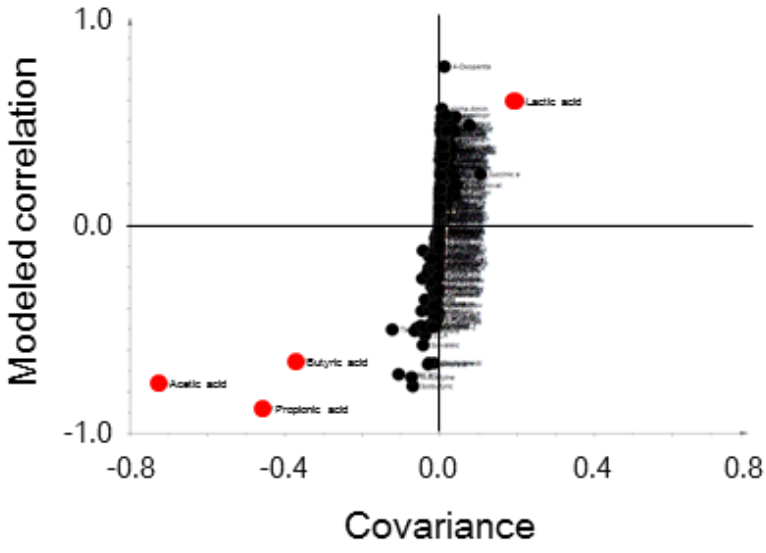
Modeled correlation
1.0
0.0
-1.0
Lactic acid
Butyric acid
Acetic acid
Propionic acid
-0.8
-0.4
0.0
0.4
0.8
Covariance

C.

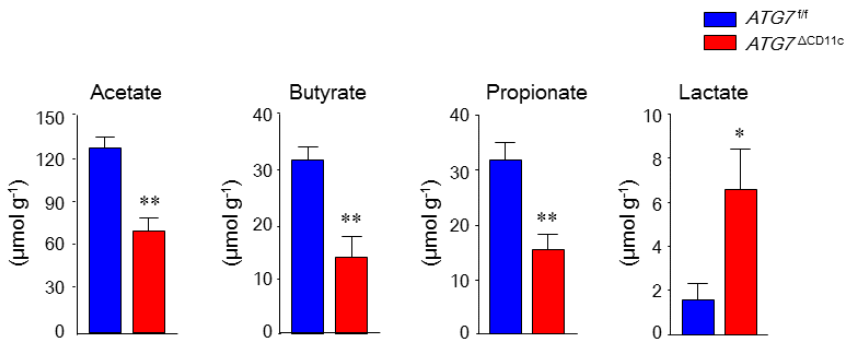

Figure 2.4. Orthogonal partial least squares discriminate analysis (OPLS-DA) in feces.

OPLS-DA on the fecal metabolome data of *Atg7*$^{f/f}$ and *Atg7*^{qCD11c} mice. **(A)** Cross-validated score plots from OPLS-DA of ^{1}H-NMR data of *Atg7*$^{f/f}$ and *Atg7*^{qCD11c} mice feces (n = 7). **(B)** S-plots for predictive component from OPLS-DA of ^{1}H-NMR data of in feces of *Atg7*$^{f/f}$ and *Atg7*^{qCD11c} mice (n = 7). **(C).** Quantification of facal SCFAs (i.e. acetate, butyrate, propionate and lactate) in *Atg7*$^{f/f}$ and *Atg7*^{qCD11c} mice (n = 5) by gas chromatography-mass spectrometry (GC-MS). All data are presented as mean ± s.e.m. Statistical analyses were done with two-tailed paired *t*-test **(C)** *P<0.05 and **P<0.01.

II-3-5. Commensal bacteria are associated with the lean phenotype of aged *Atg7*$^{\Delta CD11c}$ mice.

To address whether commensal bacteria are involved on the lean phenotype of *Atg7*$^{\Delta CD11c}$ mice, I have adopted co-housing (CH) and fecal microbiota transplantation (FMT) experiments. Both *Atg7*$^{\Delta CD11c}$ and *Atg7*$^{f/f}$ mice of 7 weeks old are sharing their feces in the same cage for 16 weeks. Of note, either body weight or fat mass were compensated each other in two groups of mice during CH period (Fig. 5A-C). To confirm whether this compensable phenotype of CH group is mediated by commensal microorganisms, I have then separated mice from sharing cage to individual cage. As shown in Fig. 5D, *Atg7*$^{\Delta CD11c}$ mice lost body weight compared to those of *Atg7*$^{f/f}$ mice as times goes by after separation. In addition, wild-type B6 mice orally transferred with fecal extracts obtained from *Atg7*$^{\Delta CD11c}$ mice for 12 weeks every day revealed significantly lower body weight and fat mass than those transferred from wild-type B6 or *Atg7*$^{f/f}$ mice (Fig. 5E). Of note, wild-type B6 mice adopted fecal extracts of *Atg7*$^{\Delta CD11c}$ mice were shown higher insulin and subsequent lower glucose levels in the serum when compared to those transferred with *Atg7*$^{f/f}$ mice (Fig. 5F). Overall, these results imply that commensal bacteria play indispensable role on the lean phenotype of *Atg7*$^{\Delta CD11c}$ mice.

A.

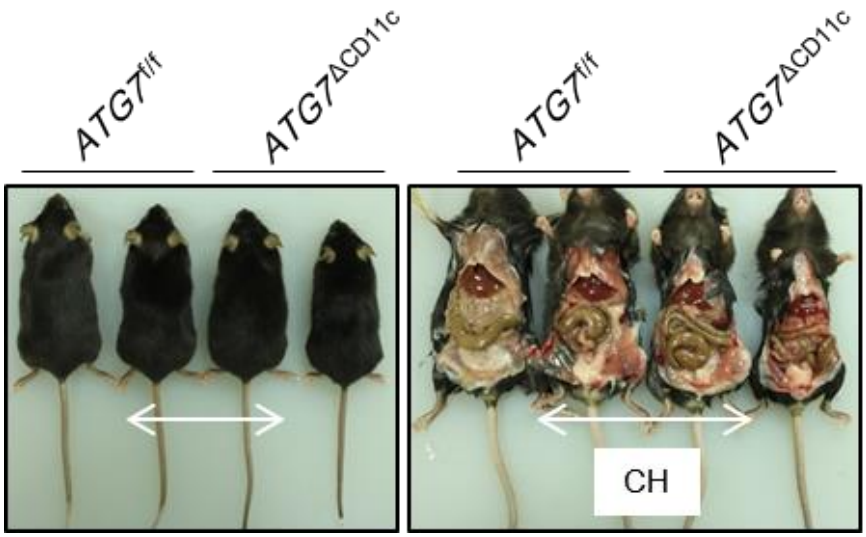
ATG7f/f
ATG7ΔCD11c
ATG7f/f
ATG7ΔCD11c
CH

B.

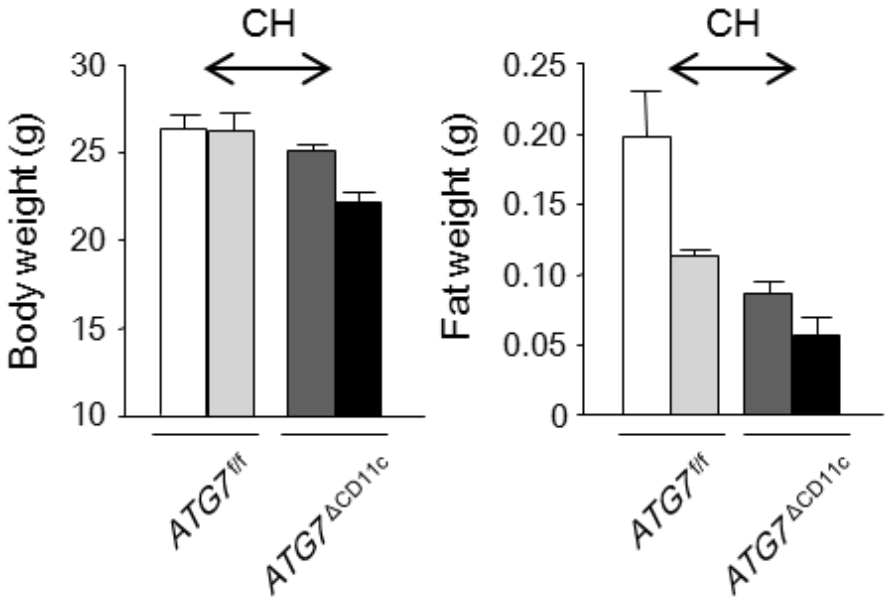
CH
Body weight (g)
30
25
20
15
10
ATG7f/f
ATG7ΔCD11c
CH
Fat weight (g)
0.25
0.20
0.15
0.10
0.05
0
ATG7f/f
ATG7ΔCD11c

C.

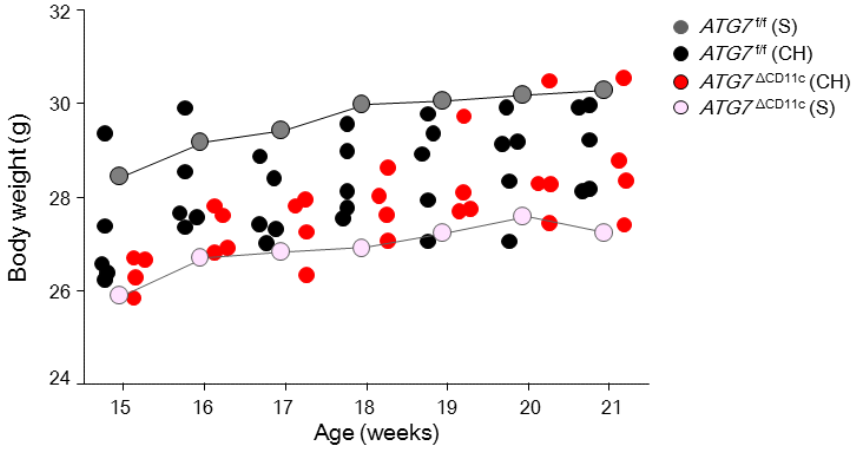
Body weight (g)
32
30
28
26
24
15
16
17
18
19
20
21
Age (weeks)
ATG7 f/f (S)
ATG7 f/f (CH)
ATG7 ΔCD11c (CH)
ATG7 ΔCD11c (S)

D.

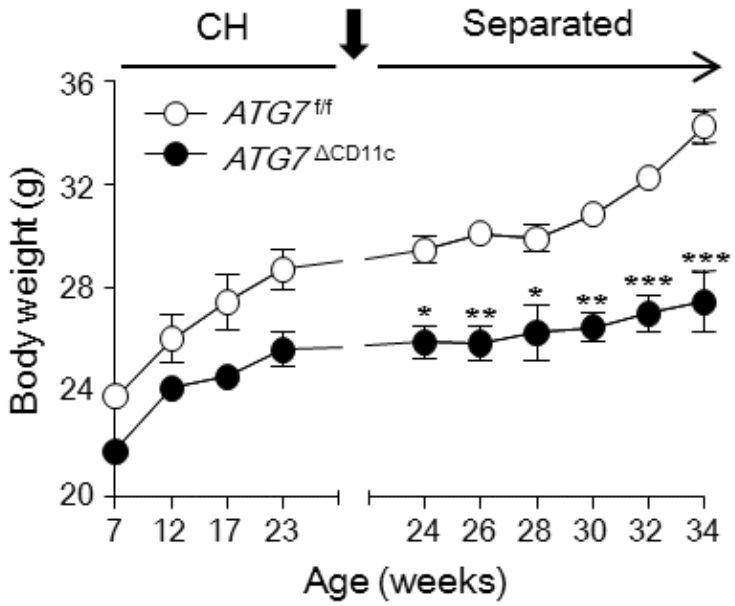
CH
Separated
ATG7 f/f
ATG7 ΔCD11c
Body weight (g)
36
32
28
24
20
7
12
17
23
24
26
28
30
32
34
Age (weeks)
*
**
*
**
***
***

E.

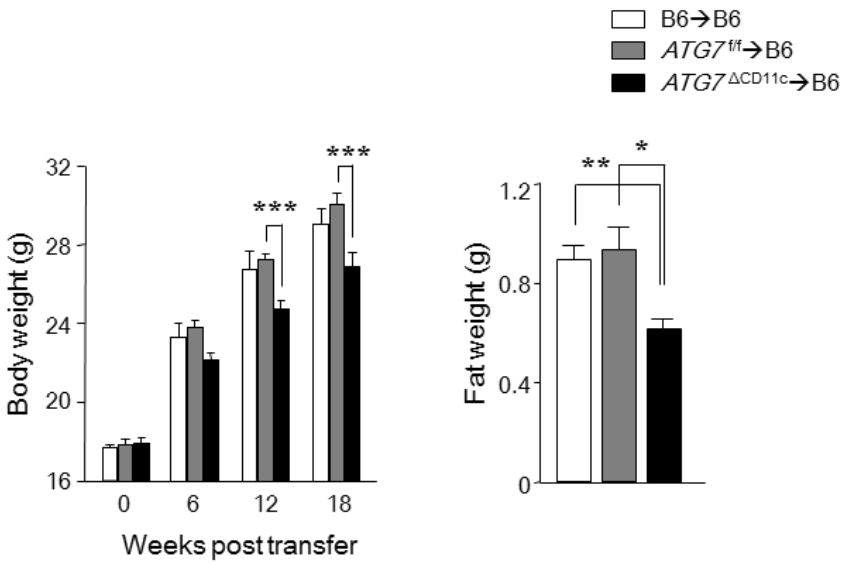
B6→B6
ATG7 f/f→B6
ATG7 ΔCD11c→B6
Body weight (g)
32
28
24
20
16
0
6
12
18
Weeks post transfer
***
***
Fat weight (g)
1.2
0.8
0.4
0
**
*

F.

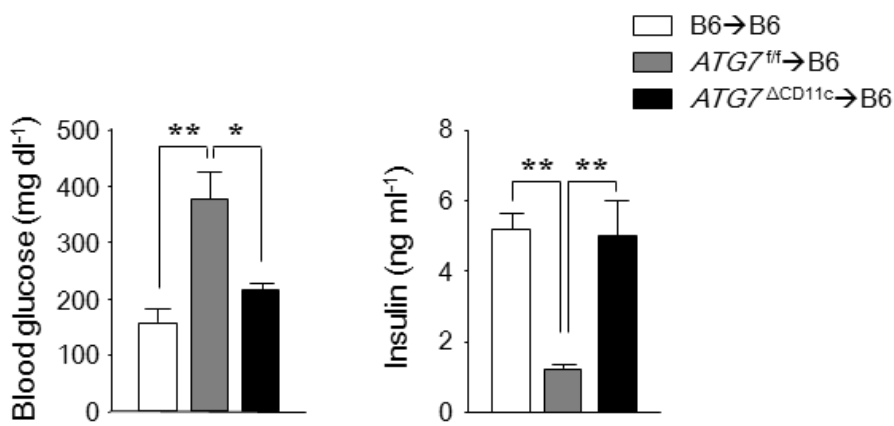
B6→B6
ATG7 f/f→B6
ATG7 ΔCD11c→B6
Blood glucose (mg dl-1)
500
400
300
200
100
0
**
*
Insulin (ng ml-1)
8
6
4
2
0
**
**

Figure 2.5. Representative photos, body / fat weight, and glucose / insulin levels of feces-transferred mice.

Lean phenotypes were originated from gut commensal bacteria. **(A).** Representative photos of 24-week-old *Atg7*$^{f/f}$ and *Atg7*$^{\Delta CD11c}$ mice after co-housing (CH; center) for 18 weeks or separated (leftmost and rightmost). (**B).** Body weight (left panel) and fat mass (right panel) of 24-week-old *Atg7*$^{f/f}$ and *Atg7*$^{\Delta CD11c}$ mice in CH- or separated- cages (n = 3-4). **(C).** Monitoring of body weight of *Atg7*$^{f/f}$ (n = 5) and *Atg7*$^{\Delta CD11c}$ (n = 4) mice in CH cages. Body weight of separated *Atg7*$^{f/f}$ and *Atg7*$^{\Delta CD11c}$ mice was drawn by linear graphs of filled circles with gray and pink color, respectively. **(D).** At 18 weeks after CH, body weight of each separated mice were monitored for further 10 weeks (n = 3-9). **(E).** Body weight (left panel) and fat mass (right panel) of naïve C57BL/6 (B6) recipient mice transferred feces of *Atg7*$^{f/f}$ or *Atg7*$^{\Delta CD11c}$ mice for 18 weeks everyday (n = 5). **(F).** Levels of glucose and insulin in serum of B6 recipient mice transferred feces of *Atg7*$^{f/f}$ or *Atg7*$^{\Delta CD11c}$ mice under non-fasting condition (n = 5). All data are presented as mean ± s.e.m. Statistical analyses were performed with two-tailed paired t-test (**B and F**) and two-way ANOVA with Bonferroni *post-hoc* test (**D** and **E**). *P<0.05, **P<0.01 and ***P<0.001.

II-3-6. Expansion of *Bacteroides acidifaciens* in the feces of *Atg7*^{qCD11c} mice.

In order to see the diversity and composition of gut commensal bacteria, I next adopted metagenomic analysis. In pyrosequencing analysis, the proportion of *Bacteroidetes*, *Firmicutes*, and *Proteobacteria*, which are well known as main populations of the gut microbiota in phylum level, were not shown any significant difference in the feces of *Atg7*$^{f/f}$ and *Atg7*^{qCD11c} mice (Fig. 6A). The proportion of *Bacteroidia* (class), *Bacteroidales* (order), *Bacteroidaceae* (family), and *Bacteroides* (genus) were also shown similar or not significantly changed (Fig. 6B). However, interestingly, when I have analyzed species levels, the ratio of *Bacteroides* (*B.*) *acidifaciens* has significantly expanded in the feces of *Atg7*^{qCD11c} mice as compared to those in *Atg7*$^{f/f}$ mice (5.48 ± 1.76 % vs. 0.77 ± 0.18 %) (Fig. 6C and red arrow in Fig. 6D). On the other hands, proportion of *B. sartorii*, another anaerobic *Bacteroides* species in the mouse commensal bacteria, was not altered in the feces of *Atg7*^{qCD11c} and *Atg7*$^{f/f}$ mice (blue arrow in Fig. 6D). To further confirm the expansion of *B. acidifaciens* in *Atg7*^{qCD11c} mice with lean phenotype, fluorescence *in situ* hybridization (*FISH*) analysis were used. As shown in Fig 6E, increased numbers of *B. acidifaciens* were detected in the lumen of the colon and few *B. acidifaciens* were internalized in the colon

intestinal epithelial cells (IECs) of *Atg7*$^{\Delta CD11c}$ mice. Taken together, *B. acidifaciens* among the commensal bacteria are skewed in the gut of *Atg7*$^{\Delta CD11c}$ mice with lean phenotype.

A.

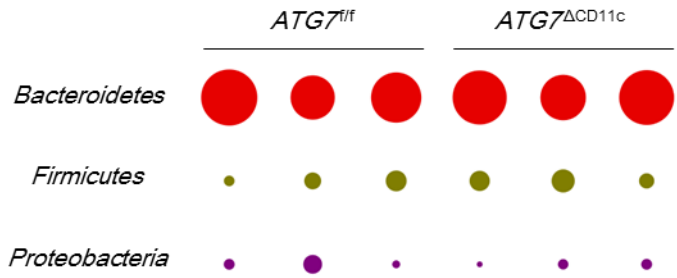
ATG7f/f
ATG7ΔCD11c
Bacteroidetes
Firmicutes
Proteobacteria

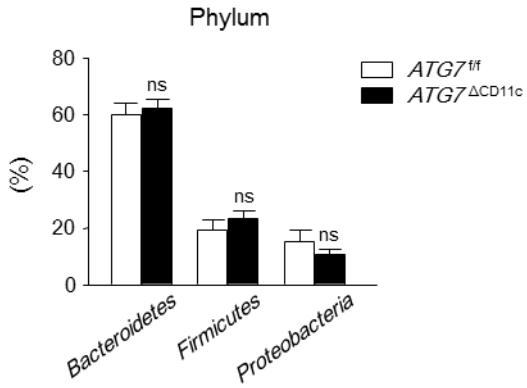
Phylum
ATG7f/f
ATG7ΔCD11c
(%)
80
60
40
20
0
ns
ns
ns
Bacteroidetes
Firmicutes
Proteobacteria

B.

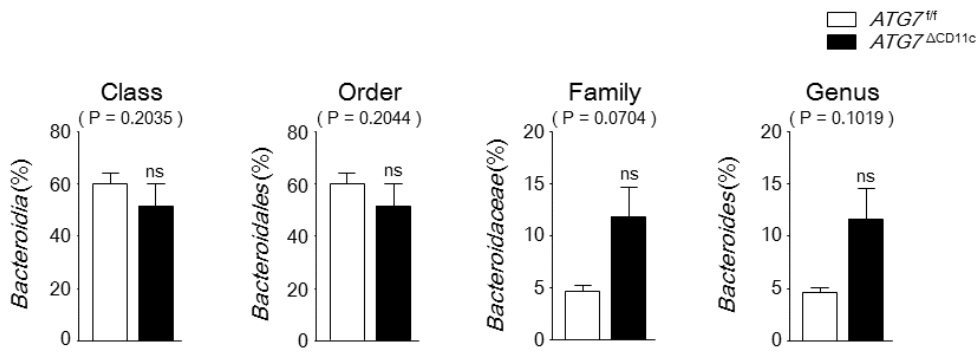
ATG7f/f
ATG7ΔCD11c
Class
(P = 0.2035)
Bacteroidia(%)
Order
(P = 0.2044)
Bacteroidales(%)
Family
(P = 0.0704)
Bacteroidaceae(%)
Genus
(P = 0.1019)
Bacteroides(%)
ns

C.

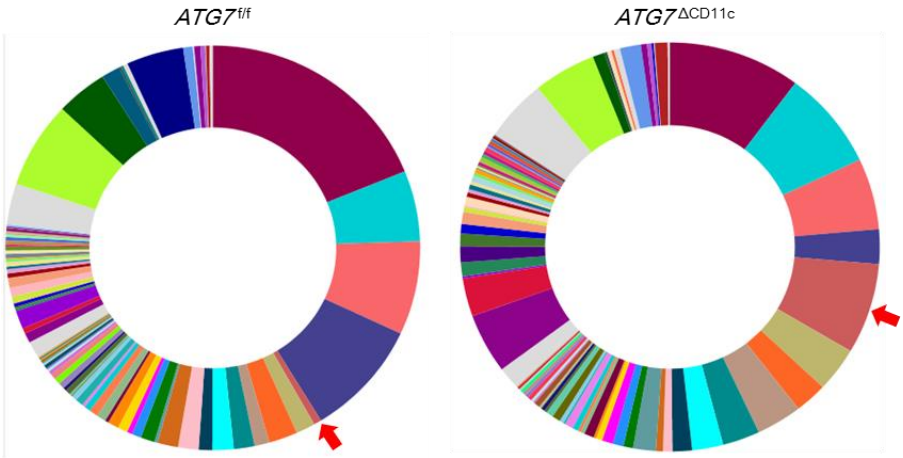
ATG7f/f
ATG7ΔCD11c

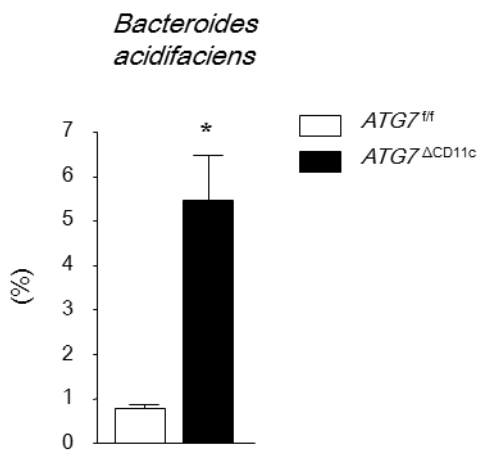
Bacteroides acidifaciens
*
ATG7f/f
ATG7ΔCD11c
(%)
0
1
2
3
4
5
6
7

D.

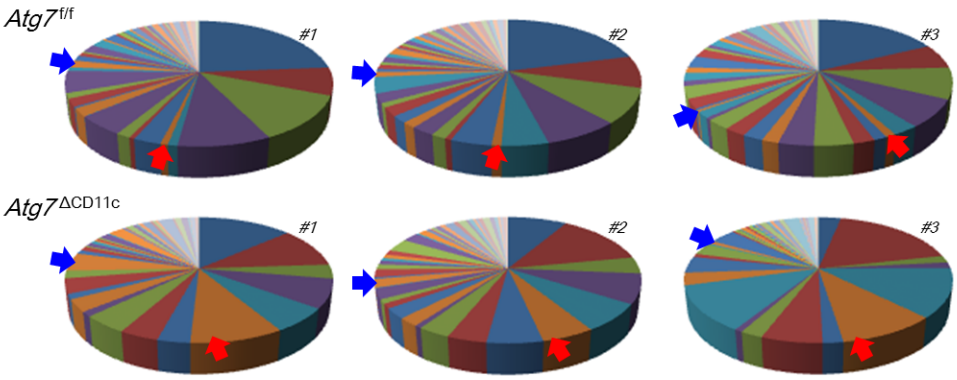

Bacteria;;;Bacteroidetes;;Bacteroidia;;Bacteroidales;;EF602759_f;EF602759_g;EF602759_s
Bacteria;;;Bacteroidetes;;Bacteroidia;;Bacteroidales;;Prevotellaceae;;Prevotella;DQ815942_s
Bacteria;;;Bacteroidetes;;Bacteroidia;;Bacteroidales;;EF602759_f;EF602759_f_uc;EF602759_f_uc_s
Bacteria;;;Bacteroidetes;;Bacteroidia;;Bacteroidales;;EF602759_f;DQ815871_g;DQ815871_g_uc
Bacteria;;;Firmicutes;;Clostridia;;Clostridiales;;Lachnospiraceae;;EF604627_g;AB606279_s
Bacteria;;;Bacteroidetes;;Bacteroidia;;Bacteroidales;;Bacteroidaceae;;Bacteroides;Bacteroides acidifaciens
Bacteria;;;Bacteroidetes;;Bacteroidia;;Bacteroidales;;EF602759_f;AY239469_g;4P003630_s
Bacteria;;;Firmicutes;;Clostridia;;Clostridiales;;Lachnospiraceae;;EU006430_g;EU006430_s
Bacteria;;;Bacteroidetes;;Bacteroidia;;Bacteroidales;;Bacteroidaceae;;Bacteroides;EF604598_s
Bacteria;;;Proteobacteria;;Betaproteobacteria;;Burkholderiales;;Sutterella_f;;Parasutterella;AJ308395_s
Bacteria;;;Tenericutes;;Mollicutes;;Acholeplasmatales;;Acholeplasmataceae;;Acholeplasma_g2;Acholeplasma_g2_uc
Bacteria;;;Bacteroidetes;;Bacteroidia;;Bacteroidales;;Porphyromonadaceae;;Parabacteroides;Parabacteroides distasonis
Bacteria;;;Deferribacteres;;Deferribacteres_c;;Deferribacterales;;Deferribacteraceae;;Mucispirillum;Mucispirillum schaedleri
Bacteria;;;Bacteroidetes;;Bacteroidia;;Bacteroidales;;EF602759_f;EU622683_g;EF406456_s
Bacteria;;;Bacteroidetes;;Bacteroidia;;Bacteroidales;;Bacteroidaceae;;Bacteroides;AB021165_s
Bacteria;;;Tenericutes;;Mollicutes;;Acholeplasmatales;;Acholeplasmataceae;;Acholeplasma_g2;EF406813_s
Bacteria;;;Firmicutes;;Clostridia;;Clostridiales;;Lachnospiraceae;;EF603662_g;EF603662_s
Bacteria;;;Bacteroidetes;;Bacteroidia;;Bacteroidales;;Bacteroidaceae;;Bacteroides;Bacteroides sartorii
Bacteria;;;Bacteroidetes;;Bacteroidia;;Bacteroidales;;Prevotellaceae;;Prevotella;EU622763_s
Bacteria;;;Bacteroidetes;;Bacteroidia;;Bacteroidales;;EF602759_f;EF602759_g;EU791194_s
Bacteria;;;Firmicutes;;Clostridia;;Clostridiales;;Ruminococcaceae;;EU791177_g;EU791177_s
Bacteria;;;Bacteroidetes;;Bacteroidia;;Bacteroidales;;Porphyromonadaceae;;Parabacteroides;EF096000_s
Bacteria;;;Bacteroidetes;;Bacteroidia;;Bacteroidales;;EF602759_f;AY239469_g;EF603769_s
Bacteria;;;Firmicutes;;Clostridia;;Clostridiales;;Ruminococcaceae;;Oscillibacter;DQ815311_s
Bacteria;;;Proteobacteria;;Deltaproteobacteria;;Desulfovibrionales;;Desulfovibrionaceae;;DQ815907_g;HM124141_s
Bacteria;;;Firmicutes;;Clostridia;;Clostridiales;;Ruminococcaceae;;Oscillibacter;JQ085130_s
Bacteria;;;Bacteroidetes;;Bacteroidia;;Bacteroidales;;Rikenellaceae;;Alistipes;DQ815748_s
Bacteria;;;Firmicutes;;Clostridia;;Clostridiales;;Lachnospiraceae;;DQ815599_g;DQ815599_s
Bacteria;;;Bacteroidetes;;Bacteroidia;;Bacteroidales;;EF602759_f;HM124280_g;EF603706_s
Bacteria;;;Bacteroidetes;;Bacteroidia;;Bacteroidales;;EF602759_f;DQ815871_g;DQ815871_s
Bacteria;;;Bacteroidetes;;Bacteroidia;;Bacteroidales;;Bacteroidales_uc;;Bacteroidales_uc_g;Bacteroidales_uc_s
Bacteria;;;Bacteroidetes;;Bacteroidia;;Bacteroidales;;EF602759_f;EF602759_g;EF097615_s
Bacteria;;;Firmicutes;;Clostridia;;Clostridiales;;HM124151_f;EF406417_g;EF406417_s
Bacteria;;;TM7;;TM7_c;;TM7_o;;TM7_f;AJ400239_g;AJ400239_s
Bacteria;;;Bacteroidetes;;Bacteroidia;;Bacteroidales;;EF602759_f;HM124280_g;EF406830_s
Bacteria;;;Bacteroidetes;;Bacteroidia;;Bacteroidales;;EF602759_f;AY239469_g;AY239469_g_uc
Bacteria;;;Bacteroidetes;;Bacteroidia;;Bacteroidales;;EF602759_f;AB606322_g;AB606322_s
Bacteria;;;TM7;;TM7_c;;TM7_o;;TM7_f;AJ400239_g;DQ777900_s
Bacteria;;;Bacteroidetes;;Bacteroidia;;Bacteroidales;;EF602759_f;FJ880046_g;EF406536_s
Bacteria;;;Proteobacteria;;Alphaproteobacteria;;EU939387_o;;AB270041_f;AB270041_g;AB270041_s
Bacteria;;;Firmicutes;;Clostridia;;Clostridiales;;Lachnospiraceae;;AB626939_g;FJ881271_s
Bacteria;;;Bacteroidetes;;Bacteroidia;;Bacteroidales;;EF602759_f;HM124280_g;HM124280_g_uc
Bacteria;;;Tenericutes;;Mollicutes;;Mycoplasmatales;;Mycoplasmataceae_f1;;Mycoplasmataceae_f1_uc;Mycoplasmataceae_f1_uc_s
Bacteria;;;Bacteroidetes;;Bacteroidia;;Bacteroidales;;EF602759_f;DQ815871_g;EF603109_s
Bacteria;;;Firmicutes;;Clostridia;;Clostridiales;;Lachnospiraceae;;DQ815599_g;HQ740248_s
Bacteria;;;Bacteroidetes;;Bacteroidia;;Bacteroidales;;EF602759_f;DQ815871_g;EF406459_s
Bacteria;;;Firmicutes;;Clostridia;;Clostridiales;;Lachnospiraceae;;Lachnospiraceae_uc;Lachnospiraceae_uc_s
Bacteria;;;Bacteroidetes;;Bacteroidia;;Bacteroidales;;EF602759_f;EF406806_g;EF406817_s
Bacteria;;;Firmicutes;;Clostridia;;Clostridiales;;Lachnospiraceae;;AB626958_g;EF604622_s
Bacteria;;;Firmicutes;;Clostridia;;Clostridiales;;Ruminococcaceae;;AM277340_g;FJ879877_s
Bacteria;;;Bacteroidetes;;Bacteroidia;;Bacteroidales;;EF602759_f;EF602759_g;EU457676_s

E.

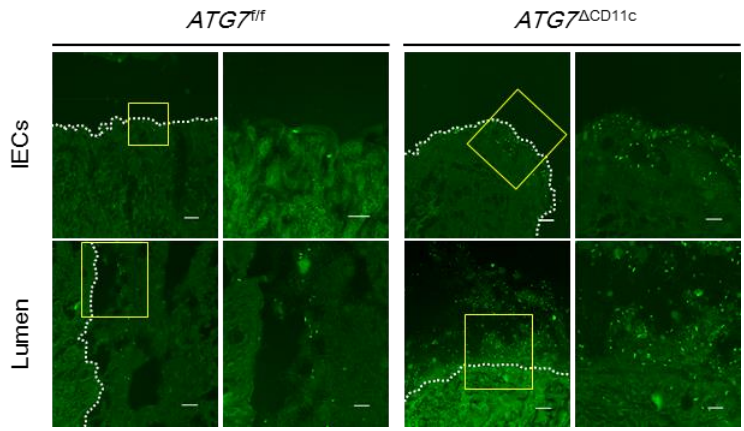

Figure 2.6. Pyrosequencing analysis in feces and confocal images of *Bacteroides acidifaciens*.

Pyrosequencing data were analyzed in terms of **(A)** phylum and **(B)** from class to genus level (n = 6). **(C).** The representative pie charts showing the proportion *B. acidifaciens* in feces detected by pyrosequencing analysis (n = 6). **(D).** Pie charts of bacterial composition in species levels of *Atg7*$^{f/f}$ and *Atg7*^{qCD11c} mice (n = 3), individually. The portion of *B. acidifaciens* and *B. sartorii* were indicated by red and blue arrow, respectively. The name of commensal bacteria was listed in top 50. **(E).** Increased numbers of *B. acidifaciens* in the intestinal epithelial cells (IECs) and lumen of colon of *Atg7*$^{f/f}$ and *Atg7*^{qCD11c} mice determined by fluorescence *in situ* hybridization (*FISH*) probe specified to *B. acidifaciens*. All data are presented as mean ± s.e.m. Statistical analyses were done with two-tailed paired *t*-test. *P<0.05.

II-3-7. Characterization of CD11c positive cells as phagocytes and antigen-presenting cells against *Bacteroides acidifaciens*.

To examine whether the expanded single commensal bacteria in *Atg7*$^{\Delta CD11c}$ mice was caused by deficiency of bacterial clearance through autophagy, I co-cultured CD11c positive cells of bone marrow-derived dendritic cells (BM-DCs) with *B. acidifaciens*. Interestingly, the number of *B. acidifaciens* inside BM-DCs at 24 hours after co-culture was significantly increased in *Atg7*$^{\Delta CD11c}$ mice, compared to that of control mice (Fig. 7A). Moreover, further analysis demonstrated that expanded *B. acidifaciens* in *Atg7*$^{\Delta CD11c}$ mice consequently affected to adaptive immune system, including elevated serum immunoglobulin G (IgG), IgA and fecal IgA specific for *B. acidifaciens*-derived antigens as well as increased co-stimulatory factors, such as CD40, CD80 and CD86 (Fig. 7B and Fig. 7C). Taken together, deleted function of autophagy in CD11c positive cells does not influence in both the capacity of antigen uptake and initiation of adaptive immunity.

A.

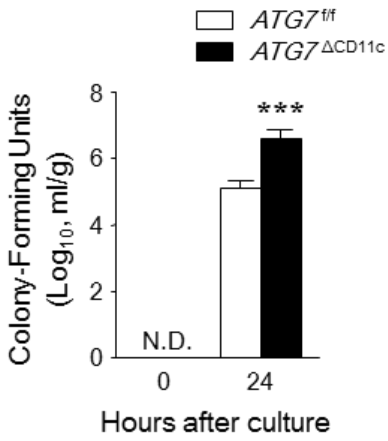
ATG7 f/f
ATG7 ΔCD11c
Colony-Forming Units
(Log10, ml/g)
8
6
4
2
0
***
N.D.
0
24
Hours after culture

B.

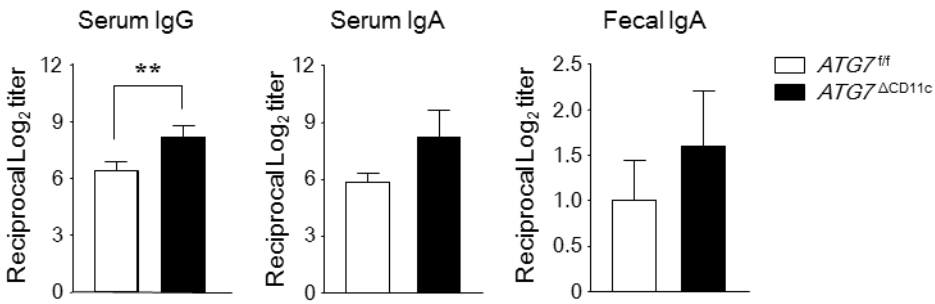
Serum IgG
Serum IgA
Fecal IgA
Reciprocal Log2 titer
12
9
6
3
0
**
2.5
2.0
1.5
1.0
0.5
ATG7 f/f
ATG7 ΔCD11c

C.

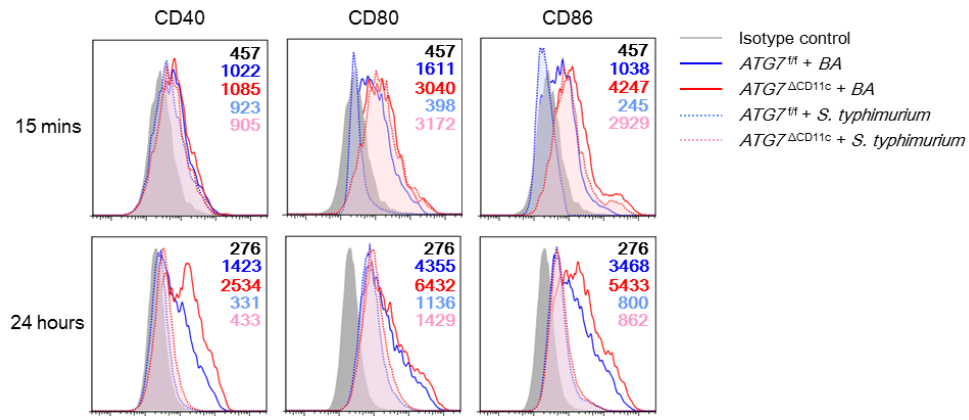
CD40
CD80
CD86
15 mins
24 hours
457
1022
1085
923
905
457
1611
3040
398
3172
457
1038
4247
245
2929
276
1423
2534
331
433
276
4355
6432
1136
1429
276
3468
5433
800
862
Isotype control
ATG7 f/f + BA
ATG7 ΔCD11c + BA
ATG7 f/f + S. typhimurium
ATG7 ΔCD11c + S. typhimurium

Figure 2.7. Colony forming units (CFUs) of *B. acidifaciens*, antibodies detection by Enzyme-linked immunosorbent assay (ELISA), and activation of co-stimulatory molecules by FACS analysis.

Lean phenotypes were originated from *B. acidifaciens* among gut commensal bacteria. **(A).** Colony-forming units (CFUs) of *B. acidifaciens* after 24 hours co-cultured with BM-DCs. **(B).** *B. acidifaciens*-specific antibodies responses were analyzed using serum and feces taken from *Atg7*$^{f/f}$ and *Atg7*$^{\Delta CD11c}$ mice by ELISA. **(C).** $CD11c^{+}$ cells differentiated from bone-marrows of *Atg7*$^{f/f}$ and *Atg7*$^{\Delta CD11c}$ mice were co-cultured with *B. acidifaciens* and *Salmonella typhimurium* as control, and then measured the expression levels of co-stimulatory molecules (i.e. CD40, CD80 and CD86) at 15 mins and 24 hours, respectively. All data are mean ± s.e.m. of at least two independent experiments. Statistical analyses were done with two-tailed paired *t*-test. **P<0.01 and ***P<0.001. N.D., not detected.

II-4. Discussion

Previous studies demonstrated that autophagy disruption would lead to insulin resistance and diabetes. For instance, mice deficient of *Atg7* in the pancreatic beta cells have significant defect on the insulin release and hyperglycemia (*26, 27*). In contrast, mice with skeletal muscle-specific deletion of *Atg7* showed decreased fat mass and diet-induced obesity, and protected from insulin resistance (*9*). Authors suggested mitochondrial dysfunction which provoked by autophagy disruption increased fibroblast growth factor 21 (Fgf21), a mitokine that contributes a strong effects on lipid mobilization. However, there are no reports about relationship between host lipid metabolisms and single commensal bacteria regulated by autophagy. I found mice with $CD11c^{+}$ cell specific autophagy deficiency revealed improved insulin sensitivity and expanded population of *Bacteroides acidifaciens*. On the other hands, while serum glucose levels were down regulated, high levels of insulin secretion were maintained in the $Atg7^{\Delta CD11c}$ mice. Therefore, I speculate that mitochondrial dysfunction by autophagy deficiency may improve insulin sensitivity but at the same time there might be uncontrolled insulin secretion by specific commensal bacteria.

B. acidifaciens were firstly isolated from the caecum of mice by Itoh K. et al (*23, 28*). These novel commensal bacteria were characterized anaerobic, gram-negative, good growth in bile acid and aesculin hydrolysis. Thereafter, their function was revealed by other group that *B. acidifaciens* possessing capacity to increase IL-6 and IL-10 production by enhancing expression of MHC class II and the co-stimulating molecules (i.e., CD80 and CD86) on antigen-presenting cells (*29*). In addition, *B. acidifaciens* is one of predominant commensal bacteria which responsible for promoting IgA Abs production in the large intestine specifically by inducing activation-induced cytidine deaminase expression (*30, 31*). Here, I noted another unique function that *B. acidifaciens* can modulate energy metabolisms and therefore applicable for therapeutic use for obesity and diabetes control.

Investigation of epidemiologic relationship between obesity and its causes revealed that environmental factors and host genetic background can influence the composition of gut commensal bacteria (*32*). The two phyla that consists the majority of gut commensal microbiota in the mammalian are the *Bacteroidetes* and the *Firmicutes*. Previous evidences in animal and human studies suggest that an increase ratio of *Firmicutes* to *Bacteroidetes* is making the gut microbiota more efficient to extract energy from the diet

and thereby can be one of causes for adiposity (*11*, *15*, *33*). In contrast, some studies described such alteration on phylum-level are too simple and insufficient to explain the mechanisms associated with adiposity and obesity (*34*, *35*). Those observations support our current finding that I could not find any changes in the proportion of *Firmicutes* and *Bacteroidetes* in feces of *Atg7*^{qCD11c} mice that are prone to lean compared to the littermate *Atg7*$^{f/f}$ mice (Fig. 6A). Instead, I found that specific species (i.e., *B. acidifaciens*) among *Bacteroidetes* phylum are largely expanded in the lean *Atg7*^{qCD11c} mice (Fig. 6C). Recent study revealed that cohousing obese mice with mice containing the lean twin's microbiota prevented the body weight increase and obesity-associated metabolic phenotypes which correlated with invasion of specific members of *Bacteroides* such as *B. cellulosilyticus*, *B. uniformis*, *B. vulgatus*, *B. thetaiotaomicron*, and *B. caccae* (*16*). Furthermore, oral administration of *B. uniformis* CECT 7771 strain improved metabolic disorders and immunological dysfunction in HFD-induced obesity mice (*36*). In this study, I firstly identify *B. acidifaciens* which might be tightly regulated in steady-state condition by autophagy machinery of CD11c^{+} cells and might be associated with gut microbiota homeostasis for energy harvest.

There are two general cascades associated with weight loss; increased energy expenditure or reduced energy utilization/storage

efficiency. A NMR-based metabolic analysis revealed that there is clear segregation between *Atg7*^{qCD11c} and *Atg7*$^{f/f}$ mice (Fig. 4A). Loading plots shows SCFAs such as butyric acids, propionic acids and acetic acids are significantly lower and conversely lactate is higher in *Atg7*^{qCD11c} mice than those in *Atg7*$^{f/f}$ control mice (Fig. 4B). This profile of SCFAs is similar to the SPF mice fed with low-fiber diet (*37*). In this regards, caloric extraction from diet fiber is upregulated in the obese animal and human compared to the healthy control (*38*). Young mice administered subtherapeutic antibiotic therapy increased adiposity and revealed substantial increases in SCFAs in the caecal contents (*15*). Thus I assume that altered microbiota condition of *Atg7*^{qCD11c} mice seems to have poor caloric extraction propertied when compare to the control *Atg7*$^{f/f}$ mice. Given that SCFAs are good energy source for the host, the decrease of SCFAs levels may reduce energy supply and resulted in lean phenotype.

In summary, deletion of *autophagy-related gene 7* (*Atg7*) in CD11c^{+} cells alters commensal bacterial composition, especially expansion of *B. acidifaciens* belonging to *Bacteroides* genus. Current discovery of *B. acidifaciens* expanded in gut of *Atg7*^{qCD11c} mice suggests that commensal bacteria might be interlinked between autophagy deficiency and lean phenotypes. Although further studies are required to figure out whether *B.*

acidifaciens have a unique function to control host lipid metabolism, my finding suggest that a single commensal bacteria can be regulated by autophagy of CD11c positive cells.

II-5. References

1. **A. Kuma, M. Hatano, M. Matsui, A. Yamamoto, H. Nakaya, T. Yoshimori, Y. Ohsumi, T. Tokuhisa, N. Mizushima.** 2004. The role of autophagy during the early neonatal starvation period. *Nature* 432, 1032-1036.
2. **B. Levine, D. J. Klionsky.** 2004. Development by self-digestion: molecular mechanisms and biological functions of autophagy. *Developmental Cell* 6, 463-477.
3. **B. Levine, N. Mizushima, H. W. Virgin.** 2011. Autophagy in immunity and inflammation. *Nature* 469, 323-335.
4. **D. J. Klionsky.** 2010. The autophagy connection. *Developmental Cell* 19, 11-12.
5. **R. Singh, S. Kaushik, Y. Wang, Y. Xiang, I. Novak, M. Komatsu, K. Tanaka, A. M. Cuervo, M. J. Czaja.** 2009. Autophagy regulates lipid metabolism. *Nature* 458, 1131-1135.
6. **L. Yang, P. Li, S. Fu, E. S. Calay, G. S. Hotamisligil.** 2010. Defective hepatic autophagy in obesity promotes ER stress and causes insulin resistance. *Cell Metabolism* 11, 467-478.
7. **Y. Zhang, S. Goldman, R. Baerga, Y. Zhao, M. Komatsu, S. Jin.** 2009. Adipose-specific deletion of autophagy-related gene 7 (*atg7*) in mice reveals a role in adipogenesis. *Proceedings of the National Academy of Sciences of the United States of America* 106, 19860-19865.
8. **R. Singh, Y. Xiang, Y. Wang, K. Baikati, A. M. Cuervo, Y. K. Luu, Y. Tang, J. E. Pessin, G. J. Schwartz, M. J. Czaja.** 2009. Autophagy regulates adipose mass and differentiation in mice. *The Journal of Clinical Investigation* 119, 3329-3339.
9. **K. H. Kim, Y. T. Jeong, H. Oh, S. H. Kim, J. M. Cho, Y. N. Kim, S. S. Kim, H. Kim do, K. Y. Hur, H. K. Kim, T. Ko, J. Han, H. L. Kim, J. Kim, S. H. Back, M. Komatsu, H. Chen, D. C. Chan, M. Konishi, N. Itoh, C. S. Choi, M. S. Lee.** 2013. Autophagy deficiency leads to protection from obesity and insulin resistance by inducing Fgf21 as a mitokine. *Nature Medicine* 19, 83-92.
10. **N. M. Delzenne, A. M. Neyrinck, F. Backhed, P. D. Cani.** 2011. Targeting gut microbiota in obesity: effects of prebiotics and probiotics. *Nature Reviews Endocrinology* 7, 639-646.
11. **R. E. Ley, F. Backhed, P. Turnbaugh, C. A. Lozupone, R. D.**

Knight, J. I. Gordon. 2005. Obesity alters gut microbial ecology. *Proceedings of the National Academy of Sciences of the United States of America* 102, 11070-11075.

12. **R. E. Ley, P. J. Turnbaugh, S. Klein, J. I. Gordon.** 2006. Microbial ecology: human gut microbes associated with obesity. *Nature* 444, 1022-1023.
13. **P. J. Turnbaugh, R. E. Ley, M. A. Mahowald, V. Magrini, E. R. Mardis, J. I. Gordon.** 2006. An obesity-associated gut microbiome with increased capacity for energy harvest. *Nature* 444, 1027-1031.
14. **M. Vijay-Kumar, J. D. Aitken, F. A. Carvalho, T. C. Cullender, S. Mwangi, S. Srinivasan, S. V. Sitaraman, R. Knight, R. E. Ley, A. T. Gewirtz. 2010.** Metabolic syndrome and altered gut microbiota in mice lacking Toll-like receptor 5. *Science* 328, 228-231.
15. **I. Cho, S. Yamanishi, L. Cox, B. A. Methe, J. Zavadil, K. Li, Z. Gao, D. Mahana, K. Raju, I. Teitler, H. Li, A. V. Alekseyenko, M. J. Blaser.** 2012. Antibiotics in early life alter the murine colonic microbiome and adiposity. *Nature* 488, 621-626.
16. **V. K. Ridaura, J. J. Faith, F. E. Rey, J. Cheng, A. E. Duncan, A. L. Kau, N. W. Griffin, V. Lombard, B. Henrissat, J. R. Bain, M. J. Muehlbauer, O. Ilkayeva, C. F. Semenkovich, K. Funai, D. K. Hayashi, B. J. Lyle, M. C. Martini, L. K. Ursell, J. C. Clemente, W. Van Treuren, W. A. Walters, R. Knight, C. B. Newgard, A. C. Heath, J. I. Gordon.** 2013. Gut microbiota from twins discordant for obesity modulate metabolism in mice. *Science* 341, 1241214.
17. **F. Backhed, H. Ding, T. Wang, L. V. Hooper, G. Y. Koh, A. Nagy, C. F. Semenkovich, J. I. Gordon.** 2004. The gut microbiota as an environmental factor that regulates fat storage. *Proceedings of the National Academy of Sciences of the United States of America* 101, 15718-15723.
18. **H. V. Lin, A. Frassetto, E. J. Kowalik, Jr., A. R. Nawrocki, M. M. Lu, J. R. Kosinski, J. A. Hubert, D. Szeto, X. Yao, G. Forrest, D. J. Marsh.** 2012. Butyrate and propionate protect against diet-induced obesity and regulate gut hormones via free fatty acid receptor 3-independent mechanisms. *PLoS One* 7, e35240.
19. **Z. Gao, J. Yin, J. Zhang, R. E. Ward, R. J. Martin, M. Lefevre, W. T. Cefalu, J. Ye.** 2009. Butyrate improves insulin sensitivity and increases energy expenditure in mice. *Diabetes* 58, 1509-1517.
20. **I. Kimura, K. Ozawa, D. Inoue, T. Imamura, K. Kimura, T. Maeda, K. Terasawa, D. Kashihara, K. Hirano, T. Tani, T.**

Takahashi, S. Miyauchi, G. Shioi, H. Inoue, G. Tsujimoto. 2013. The gut microbiota suppresses insulin-mediated fat accumulation via the short-chain fatty acid receptor GPR43. *Nature Communications* 4, 1829.

21. **B. P. Willing, A. Vacharaksa, M. Croxen, T. Thanachayanont, B. B. Finlay.** 2011. Altering host resistance to infections through microbial transplantation. *PLoS One* 6, e26988.
22. **T. H. Sannasiddappa, A. Costabile, G. R. Gibson, S. R. Clarke.** 2011. The influence of *Staphylococcus aureus* on gut microbial ecology in an in vitro continuous culture human colonic model system. *PloS One* 6, e23227
23. **Y. Momose, S. H. Park, Y. Miyamoto, K. Itoh.** 2011. Design of species-specific oligonucleotide probes for the detection of Bacteroides and Parabacteroides by fluorescence in situ hybridization and their application to the analysis of mouse caecal *Bacteroides-Parabacteroides* microbiota. *Journal of Applied Microbiology* 111, 176-184.
24. **G. F. Sonnenberg, L. A. Monticelli, T. Alenghat, T. C. Fung, N. A. Hutnick, J. Kunisawa, N. Shibata, S. Grunberg, R. Sinha, A. M. Zahm, M. R. Tardif, T. Sathaliyawala, M. Kubota, D. L. Farber, R. G. Collman, A. Shaked, L. A. Fouser, D. B. Weiner, P. A. Tessier, J. R. Friedman, H. Kiyono, F. D. Bushman, K. M. Chang, D. Artis.** 2012. Innate lymphoid cells promote anatomical containment of lymphoid-resident commensal bacteria. *Science* 336, 1321-1325.
25. **Y. W. Lim, B. K. Kim, C. Kim, H. S. Jung, B. S. Kim, J. H. Lee, J. Chun.** 2010. Assessment of soil fungal communities using pyrosequencing. *Journal of Microbiology* 48, 284-289**.**
26. **C. Ebato, T. Uchida, M. Arakawa, M. Komatsu, T. Ueno, K. Komiya, K. Azuma, T. Hirose, K. Tanaka, E. Kominami, R. Kawamori, Y. Fujitani, H. Watada.** 2008. Autophagy is important in islet homeostasis and compensatory increase of beta cell mass in response to high-fat diet. *Cell Metabolism* 8, 325-332**.**
27. **H. S. Jung, K. W. Chung, J. Won Kim, J. Kim, M. Komatsu, K. Tanaka, Y. H. Nguyen, T. M. Kang, K. H. Yoon, J. W. Kim, Y. T. Jeong, M. S. Han, M. K. Lee, K. W. Kim, J. Shin, M. S. Lee.** 2008. Loss of autophagy diminishes pancreatic beta cell mass and function with resultant hyperglycemia. *Cell Metabolism* 8, 318-324.
28. **Y. Miyamoto, K. Itoh.** 2000. *Bacteroides acidifaciens* sp. isolated from the caecum of mice. *International Journal of Systematic and*

Evolutionary Microbiology 50 Pt 1, 145-148.

29. **M. Tsuda, A. Hosono, T. Yanagibashi, S. Hachimura, K. Hirayama, K. Itoh, K. Takahashi, S. Kaminogawa.** 2007. Prior stimulation of antigen-presenting cells with *Lactobacillus* regulates excessive antigen-specific cytokine responses in vitro when compared with *Bacteroides*. *Cytotechnology* 55, 89-101.
30. **T. Yanagibashi, A. Hosono, A. Oyama, M. Tsuda, S. Hachimura, Y. Takahashi, K. Itoh, K. Hirayama, K. Takahashi, S. Kaminogawa.** 2009. *Bacteroides* induce higher IgA production than *Lactobacillus* by increasing activation-induced cytidine deaminase expression in B cells in murine Peyer's patches. *Bioscience, Biotechnology, and Biochemistry* 73, 372-377.
31. **T. Yanagibashi, A. Hosono, A. Oyama, M. Tsuda, A. Suzuki, S. Hachimura, Y. Takahashi, Y. Momose, K. Itoh, K. Hirayama, K. Takahashi, S. Kaminogawa.** 2013. IgA production in the large intestine is modulated by a different mechanism than in the small intestine: *Bacteroides acidifaciens* promotes IgA production in the large intestine by inducing germinal center formation and increasing the number of IgA^+ B cells. *Immunobiology* 218, 645-651.
32. **A. Spor, O. Koren, R. Ley.** 2011. Unravelling the effects of the environment and host genotype on the gut microbiome. *Nature Reviews Microbiology* 9, 279-290.
33. **P. J. Turnbaugh, F. Backhed, L. Fulton, J. I. Gordon.** 2008. Diet-induced obesity is linked to marked but reversible alterations in the mouse distal gut microbiome. *Cell Host & Microbe* 3, 213-223.
34. **E. F. Murphy, P. D. Cotter, S. Healy, T. M. Marques, O. O'Sullivan, F. Fouhy, S. F. Clarke, P. W. O'Toole, E. M. Quigley, C. Stanton, P. R. Ross, R. M. O'Doherty, F. Shanahan. 2010.** Composition and energy harvesting capacity of the gut microbiota: relationship to diet, obesity and time in mouse models. *Gut* 59, 1635-1642.
35. **C. K. Fleissner, N. Huebel, M. M. Abd El-Bary, G. Loh, S. Klaus, M. Blaut.** 2010. Absence of intestinal microbiota does not protect mice from diet-induced obesity. *The British Journal of Nutrition* 104, 919-929.
36. **P. Gauffin Cano, A. Santacruz, A. Moya, Y. Sanz.** 2012. Bacteroides uniformis CECT 7771 ameliorates metabolic and immunological dysfunction in mice with high-fat-diet induced obesity. *PLoS One* 7, e41079.
37. **Y. Furusawa, Y. Obata, S. Fukuda, T. A. Endo, G. Nakato, D.**

Takahashi, Y. Nakanishi, C. Uetake, K. Kato, T. Kato, M. Takahashi, N. N. Fukuda, S. Murakami, E. Miyauchi, S. Hino, K. Atarashi, S. Onawa, Y. Fujimura, T. Lockett, J. M. Clarke, D. L. Topping, M. Tomita, S. Hori, O. Ohara, T. Morita, H. Koseki, J. Kikuchi, K. Honda, K. Hase, H. Ohno. 2013. Commensal microbe-derived butyrate induces the differentiation of colonic regulatory T cells. *Nature* 504, 446-450.

38. **H. Tilg, A. Kaser.** 2011. Gut microbiome, obesity, and metabolic dysfunction. *The Journal of Clinical Investigation* 121, 2126-2132.

Chapter III. Gut commensal *Bacteroides acidifaciens* improves insulin sensitivity and prevents obesity in mice

III-1. Introduction

Bacteroides is a Gram-negative, obligately anaerobe, motile or nonmotile, and non-endospore forming bacterium belonging to the Enterobacteriaceae family. *Bacteroides* is one of the subcategory of *Bacteroidetes* phylum (*1*). *Bacteroides* are primary fermenters that lead carbohydrates to enter the network of syntrophic links within gut microflora. *Bacteroides* degrade carbohydrates to their component monosaccharides, which are metabolized to produce phosphenolpyruvate (PEP) converted to fermentation end products such as succinate and acetate. These products can be changed to butyrate by *Firmicutes*, which in turn can be taken up by the host and increase mucus production (*2*).

Obesity is one of leading social issue worldwide due to potentials to cause type 2 diabetes, cardiovascular disorder, cancer, and asthma (*3*). Although therapeutic trials to obesity become more complicated due to diverse life styles and genetic polymorphisms, it is obvious that obesity is caused by energy imbalance (*4*). Therefore, lots of scientific efforts are attempting to find contributing environmental factors that influence on the energy balance.

Bile acids are the main organic materials forming bile juice, and

especially play a critical physiological role in the liver and gastrointestinal organ (*5*). Bile acids are classified into primary- and secondary bile acids depending on their places to be created. The primary bile acids are synthesized from cholesterol to cholic acid (CA) and chenodeoxycholic acid (CDCA) by a variety of enzymes in liver (*5*). The commensal bacteria deconjugate residues that increase the water solubility of bile acids, and produce secondary bile acids like deoxycholic acid (DCA), lithocholic acid (LCA), ursodeoxycholic acid (UDCA) (*6*, *7*). Once the fat is entered into the gastrointestinal tract, the stored bile is secreted into the small intestine inside. Bile acid of 95 % remained in the intestinal area immediately after the completion of the function as digestive enzymes are mostly reabsorbed by active transport in ileum of small intestine, and repeats enterohepatic circulation (*8*).

To clarify the function of *Bacteroides acidifaciens* expanded in *Atg7*^{qCD11c} mice showing lean phenotypes, I orally administrated these bacteria to C57BL/6 mice everyday. Remarkably, *B. acidifaciens*-fed mice were shown the amelioration of metabolic disorders through TGR5-PPARŬ signals. My results suggest that single strain of commensal bacteria can be used as therapeutic agents for modulating metabolic disorders such as obesity.

III-2. Materials and Methods

III-2-1. Ethics statement

All animal experiments were approved by the Institutional Animal Care and Use Committee of the Asan biomedical research center (Approval No: PN 2014-13-069). All experiment was performed under anesthesia with a mixture of ketamine (100 mg/kg) and xylazine (20 mg/kg), and all efforts were made to minimize suffering.

III-2-2. Mice and bacteria strains

C57BL/6 (B6) and *CD11c*^{cre} mice were purchased from Charles River Laboratories (Orient Bio Inc., Sungnam, Korea) and Jackson Laboratory (Bar Harbor, ME), respectively. *ATG7*$^{flox/flox}$ mice were kindly provided by Dr. Masaaki Komatsu (Tokyo Metroplitan Institue of Medical Science, Japan). All mice were maintained under specific pathogen-free conditions in the animal facility at the Asan biomedical research center (Seoul, Korea) where they received sterilized food and water *ad libitum*. *Bacteroides* (*B.*) *acidifaciens* (JCM10556) and *B. sartorii* (JCM17136) used in this study were purchased from Japan Collection of Microorganisms (JCM) at RIKEN BioResource Center.

III-2-3. Bacteria culture and administration

B. acidifaciens and *B. sartorii* were grown in peptone-yeast-glucose (PYG) broth at 37 ^{o}C for 48 hours anaerobically with BBL^{TM} GasPak 100^{TM} EZ gas generating container (Becton Dickinson, Sparks, MD). The bacteria were concentrated by centrifuging for 15 minutes at 5,000 g and resuspended with sterile PBS. For therapeutic studies, mice were orally administered *B. acidifaciens* (5 ∃ 10^{10} CFU/ml) or *B. sartorii* (5 ∃ 10^{10} CFU/ml) everyday for a period of 10 weeks. The actual bacterial dose given was confirmed by plating serial dilutions onto EG blood agar plates.

III-2-4. Magnetic resonance imaging (MRI) analysis

All MRI experiments were performed at 9.4 T / 160 mm by Agilent MRI scanner (Agilent Technologies, Santa Clara, CA) using a millipede-shaped volume radiofrequency coil. All animals were anesthetized through a mask by spontaneous inhalation of 1.5 ~ 2% isoflurane. Shimming was performed to minimize B0 inhomogeneity prior to MR scanning both automatically and manually. The axial T1-weighted (T1-WI) fast spin echo (FSE) images was used to cover both kidneys completely. The parameters of T1-WI image were TR = 1100 msec, kzero = 1, echo spacing (ESP) =

9.82 msec (effective TE = 48 msec), 48 segments, echo train length (ETL) = 4, 4 averages, matrix = 192 ∃ 192, the field of view (FOV) = 25 ∃ 30 mm, slice thickness = 1.0 mm; and total scan time = 3 min 33 sec, respectively. During MR scanning, external triggering was used to eliminate respiratory motion artifacts.

III-2-5. MRI data analysis

Image J software (US National Institutes of Health, Bethesda, MD; http://rsb.info.nih.gov/ij/) was used for segmentation and measurement of compartments for MR images. We chose two representative MRI sections at the center of kidney level and at the kidney low pole. Then, the regions of interest were manually drawn to encompass the entire abdomen in order to calculate the total abdominal area and to encompass the peritoneal cavity for calculation of a visceral fat area. Contours of the visceral fat area were then generated semi-automatically based on the threshold of signal intensity to select fatty tissue. If there was a non-fat component within the contours, we manually removed those components.

III-2-6. Fluorescence *in situ* hybridization (*FISH*) analysis

The localization of *B. acidifaciens* in the gut mucosa was detected by *FISH* method as previously described (*9*). In brief, the large intestines were isolated and fixed with 4 % formaldehyde and dehydrated with 15 % - and 30 % - sucrose in PBS consecutively. Then dehydrated tissues were embedded in OCT compound (Sakura Finetek, Tokyo, Japan), frozen, sliced into 5-μm sections, and dried thoroughly. Hybridization buffer containing 5 ng of oligonucleotide probe μl^{-1} [Bacid2 (5′-AACATGTTTCCACATTATT CAGG-3′)] was applied to the slide and incubated at 50 °C for 2 hours. Oligonucleotide probes labeled with FAM were synthesized by Bioneer Corporation (Daejeon, Korea). The slides were rinsed with washing buffer at 50 °C for 10 min. After mounting with PermaFluor (Thermo scientific, Fremont, CA), slides were viewed under a confocal laser microscope (Zeiss, Göttingen, Germany).

III-2-7. Histology

The visceral adipose tissues were washed with PBS and fixed in 4 % formaldehyde for 1 hour at 4 °C. Tissues were dehydrated by gradually soaking in alcohol and xylene and then embedded in paraffin. The paraffin-

embedded specimens were cut into 5-μm sections, stained with H&E, and viewed with a digital light microscope (Olympus, Tokyo, Japan).

III-2-8. Real-time PCR for tissues

Tissue RNA was extracted using TRIzol® (Invitrogen), and total RNA (0.5 μg) was reverse-transcribed into cDNA according to the manufacturer's instructions. All signal mRNAs were normalized to GAPDH mRNA. Specific primer sets are listed in table 3.1. All reactions were performed in the same manner: 95 °C for 10 seconds, followed by 45 cycles of 95 °C for 15 seconds and 60 °C for 1 minute. The results were analyzed with real-time system AB 7900HT software (Life Technologies), and all values were normalized to the levels of GAPDH.

III-2-9. Analysis of metabolic parameters

Serum glucose, total cholesterol and triglyceride concentrations were determined using commercially available enzymatic assay kits (Asan Pharmacology, Seoul, Korea). Serum insulin levels were measured with an ultra-sensitive mouse insulin ELISA kit (Shibayagi, Gunma, Japan).

Table 3.1. List of specific primer sets used for real time-PCR

Target gene Symbol	Forward sequence	Reverse sequence
FasN	AGCACTGCCTTCGGTTCAGTC	AAGAGCTGTGGAGGCCACTTG
HSL	TCCTGGAACTAAGTGGACGCAAG	CAGACACACTCCTGCGCATAGAC
PEPCK	GTGTTTGTAGGAGCAGCCATGAGA	GCCAGGTATTTGCCGAAGTTGTAG
SCD1	TCGCCCCTACGACAAGAACA	GTAAGCCAGGCCCA
PPAR ɔ	TGTCGGTTTCAGAAGTGCCTTG	TTCAGCTGGTCGATATCACTGGAG
P P A R Ŭ	ACGCTCCCGACCCATCTTTAG	TCCATAAATCGGCACCAGGAA
PRDM16	CCTAGCCCTGAGCGATACTGTGA	ACAGACAATGGCTGGAATGGTG
PGC1 Ŭ	CCGTAAATCTGCGGGATGATG	CAGTTTCGTTCGACCTGCGTAA
Cidea	CTGTCTCAATGTCAAAGCCACGA	TGTGCAGCATAGGACATAAACCTCA
GLUT4	CTGTAACTTCATTGTCGGCATGG	AGGCAGCTGAGATCTGGTCAAAC
TGR5	GGCCTGGAACTCTGTTATCG	GTCCCTCTTGGCTCTTCCTC
GAPDH	CTGGAGAAACCTGCCAAGTA	AGTGGGAGTTGCTGTTGAAG

III-2-10. Measurement of glucagon-like peptide-1 (GLP-1)

Blood samples were taken from control and *B. acidifaciens*-fed mice, and then centrifuged for 30 minutes at 1800 g at 4 ^{o}C. DPP4 inhibitor was added to separated serum, GLP-1 concentrations were determined using GLP-1 ELISA kit (Shibayagi, Gunma, Japan).

III-2-11. Measurement of dipeptidyl peptidase-4 (DPP-4)

The DPP-4 activity was performed as previously described (*10*). In brief, mice were orally administrated with 5 x 10^{10} CFU / ml of *B. acidifaciens*, its supernatents, and fresh growth medium after fasting for 6 hours, and then additionally administrated glucose 30 minutes later. After 15 min, the intestinal epithelial cells of ileum were taken from pre-treated mice, and washed with PBS to remove luminal contents. The minced tissues were spun down by centrifugation (8,000 rpm, 4 ^{o}C, 5 min), and then 50 μl of the supernatant is incubated with kit reagents for 2 hours at 37 ^{o}C using DPP-4 Glo protease assay (Promega, Madison, WI). Relative DPP-4 activity was converted into a percentage based on the values of media group.

III-2-12. Comprehensive laboratory animal monitoring system (CLAMS)

Individually, eleven- to twelve-week-old *B. acidifaciens*-fed mice and controls placed in CLAMS (Columbus Instruments, Columbus, OH) cages and monitored over a 5-day period. The hourly file displays all measurements for each parameter: volume of oxygen consumed (VO_2; ml/kg/h), volume of carbon dioxide produced (VCO_2; ml/kg/h), respiratory exchange ratio, heat (kcal/h), activity (XY total-, XY ambulatory-, and Z activity). The data were recorded during the 30 seconds sampling period.

III-2-13. Capillary electrophoresis time-of-flight mass spectrometry (CE-TOFMS) measurement

A quantitative analysis of charged metabolites by CE-TOFMS was performed as described previously with slight modification (*11*). Briefly, 10 mg of freeze-dried fecal samples were disrupted using 3 mm zirconia/silica beads (BioSpec Products, Bartlesville, OK) and homogenized with 400 µl MeOH containing 20 µM each of methionine sulfone (Wako, Osaka, Japan) for cations, MES (Dojindo, Kumamoto, Japan) and CSA (D-Camphol-10-sulfonic acid, Wako, Osaka, Japan) for anions as internal standards. Then, 200 µl of de-ionized water and 500 µl of chloroform were added. After

vigorous shaking using Shakemaster neo (Bio Medical Science, Tokyo, Japan) at 1,500 r.p.m. for 10 min, the solution was centrifuged at 4,600 so*g* for 15 min at 4 lution was centrifuged at 4 roductsads [BioSpec Profiltered through a Millipore 5,000 Da cutoff filter (Millipore, Billerica, MA)] to remove proteins. The filtrate was lyophilized and dissolved in 25 µl of water containing 200 µM each of 3-aminopyrrolidine (Sigma Aldrich, St. Louis, MO) and trimesate (Wako, Osaka, Japan) as reference compounds. All CE-TOFMS experiments were performed using an Agilent CE capillary electrophoresis system (Agilent Technologies, Santa Clara, CA), an Agilent G3250AA LC/ MSD TOF system, an Agilent 1100 series binary HPLC pump, and the G1603A Agilent CE-MS adapter and G1607A Agilent CE-ESI-MS sprayer kit. To identify peak annotation and quantification, the obtained data were processed using in-house software (MasterHands) (*12*).

III-2-14. Statistics

GraphPad Prism software (GraphPad, La Jolla, CA) was used for statistical analysis. Significant differences between two groups were analyzed with two-tailed paired *t*-test or Mann-Whitney *t*-test. Multiple groups were analyzed by two-way ANOVA followed by Bonferroni *post-hoc* test (*, $P < 0.05$; **, $P < 0.01$; ***, $P < 0.001$).

III-3. Results

III-3-1. The scheme of oral administration with *B. acidifaciens.*

To clarify whether expanded *B. acidifaciens* can regulate lipid metabolisms, I obtained *B. acidifaciens* from RIKEN (JCM10556), cultured for large volume, and fed to na μe B6 mice. In order to determine optimal condition for administration, quantification of *B. acidifaciens* were examined in colon tissue and feces of mice fed with *B. acidifaciens* (5 ∃ 10^{10} CFU/ml) using *FISH* analysis. The numerous *B. acidifaciens* were detected in lumen and tip of colon epithelium cells at 1 day following oral administration (Fig. 1A) and disappeared thereafter (data not shown). In addition, *B. acidifaciens* were recovered in feces at peak of 2 days after oral feeding, and rapidly disappeared (Fig. 1B). Therefore, I concluded the scheme of oral administration with *B. acidifaciens* (5 ∃ 10^{10} CFU/ml, everyday)

A.

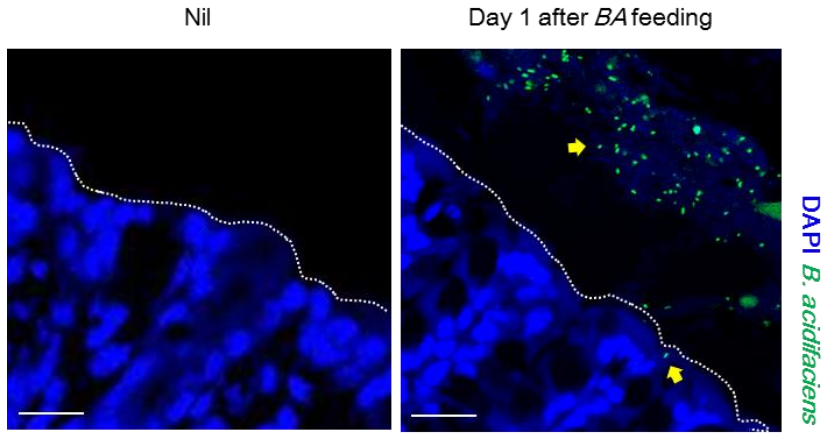
Nil
Day 1 after *BA* feeding
DAPI *B. acidifaciens*

B.

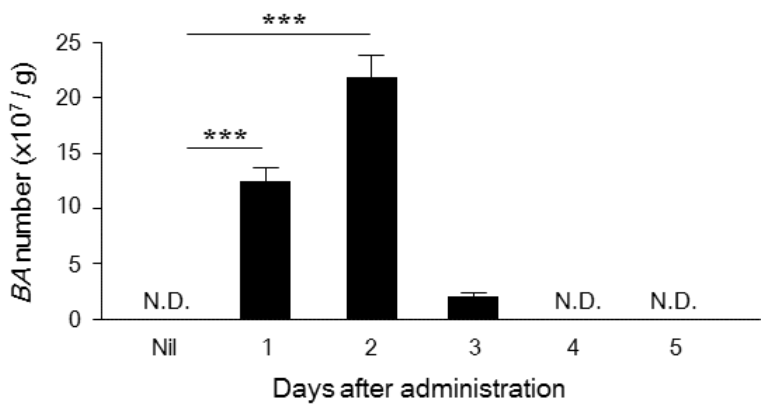
***
***
25
20
15
10
5
0
BA number (x10^7 / g)
N.D.
N.D.
N.D.
Nil
1
2
3
4
5
Days after administration

Figure 3.1. Confocal images of *B. acidifaciens* in colon and feces.

B. acidifaciens (*BA*) can temporarily reside in colon. Colon tissue and feces were obtained at nil, 1, 2, 3, 4, and 5 days after oral administration of *B. acidifaciens* (5 x 10^{10} CFU/ml), and then stained with *B. acidifaciens*-specific *FISH* probes. **(A).** Representative confocal images of *B. acidifaciens* (yellow arrow). **(B).** Quantification of *B. acidifaciens* in fecal extract at indicated time point. Numbers of *B. acidifaciens* were counted at least 20 regions per slide. Data are mean ± s.e.m. of three independent experiments. Statistical analyses were done with two-way ANOVA with Bonferroni *post-hoc* test. ***P<0.001. N.D., not detected.

III-3-2. Oral administration of *B. acidifaciens* leads to lean phenotypes in NCD- or HFD-fed B6 mice.

Wild-type B6 mice fed with *B. acidifaciens* for 10 weeks were shown reduced body weight and fat mass while similar levels of food intake between groups fed normal-chow diet (NCD) or high-fat diet (HFD) were detected (Fig. 2A-C). In contrast, *B. sartorri*-fed mice used as control anaerobic strain were not shown any loss of body weight (Fig. 2D). In addition, the size of a single adipocyte in epididymal adipose tissues taken from *B. acidifaciens*- and HFD-fed B6 mice was significantly smaller than that of PBS-fed HFD-fed mice (Fig. 2E). Collectively, long-term administration with *B. acidifaciens* promotes energy expenditure and consequently causes dominant lean phenotypes in diet-induced obesity mice.

A.

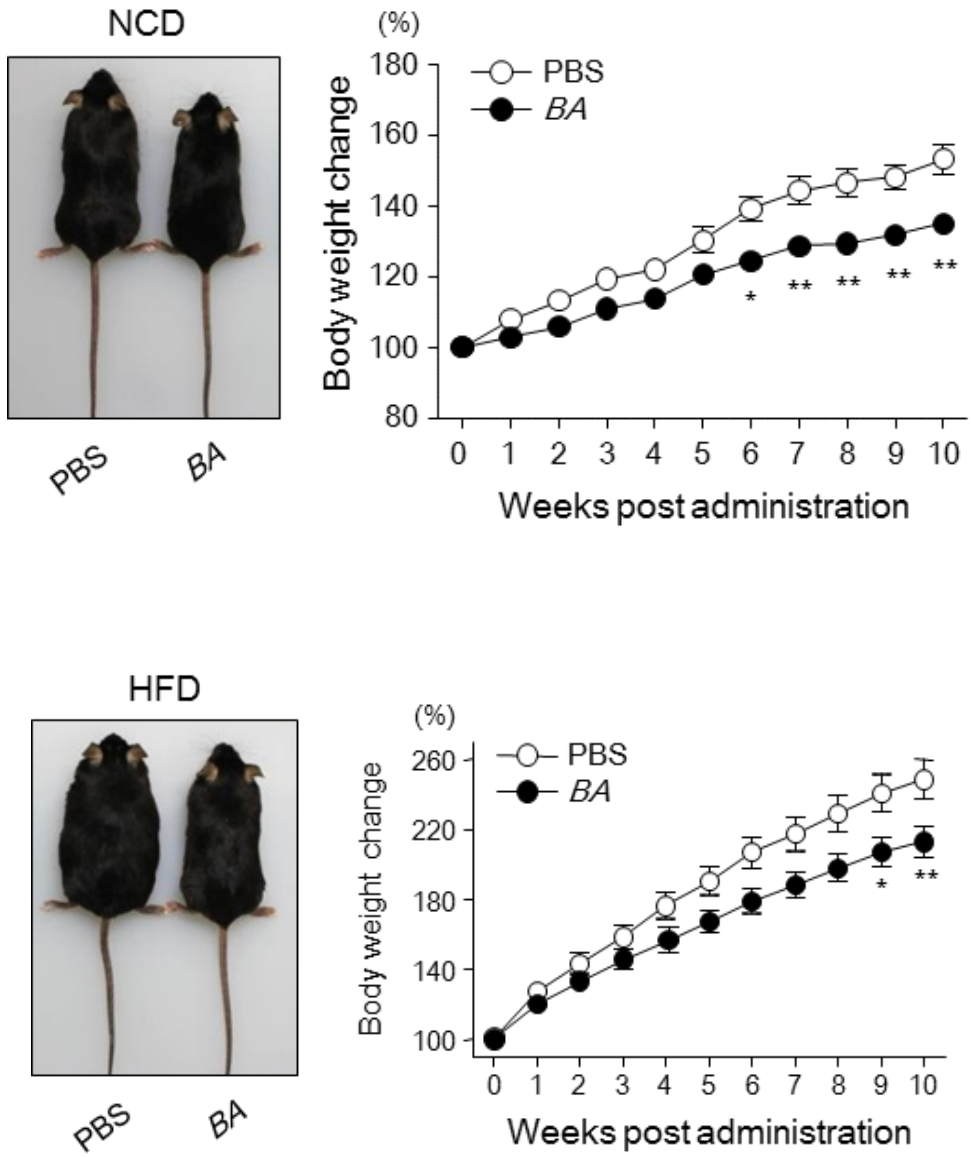
NCD
PBS
BA
(%)
Body weight change
PBS
BA
Weeks post administration
HFD
PBS
BA
(%)
Body weight change
PBS
BA
Weeks post administration

B.

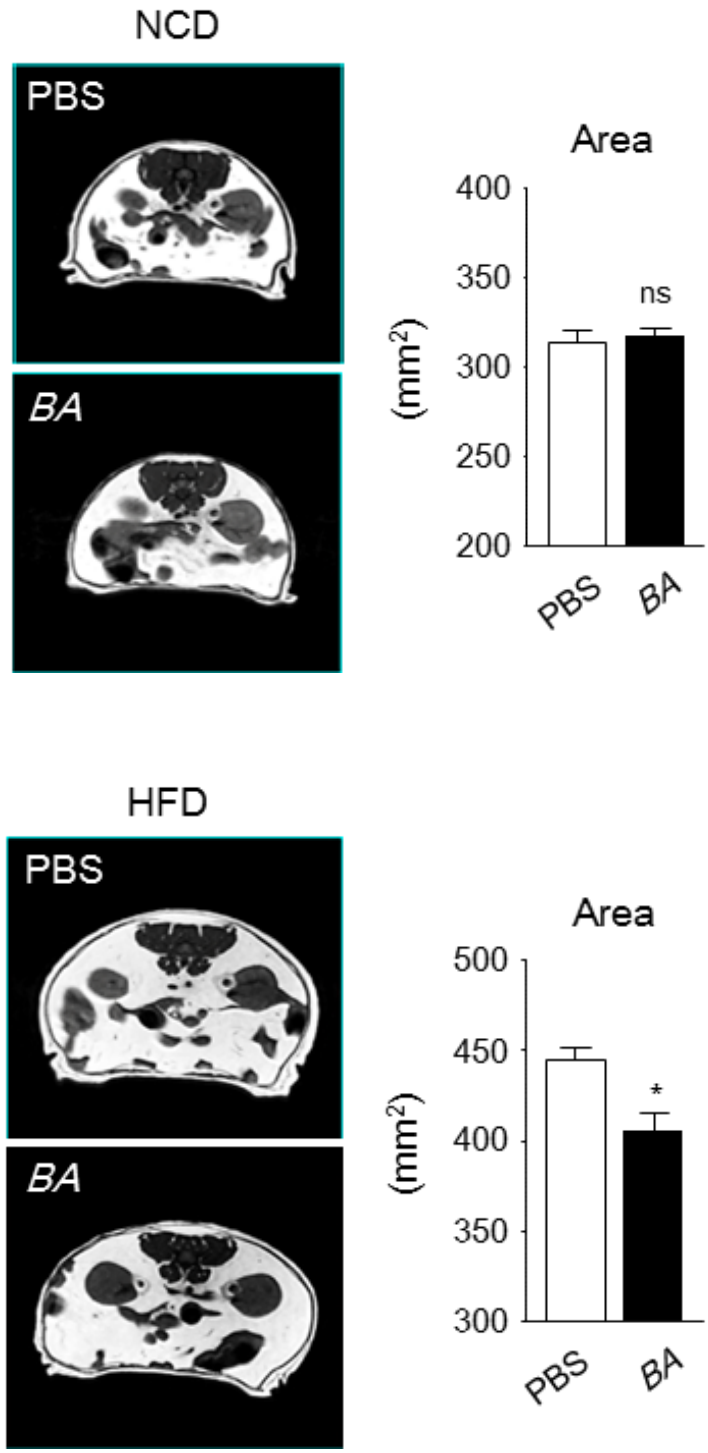
NCD
PBS
BA
Area
400
350
300
250
200
(mm²)
ns
PBS
BA
HFD
PBS
BA
Area
500
450
400
350
300
(mm²)
*
PBS
BA

C.

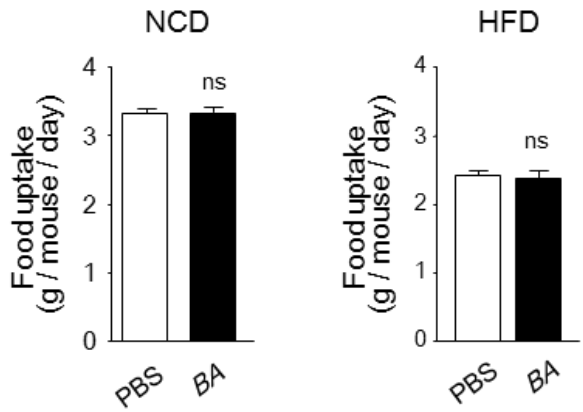
NCD
HFD
Food uptake
(g / mouse / day)
4
3
2
1
0
ns
ns
PBS
BA
PBS
BA

D.

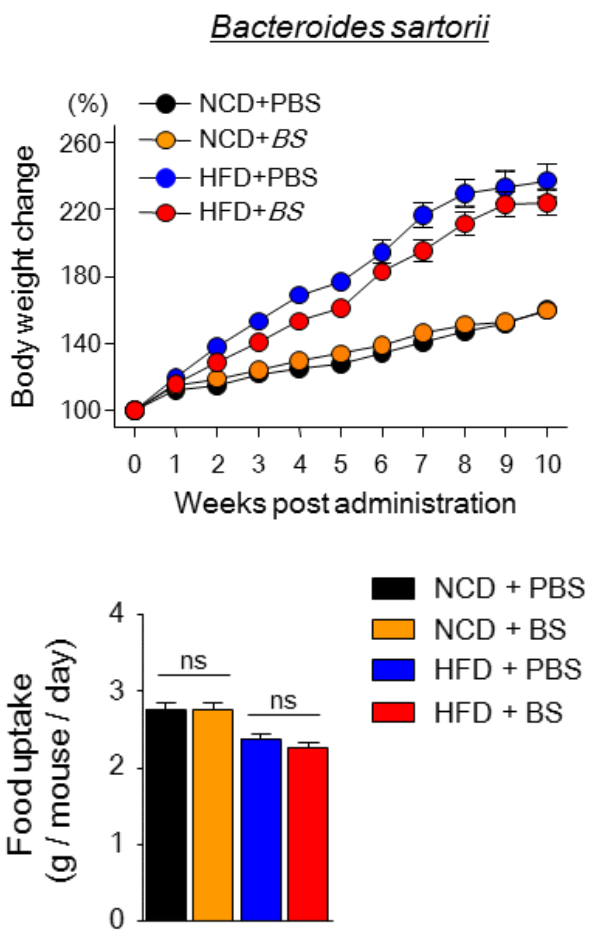
Bacteroides sartorii
(%)
NCD+PBS
NCD+BS
HFD+PBS
HFD+BS
Body weight change
260
220
180
140
100
0 1 2 3 4 5 6 7 8 9 10
Weeks post administration
NCD + PBS
NCD + BS
HFD + PBS
HFD + BS
Food uptake
(g / mouse / day)
4
3
2
1
0
ns
ns

E.

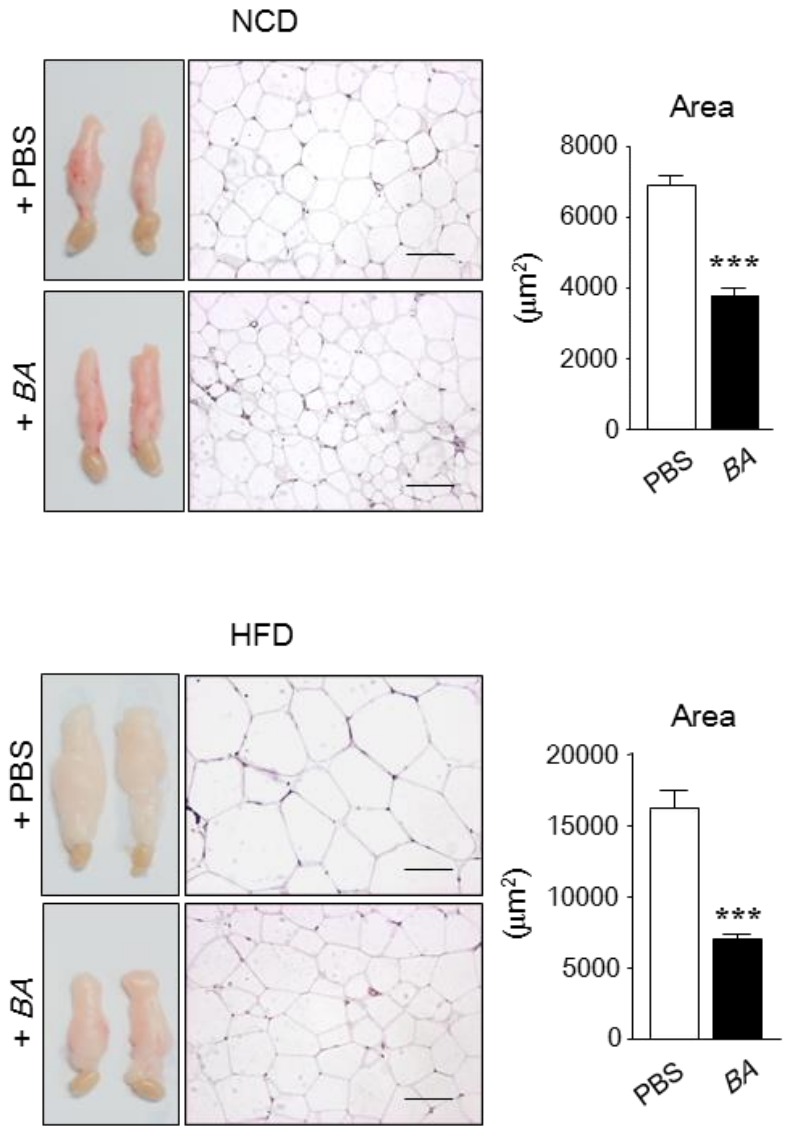
NCD
+ PBS
+ BA
Area
8000
6000
4000
2000
0
(μm²)
***
PBS
BA
HFD
+ PBS
+ BA
Area
20000
15000
10000
5000
0
(μm²)
***
PBS
BA

Figure 3.2. Representative photos, magnetic resonance imaging (MRI) analysis, and body / fat weight, and histologic analysis of adipose tissues. Effective functions of *B. acidifaciens* (BA) to regulate body weight and fat mass in diet-induced obesity mice. **(A).** Representative photos of PBS- and *B. acidifaciens*-fed B6 mice (left panel) and the body weight of each group was monitored for 10 weeks (right panel) during NCD (upper) and HFD (bottom). *B. acidifaciens* were orally administered ($5x10^{10}$ CFU/ml) everyday. **(B).** MRI analysis was examined with PBS- and *B. acidifaciens*-fed B6 mice. **(C).** Food intakes were checked everyday during *B. acidifaciens* feeding period. **(D**; upper panel**).** Monitoring of body weight for 10 weeks following oral administration of *B. sartorii* (5×10^{10} CFU/ml, everyday). **(D**; bottom panel**).** The food intakes were checked during oral feeding with PBS or *B. sartorii.* **(E).** Histological changes of adipose tissues (left panel) and size of adipocytes (right panel) of PBS- and *B. acidifaciens*-fed B6 mice. Scale bars = 50 ㎛. All data are presented as mean ± s.e.m. Statistical analyses were done with two-tailed paired *t*-test (**B, C**, and **E**) and two-way ANOVA with Bonferroni *post-hoc* test (**A** and **D**). *P<0.05, **P<0.01 and ***P<0.001. ns, not significant.

III-3-3. Increased insulin levels in serum and energy expenditure were detected in *B. acidifaciens*-fed B6 mice.

Of note, *B. acidifaciens*- and HFD-fed B6 mice were shown higher levels of insulin and lower levels of glucose than PBS- and HFD-fed B6 mice (Fig. 3A). Additionally, insulin resistance as determined by GTT and ITT was significantly improved in *B. acidifaciens*- and HFD-fed mice as compared to PBS- and HFD-fed mice (Fig. 3B). To further assess the energy expenditure, activity and substrate utilization, I next monitored mice fed with *B. acidifaciens* following individually housing in comprehensive laboratory animal monitoring system (CLAMS) cages for 5 days. Although groups of mice fed PBS or *B. acidifaciens* exhibited similar locomotor activity and respiratory exchange ratio (RER), HFD-B6 mice fed with *B. acidifaciens* revealed increased energy expenditure as compared to those mice fed PBS (Fig. 3C-E). Similar effects of oral *B. acidifaciens* were determined in the NCD-fed mice except energy expenditure (Fig. 3A-E). Collectively, long-term administration with *B. acidifaciens* promotes energy expenditure and consequently causes dominant lean phenotypes in diet-induced obesity mice.

A.

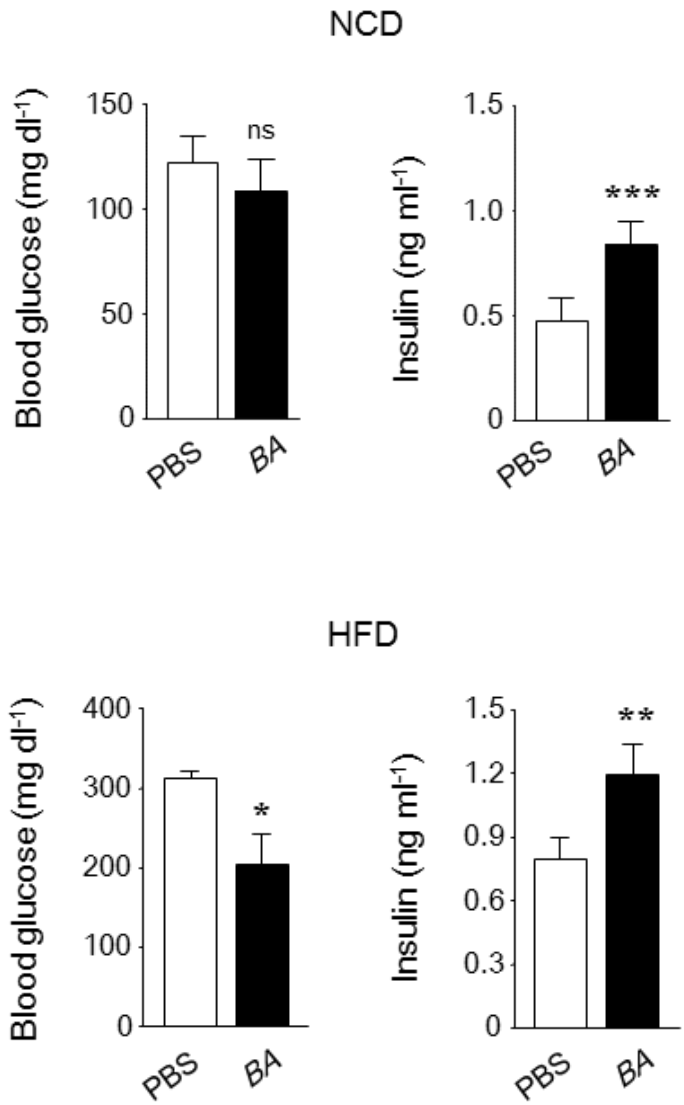
NCD
Blood glucose (mg dl-1)
150
100
50
0
ns
PBS
BA
Insulin (ng ml-1)
1.5
1.0
0.5
0
***
PBS
BA
HFD
Blood glucose (mg dl-1)
400
300
200
100
0
*
PBS
BA
Insulin (ng ml-1)
1.5
1.2
0.9
0.6
0.3
0
**
PBS
BA

B.

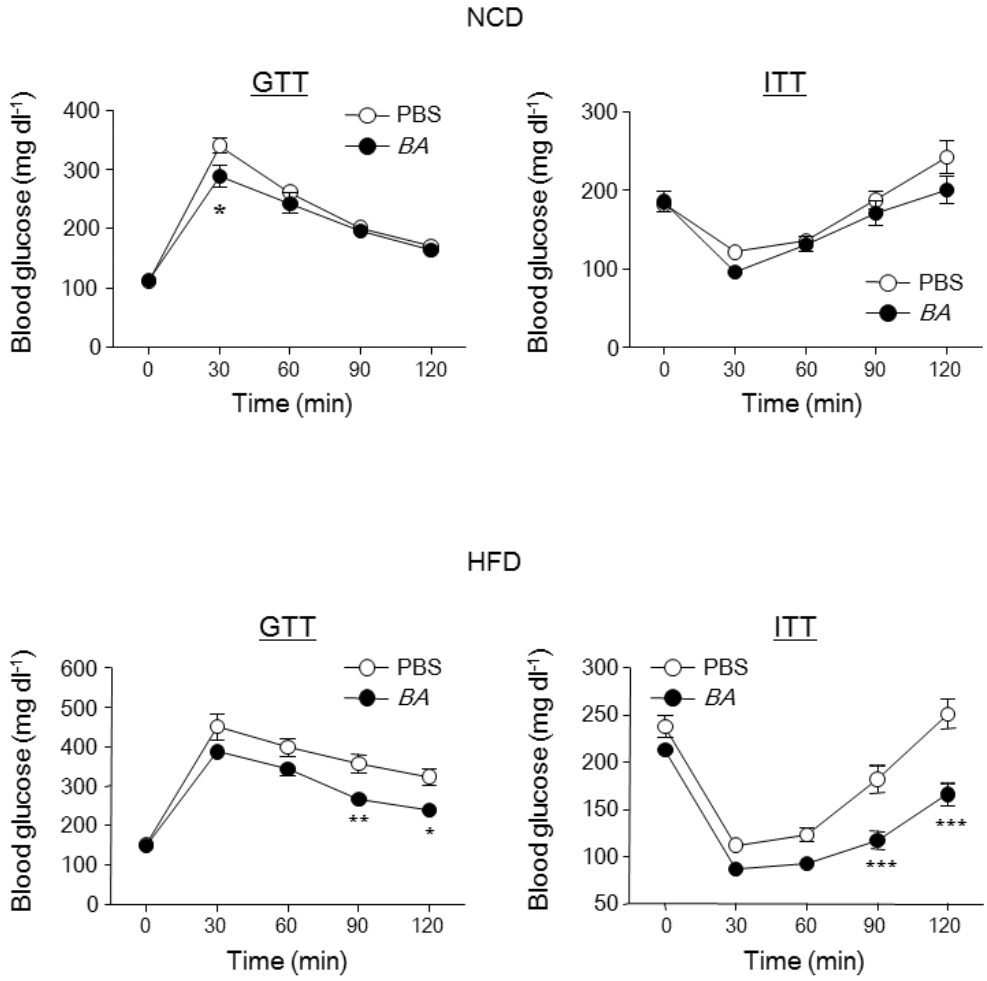
NCD
GTT
ITT
PBS
BA
Blood glucose (mg dl-1)
Time (min)
0
30
60
90
120
HFD
*
**
***

C.

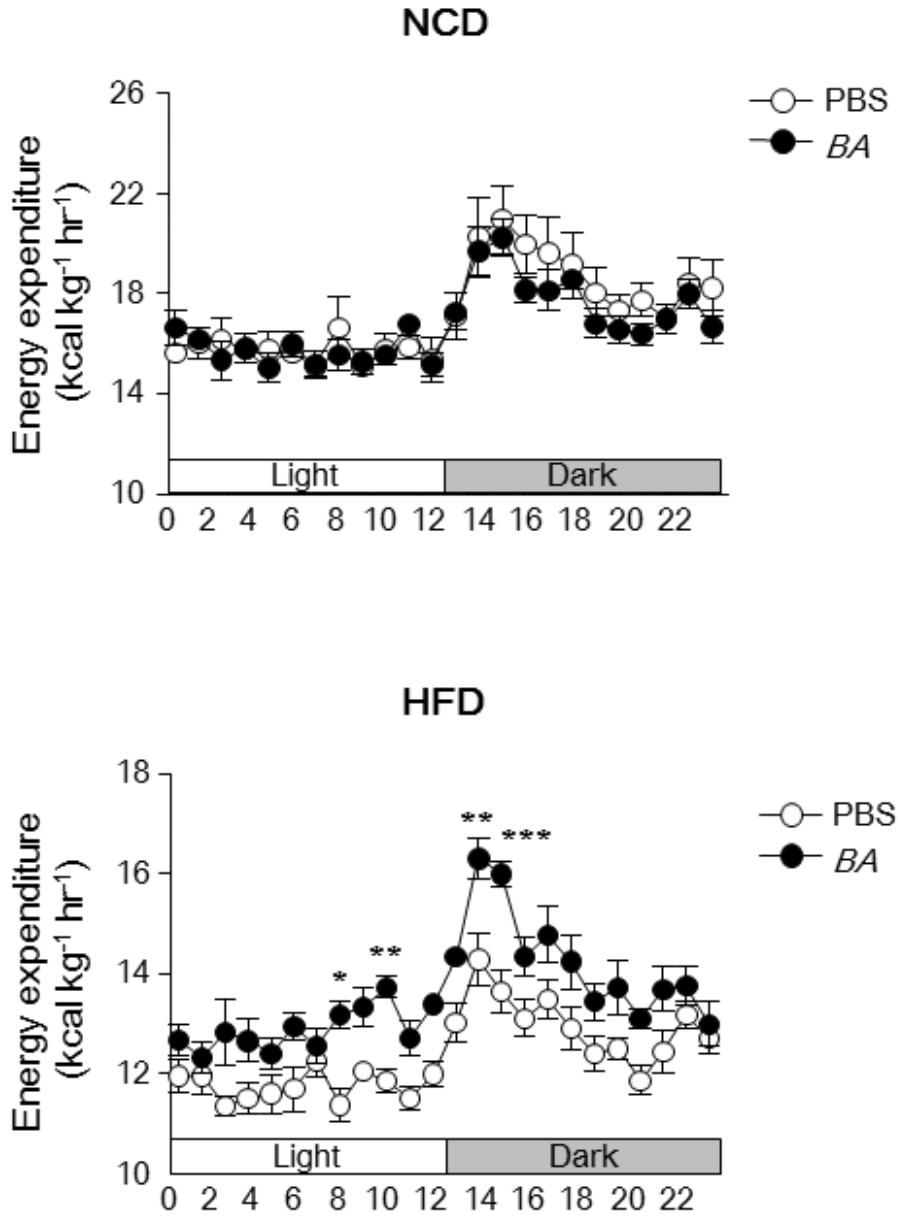
NCD
Energy expenditure (kcal kg-1 hr-1)
PBS
BA
Light
Dark
HFD
Energy expenditure (kcal kg-1 hr-1)
PBS
BA
Light
Dark
*
**
**
***

D.

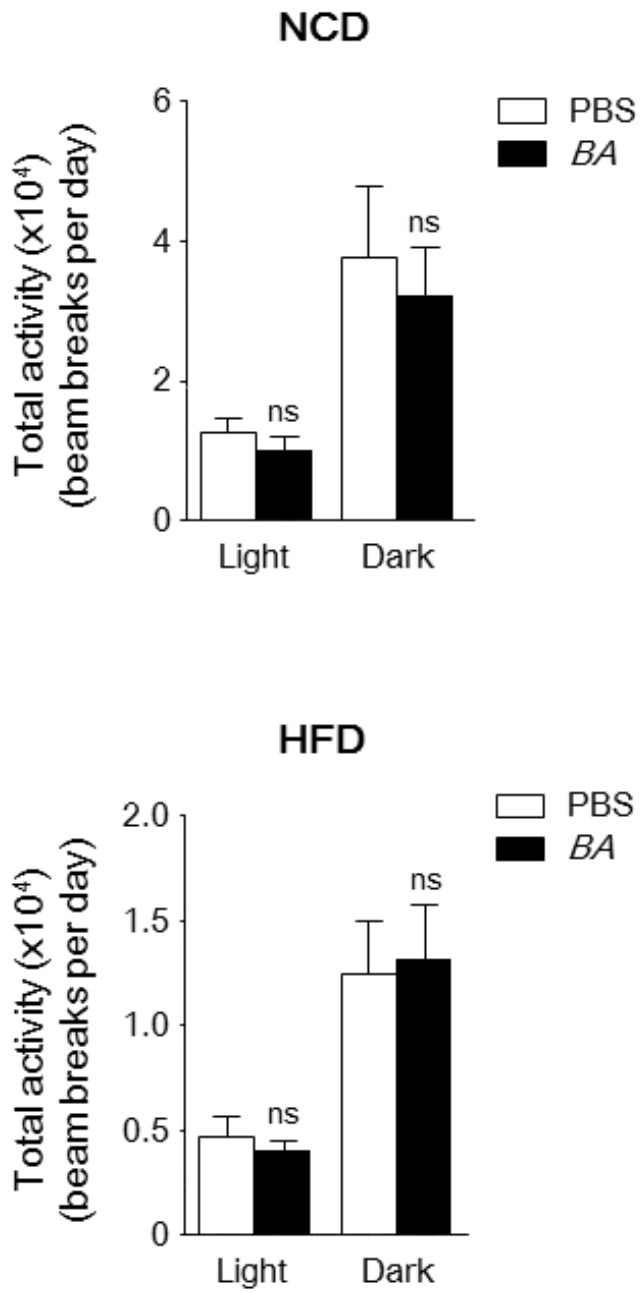
NCD
Total activity (x10⁴)
(beam breaks per day)
6
4
2
0
PBS
BA
ns
ns
Light
Dark
HFD
Total activity (x10⁴)
(beam breaks per day)
2.0
1.5
1.0
0.5
0
PBS
BA
ns
ns
Light
Dark

E.

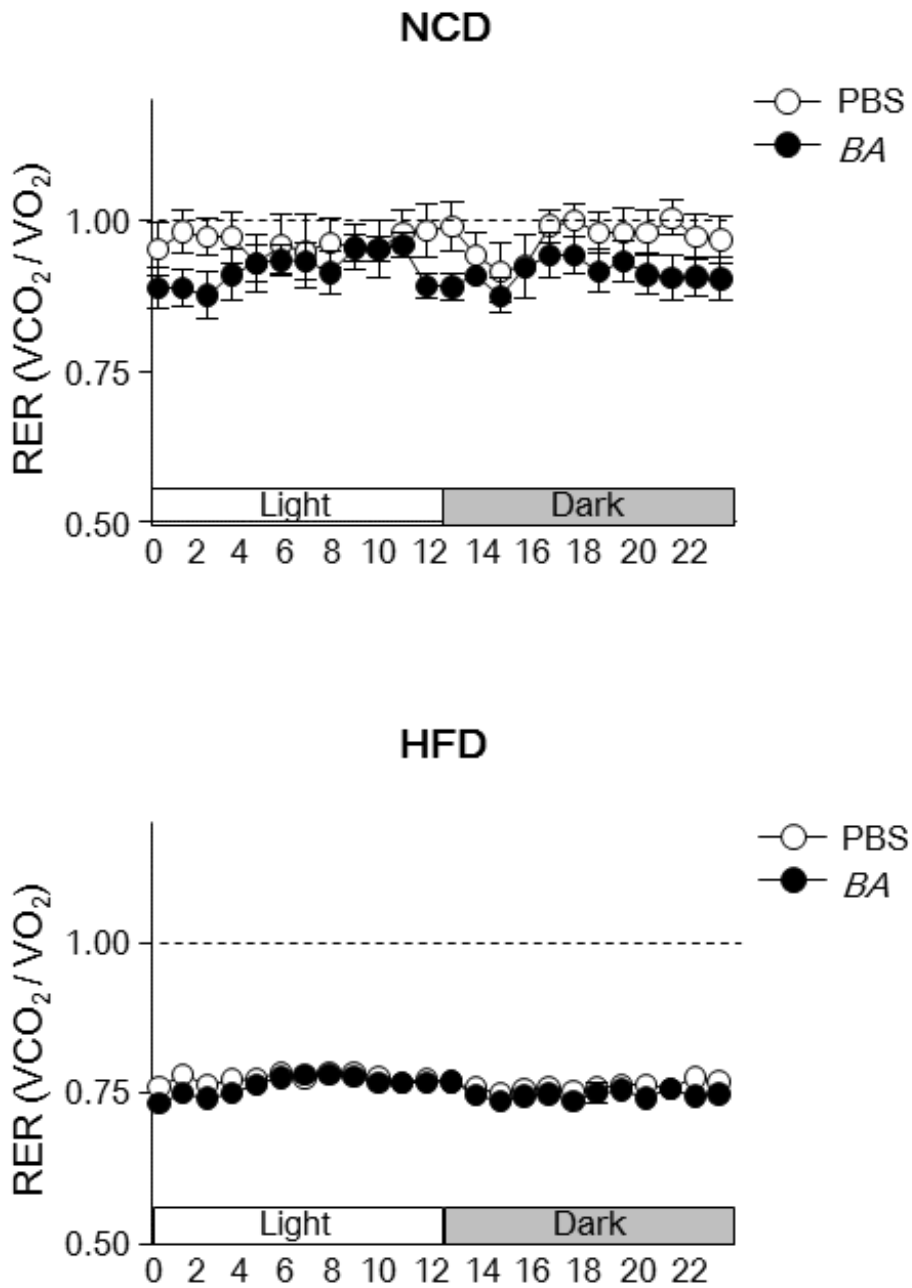
NCD
PBS
BA
RER (VCO2 / VO2)
1.00
0.75
0.50
Light
Dark
0 2 4 6 8 10 12 14 16 18 20 22
HFD
PBS
BA
RER (VCO2 / VO2)
1.00
0.75
0.50
Light
Dark
0 2 4 6 8 10 12 14 16 18 20 22

Figure 3.3. Glucose / insulin levels, GTT / ITT analysis, and comprehensive laboratory animal monitoring system (CLAMS) analysis.

(A). Levels of glucose and insulin in serum of PBS- and *B. acidifaciens*-fed B6 mice for 10 weeks everyday (n = 5). **(B).** GTT (left panel, n = 8-9) and ITT (right panel, n = 7-12) were analyzed using serum of PBS- and *B. acidifaciens*-fed B6 mice at the indicated time point after i.p. injection of glucose or insulin, respectively. **(C).** Energy expenditure of *B. acidifaciens*-administered B6 mice (n = 6). **(D).** Total activity in *B. acidifaciens*-administered B6 mice (n = 4). **(E).** RER of *B. acidifaciens*-administered B6 mice (n = 6). All data are presented as mean Õ s.e.m. Statistical analyses were done with two-tailed paired *t*-test **(A)** and with two-way ANOVA with Bonferroni *post-hoc* test. *P<0.05, **P<0.01 and ***P<0.001. ns, not significant.

III-3-4. Mice having lean phenotypes exhibited enhanced peroxisome proliferator activated receptor (PPAR) Ŭ expression in their adipose tissues.

Because decreased body weight and fat mass were previously detected in *Atg7*$^{\Delta CD11c}$, FMT B6, and *B. acidifaciens*-fed B6 mice, I further analyzed gene expression levels related with lipid metabolisms in adipose tissue, liver, and small intestine. Of note, gene expressions related to lipid ß-oxidation, especially PPARŬ was significantly enhanced only in WAT (abdominal and subcutaneous) of *Atg7*$^{\Delta CD11c}$ mice as compared to *Atg7*$^{f/f}$ mice (Fig. 4A). No significant changes of this gene were seen in small intestine and liver (Fig. 4D-E). Consistent with these results, expression of PPARŬ was significantly upregulated in WAT (epididymal) of B6 mice transferred with fecal extracts of *Atg7*$^{\Delta CD11c}$ mice or fed with HFD and *B. acidifaciens* (Fig. 4B-C). Of interest, mRNA levels of PPARŬ in WAT of B6 mice were significantly enhanced 2 weeks after *B. acidifaciens* administration (Fig. 4F). We also assessed the expression levels of TGR5, a G-protein-coupled bile acid receptor that can stimulate energy expenditure through PPARŬ activation (*13, 14*). We found elevated TGR5 expression levels in adipose tissues following *B. acidifaciens* administration (Fig. 4G). These results suggest that lean phenotypes mediated by *B. acidifaciens*

might begin with lipid oxidation in adipose tissue through TGR5-PPARŭ activation.

A.

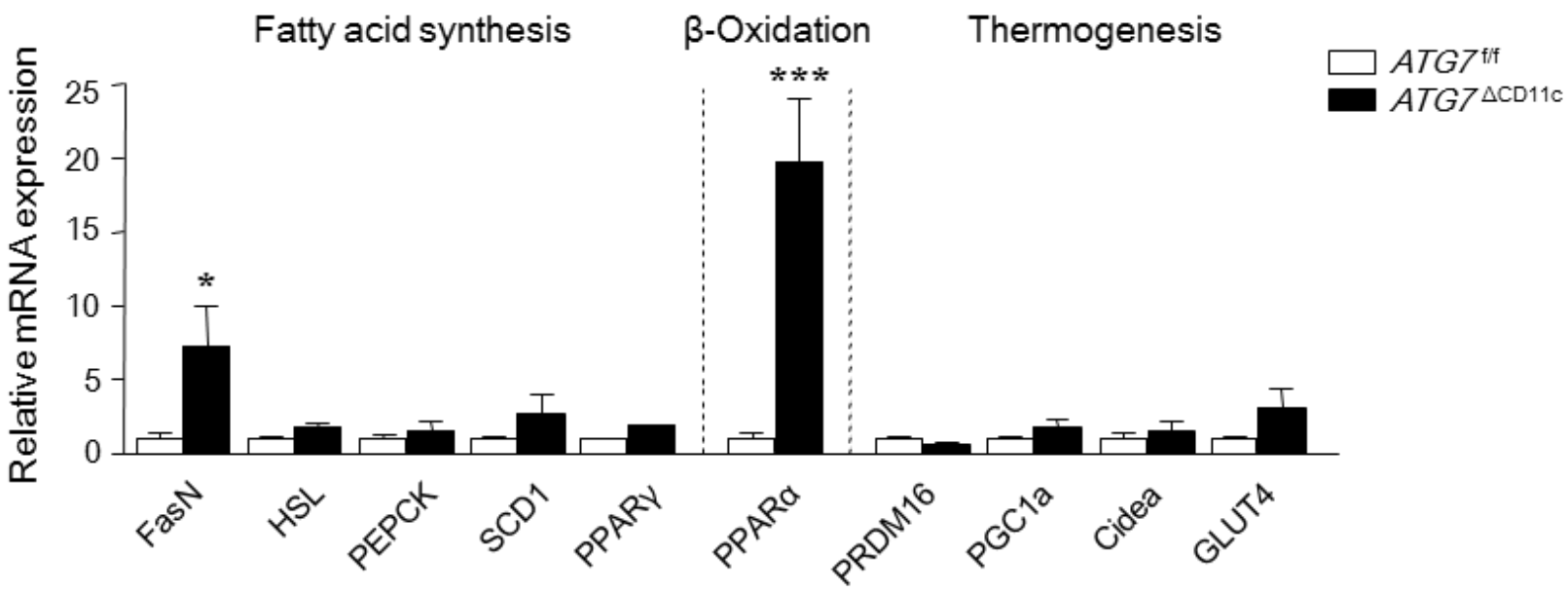
Fatty acid synthesis
β-Oxidation
Thermogenesis
ATG7 f/f
ATG7 ΔCD11c
Relative mRNA expression
25
20
15
10
5
0
*
***
FasN
HSL
PEPCK
SCD1
PPARγ
PPARα
PRDM16
PGC1a
Cidea
GLUT4

B.

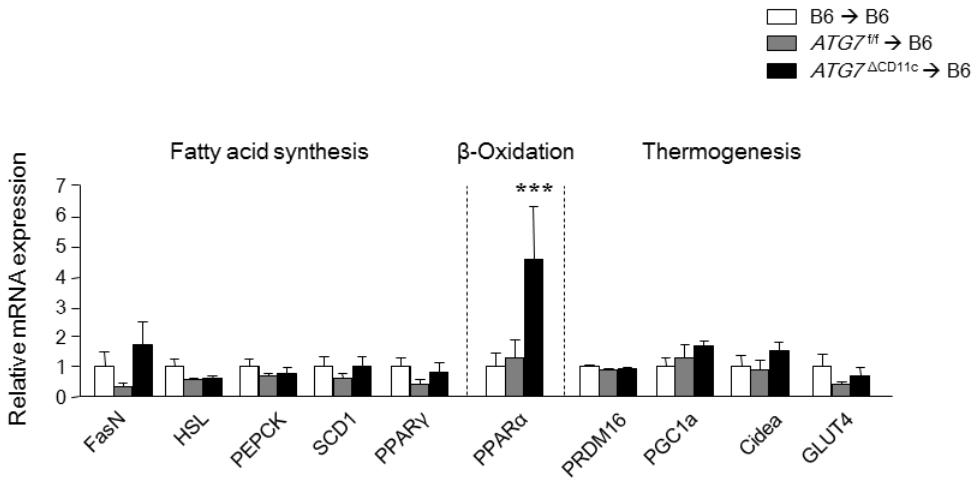
B6 → B6
ATG7f/f → B6
ATG7ΔCD11c → B6
Fatty acid synthesis
β-Oxidation
Thermogenesis
Relative mRNA expression
***
FasN
HSL
PEPCK
SCD1
PPARγ
PPARα
PRDM16
PGC1a
Cidea
GLUT4

C.

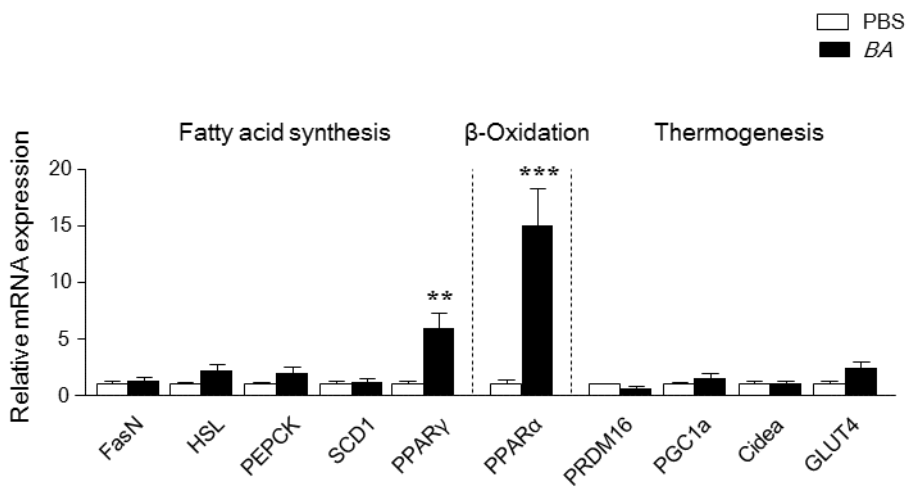
PBS
BA
Fatty acid synthesis
β-Oxidation
Thermogenesis
Relative mRNA expression
**
***
FasN
HSL
PEPCK
SCD1
PPARγ
PPARα
PRDM16
PGC1a
Cidea
GLUT4

D.

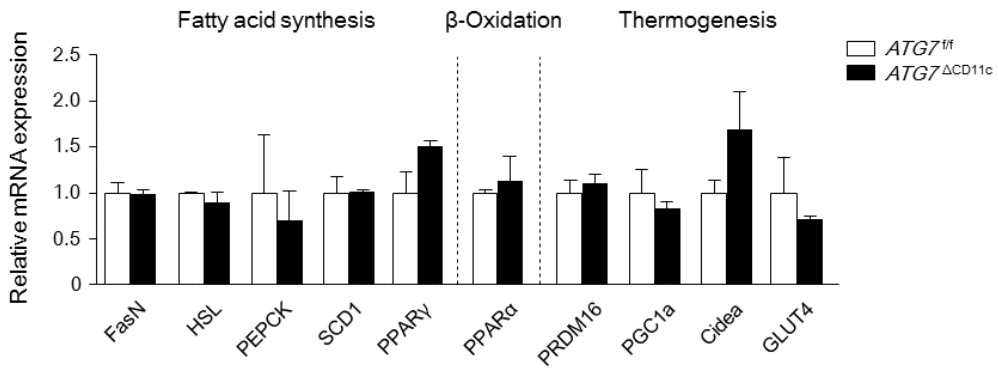
Fatty acid synthesis
β-Oxidation
Thermogenesis
Relative mRNA expression
2.5
2.0
1.5
1.0
0.5
0
ATG7 f/f
ATG7 ΔCD11c
FasN
HSL
PEPCK
SCD1
PPARγ
PPARα
PRDM16
PGC1a
Cidea
GLUT4

E.

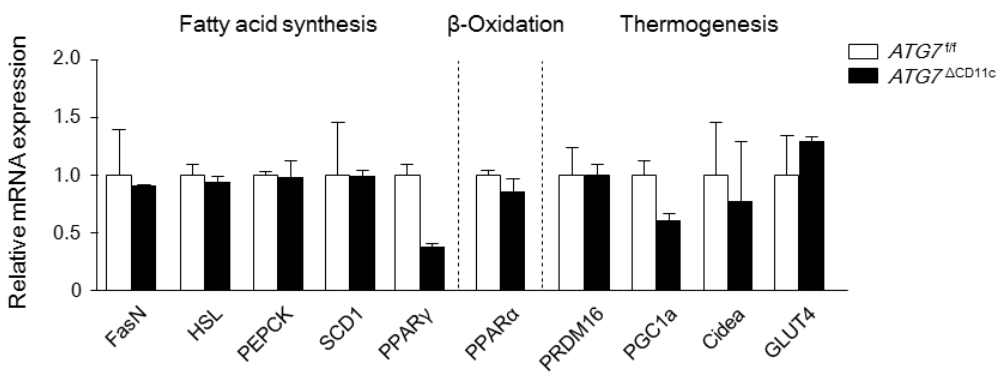
Fatty acid synthesis
β-Oxidation
Thermogenesis
Relative mRNA expression
2.0
1.5
1.0
0.5
0
ATG7 f/f
ATG7 ΔCD11c
FasN
HSL
PEPCK
SCD1
PPARγ
PPARα
PRDM16
PGC1a
Cidea
GLUT4

F.

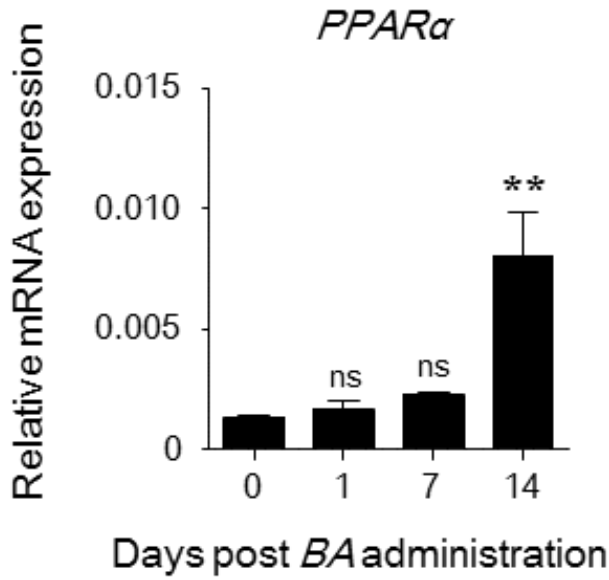
PPARα
Relative mRNA expression
0.015
0.010
0.005
0
ns
ns
**
0
1
7
14
Days post BA administration

G

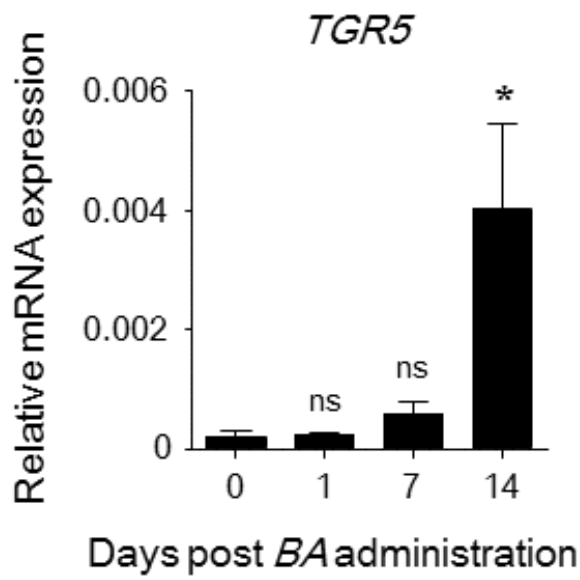
TGR5
Relative mRNA expression
0.006
0.004
0.002
0
ns
ns
*
0
1
7
14
Days post BA administration

Figure 3.4. mRNA expression levels of fatty acid synthesis, ß-oxidation , and thermogenesis by RT-PCR.

B. acidifaciens (*BA*) promotes fat oxidation in the adipose tissues through PPARŬactivation. Expression level of mRNA genes related with fatty acid synthesis (FasN, HSL, PEPCK, SCD1, and PPARɔ), ß-oxidation (PPARŬ), and thermogenesis (PRDM16, PGC1a, Cidea, and GLUT4) were determined by real-time PCR using adipose tissues taken from *Atg7*$^{f/f}$ and *Atg7*^{qCD11c} mice (**A**), fecal microbiota transplanted mice (**B**), and *B. acidifaciens*-fed mice (**C**) at the end point of each experiments. The mRNA expression of equal candidates as above was measured in liver **(D)** and intestine **(E)**. Expression levels of PPARŬ**(F)** and TGR5 **(G)** in adipose tissue were analyzed by RT-PCR 1, 7, and 14 days after daily *BA* administration. All data are mean Õ s.e.m of ×2 independent experiments. Statistical analyses were done with two-way ANOVA with Bonferroni *post-hoc* test **(A-E)** and with Mann-Whitney *t*-test **(F** and **G)**. *P < 0.05, **P < 0.01, ***P<0.001; ns, not significant.

III-3-5. *B. acidifaciens* modulates GLP-1 production by regulating DPP-4 enzyme in small intestine.

In order to investigate the underlying mechanism of high levels of insulin secretion in *B. acidifaciens*-fed lean mice, I next studied the glucagon-like protein-1 (GLP-1) levels that could stimulate insulin release to blood (*15*). The GLP-1 levels in serum were dramatically enhanced following administration of *B. acidifaciens* in NCD- and HFD-fed mice (Fig. 5A). Of note, the levels of dipeptidyl peptidase-4 (DPP-4), a well-known enzyme responsible for the degradation of GLP-1 (*16*), was decreased in the small intestine ileum after oral administration of *B. acidifaciens* or culture supernatants (Fig. 5B). Previous studies suggested that bile acids play a pivotal role in glucose homeostasis by stimulating GLP-1 secretion through TGR5 activation (*17, 18*). I found significantly increased levels of cholate, salts of cholic acid (CA), and taurine deconjugated from primary bile acid in feces of B6 mice fed with *B. acidifaciens* for 10 weeks but no significant loss of cholesterol (Fig. 5C-D). These results indicate that *B. acidifaciens* and/or their metabolites may reduce DPP-4 enzyme activity and subsequently result in GLP-1 activation, improving insulin sensitivity and glucose tolerance.

A.

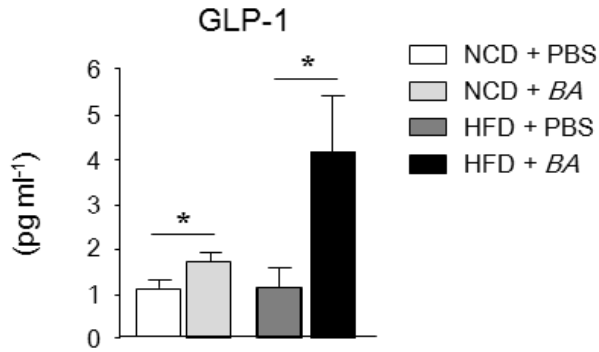
GLP-1
(pg ml-1)
0
1
2
3
4
5
6
*
*
NCD + PBS
NCD + BA
HFD + PBS
HFD + BA

B.

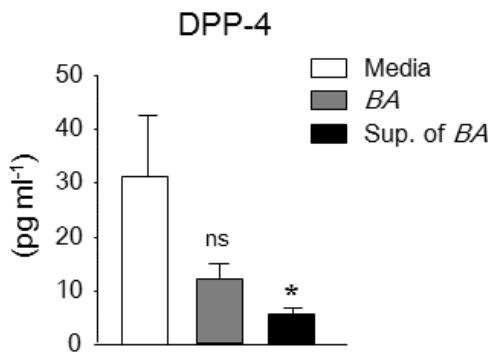
DPP-4
(pg ml-1)
0
10
20
30
40
50
ns
*
Media
BA
Sup. of BA

C.

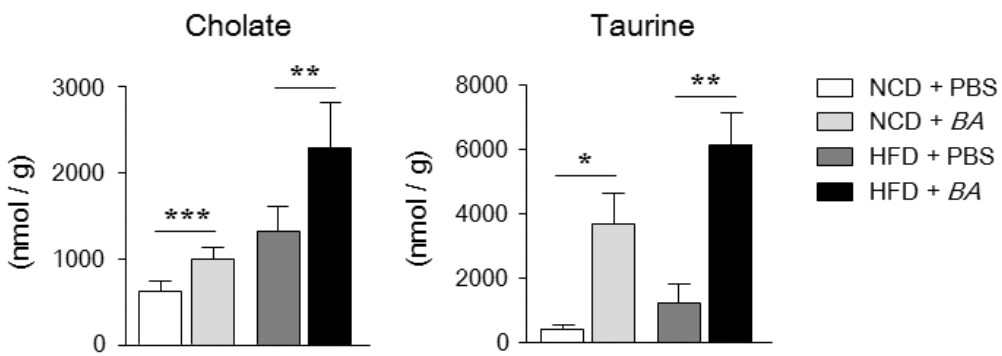
Cholate
(nmol / g)
0
1000
2000
3000
***
**
Taurine
(nmol / g)
0
2000
4000
6000
8000
*
**
NCD + PBS
NCD + BA
HFD + PBS
HFD + BA

D.

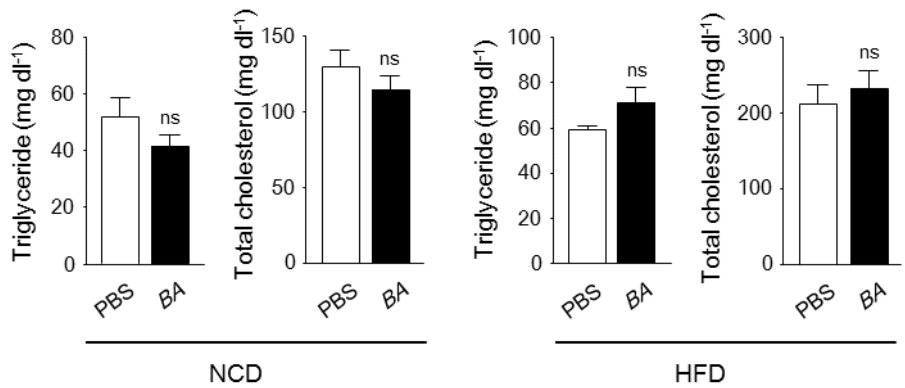

Figure 3.5. *B. acidifaciens* (BA) can regulate intestinal dipeptidal peptidase-4 (DPP-4) secretion and subsequently induce glucagon-like peptide 1 (GLP-1) production in B6 mice.

Active GLP-1 **(A)** in serum of PBS- and BA-fed mice (normal chow diet, NCD; high-fat diet, HFD; n = 5). **(B).** At 1 hour after BA administration or supernatant of BA culture or medium alone into na μe B6 mice, DPP-4 levels in the small intestine were detected by luminescent assay. **(C).** Quantification of cholate and taurine in feces of PBS- and BA-fed mice (n = 5) by capillary electrophoresis-mass spectrometry. Concentrations of serum triglycerides and total cholesterol were analyzed using enzymatic assay kits in BA-fed mice **(D**; n = 5**)**. All data are mean Õ s.e.m of ×2 independent experiments. Statistical analyses were done with two-tailed paired *t*-test. *P < 0.05, **P < 0.01, ***P<0.001; ns, not significant.

III-4. Discussion

Bacteroides (B.) acidifaciens were firstly isolated from the caecum of mice by Itoh K. et al (*9, 19*). These novel commensal bacteria were characterized anaerobic, gram-negative, good growth in bile acid and aesculin hydrolysis. Thereafter, their function was revealed by other group that *B. acidifaciens* possessing capacity to increase IL-6 and IL-10 production by enhancing expression of MHC class II and the co-stimulating molecules (i.e., CD80 and CD86) on antigen-presenting cells (*20*). In addition, *B. acidifaciens* is one of predominant commensal bacteria which responsible for promoting IgA Abs production in the large intestine specifically by inducing activation-induced cytidine deaminase expression (*1, 21*). Here, I noted another unique function that *B. acidifaciens* can modulate energy metabolisms and therefore applicable for therapeutic use for obesity and diabetes control.

PPARŭ is a nuclear receptor contr

aspects of lipid metabolism (*22*). Previous studies have demonstrated that PPARŭ activation through its sight by gonists regulating satiety, and ameliorate obesity-derived inflammation in adipose tissue (*23, 24*) . Although -/- mice fed HAD showed several obesity

phenotypes in terms of body weight, fat mass and fat droplets (*25*), the two major mechanisms for PPARŭ to regulat for regulating fatty acids (FAs) cellular uptake or for stimulating FA oxidation (*26, 27*). In my studies, enhanced mRNA expression levels of PPARŭ were constantly detected only i *Atg7*$^{\varphi CD11c}$ mice, FMT mice, and *B. acidifaciens*-fed mice (Fig. 4), indicating that ß-oxidation through PPARŭ signali a mechanism for protection to obesity provoked by specific commensal bacteria *B. acidifaciens*.

The gastrointestinal tract is a locus of incretin hormone products such as glucagon-like peptide 1 (GLP-1) that stimulates insulin release and decreases blood glucose levels (*15*). The GLP-1 is inactivated by the enzyme dipeptidyl peptidase-4 (DPP-4) and thus DPP-4 inhibitor is a class of oral hypoglycemic (*16*). I found similar patterns of low glucose and high insulin levels in the serum of *Atg7*$^{\varphi CD11c}$ mice, FMT mice, and *B. acidifaciens*-fed mice (Fig. 3A, Fig. 5F of part II, and Fig. 3A). Notably, there are significantly decreased levels of DPP4 in ileum and increased levels of GLP-1 in the serum of *B. acidifaciens*-fed mice (Fig. 5A-B). It seems likely that unknown metabolites synthesized by *B. acidifaciens* or bacteria itself may directly interact with gut epithelial cells and inhibit DPP-

4 activation, and thereby increase circulating GLP-1.

In mice, cholic acid (CA), a primary bile acid, is secreted as a taurine-conjugated form from the gallbladder into the duodenum and then is deconjugated in the ileum by commensal bacteria (*28*). Recent studies have shown that the bile acid profiles in the small intestine, feces, and serum of conventionally raised mice is totally different from those of germ-free mice, suggesting that commensal bacteria can modulate gene expression levels related to bile acid synthesis, conjugation, and reabsorption (*7*). In the present study, significantly elevated levels of cholate and taurine were determined in feces (Fig. 5C) and their receptor TGR5 in adipose tissues (Fig. 4G) of B6 mice fed *B. acidifaciens*. Others have shown that administration of the TGR5 agonists CA and taurine result in significant improvement of body weight and fat mass in HFD-fed mice (*18, 29*). The authors suggest that the bile acid-TGR5-cAMP signaling pathways increase energy expenditure in adipose tissue and skeletal muscle. Thus, I propose that bile acids activated by *B. acidifaciens* serve as ligands for TGR5-mediated regulation of energy expenditure through PPAR Ŭactivation.

In summary, expansion of *B. acidifaciens* leads to increased insulin production and ɓoxidation, and finally to protect host from obesity. Although further studies are required to figure out the efficiency of *B.*

acidifaciens on diverse combination of genetic and environment factors, my finding suggest that a single commensal bacteria can be used as a potent ñprobioticsò for metabolic diseases su

III-5. References

1. **T. Yanagibashi, A. Hosono, A. Oyama, M. Tsuda, A. Suzuki, S. Hachimura, Y. Takahashi, Y. Momose, K. Itoh, K. Hirayama, K. Takahashi, S. Kaminogawa.** 2013. IgA production in the large intestine is modulated by a different mechanism than in the small intestine: *Bacteroides acidifaciens* promotes IgA production in the large intestine by inducing germinal center formation and increasing the number of IgA^+ B cells. *Immunobiology* 218, 645-651.
2. **A. Spor, O. Koren, R. Ley.** 2011. Unravelling the effects of the environment and host genotype on the gut microbiome. *Nature Reviews. Microbiology* 9, 279-290.
3. **P. G. Kopelman.** 2000. Obesity as a medical problem. *Nature* 404, 635-643.
4. **X. Zhang, G. Zhang, H. Zhang, M. Karin, H. Bai, D. Cai.** 2008. Hypothalamic IKKbeta/NF-kappaB and ER stress link overnutrition to energy imbalance and obesity. *Cell* 135, 61-73.
5. **J. Y. Chiang.** 2009. Bile acids: regulation of synthesis. *Journal of Lipid Research* 50, 1955-1966.
6. **D. W. Russell.** 2009. Fifty years of advances in bile acid synthesis and metabolism. *Journal of Lipid Research* 50 Suppl, S120-125.
7. **S. I. Sayin, A. Wahlstrom, J. Felin, S. Jantti, H. U. Marschall, K. Bamberg, B. Angelin, T. Hyotylainen, M. Oresic, F. Backhed.** 2013. Gut microbiota regulates bile acid metabolism by reducing the levels of tauro-beta-muricholic acid, a naturally occurring FXR antagonist. *Cell Metabolism* 17, 225-235.
8. **J. Y. Chiang.** 2013. Bile acid metabolism and signaling. *Comprehensive Physiology* 3, 1191-1212.
9. **Y. Momose, S. H. Park, Y. Miyamoto, K. Itoh.** 2011. Design of species-specific oligonucleotide probes for the detection of *Bacteroides* and *Parabacteroides* by fluorescence in situ hybridization and their application to the analysis of mouse caecal *Bacteroides-Parabacteroides* microbiota. *Journal of Applied Microbiology* 111, 176-184.
10. **A. Waget, C. Cabou, M. Masseboeuf, P. Cattan, M. Armanet, M. Karaca, J. Castel, C. Garret, G. Payros, A. Maida, T. Sulpice, J. J. Holst, D. J. Drucker, C. Magnan, R. Burcelin.** 2011. Physiological and pharmacological mechanisms through which the

DPP-4 inhibitor sitagliptin regulates glycemia in mice. *Endocrinology* 152, 3018-3029.

11. **E. Mishima, S. Fukuda, H. Shima, A. Hirayama, Y. Akiyama, Y. Takeuchi, N. N. Fukuda, T. Suzuki, C. Suzuki, A. Yuri, K. Kikuchi, Y. Tomioka, S. Ito, T. Soga, T. Abe.** 2014. Alteration of the intestinal environment by lubiprostone is associated with amelioration of adenine-induced CKD. *Journal of the American Society of Nephrology* 10, 1681/ASN.2014060530.
12. **M. Sugimoto, D. T. Wong, A. Hirayama, T. Soga, M. Tomita.** 2010. Capillary electrophoresis mass spectrometry-based saliva metabolomics identified oral, breast and pancreatic cancer-specific profiles. *Metabolomics* 6, 78-95.
13. **M. Watanabe, S. M. Houten, C. Mataki, M. A. Christoffolete, B. W. Kim, H. Sato, N. Messaddeq, J. W. Harney, O. Ezaki, T. Kodama, K. Schoonjans, A. C. Bianco, J. Auwerx.** 2006. Bile acids induce energy expenditure by promoting intracellular thyroid hormone activation. *Nature* 439, 484-489.
14. **V. Stepanov, K. Stankov, M. Mikov.** 2013. The bile acid membrane receptor TGR5: a novel pharmacological target in metabolic, inflammatory and neoplastic disorders. *Journal of Receptor and Signal Transduction Research* 33, 213-223.
15. **D. J. Drucker, M. A. Nauck.** 2006. The incretin system: glucagon-like peptide-1 receptor agonists and dipeptidyl peptidase-4 inhibitors in type 2 diabetes. *Lancet* 368, 1696-1705.
16. **B. Ahren, O. Schmitz.** 2004. GLP-1 receptor agonists and DPP-4 inhibitors in the treatment of type 2 diabetes. *Hormone and Metabolic Research* 36, 867-876.
17. **S. Katsuma, A. Hirasawa, G. Tsujimoto.** 2005. Bile acids promote glucagon-like peptide-1 secretion through TGR5 in a murine enteroendocrine cell line STC-1. *Biochemical and Biophysical Research Communications* 329, 386-390.
18. **H. Sato, C. Genet, A. Strehle, C. Thomas, A. Lobstein, A. Wagner, C. Mioskowski, J. Auwerx, R. Saladin.** 2007. Anti-hyperglycemic activity of a TGR5 agonist isolated from Olea europaea. *Biochemical and Biophysical Research Communications* 362, 793-798.
19. **Y. Miyamoto, K. Itoh.** 2000. *Bacteroides acidifaciens sp.* nov., isolated from the caecum of mice. *International Journal of Systematic and Evolutionary Microbiology* 50 Pt 1, 145-148.
20. **M. Tsuda, A. Hosono, T. Yanagibashi, S. Hachimura, K.**

Hirayama, K. Itoh, K. Takahashi, S. Kaminogawa. 2007. Prior stimulation of antigen-presenting cells with *Lactobacillus* regulates excessive antigen-specific cytokine responses in vitro when compared with *Bacteroides*. *Cytotechnology* 55, 89-101.

21. **T. Yanagibashi, A. Hosono, A. Oyama, M. Tsuda, S. Hachimura, Y. Takahashi, K. Itoh, K. Hirayama, K. Takahashi, S. Kaminogawa.** 2009. *Bacteroides* induce higher IgA production than *Lactobacillus* by increasing activation-induced cytidine deaminase expression in B cells in murine Peyer's patches. *Bioscience, Biotechnology, and Biochemistry* 73, 372-377.
22. **P. Lefebvre, G. Chinetti, J. C. Fruchart, B. Staels.** 2006. Sorting out the roles of PPAR alpha in energy metabolism and vascular homeostasis. *The Journal of Clinical Investigation* 116, 571-580.
23. **J. Fu, S. Gaetani, F. Oveisi, J. Lo Verme, A. Serrano, F. Rodriguez De Fonseca, A. Rosengarth, H. Luecke, B. Di Giacomo, G. Tarzia, D. Piomelli.** 2003. Oleylethanolamide regulates feeding and body weight through activation of the nuclear receptor PPAR-alpha. *Nature* 425, 90-93.
24. **A. Tsuchida, T. Yamauchi, S. Takekawa, Y. Hada, Y. Ito, T. Maki, T. Kadowaki.** 2005. Peroxisome proliferator-activated receptor (PPAR)alpha activation increases adiponectin receptors and reduces obesity-related inflammation in adipose tissue: comparison of activation of PPARalpha, PPARgamma, and their combination. *Diabetes* 54, 3358-3370.
25. **B. H. Kim, Y. S. Won, E. Y. Kim, M. Yoon, K. T. Nam, G. T. Oh, D. Y. Kim.** 2003. Phenotype of peroxisome proliferator-activated receptor-alpha(PPARalpha)deficient mice on mixed background fed high fat diet. *Journal of Veterinary Science* 4, 239-244.
26. **K. Motojima, P. Passilly, J. M. Peters, F. J. Gonzalez, N. Latruffe.** 1998. Expression of putative fatty acid transporter genes are regulated by peroxisome proliferator-activated receptor alpha and gamma activators in a tissue- and inducer-specific manner. *The Journal of Biological Chemistry* 273, 16710-16714.
27. **C. Ribet, E. Montastier, C. Valle, V. Bezaire, A. Mazzucotelli, A. Mairal, N. Viguerie, D. Langin.** 2010. Peroxisome proliferator-activated receptor-alpha control of lipid and glucose metabolism in human white adipocytes. *Endocrinology* 151, 123-133.
28. **J. M. Ridlon, D. J. Kang, P. B. Hylemon.** 2006. Bile salt biotransformations by human intestinal bacteria. *Journal of Lipid Research* 47, 241-259.

29. **N. Tsuboyama-Kasaoka, C. Shozawa, K. Sano, Y. Kamei, S. Kasaoka, Y. Hosokawa, O. Ezaki.** 2006. Taurine (2-aminoethanesulfonic acid) deficiency creates a vicious circle promoting obesity. *Endocrinology* 147, 3276-3284.

Chapter IV. Overall conclusion

IV-1. Gut commensal *Bacteroides acidifaciens* expanded in *Atg7*$^{\Delta CD11c}$ mice improves insulin sensitivity and prevents obesity

I found lean phenotypes (i.e., reduced body weight and fat mass) in aged conditional knock-out mice (*Atg7*$^{\Delta CD11c}$) with CD11c^{+} cells with specific deletion of autophagy-related gene 7 when compared with littermate control mice (*Atg7*$^{f/f}$). Interestingly, body weight and fat mass were compensated in both *Atg7*$^{f/f}$ and *Atg7*$^{\Delta CD11c}$ mice through co-housing or fecal extracts transplantation, indicating that lean phenotypes might be mediated by commensal bacteria of *Atg7*$^{\Delta CD11c}$ mice. By pyrosequencing analysis, I found that *Bacteroides acidifaciens* were significantly increased (>5%) in feces of *Atg7*$^{\Delta CD11c}$ mice compared with those of control *Atg7*$^{f/f}$ mice. Taken together, these findings suggest that *B. acidifaciens* regulated by autophagy in CD11c^{+} cells could be a novel therapeutic agent related to obesity.

I further investigate a novel function of *B. acidifaciens* expanded in the gut of *Atg7*$^{\Delta CD11c}$ mice whether these single commensal bacteria can modulate host lipid metabolisms. I found B6 mice daily fed *B. acidifaciens* for 10 weeks were more likely to lose body weights and fat masses than a

group fed PBS, even though both groups were taken the same amount of food. Of note, predominant expression of PPARŬwas consistently found in the adipose tissues of *Atg7*^{qCD11c} mice, wild-type B6 mice transferred with fecal microbiota of *Atg7*^{qCD11c} mice, and *B. acidifaciens*-feeding wild-type B6 mice, not in liver and ileum. In addition, the expression of TGR5, well known as bile acid receptors, were also increased in adipose tissue by short-term treatment of *B. acidifaciens*, indicating that enhanced glucose homeostasis found in B6 mice fed with *B. acidifaciens* might be closely related with increased GLP-1 secretion through TGR5 activation. I also found elevated insulin levels following oral administration with *B. acidifaciens* were closely related to increased glucagon-like peptide 1 (GLP-1) and decreased dipeptidyl peptidase-4 (DPP-4). In addition, significantly increased levels of cholate and taurine were found in feces of B6 mice fed with *B. acidifaciens* for 10 weeks. Collectively, these finding suggest that *B. acidifaciens* could be a novel therapeutic agent related to obesity mediated by a TGR5-PPARŬdependent pathway.

1. Lean phenotypes with reduced body weight and fat mass were detected in aged *Atg7*^{qCD11c} mice regardless gender. Other conditional knock-out mice such as *Atg7*^{qvillin} and *Atg7*^{qMǩ} mice were shown no difference on their body weight.

2. The levels of insulin in serum of *Atg7*$^{\Delta CD11c}$ mice were significantly elevated, even though *Atg7*$^{\Delta CD11c}$ mice have shown lower levels of serum glucose compare to that of *Atg7*$^{f/f}$ mice.

3. Body weight and fat mass of *Atg7*$^{f/f}$ and *Atg7*$^{\Delta CD11c}$ mice in co-housing cage were compensated. In addition, C57BL/6 mice fed with fecal extracts of *Atg7*$^{\Delta CD11c}$ mice for 18 weeks were shown significant loss of body weight compared to that of control group, indicating that commensal bacteria can be a ĩransporter Śo f host fat metabolism.

4. From Phylum to Genus level, the composition of commensal bacteria in feces was identical between *Atg7*$^{f/f}$ mice and *Atg7*$^{\Delta CD11c}$ mice. However, in the Species levels, *B. acidifaciens* were significantly expanded in the lumen and some of them are localized in the epithelial cells of the large intestine from *Atg7*$^{\Delta CD11c}$ mice.

5. B6 mice fed with *B. acidifaciens* for 10 weeks were shown significant body weight loss in normal-chow diet (17%) and in high-fat diet (43%) compared to that of B6 mice fed with PBS. In contrast, B6 mice fed with *B. sartorii*, as internal control strain which were included in same genus, were shown no effects on the body weight.

6. The increased levels of insulin and improved insulin sensitivity were detected in serum of B6 mice fed with *B. acidifaciens* which are consistant results from *Atg7*$^{\Delta CD11c}$ mice and B6 mice transferred with fecal extracts of *Atg7*$^{\Delta CD11c}$ mice. In addition, B6 mice fed with *B. acidifaciens* revealed highly enhanced energy expenditure in HFD condition, suggesting that *B. acidifaciens* may regulate host lipid metabolisms by activating the induction of fat consumption.

7. The expression levels of PPARŬwere significantly increased in adipose tissues of all mice shown lean phenotypes (*Atg7*$^{\Delta CD11c}$ mice, B6 mice transferred with fecal extracts of *Atg7*$^{\Delta CD11c}$ mice and fed with HFD and *B. acidifaciens*), indicating that lean phenotypes mediated by *B. acidifaciens* might begin with lipid oxidation in adipose tissue through PPARŬactivation.

8. ELISA analysis revealed that the levels of both glucagon-like peptide 1 (GLP-1) and dipeptidyl peptidase-4 (DPP-4) were closely connected with *B. acidifaciens* and/or their metabolites. On the other hand, the elevated levels of cholate and taurine were found in feces of B6 mice fed with *B. acidifaciens*. These results suggest that unknown metabolites synthesized by *B. acidifaciens* or bacteria itself may directly interact with gut epithelial cells to modulate gut

hormone and may plays a critical role of deconjugation of primary bile acids.

IV-2. Proposed model of *B. acidifaciens* to clean by protect host against insulin resistance and obesity

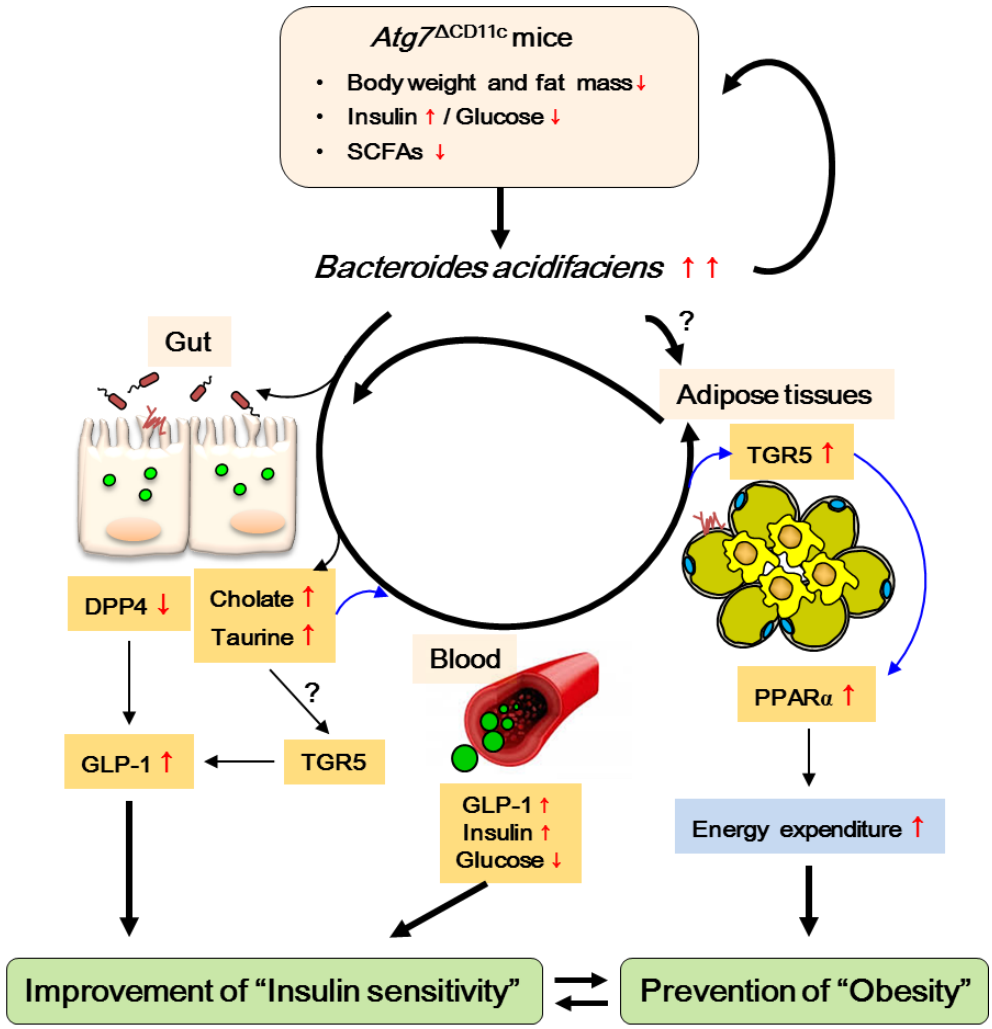

Figure 4.1.. The scheme of this study.

Specific gut commensal bacteria (i.e., *B. acidifaciens*) were expanded in *Atg7*^{qCD11c} mice with lean phenotypes. Administration of *B. acidifaciens* resulted in activation of fat oxidation through the bile acid-TGR5-PPARŮ axis in adipose tissues, which may lead to high energy expenditure. At the same time, *B. acidifaciens* activate DPP-4 in the gut and subsequently increase GLP-1, which may contribute to glucose homeostasis. Bile acids, cholate, and taurine may also contribute to GLP-1 activation through TGR5 and result in improved insulin sensitivity. Overall, *B. acidifaciens* may play a role in prevention of metabolic diseases such as diabetes and obesity.

.

. CD11c

(*Atg7*) (*Atg7* $^{\text{CD11c}}$)

(*Atg7* $^{\text{f/f}}$ mice)

.

Atg7 $^{\text{CD11c}}$

. *Atg7* $^{\text{f/f}}$ *Atg7* $^{\text{CD11c}}$

.

Bacteroides acidifaciens *Atg7* $^{\text{CD11c}}$

(5%)

. *Bacteroides*

B. sartorii

. *B. acidifaciens*

. *B. acidifaciens* B6

, PBS

.

B. sartorii B6

, *B. acidifacien s*

.

B. acidifaciens

.

Atg7 $^{\text{qCD11c}}$, *Atg7* $^{\text{qCD11c}}$

B6 , *B. acidifaciens* B6

PPAR .

PPAR

. CE- TOFMS

10 *B. acidifaciens*

. ,

G TGR5 *B. acidifaciens*

, *B.*

acidifaciens - TGR5 - PPAR

,

. *B. acidifaciens*

1 .

B. acidifaciens

.

: (*Bacteroides acidifaciens*),

, PPAR , 1,

: 2011 - 31031

Chapter I. General Introduction

I-1. Gastrointestinal immunity

I-1-1. Introduction

Mucosal tissues of the human body (i.e., respiratory, gastro-intestinal, and uro-genital tracts) are covered by mucus layers and are linked directly with various exogeneous antigens and symbiotic microorganisms (i.e., commensal bacteria) (*1*). Mucosal membrane consists of epithelial cells connected by tight junction, so that works as first physical defense barrier. The mucosal immune systems play critical roles for development of innate immune responses that protect the host within a few minutes and hours after infection of pathogens (*2*). Therefore, the study of the cross-talk mechanism between host and symbiotic/pathogenic microorganisms will be able to reveal the pathogenesis of diverse diseases and contribute to the development of new therapies.

I-1-2. Gastrointestinal defense mechanism

I-1-2-1. Secretory immunoglobulin A (sIgA)

IgA is a secretory antibody that mainly found in mucus secretions such as tears, saliva, and vaginal secretion, and that plays an essential role in mucosal immunity as humoral defense factors. The numerous IgA-producing cells in the gut can secrete IgA into lumen area between two and

five grams per day and play an important role on the host defense (*3*). Secretory IgA (sIgA) can exist in a dimeric form, which is connected by J chain, and can exist intact form in the gut because sIgA is resistant to proteolysis (*4*). The primary defense mechanism of sIgA against pathogens is to prevent attachment to mucosal surfaces and penetration into the gut (*5*).

I-1-2-2. Intestinal epithelial cells (IECs)

The mucosal surfaces are formed by layers of epithelial cells covered with complex of glycoproteins. Of note, the IECs are maintained on a network of interconnected enterocytes, goblet cells, enteroendocrine cells (L cells), and paneth cells. Mucosal barrier function of IECs is closely related with nervous system, which can increase tight junction between adjacent cells (*6*). Secretory bioactive factors produced by commensal bacteria can also elevate epithelial barrier function (*7*). Further, various types of epithelial cells involve in mucosal defense function. The most frequent cells are conventional enterocytes which construct mechanic barrier. Both goblet cells producing mucin and Paneth cells secreting antibiotic peptides-defensins preclude the invasion of exogenous pathogens (*8, 9*). Enteroendocrine cells produce gut hormones such as glucagon-like peptides (GLPs) and peptide YY (PYY) (*10*). Of the many important roles of IECs, it

is the distinct responsibility to discriminate between harmful and beneficial antigens (*6*).

I-2. Autophagy

I-2-1. Introduction

Autophagy is a “key” machinery to maintain homeostatic condition of human body. Autophagy is essential to degrade cellular proteins and organelles, to recycle them for cell survival. This mechanism is active at a basal level in most cells and contributes to the routine turnover of cytoplasmic components (*11*).

I-2-2. The autophagic pathway

There are four stages of autophagy and many proteins (autophagy protein, ATG) involved in each step of autophagic responses, respectively. First, autophagy can be induced by diverse situations such as starvation, depletion of growth factor and immune signals (*12*). Autophagy is inhibited under nutrient-rich conditions and therefore simulated by starvation mediated by Tor/mTOR signal. Inactivation of mTOR under starvation is leading to induction of autophagy. In addition, Tor inactivation leads to downstream dephosphorylation resulting in transcriptional activation of autophagy genes, like *Atg1* and *Atg13* (*13*). Secondly, a double membrane vesicle forms autophagosome in the cytosol, and sequester those cytoplasmic components for degradation. Although the mechanism of

formation of double membrane is not fully defined, the *ATG* genes involved in vesicle formation are well identified. The *Atg5-Atg12* conjugate induces both the recruitment of LC3 and the conversion of LC3 to its phosphatidylethanolamine-conjugated LC3-II form. Formation of large complex with Atg16L1 also requires the *Atg5-Atg12* conjugate (*14*). Of note, *Atg7* is required for two ubiquitin-like conjugation pathways as mentioned before, indicating that *Atg7* is a key regulator in the generation of the autophagosome (*15*). Thirdly, the autophagosome meet with the lysosome, and thus the contents of the autophagosome are exposed to the lysosome for degradation by lysosomal proteases (*16*). Finally, following fusion of these two vesicle bodies, the membrane of autophagosome is broken down by the lysosomal proteases (*17*).

I-3. Gut microbiota

I-3-1. Introduction

Commensal bacteria means “beneficial” bacteria to host that reside on host barrier surfaces covered by epithelial cells. It is well established that five bacterial phyla (i.e. *Firmicutes*, *Bacteroidetes*, *Actinobacteria*, *Proteobacteria* and *Verruco-microbia*) are dominant gut microbiota in human (*18*). The duodenum and jejunum of the small intestine have only a few bacteria because of low pH conditions. However, numerous microbes in ileum (about 10^7 ml^{-1}) and colon (about 10^{14} ml^{-1}) inhabit the gut lumen and contents (*19*). The gut microbiota is heavily diverse and varies between individulas. More than 90% of the bacterial populations are Gram negative anaerobes and predominant species can list as follow; *Bacteroides*, *Eubacterium*, *Bifidobacterium*, *Fusobacterium*, and others (*20*). Over 100 trillions of gut microbiota plays indispensable roles in carbohydrate fermentation and nutrient absorption (*21*), protection of pathogenic bacteria (*22*, *23*), stimulation of innate/adaptive immunity (*24*, *25*), and regulation of metabolic disorders including obesity (*26*). However, under specific conditions like the treatment of antibiotics or medicines, some commensal bacteria are prone to change its characteristic to pathogenic bacteria to provoke inflammation or cancer (*27*).

I-3-2. The role of intestinal commensal microbes

The host intestinal area has a unique and complex circumstance which is exposed to numerous antigens like a daily food and exogenous bacteria. Resident gut microbiota contains a number of components able to activate innate and adaptive immunity. For examples, the majority of the intestinal bacteria are Gram-negative anaerobes having diverse structural agents, such as lipopolysaccharide (LPS) and flagella, give continuously signals to intestinal epithelial cells (IECs) through toll-like receptors (TLRs) (*28*, *29*). Segmented filamentous bacteria (SFB) embedded in the ileum can also stimulate to induce T helper 17 cell (T_H17) responses and induce the production of mucosal IgA (*30*). In addition, innate lymphoid cells (ILCs) directly regulate specific commensal bacteria (*31*) or indirectly modulate $CD4^+$ T cells that promoted intestinal inflammation (*32*).

Commensal bacteria have enzymes which does not produced by human cells, thus can help for human to digest and absorb some carbohydrates (*33*). Gut microbiome, meanwhile, can be changed by dietary habits. For instances, *Bacteroides* genus is predominantly detected in people who usally eat diet including high fat and protein, whereas *Prevotella* genus is mainly found in people who have diatary patterns based on carbohydrates (*34*).

I-4. Obesity

I-4-1. Introduction

Obesity represents the situation that body mass index (BMI) is more than 30 kg / m^2, and provoke secondary complications which may be caused from excessive body fat such as cardiovascular diseases, diabetes, and osteoarthritis (*35*). In world health organization (WHO) reports, obesity is not only considered as a simple risk factor for other diseases, but also classified as a disease to be managed and treated (*36*). According to the 2012 national health statistics, the prevalence of obesity was 32.8% in Korea, and person who has 30 kg / m^2 or more in BMI is increasing with 4.8 % in the population 19 years old or elder. Direct or indirect costs due to overweight and obesity accounted for 3.7% of national health care spending by 1.8 trillion won, suggesting that the time required aggressive weight management at the national level (*37*).

I-4-2. Commensal microbiota in host metabolism

Gut microbiota has also been implicated in obesity and metabolic syndrome. In support, altering composition of gut microbiota using antibiotic treatment increased host adiposity (*38*). Moreover, gnotobiotic mice transplanted with fecal microbiota from obese or lean volunteers

provide representing donor′s phenotypes (*39*). Dietary habits influence numbers and diversity of gut microbes. Several studies suggest that dietary consumption patterns might cause changes in the microbiota with consequences for host nutritional status and immune responses (*40*). For instance, rural African children revealed higher bacterial richness and a lower proportion of *Bacteroides* than European children (*41*). Inversely, the commensal microbiota involve in synthesizing a variety of vitamins and the absorption of minerals, which can adversely impact immune system (*42*).

I-4-3. Application of commensal microbiota: Bacteriotherapy

Many groups have tried to develop “Bacteriotherapy” by fecal microbiota transplantation (FMT) which commensal bacteria taken from a healthy donor transfer its beneficial function to recipients. *Enterobacter cloacae* B29 which were expanded in obese mice can induce obesity after feces transplantation to germ-free mice (*43*). In addition, infusion of fecal microbiota harvested from lean donor can increase insulin sensitivity and alter butyrate-producing commensal bacteria (*44*), indicating that commensal bacteria is the potential as therapeutic agents to metabolic diseases.

I-5. Objectives

Commensal bacteria play pivotal roles to regulate gut homeostasis by competing with pathogenic bacteria and to control host metabolisms by regulating food digestion. In this respect, I was tried to figure out these basal questions and performed several experiments with the objectives below.

1. **Identification of commensal bacteria regulated by host autophagic reaction in species levels and investigation of phenotypes can be modulated by microflora.**
2. **Investigation of the correlation between single commensal bacteria and host lipid metabolism, and mechanism how they modulate.**

I-6. References

1. **J. Mestecky, H. Nguyen, C. Czerkinsky, H. Kiyono.** 2008. Oral immunization: an update. *Current Opinion in Gastroenterology* 24, 713-719.
2. **C. A. Janeway, Jr., R. Medzhitov.** 2002. Innate immune recognition. *Annual Review of Immunology* 20, 197-216.
3. **P. Brandtzaeg, R. Pabst.** 2004. Let's go mucosal: communication on slippery ground. *Trends in Immunology* 25, 570-577.
4. **E. E. Max, S. J. Korsmeyer.** 1985. Human J chain gene. Structure and expression in B lymphoid cells. *The Journal of Experimental Medicine* 161, 832-849.
5. **S. Fagarasan, T. Honjo.** 2003. Intestinal IgA synthesis: regulation of front-line body defences. *Nature Reviews Immunology* 3, 63-72.
6. **D. C. Baumgart, A. U. Dignass.** 2002. Intestinal barrier function. *Current Opinion in Clinical Nutrition and Metabolic Care* 5, 685-694.
7. **B. Sanchez, M. C. Urdaci, A. Margolles.** 2010. Extracellular proteins secreted by probiotic bacteria as mediators of effects that promote mucosa-bacteria interactions. *Microbiology* 156, 3232-3242.
8. **M. E. Johansson, G. C. Hansson.** 2013. Mucus and the goblet cell. *Digestive Diseases* 31, 305-309.
9. **N. H. Salzman, D. Ghosh, K. M. Huttner, Y. Paterson, C. L. Bevins.** 2003. Protection against enteric salmonellosis in transgenic mice expressing a human intestinal defensin. *Nature* 422, 522-526.
10. **D. J. Drucker, M. A. Nauck.** 2006. The incretin system: glucagon-like peptide-1 receptor agonists and dipeptidyl peptidase-4 inhibitors in type 2 diabetes. *Lancet* 368, 1696-1705.
11. **B. Levine, N. Mizushima, H. W. Virgin.** 2011. Autophagy in immunity and inflammation. *Nature* 469, 323-335.
12. **S. T. Shibutani, T. Yoshimori.** 2014. A current perspective of autophagosome biogenesis. *Cell Research* 24, 58-68.
13. **C. H. Jung, S. H. Ro, J. Cao, N. M. Otto, D. H. Kim.** 2010. mTOR regulation of autophagy. *FEBS Letters* 584, 1287-1295.
14. **N. Mizushima, T. Noda, T. Yoshimori, Y. Tanaka, T. Ishii, M. D. George, D. J. Klionsky, M. Ohsumi, Y. Ohsumi.** 1998. A protein conjugation system essential for autophagy. *Nature* 395, 395-398.
15. **A. M. Taherbhoy, S. W. Tait, S. E. Kaiser, A. H. Williams, A.**

Deng, A. Nourse, M. Hammel, I. Kurinov, C. O. Rock, D. R. Green, B. A. Schulman. 2011. Atg8 transfer from Atg7 to Atg3: a distinctive E1-E2 architecture and mechanism in the autophagy pathway. *Molecular Cell* 44, 451-461.

16. **I. G. Ganley, P. M. Wong, N. Gammoh, X. Jiang.** 2011. Distinct autophagosomal-lysosomal fusion mechanism revealed by thapsigargin-induced autophagy arrest. *Molecular Cell* 42, 731-743.
17. **I. Tanida, N. Minematsu-Ikeguchi, T. Ueno, E. Kominami.** 2005. Lysosomal turnover, but not a cellular level, of endogenous LC3 is a marker for autophagy. *Autophagy* 1, 84-91.
18. **G. Vedantam, D. W. Hecht.** 2003. Antibiotics and anaerobes of gut origin. *Current Opinion in Microbiology* 6, 457-461.
19. **R. D. Berg.** 1996. The indigenous gastrointestinal microflora. *Trends in Microbiology* 4, 430-435.
20. **F. Guarner, J. R. Malagelada.** 2003. Gut flora in health and disease. *Lancet* 361, 512-519.
21. **J. Qin, R. Li, J. Raes, M. Arumugam, K. S. Burgdorf, C. Manichanh, T. Nielsen, N. Pons, F. Levenez, T. Yamada, D. R. Mende, J. Li, J. Xu, S. Li, D. Li, J. Cao, B. Wang, H. Liang, H. Zheng, Y. Xie, J. Tap, P. Lepage, M. Bertalan, J. M. Batto, T. Hansen, D. Le Paslier, A. Linneberg, H. B. Nielsen, E. Pelletier, P. Renault, T. Sicheritz-Ponten, K. Turner, H. Zhu, C. Yu, S. Li, M. Jian, Y. Zhou, Y. Li, X. Zhang, S. Li, N. Qin, H. Yang, J. Wang, S. Brunak, J. Dore, F. Guarner, K. Kristiansen, O. Pedersen, J. Parkhill, J. Weissenbach, H. I. T. C. Meta, P. Bork, S. D. Ehrlich, J. Wang.** 2010. A human gut microbial gene catalogue established by metagenomic sequencing. *Nature* 464, 59-65.
22. **N. Kamada, Y. G. Kim, H. P. Sham, B. A. Vallance, J. L. Puente, E. C. Martens, G. Nunez.** 2012. Regulated virulence controls the ability of a pathogen to compete with the gut microbiota. *Science* 336, 1325-1329.
23. **J. Behnsen, S. Jellbauer, C. P. Wong, R. A. Edwards, M. D. George, W. Ouyang, M. Raffatellu.** 2014. The cytokine IL-22 promotes pathogen colonization by suppressing related commensal bacteria. *Immunity* 40, 262-273.
24. **T. Karrasch, J. S. Kim, M. Muhlbauer, S. T. Magness, C. Jobin.** 2007. Gnotobiotic IL-$10^{-/-}$;NF-kappa B (EGFP) mice reveal the critical role of TLR/NF-kappa B signaling in commensal bacteria-induced colitis. *Journal of Immunology* 178, 6522-6532.

25. **I. Jarchum, E. G. Pamer.** 2011. Regulation of innate and adaptive immunity by the commensal microbiota. *Current Opinion in Immunology* 23, 353-360.
26. **L. Trasande, J. Blustein, M. Liu, E. Corwin, L. M. Cox, M. J. Blaser.** 2013. Infant antibiotic exposures and early-life body mass. *International Journal of Obesity* 37, 16-23.
27. **M. V. Pirotta, S. M. Garland.** 2006. Genital Candida species detected in samples from women in Melbourne, Australia, before and after treatment with antibiotics. *Journal of Clinical Microbiology* 44, 3213-3217.
28. **J. L. Round, S. M. Lee, J. Li, G. Tran, B. Jabri, T. A. Chatila, S. K. Mazmanian.** 2011. The Toll-like receptor 2 pathway establishes colonization by a commensal of the human microbiota. *Science* 332, 974-977.
28. **M. M. Heimesaat, A. Fischer, H. K. Jahn, J. Niebergall, M. Freudenberg, M. Blaut, O. Liesenfeld, R. R. Schumann, U. B. Gobel, S. Bereswill.** 2007. Exacerbation of murine ileitis by Toll-like receptor 4 mediated sensing of lipopolysaccharide from commensal Escherichia coli. *Gut* 56, 941-948.
30. **Ivanov, II, K. Atarashi, N. Manel, E. L. Brodie, T. Shima, U. Karaoz, D. Wei, K. C. Goldfarb, C. A. Santee, S. V. Lynch, T. Tanoue, A. Imaoka, K. Itoh, K. Takeda, Y. Umesaki, K. Honda, D. R. Littman.** 2009. Induction of intestinal Th17 cells by segmented filamentous bacteria. *Cell* 139, 485-498.
31. **G. F. Sonnenberg, L. A. Monticelli, T. Alenghat, T. C. Fung, N. A. Hutnick, J. Kunisawa, N. Shibata, S. Grunberg, R. Sinha, A. M. Zahm, M. R. Tardif, T. Sathaliyawala, M. Kubota, D. L. Farber, R. G. Collman, A. Shaked, L. A. Fouser, D. B. Weiner, P. A. Tessier, J. R. Friedman, H. Kiyono, F. D. Bushman, K. M. Chang, D. Artis.** 2012. Innate lymphoid cells promote anatomical containment of lymphoid-resident commensal bacteria. *Science* 336, 1321-1325.
32. **M. R. Hepworth, L. A. Monticelli, T. C. Fung, C. G. Ziegler, S. Grunberg, R. Sinha, A. R. Mantegazza, H. L. Ma, A. Crawford, J. M. Angelosanto, E. J. Wherry, P. A. Koni, F. D. Bushman, C. O. Elson, G. Eberl, D. Artis, G. F. Sonnenberg.** 2013. Innate lymphoid cells regulate $CD4^+$ T-cell responses to intestinal commensal bacteria. *Nature* 498, 113-117.
33. **S. C. Resta.** 2009. Effects of probiotics and commensals on intestinal epithelial physiology: implications for nutrient handling.

The Journal of Physiology 587, 4169-4174.

34. **G. D. Wu, J. Chen, C. Hoffmann, K. Bittinger, Y. Y. Chen, S. A. Keilbaugh, M. Bewtra, D. Knights, W. A. Walters, R. Knight, R. Sinha, E. Gilroy, K. Gupta, R. Baldassano, L. Nessel, H. Li, F. D. Bushman, J. D. Lewis.** 2011. Linking long-term dietary patterns with gut microbial enterotypes. *Science* 334, 105-108.
35. **D. W. Haslam, W. P. James.** 2005. Obesity. *Lancet* 366, 1197-1209.
36. **W. P. James.** 2008. WHO recognition of the global obesity epidemic. *International Journal of Obesity* 32 Suppl 7, S120-126.
37. **M. K. Kim, W. Y. Lee, J. H. Kang, J. H. Kang, B. T. Kim, S. M. Kim, E. M. Kim, S. H. Suh, H. J. Shin, K. R. Lee, K. Y. Lee, S. Y. Lee, S. Y. Lee, S. K. Lee, C. B. Lee, S. Chung, I. K. Jeong, K. Y. Hur, S. S. Kim, J. T. Woo, G.** 2014. 2014 clinical practice guidelines for overweight and obesity in Korea. *Endocrinology and Metabolism* 29, 405-409.
38. **I. Cho, S. Yamanishi, L. Cox, B. A. Methe, J. Zavadil, K. Li, Z. Gao, D. Mahana, K. Raju, I. Teitler, H. Li, A. V. Alekseyenko, M. J. Blaser.** 2012. Antibiotics in early life alter the murine colonic microbiome and adiposity. *Nature* 488, 621-626.
39. **V. K. Ridaura, J. J. Faith, F. E. Rey, J. Cheng, A. E. Duncan, A. L. Kau, N. W. Griffin, V. Lombard, B. Henrissat, J. R. Bain, M. J. Muehlbauer, O. Ilkayeva, C. F. Semenkovich, K. Funai, D. K. Hayashi, B. J. Lyle, M. C. Martini, L. K. Ursell, J. C. Clemente, W. Van Treuren, W. A. Walters, R. Knight, C. B. Newgard, A. C. Heath, J. I. Gordon.** 2013. Gut microbiota from twins discordant for obesity modulate metabolism in mice. *Science* 341, 1241214.
40. **P. J. Turnbaugh, F. Backhed, L. Fulton, J. I. Gordon. 2008.** Diet-induced obesity is linked to marked but reversible alterations in the mouse distal gut microbiome. *Cell Host & Microbe* 3, 213-223.
41. **J. Ou, F. Carbonero, E. G. Zoetendal, J. P. DeLany, M. Wang, K. Newton, H. R. Gaskins, S. J. O'Keefe.** 2013. Diet, microbiota, and microbial metabolites in colon cancer risk in rural Africans and African Americans. *The American Journal of Clinical Nutrition* 98, 111-120.
42. **S. C. Resta.** 2009. Effects of probiotics and commensals on intestinal epithelial physiology: implications for nutrient handling. *The Journal of Physiology* 587, 4169-4174.
43. **N. Fei, L. Zhao.** 2013. An opportunistic pathogen isolated from the gut of an obese human causes obesity in germfree mice. *The ISME Journal* 7, 880-884.

44. **A. Vrieze, E. Van Nood, F. Holleman, J. Salojarvi, R. S. Kootte, J. F. Bartelsman, G. M. Dallinga-Thie, M. T. Ackermans, M. J. Serlie, R. Oozeer, M. Derrien, A. Druesne, J. E. Van Hylckama Vlieg, V. W. Bloks, A. K. Groen, H. G. Heilig, E. G. Zoetendal, E. S. Stroes, W. M. de Vos, J. B. Hoekstra, M. Nieuwdorp.** 2012. Transfer of intestinal microbiota from lean donors increases insulin sensitivity in individuals with metabolic syndrome. *Gastroenterology* 143, 913-916 e917.

Chapter II. Specific deletion of autophagy-related gene *(atg7)* in $CD11c^+$ cells alter murine gut microbiota

II-1. Introduction

Autophagy, self-eating pathway, has been firstly known as an innate adaptation to starvation (*1*, *2*). Autophagy machinery play indispensable roles in the maintain host homeostasis due to their ability for removing misfolded proteins and damaged organelles (*3*). Over recent years, autophagy has been implicated in several pathological and physiological conditions such as infectious diseases, cancer, autoimmune diseases, and metabolic disorders including obesity (*4*). Previous studies demonstrated that inhibition of autophagy with 3-methylademine (3MA) in vitro lead to increased triglycerides and lipid droplets accumulation in hepatocytes (*5*) and defective hepatic autophagy-related gene 7 (*Atg*7) in obesity causes insulin resistance (*6*). On the other hand, adipose-specific *Atg*7 deleted mice exhibited lower body weight, decreased white adipose tissues (WATs), and increased insulin sensitivity which contributing resistant to diet-induced obesity (*7*, *8*). In addition, skeletal muscle-specific *Atg*7 deleted mice showed ″lean″ phenotypes supported by decreased fat mass and amelioration of insulin resistance (*9*), indicating that autophagy is one of key mechanisms to regulate host lipid metabolism. However, it is still unveiled whether controlling autophagy pathway could be one of

environmental factors for regulating energy balance.

Obesity is associated with substantial changes in the composition and metabolic function of the gut microbiota which has emerged for therapeutic potential (*10*). In initial studies, data from mice models and human volunteers with lean and obese phenotypes revealed that change of relative abundance of specific phyla such as *Firmicutes* and *Bacteroidetes* are associated with obesity (*11, 12*). It has been hypothesized that these distinct abundances in the gut microbiota resulted in different yield to harvest energy from the diet (*13*). Mice deficient in TLR5 developed metabolic syndrome including insulin resistance and increased adiposity which closely related with changes in the composition of their gut microbiota (*14*). In support, altering composition of gut microbiota using antibiotic treatment increased host adiposity (*15*). Moreover, gnotobiotic mice transplanted with fecal microbiota from obese or lean volunteers provide representing donor′s phenotypes (*16*). In terms of energy expenditure, commensal microbes can contribute to obesity by providing digestive enzymes, by regulating fat storage (*17*), and by producing short-chain fatty acids (SCFAs) (*18, 19*).

Here, I unexpectedly identified lean phenotypes in *Atg7*$^{\Delta CD11c}$ mice including lower levels of body weight / fat mass and glucose in serum,

which were associated with increased production of insulin. Interestingly, I got the clues that commensal bacteria are closely related in these phenomenons using co-housing and fecal extracts transplantation. In depth, pyrosequencing analysis revealed that specific commensal bacteria, especially *Bacteroides acidifaciens*, were expanded in feces and colon epithelial cells of *Atg7*$^{\Delta CD11c}$ mice. My results suggest that single strain of commensal bacteria can be regulated by autophagy of CD11c positive cells and those bacteria might be related with host lipid metabolism.

II-2. Materials and Methods

II-2-1. Ethics statement

All animal experiments were approved by the Institutional Animal Care and Use Committee of the Asan biomedical research center (Approval No: PN 2014-13-069). All experiment was performed under anesthesia with a mixture of ketamine (100 mg/kg) and xylazine (20 mg/kg), and all efforts were made to minimize suffering.

II-2-2. Mice and bacteria strains

C57BL/6 (B6) and *CD11c*^{cre} mice were purchased from Charles River Laboratories (Orient Bio Inc., Sungnam, Korea) and Jackson Laboratory (Bar Harbor, ME), respectively. *ATG7*$^{flox/flox}$ mice were kindly provided by Dr. Masaaki Komatsu (Tokyo Metroplitan Institue of Medical Science, Japan). All mice were maintained under specific pathogen-free conditions in the animal facility at the Asan biomedical research center (Seoul, Korea) where they received sterilized food and water *ad libitum*. *Bacteroides* (*B.*) *acidifaciens* (JCM10556) and *B. sartorii* (JCM17136) used in this study were purchased from Japan Collection of Microorganisms (JCM) at RIKEN BioResource Center.

II-2-3. Bacteria culture

B. acidifaciens and *B. sartorii* were grown in peptone-yeast-glucose (PYG) broth at 37 ^{o}C for 48 hours anaerobically with BBL^{TM} GasPak 100^{TM} EZ gas generating container (Becton Dickinson, Sparks, MD). The bacteria were concentrated by centrifuging for 15 minutes at 5,000 g and resuspended with sterile PBS. The actual bacterial dose given was confirmed by plating serial dilutions onto Eggerth-Gangon (EG) blood agar plates.

II-2-4. Glucose tolerance test (GTT) and insulin tolerance test (ITT)

GTT and ITT were done as previously described (*20*). For GTT, in brief, 16 hours-fasted mice were injected 2 mg of glucose per gram of body weight through intraperitoneal (i.p.) route. For ITT, 6 hours-fasted mice were injected 0.75 Unit of insulin through i.p. route. The concentration of plasma glucose was monitored at 0, 30, 60, 90 and 120 min after injection of glucose or insulin, respectively.

II-2-5. Fecal microbiota transplantation

Transfer of feces was done as previously described (*21*). In brief, fresh feces were harvested and thoroughly mashed up with sterile PBS containing 0.05 % cysteine HCl (Sigma-Aldrich) on 100 μm cell strainers. The resulting suspension after passing through strainers was briefly centrifuged at 100 g to remove large aggregates and then administrated daily for 18 weeks to mice by needleless intubation tools.

II-2-6. Magnetic resonance imaging (MRI) analysis

All MRI experiments were performed at 9.4 T / 160 mm by Agilent MRI scanner (Agilent Technologies, Santa Clara, CA) using a millipede-shaped volume radiofrequency coil. All animals were anesthetized through a mask by spontaneous inhalation of 1.5 ~ 2% isoflurane. Shimming was performed to minimize B0 inhomogeneity prior to MR scanning both automatically and manually. The axial T1-weighted (T1-WI) fast spin echo (FSE) images was used to cover both kidneys completely. The parameters of T1-WI image were TR = 1100 msec, kzero = 1, echo spacing (ESP) = 9.82 msec (effective TE = 48 msec), 48 segments, echo train length (ETL) =

4, 4 averages, matrix = 192 × 192, the field of view (FOV) = 25 × 30 mm, slice thickness = 1.0 mm; and total scan time = 3 min 33 sec, respectively. During MR scanning, external triggering was used to eliminate respiratory motion artifacts.

II-2-7. Gas chromatography mass spectrometry (GC-MS) measurement

Organic acid concentrations of feces were determined by gas chromatography–mass spectrometer (*22*). In brief, aliquots (80 ml) of ether extracts of feces were mixed with 16 ml N-tert-butyldimethylsilyl-Nmethyltrifluoroacet amide (MTBSTFA). The vials were sealed tightly, heated at 80 ^{o}C for 20 min in a water bath, and then left at room temperature for 48 h for derivatization. The derivatized samples were run through a 6890N Network GC System (Agilent Technologies, *Santa Clara*, CA) equipped with an HP-5MS column (0.25 mm × 30 m × 0.25 mm) and a 5973 Network Mass Selective Detector (Agilent Technologies). Pure helium (99.9999%) was used as carrier gas and delivered at a flow rate of 1.2 ml min^{-1}. The head pressure was set at 97 kPa with split 20:1. The inlet and transfer line temperatures were 250 and 260 ^{o}C, respectively. The following temperature program was used: 60 ^{o}C (3 min), 60-120 ^{o}C (5^{o}C /min), 120-

300 ^{o}C (20^{o}C /min). Then, 1 μl of each sample was injected with a runtime of 30 min. Organic acid concentrations were quantified by comparing their peak areas with standards.

II-2-8. Fluorescence *in situ* hybridization (*FISH*) analysis

Localization of *B. acidifaciens* in the gut mucosa was detected by *FISH* method as previously described (*23*). In brief, the large intestines were isolated and fixed with 4 % formaldehyde and dehydrated with 15 % - and 30 % - sucrose in PBS consecutively. Then dehydrated tissues were embedded in OCT compound (Sakura Finetek, Tokyo, Japan), frozen, sliced into 5-μm sections, and dried thoroughly. Hybridization buffer containing 5 ng of oligonucleotide probe μl^{-1} [Bacid2 (5′-AACATGTTTCCACATTATT CAGG-3′)] was applied to the slide and incubated at 50 ^{o}C for 2 hours. Oligonucleotide probes labeled with fluorescein were synthesized by Bioneer Corporation (Daejeon, Korea). The slides were rinsed with washing buffer at 50 ^{o}C for 10 min. After mounting with PermaFluor (Thermo scientific, Fremont, CA), slides were viewed under a confocal laser microscope (Zeiss, Göttingen, Germany).

II-2-9. Cytokine levels in serum

Cytokine levels in serum measured using the Cytometric Bead Array-mouse inflammation kit (BD Biosciences, San Jose, CA) according to the manufacturers′ instructions.

II-2-10. Histology

The visceral adipose tissues were washed with PBS and fixed in 4 % formaldehyde for 1 hour at 4 ^{o}C. Tissues were dehydrated by gradually soaking in alcohol and xylene and then embedded in paraffin. The paraffin-embedded specimens were cut into 5-μm sections, stained with H&E, and viewed with a digital light microscope (Olympus, Tokyo, Japan).

II-2-11. Bacterial antigen preparation and *B. acidifaciens*-specific ELISA

The commensal bacteria specific ELISA was performed as previously described (*24*). In brief, bacteria cultured in mass volume for 48 hours were centrifuged at 5,000 g for 15 min and washed in sterile PBS twice by centrifuging for 1 minute at 8,000 rpm. On the last wash bacteria were resuspended in 2 ml ice-cold PBS and sonicated on ice (0.2 mV pulse,

20 seconds). After spin-down with 20,000 g for 10 min at 4 ^{o}C, and recovered supernatants used for *B. acidifaciens*-specific ELISA as antigen. 5 μg/ml of *B. acidifaciens´* antigen in 50 mM sodium bicarbonate was coated for overnight at 4 ^{o}C. After a blocking step, two-fold serially diluted samples (serums and feces) were applied onto plates and incubated for 2 hours at 37 ^{o}C. HRP-conjugated goat anti-mouse IgG and IgA antibody (Southern Biotechnology Associates, Birmingham, AL) (1:3000 in 0.1 % BSA in PBS plus 0.1 % Tween 20) was added. Plates were developed with TMB substrate solution (Moss, INC), stopped by adding 0.5 N HCl, and measured at 450 nm on an ELISA reader (Microplate spectrophotometer; Molecular Devices).

II-2-12. 454 pyrosequencing analysis

cDNA was extracted from the feces using QIAamp DNA stool mini kits (QIAGEN, Venlo, Netherlands). PCR amplification was performed using primers targeting from V1 to V3 regions of the 16S rRNA gene with extracted cDNA. For bacterial amplification, barcoded primers of 9F (5′-CCTATCCCCTGTGTGCCTTGGCAGTC-TCAG-AC-AGAGTTTGATCM TGGCTCAG-3′; underlining sequence indicates the target region primer) and 541R (5′-CCATCTCATCCCTGCGTGTCTCCGAC-TCAG-X-AC-

ATTACCGCGGCTGCTGG-3′; ′X′ indicates the unique barcode for each subject) (http://oklbb.ezbiocloud.net/content/1001). The amplifications was carried out under the following conditions: initial denaturation at 95 ^{o}C for 5 min, followed by 30 cycles of denaturation at 95 ^{o}C for 30 sec, primer annealing at 55 ^{o}C for 30 sec, and extension at 72 ^{o}C for 30 sec, with a final elongation at 72 ^{o}C for 5 min. The amplified products were purified with the QIAquick PCR purification kit (Qiagen, Valencia, CA). Equal concentrations of purified products were pooled together and short fragments (non-target products) were removed with an AMPure bead kit (Agencourt Bioscience, Beverly, MA). The quality and product size were assessed on a Bioanalyzer 2100 (Agilent, Palo Alto, CA) using a DNA 7500 chip. Mixed amplicons were conducted by using emulsion PCR and then deposited on picotiter plates. The sequencing was carried out at Chunlab, Inc. (Seoul, Korea) by GS Junior Sequencing System (Roche, Branford, CT) according to the manufacturer′s instructions. Pyrosequencing data analysis was performed as previously described (*25*).

II-2-13. Real-time PCR for tissues

Tissue RNA was extracted using TRIzol® (Invitrogen), and total RNA (0.5 μg) was reverse-transcribed into cDNA according to the

manufacturer′s instructions. All signal mRNAs were normalized to GAPDH mRNA. The following primers were used to determine the relative gene expression. *F4/80*: FP, 5′-GCCTGGACGAATCCTGTGAA-3′; RP, 5′-GCTAGATGCAAAGCCAGGGT-3′. *TNF-α*: FP, 5′-GGCAGGTCTACTTT GGAGTC-3′; RP, 5′-TCGAGGCTCCAGTGAATTCG-3′. All reactions were performed in the same manner: 95 ^{o}C for 10 seconds, followed by 45 cycles of 95 ^{o}C for 15 seconds and 60 ^{o}C for 1 minute. The results were analyzed with real-time system AB 7900HT software (Life Technologies), and all values were normalized to the levels of GAPDH.

II-2-14. Analysis of metabolic parameters

Serum glucose, total cholesterol and triglyceride concentrations were determined using commercially available enzymatic assay kits (Asan Pharmacology, Seoul, Korea). Serum insulin levels were measured with an ultra-sensitive mouse insulin ELISA kit (Shibayagi, Gunma, Japan).

II-2-15. Statistics

GraphPad Prism software (GraphPad, La Jolla, CA) was used for statistical analysis. Significant differences between two groups were analyzed with two-tailed paired *t*-test or Mann-Whitney *t*-test. Multiple

groups were analyzed by two-way ANOVA followed by Bonferroni *post-hoc* test (*, $P < 0.05$; **, $P < 0.01$; ***, $P < 0.001$).

II-3. Results

II-3-1. *Atg7*$^{\Delta CD11c}$ mice showed lean phenotypes with reduced body weight and fat mass.

In order to address a role of autophagy on the development of metabolic disorders, I carefully monitored the body weight and behavior of three different kinds of *Atg7* conditional knockout mice in dendritic cells (*Atg7*$^{\Delta CD11c}$), gut epithelial cells (*Atg7*$^{\Delta villin}$), or macrophages (*Atg7*$^{\Delta M\Phi}$) with normal chow diet (NCD) feeding. As mice aged, I unexpectedly found that *Atg7*$^{\Delta CD11c}$ mice of 24 weeks old showed significantly lower body weight and fat mass than those of control littermates (*Atg7*$^{flox/flox\ (f/f)}$) (Fig. 1A-C). No significant body weight changes were found in *Atg7*$^{\Delta villin}$ and *Atg7*$^{\Delta M\Phi}$ mice of same ages (Fig. 1D-E). The difference of body weight between *Atg7*$^{\Delta CD11c}$ and *Atg7*$^{f/f}$ mice were gradually increased with age (Fig. 1F). Those lean phenotypes of *Atg7*$^{\Delta CD11c}$ mice were detected both male and female (Fig. 1G). When *Atg7*$^{\Delta CD11c}$ and *Atg7*$^{f/f}$ mice of 9 weeks old were fed high fat diet (HFD) for four weeks, body weight loss were also found in the *Atg7*$^{\Delta CD11c}$ mice (Fig. 1H). Magnetic resonance imaging (MRI) analysis further revealed that mass of the abdominal adipose tissues both in axial and colonal derection were significantly reduced in the *Atg7*$^{\Delta CD11c}$ mice when

compared with those of littermate *Atg7*$^{f/f}$ mice (Fig. 1I). In addition, the size of a single adipocyte in visceral adipose tissues obtained from *Atg7*$^{\Delta CD11c}$ mice was significantly smaller than that of *Atg7*$^{f/f}$ mice (Fig. 1J).

A.

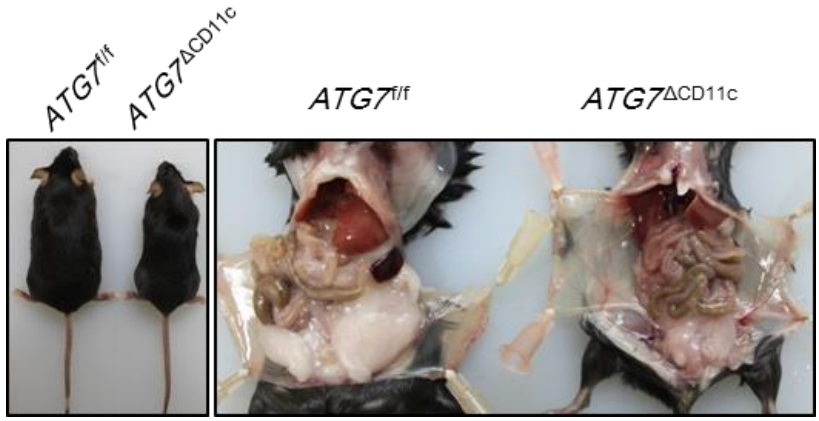
ATG7f/f
ATG7ΔCD11c
ATG7f/f
ATG7ΔCD11c

B.

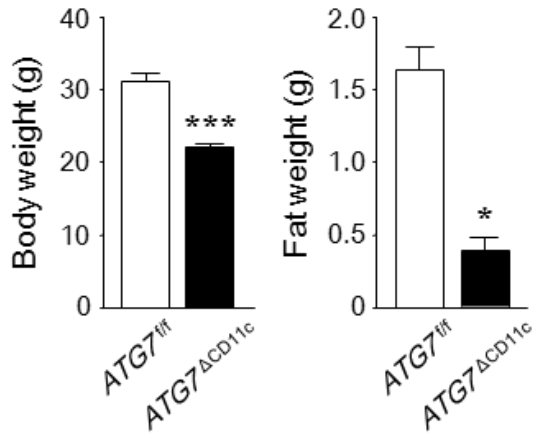
Body weight (g)
40
30
20
10
0
***
ATG7f/f
ATG7ΔCD11c
Fat weight (g)
2.0
1.5
1.0
0.5
0
*
ATG7f/f
ATG7ΔCD11c

C.

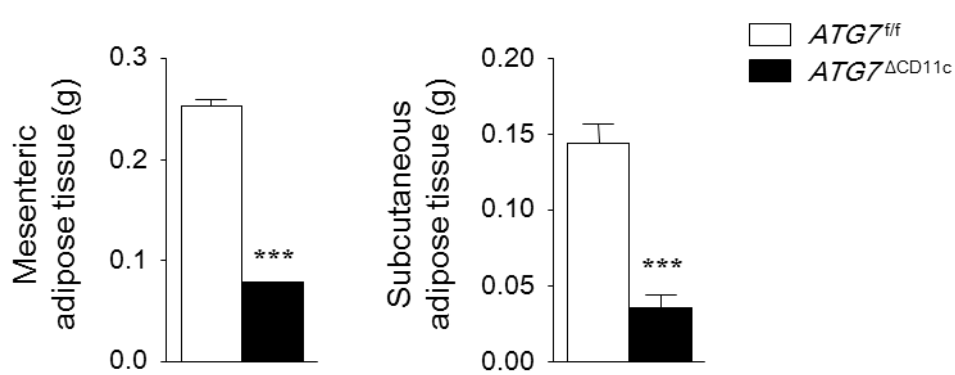
ATG7f/f
ATG7ΔCD11c
Mesenteric adipose tissue (g)
0.3
0.2
0.1
0.0
***
Subcutaneous adipose tissue (g)
0.20
0.15
0.10
0.05
0.00
***

D.

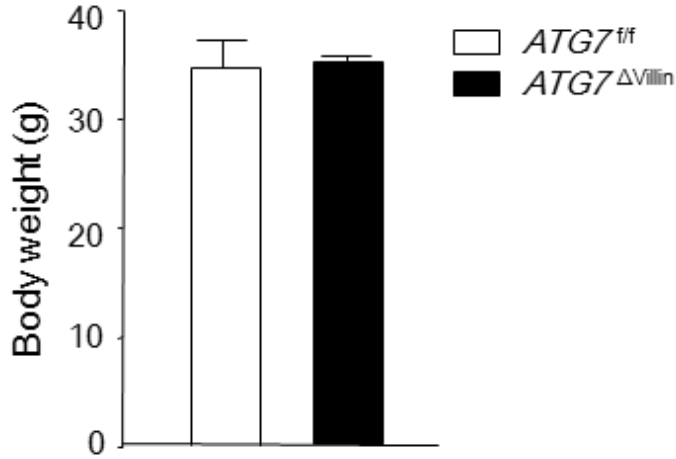
40
30
20
10
0
Body weight (g)
ATG7 f/f
ATG7 ΔVillin

E.

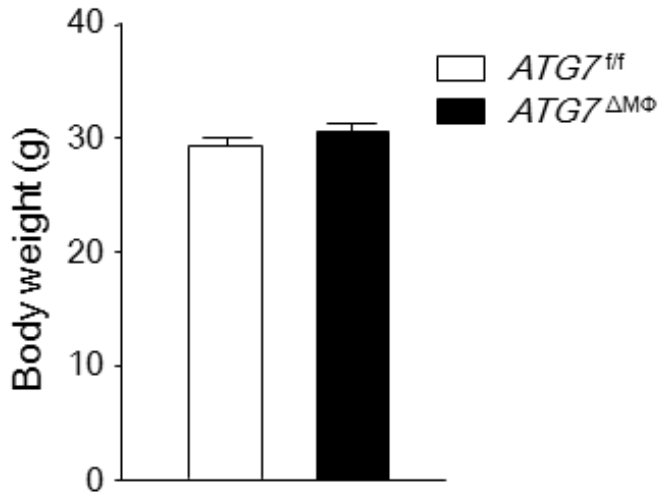
40
30
20
10
0
Body weight (g)
ATG7 f/f
ATG7 ΔMΦ

F.

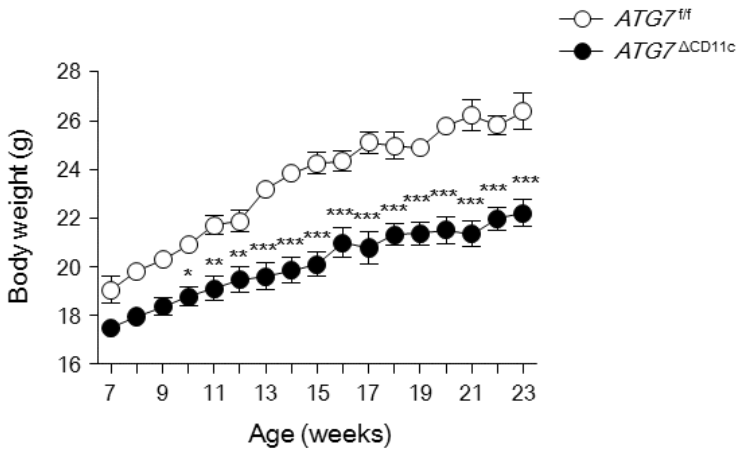
ATG7f/f
ATG7ΔCD11c
Body weight (g)
28
26
24
22
20
18
16
7
9
11
13
15
17
19
21
23
Age (weeks)
*
**
**
***
***
***
***
***
***
***
***
***
***

G.

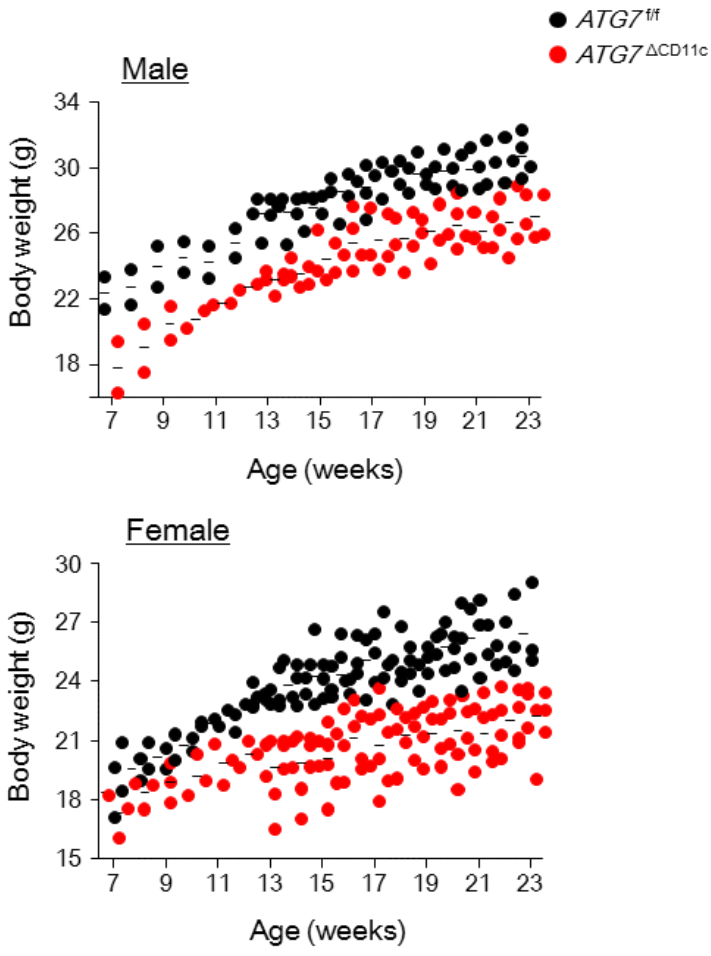
ATG7f/f
ATG7ΔCD11c
Male
Body weight (g)
34
30
26
22
18
7
9
11
13
15
17
19
21
23
Age (weeks)
Female
Body weight (g)
30
27
24
21
18
15
7
9
11
13
15
17
19
21
23
Age (weeks)

H.

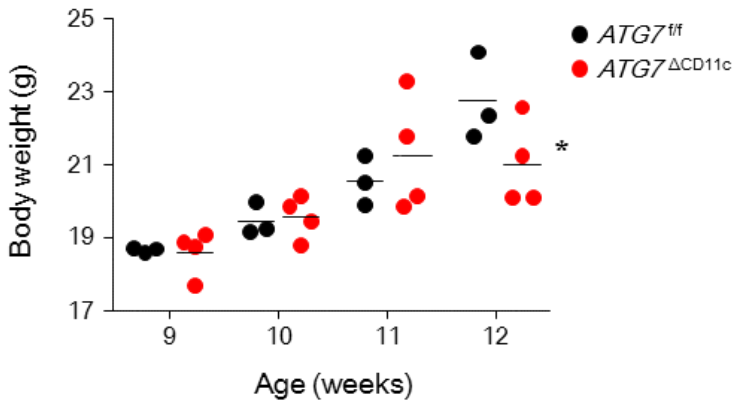
25
23
21
19
17
Body weight (g)
9
10
11
12
Age (weeks)
ATG7 f/f
ATG7 ΔCD11c
*

I.

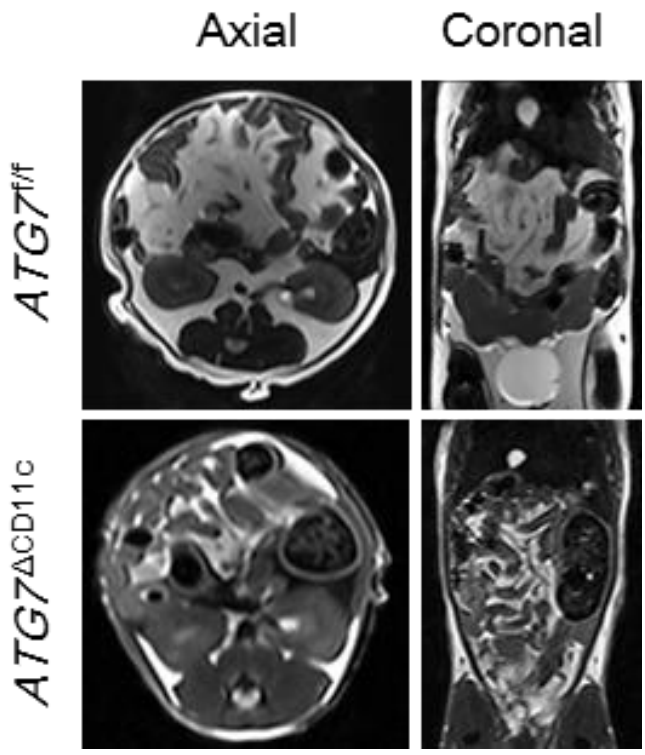
Axial
Coronal
ATG7f/f
ATG7ΔCD11c

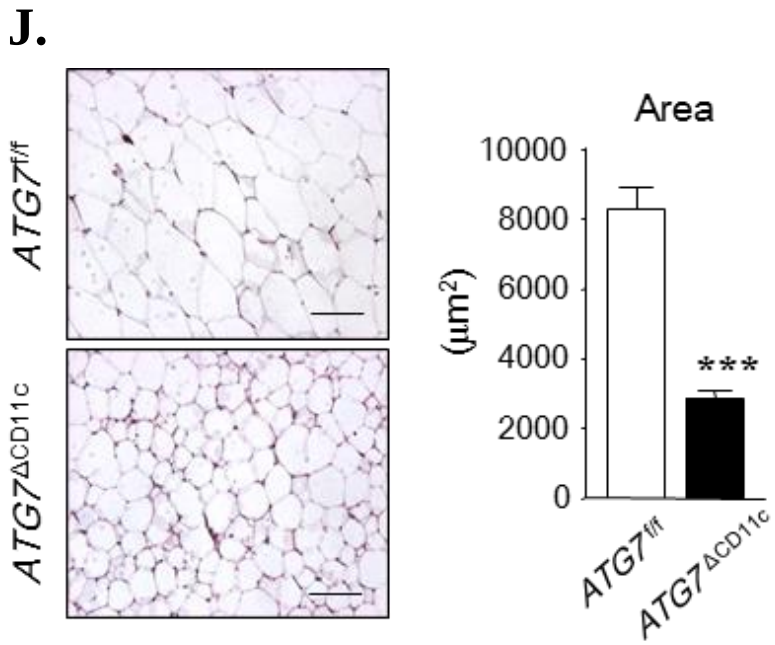

Figure 2.1. Morphological characteristics of *Atg7*$^{\Delta CD11c}$ mice.

Lean phenotypes were discovered in *Atg7*$^{\Delta CD11c}$ mice. **(A).** Representative photos of 24-week-old *Atg7*$^{f/f}$ and *Atg7*$^{\Delta CD11c}$ mice. **(B).** Body weight (left panel) and fat mass (right panel) of 24-week-old male *Atg7*$^{f/f}$ and *Atg7*$^{\Delta CD11c}$ mice fed normal chow diet (NCD; n = 5-8). **(C).** The specific fat depot were further analysed. The comparison of body weight between littermate control and conditional KO mice (n = 3) having an impaired autophagy function in intestinal villi **(D**; male, n = 3**)** and macrophages **(E**; female, n = 5**)**. **(F).** Body weight changes of *Atg7*$^{f/f}$ and *Atg7*$^{\Delta CD11c}$ mice (n = 8) were monitored for 23 weeks. **(G).** Monitoring of body weight for 23 weeks in male (upper) and female (bottom) *Atg7*$^{f/f}$ and *Atg7*$^{\Delta CD11c}$ mice fed NCD. **(H).** Monitoring

of body weight for 12 weeks in male *Atg7*$^{f/f}$ (n = 3) and *Atg7*$^{\Delta CD11c}$ (n = 4) mice fed HFD. **(I).** The abdominal adipose tissues from 24-week-old male *Atg7*$^{f/f}$ and *Atg7*$^{\Delta CD11c}$ mice fed NCD were analyzed by magnetic resonance imaging (MRI). **(J).** Histological changes of adipose tissues (left panel) and size of adipocytes (right panel) of *Atg7*$^{f/f}$ and *Atg7*$^{\Delta CD11c}$ mice. Scale bars=50 μm. All data are presented as mean ± s.e.m. Statistical analyses were done with two-tailed paired *t*-test (**B**-**E** and **J**) and two-way ANOVA with Bonferroni *post-hoc* test (**F** and **H**). *P<0.05, **P<0.01, and ***P<0.001.

II-3-2. *Atg7*$^{\Delta CD11c}$ mice shown lean phenotypes were not related with inflammation.

To clarify involvement of systemic and mucosal inflammation on the lean phenotype of *Atg7*$^{\Delta CD11c}$ mice, I have measured proinflammatory cytokine levels in serum, mRNA expression of F4/80 and TNFα in visceral adipose tissues, and did histological analysis of small and large intestines. I found similar or even decreased levels of several indicators for systemic and mucosal inflammation in the *Atg7*$^{\Delta CD11c}$ mice, indicating lean phenotype chronically shown in *Atg7*$^{\Delta CD11c}$ mice is not associated with inflammation issues (Fig. 2A-C).

A.

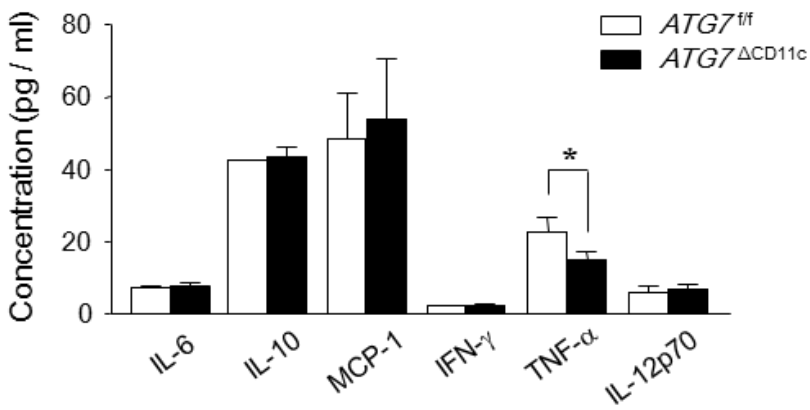
Concentration (pg / ml)
80
60
40
20
0
ATG7 f/f
ATG7 ΔCD11c
*
IL-6
IL-10
MCP-1
IFN-γ
TNF-α
IL-12p70

B.

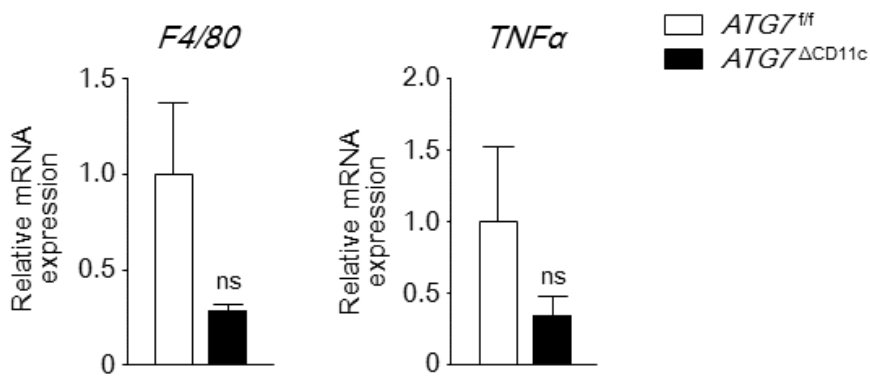
F4/80
TNFα
ATG7 f/f
ATG7 ΔCD11c
Relative mRNA expression
1.5
1.0
0.5
0
ns
Relative mRNA expression
2.0
1.5
1.0
0.5
0
ns

C.

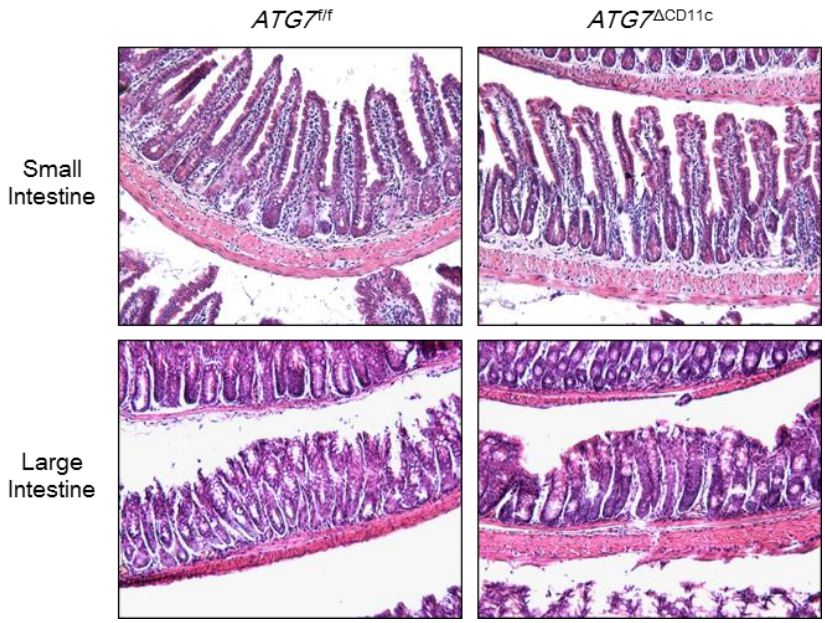

Figure 2.2. No inflammatory phenomenons in serum, adipose tissue, and intestinal area of *Atg7*$^{\Delta CD11c}$ mice.

(A). Proinflammatory cytokine levels in serum taken from 24-week-old *Atg7*$^{f/f}$ and *Atg7*$^{\Delta CD11c}$ mice (n = 7) by CBA mouse-inflammatory kit (BD Biosciences). (**B).** The mRNA expression levels of *F4/80* (left) and *TNFα* (right) in adipose tissue by real-time PCR. **(C).** Hematoxylin-eosin (H&E) staining of small intestine and large intestine taken from 24-week-old *Atg7*$^{f/f}$ and *Atg7*$^{\Delta CD11c}$ mice. Scale bar = 100 μm. All data are presented as mean ± s.e.m. Statistical analyses were done with one-way ANOVA with Bonferroni *post-hoc* test (**A**) and two-tailed paired *t*-test (**B**). *P<0.05. ns, not significant.

II-3-3. Insulin sensitivity was improved in *Atg7*$^{\Delta CD11c}$ mice.

Of note, higher insulin and subsequent lower glucose levels were detected in the serum of *Atg7*$^{\Delta CD11c}$ mice then those of *Atg7*$^{f/f}$ mice under the non-fasting condition. (Fig. 3A). Moreover, insulin resistance as determined by glucose tolerance test (GTT) and insulin tolerance test (ITT) was significantly improved in *Atg7*$^{\Delta CD11c}$ mice when compared with littermate *Atg7*$^{f/f}$ mice (Fig. 3B). Taken together, these data indicate that aged *Atg7*$^{\Delta CD11c}$ mice showed the improved glucose homeostasis with lean phenotypes of reduced body weight and fat mass.

A.

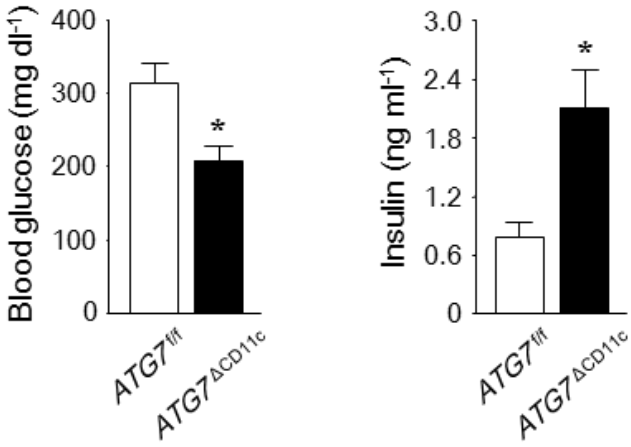
Blood glucose (mg dl-1)
400
300
200
100
0
*
ATG7f/f
ATG7ΔCD11c
Insulin (ng ml-1)
3.0
2.4
1.8
1.2
0.6
0
*
ATG7f/f
ATG7ΔCD11c

B.

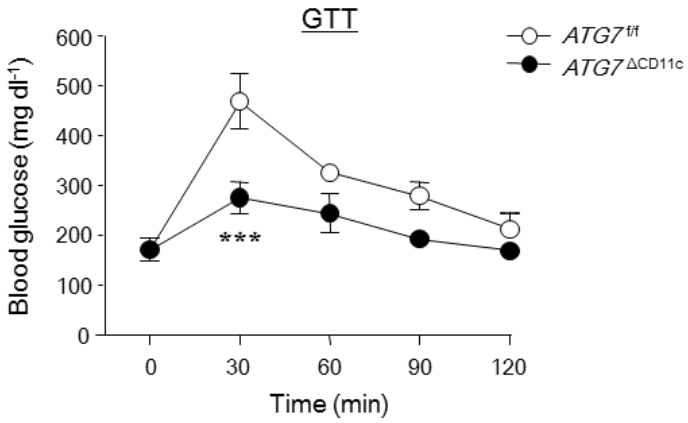
GTT
ATG7f/f
ATG7ΔCD11c
Blood glucose (mg dl-1)
600
500
400
300
200
100
0
***
0
30
60
90
120
Time (min)

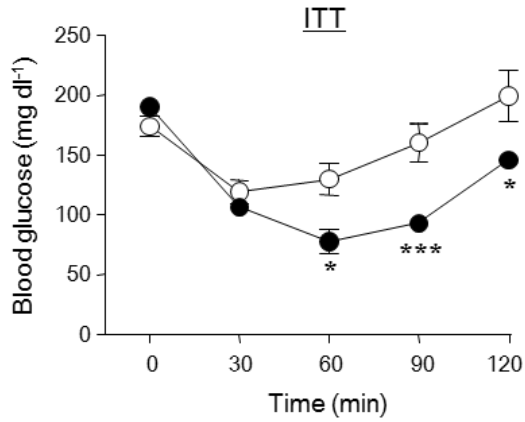
ITT
Blood glucose (mg dl-1)
250
200
150
100
50
0
*
***
*
0
30
60
90
120
Time (min)

Figure 2.3. Glucose / insulin levels in serum of *Atg7*$^{\Delta CD11c}$ mice

(A). Non-fasting glucose and insulin concentration in NCD-fed *Atg7*$^{f/f}$ and *Atg7*$^{\Delta CD11c}$ mice (n = 3). **(B).** Concentrations of serum triglycerides and total cholesterol were analyzed using enzymatic assay kits in *Atg7*$^{f/f}$ and *Atg7*$^{\Delta CD11c}$ mice (n = 3). **(C).** Glucose tolerance test (GTT) and insulin tolerance test (ITT) in male *Atg7*$^{f/f}$ and *Atg7*$^{\Delta CD11c}$ mice (n = 7). All data are presented as mean ± s.e.m. Statistical analyses were done with two-tailed paired *t*-test (**A** and **B**) and two-way ANOVA with Bonferroni *post-hoc* test (**C**). *P<0.05, and ***P<0.001.

II-3-4. Low levels of short-chain fatty acids (SCFAs) in the feces of *Atg7*$^{\Delta CD11c}$ mice.

Because aged *Atg7*$^{\Delta CD11c}$ mice had shown a decreased body weight and fat mass, I next assessed metabolome analysis in the feces to investigate the correlation between lean phenotypes and energy utilization. Although principal component analysis (PCA) revealed a weak correlation (data not shown), individual spots of *Atg7*$^{\Delta CD11c}$ mice in orthogonal partial least squares discriminate analysis (OPLS-DA) were clearly segregated from those of *Atg7*$^{f/f}$ mice (Fig. 4A). Moreover, some of short-chain fatty acids (SCFAs) such as acetate, propionate, butyrate and lactate, were located at remote spots from the axis (Fig. 4B), indicating that those factors contribute to separate the class between *Atg7*$^{f/f}$ and *Atg7*$^{\Delta CD11c}$ mice. I then further investigated the concentration of SCFAs and all sorts of compounds in feces using gas chromatography-mass spectrometry (GC-MS). While the level of lactate in *Atg7*$^{\Delta CD11c}$ mice was higher than that of *Atg7*$^{f/f}$ mice, the amounts of acetate, butyrate and propionate in *Atg7*$^{\Delta CD11c}$ mice were significantly decreased (Fig. 4C).

A.

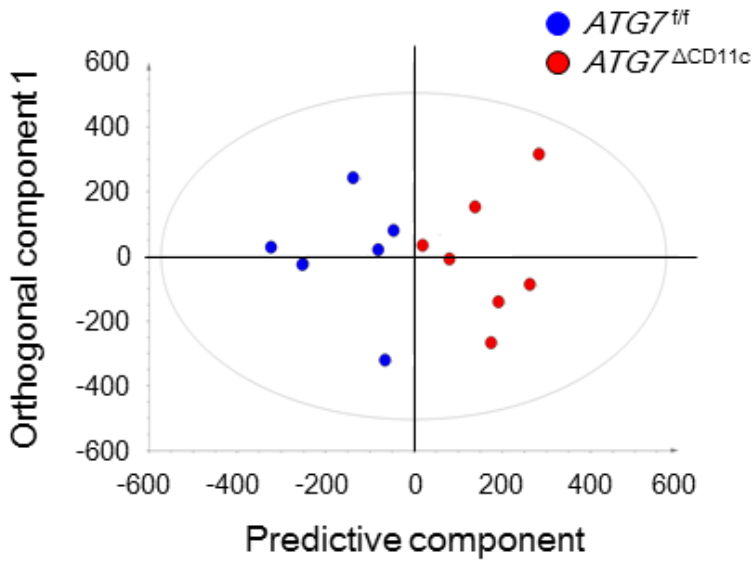
ATG7 f/f
ATG7 ΔCD11c
Orthogonal component 1
600
400
200
0
-200
-400
-600
-600
-400
-200
0
200
400
600
Predictive component

B.

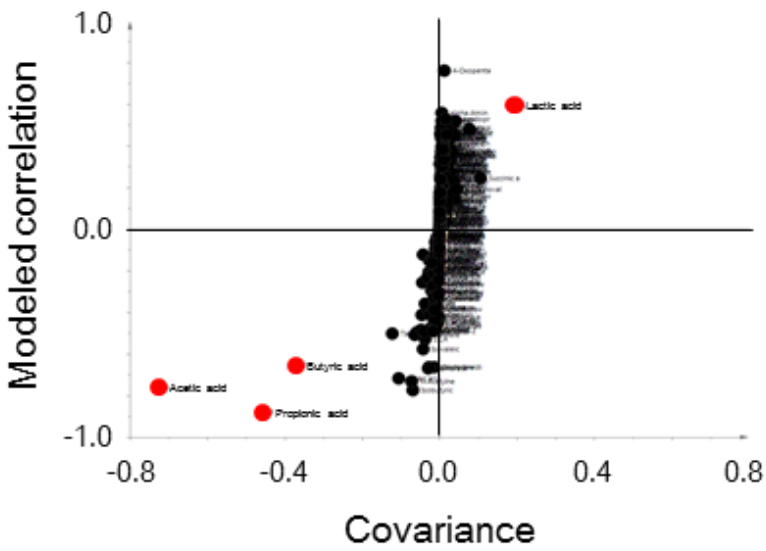
Modeled correlation
1.0
0.0
-1.0
Lactic acid
Butyric acid
Acetic acid
Propionic acid
-0.8
-0.4
0.0
0.4
0.8
Covariance

C.

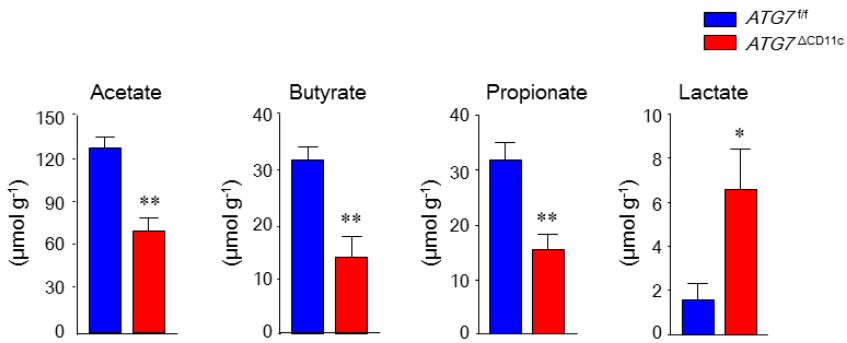

Figure 2.4. Orthogonal partial least squares discriminate analysis (OPLS-DA) in feces.

OPLS-DA on the fecal metabolome data of *Atg7*$^{f/f}$ and *Atg7*$^{\Delta CD11c}$ mice. **(A)** Cross-validated score plots from OPLS-DA of ^{1}H-NMR data of *Atg7*$^{f/f}$ and *Atg7*$^{\Delta CD11c}$ mice feces (n = 7). **(B)** S-plots for predictive component from OPLS-DA of ^{1}H-NMR data of in feces of *Atg7*$^{f/f}$ and *Atg7*$^{\Delta CD11c}$ mice (n = 7). **(C).** Quantification of facal SCFAs (i.e. acetate, butyrate, propionate and lactate) in *Atg7*$^{f/f}$ and *Atg7*$^{\Delta CD11c}$ mice (n = 5) by gas chromatography-mass spectrometry (GC-MS). All data are presented as mean ± s.e.m. Statistical analyses were done with two-tailed paired *t*-test **(C)** *P<0.05 and **P<0.01.

II-3-5. Commensal bacteria are associated with the lean phenotype of aged *Atg7*$^{\Delta CD11c}$ mice.

To address whether commensal bacteria are involved on the lean phenotype of *Atg7*$^{\Delta CD11c}$ mice, I have adopted co-housing (CH) and fecal microbiota transplantation (FMT) experiments. Both *Atg7*$^{\Delta CD11c}$ and *Atg7*$^{f/f}$ mice of 7 weeks old are sharing their feces in the same cage for 16 weeks. Of note, either body weight or fat mass were compensated each other in two groups of mice during CH period (Fig. 5A-C). To confirm whether this compensable phenotype of CH group is mediated by commensal microorganisms, I have then separated mice from sharing cage to individual cage. As shown in Fig. 5D, *Atg7*$^{\Delta CD11c}$ mice lost body weight compared to those of *Atg7*$^{f/f}$ mice as times goes by after separation. In addition, wild-type B6 mice orally transferred with fecal extracts obtained from *Atg7*$^{\Delta CD11c}$ mice for 12 weeks every day revealed significantly lower body weight and fat mass than those transferred from wild-type B6 or *Atg7*$^{f/f}$ mice (Fig. 5E). Of note, wild-type B6 mice adopted fecal extracts of *Atg7*$^{\Delta CD11c}$ mice were shown higher insulin and subsequent lower glucose levels in the serum when compared to those transferred with *Atg7*$^{f/f}$ mice (Fig. 5F). Overall, these results imply that commensal bacteria play indispensable role on the lean phenotype of *Atg7*$^{\Delta CD11c}$ mice.

A.

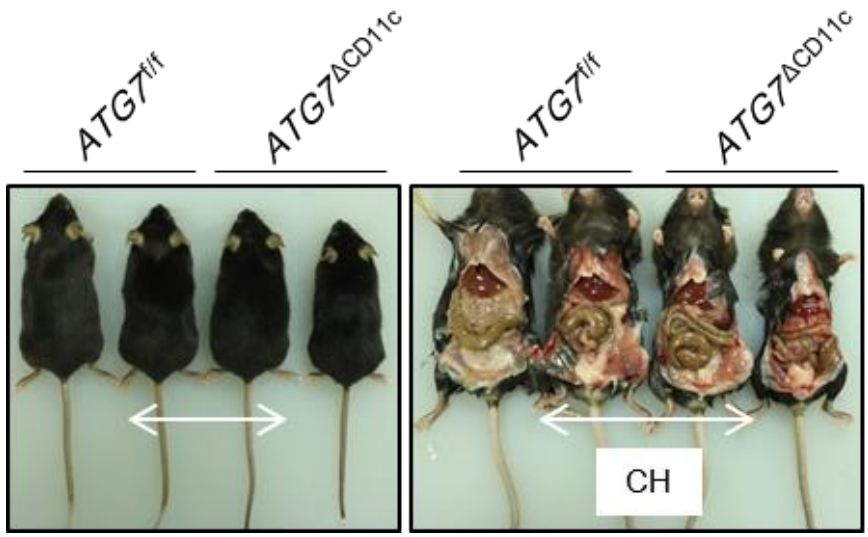
ATG7f/f
ATG7ΔCD11c
ATG7f/f
ATG7ΔCD11c
CH

B.

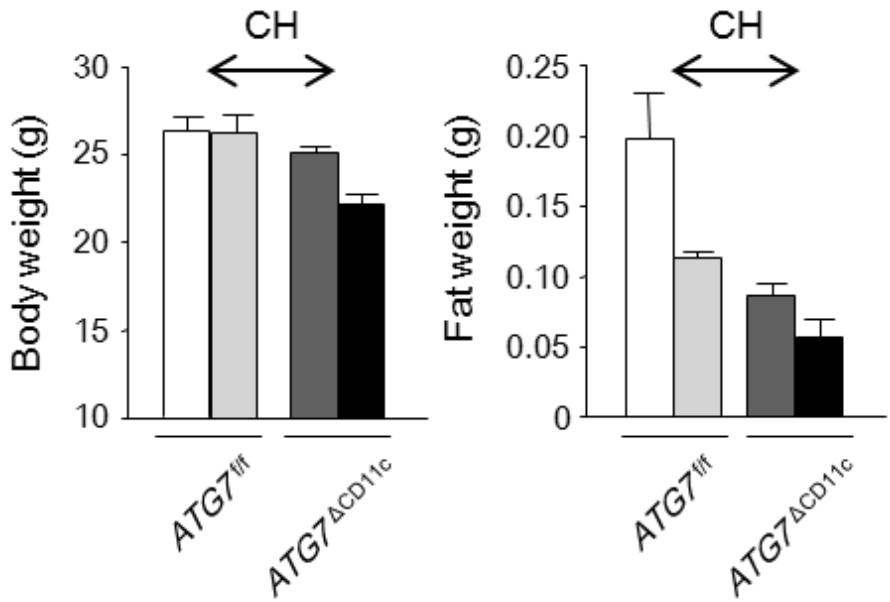
CH
Body weight (g)
30
25
20
15
10
ATG7f/f
ATG7ΔCD11c
CH
Fat weight (g)
0.25
0.20
0.15
0.10
0.05
0
ATG7f/f
ATG7ΔCD11c

C.

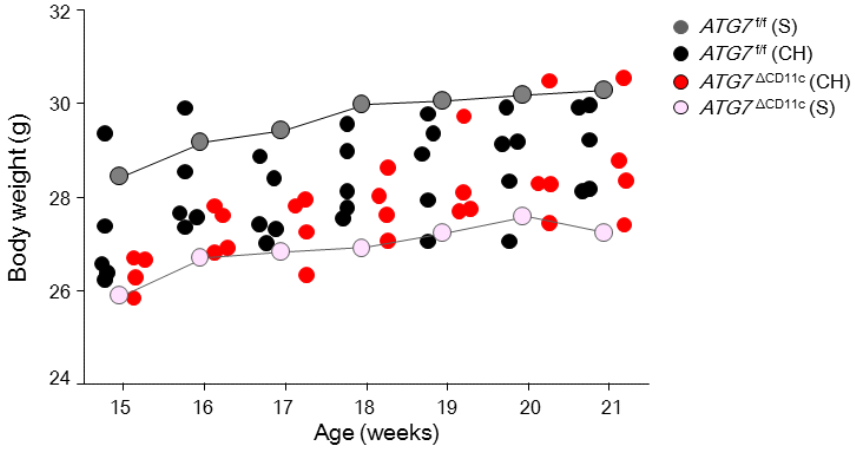
Body weight (g)
32
30
28
26
24
15
16
17
18
19
20
21
Age (weeks)
ATG7 f/f (S)
ATG7 f/f (CH)
ATG7 ΔCD11c (CH)
ATG7 ΔCD11c (S)

D.

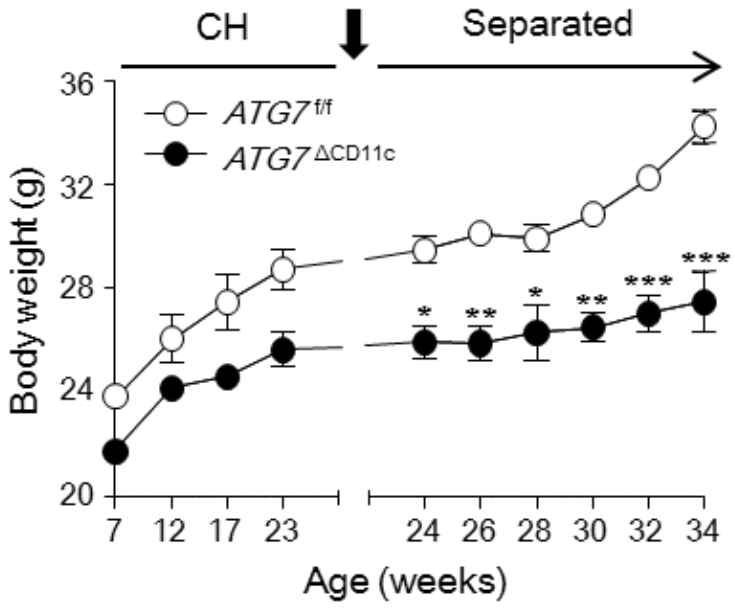
CH
Separated
ATG7 f/f
ATG7 ΔCD11c
Body weight (g)
36
32
28
24
20
7
12
17
23
24
26
28
30
32
34
Age (weeks)
*
**
*
**
***
***

E.

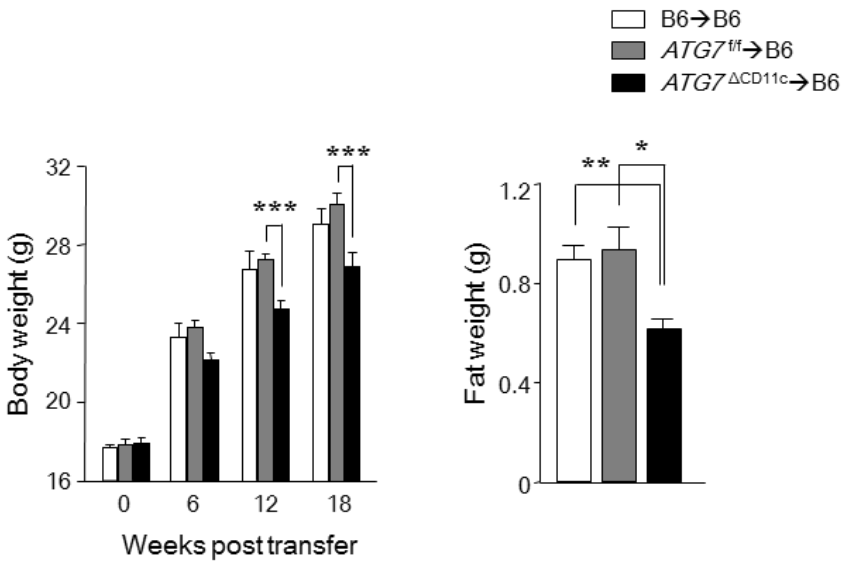
B6→B6
ATG7 f/f→B6
ATG7 ΔCD11c→B6
Body weight (g)
32
28
24
20
16
0
6
12
18
Weeks post transfer
***
***
Fat weight (g)
1.2
0.8
0.4
0
**
*

F.

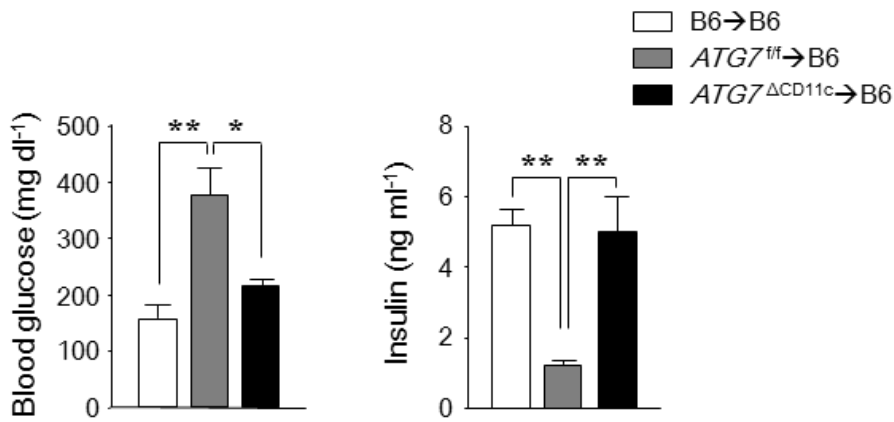
B6→B6
ATG7 f/f→B6
ATG7 ΔCD11c→B6
Blood glucose (mg dl-1)
500
400
300
200
100
0
**
*
Insulin (ng ml-1)
8
6
4
2
0
**
**

Figure 2.5. Representative photos, body / fat weight, and glucose / insulin levels of feces-transferred mice.

Lean phenotypes were originated from gut commensal bacteria. **(A).** Representative photos of 24-week-old *Atg7*$^{f/f}$ and *Atg7*$^{\Delta CD11c}$ mice after co-housing (CH; center) for 18 weeks or separated (leftmost and rightmost). (**B).** Body weight (left panel) and fat mass (right panel) of 24-week-old *Atg7*$^{f/f}$ and *Atg7*$^{\Delta CD11c}$ mice in CH- or separated- cages (n = 3-4). **(C).** Monitoring of body weight of *Atg7*$^{f/f}$ (n = 5) and *Atg7*$^{\Delta CD11c}$ (n = 4) mice in CH cages. Body weight of separated *Atg7*$^{f/f}$ and *Atg7*$^{\Delta CD11c}$ mice was drawn by linear graphs of filled circles with gray and pink color, respectively. **(D).** At 18 weeks after CH, body weight of each separated mice were monitored for further 10 weeks (n = 3-9). **(E).** Body weight (left panel) and fat mass (right panel) of naïve C57BL/6 (B6) recipient mice transferred feces of *Atg7*$^{f/f}$ or *Atg7*$^{\Delta CD11c}$ mice for 18 weeks everyday (n = 5). **(F).** Levels of glucose and insulin in serum of B6 recipient mice transferred feces of *Atg7*$^{f/f}$ or *Atg7*$^{\Delta CD11c}$ mice under non-fasting condition (n = 5). All data are presented as mean ± s.e.m. Statistical analyses were performed with two-tailed paired t-test (**B and F**) and two-way ANOVA with Bonferroni *post-hoc* test (**D** and **E**). *P<0.05, **P<0.01 and ***P<0.001.

II-3-6. Expansion of *Bacteroides acidifaciens* in the feces of *Atg7*$^{\Delta CD11c}$ mice.

In order to see the diversity and composition of gut commensal bacteria, I next adopted metagenomic analysis. In pyrosequencing analysis, the proportion of *Bacteroidetes*, *Firmicutes*, and *Proteobacteria*, which are well known as main populations of the gut microbiota in phylum level, were not shown any significant difference in the feces of *Atg7*$^{f/f}$ and *Atg7*$^{\Delta CD11c}$ mice (Fig. 6A). The proportion of *Bacteroidia* (class), *Bacteroidales* (order), *Bacteroidaceae* (family), and *Bacteroides* (genus) were also shown similar or not significantly changed (Fig. 6B). However, interestingly, when I have analyzed species levels, the ratio of *Bacteroides* (*B.*) *acidifaciens* has significantly expanded in the feces of *Atg7*$^{\Delta CD11c}$ mice as compared to those in *Atg7*$^{f/f}$ mice (5.48 ± 1.76 % vs. 0.77 ± 0.18 %) (Fig. 6C and red arrow in Fig. 6D). On the other hands, proportion of *B. sartorii*, another anaerobic *Bacteroides* species in the mouse commensal bacteria, was not altered in the feces of *Atg7*$^{\Delta CD11c}$ and *Atg7*$^{f/f}$ mice (blue arrow in Fig. 6D). To further confirm the expansion of *B. acidifaciens* in *Atg7*$^{\Delta CD11c}$ mice with lean phenotype, fluorescence *in situ* hybridization (*FISH*) analysis were used. As shown in Fig 6E, increased numbers of *B. acidifaciens* were detected in the lumen of the colon and few *B. acidifaciens* were internalized in the colon

intestinal epithelial cells (IECs) of *Atg7*$^{\Delta CD11c}$ mice. Taken together, *B. acidifaciens* among the commensal bacteria are skewed in the gut of *Atg7*$^{\Delta CD11c}$ mice with lean phenotype.

A.

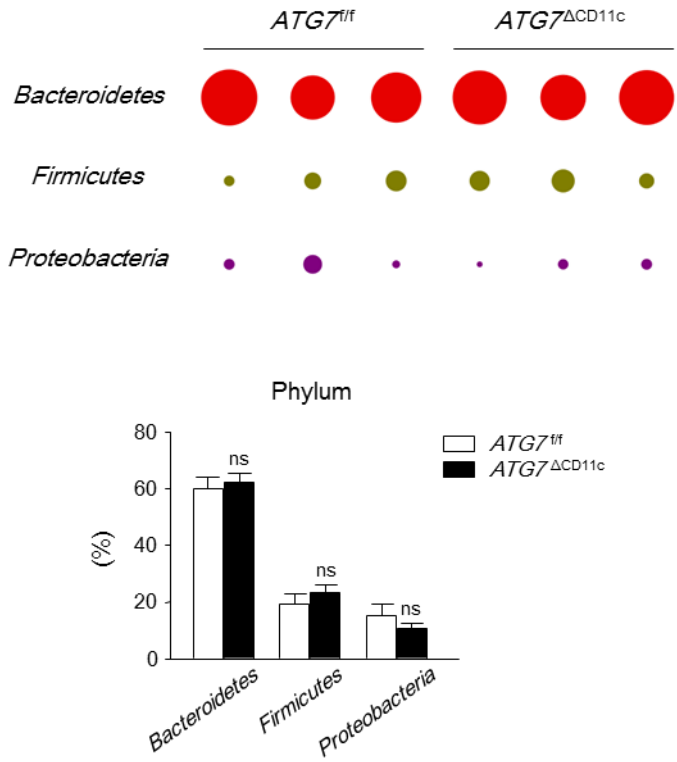
ATG7f/f
ATG7ΔCD11c
Bacteroidetes
Firmicutes
Proteobacteria
Phylum
ATG7f/f
ATG7ΔCD11c
(%)
80
60
40
20
0
ns
ns
ns
Bacteroidetes
Firmicutes
Proteobacteria

B.

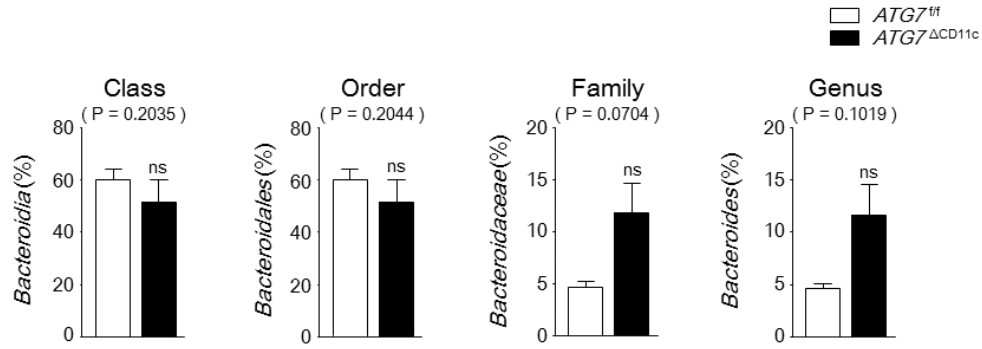
ATG7f/f
ATG7ΔCD11c
Class
(P = 0.2035)
Bacteroidia(%)
Order
(P = 0.2044)
Bacteroidales(%)
Family
(P = 0.0704)
Bacteroidaceae(%)
Genus
(P = 0.1019)
Bacteroides(%)
ns

C.

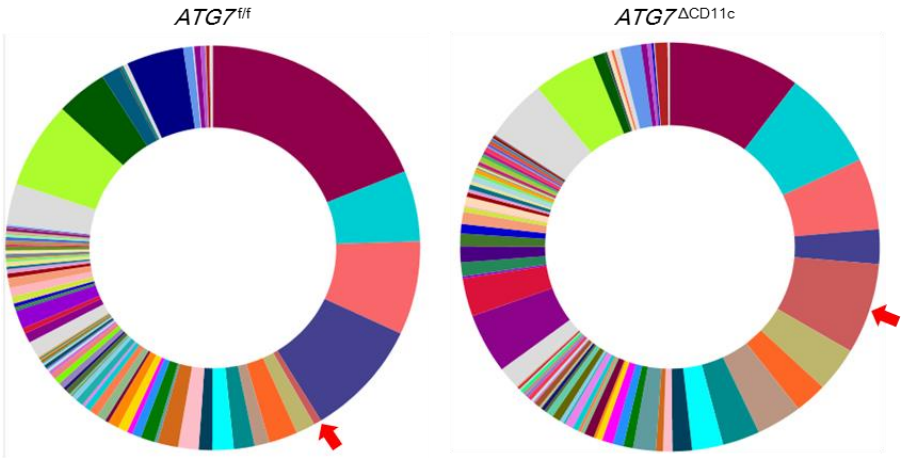
ATG7f/f
ATG7ΔCD11c

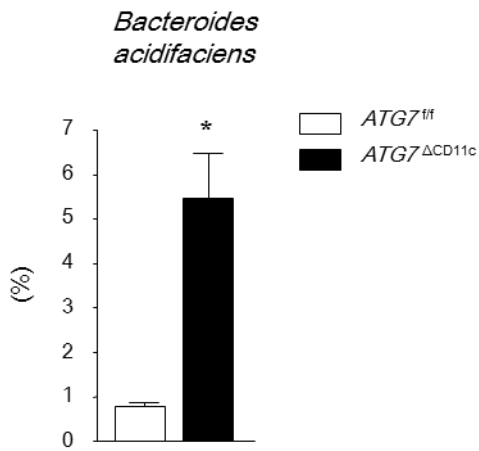
Bacteroides acidifaciens
*
ATG7f/f
ATG7ΔCD11c
(%)
0
1
2
3
4
5
6
7

D.

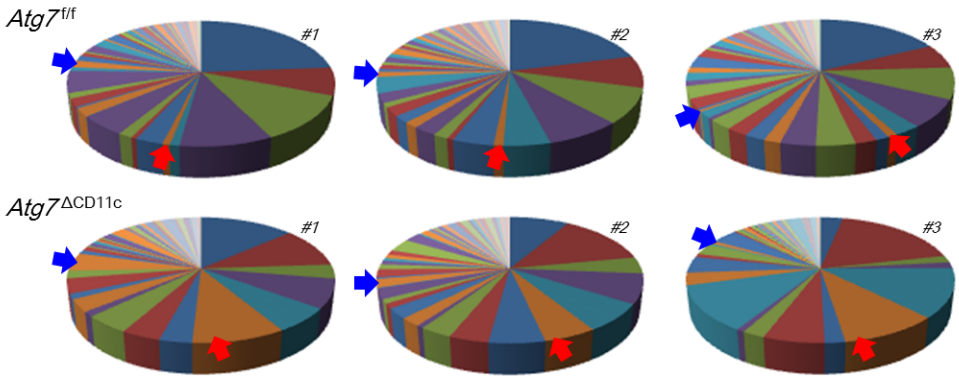

Bacteria;;;Bacteroidetes;;Bacteroidia;;Bacteroidales;;EF602759_f;EF602759_g;EF602759_s
Bacteria;;;Bacteroidetes;;Bacteroidia;;Bacteroidales;;Prevotellaceae;;Prevotella;DQ815942_s
Bacteria;;;Bacteroidetes;;Bacteroidia;;Bacteroidales;;EF602759_f;EF602759_f_uc;EF602759_f_uc_s
Bacteria;;;Bacteroidetes;;Bacteroidia;;Bacteroidales;;EF602759_f;DQ815871_g;DQ815871_g_uc
Bacteria;;;Firmicutes;;Clostridia;;Clostridiales;;Lachnospiraceae;;EF604627_g;AB606279_s
Bacteria;;;Bacteroidetes;;Bacteroidia;;Bacteroidales;;Bacteroidaceae;;Bacteroides;Bacteroides acidifaciens
Bacteria;;;Bacteroidetes;;Bacteroidia;;Bacteroidales;;EF602759_f;AY239469_g;4P003630_s
Bacteria;;;Firmicutes;;Clostridia;;Clostridiales;;Lachnospiraceae;;EU006430_g;EU006430_s
Bacteria;;;Bacteroidetes;;Bacteroidia;;Bacteroidales;;Bacteroidaceae;;Bacteroides;EF604598_s
Bacteria;;;Proteobacteria;;Betaproteobacteria;;Burkholderiales;;Sutterella_f;;Parasutterella;AJ308395_s
Bacteria;;;Tenericutes;;Mollicutes;;Acholeplasmatales;;Acholeplasmataceae;;Acholeplasma_g2;Acholeplasma_g2_uc
Bacteria;;;Bacteroidetes;;Bacteroidia;;Bacteroidales;;Porphyromonadaceae;;Parabacteroides;Parabacteroides distasonis
Bacteria;;;Deferribacteres;;Deferribacteres_c;;Deferribacterales;;Deferribacteraceae;;Mucispirillum;Mucispirillum schaedleri
Bacteria;;;Bacteroidetes;;Bacteroidia;;Bacteroidales;;EF602759_f;EU622683_g;EF406456_s
Bacteria;;;Bacteroidetes;;Bacteroidia;;Bacteroidales;;Bacteroidaceae;;Bacteroides;AB021165_s
Bacteria;;;Tenericutes;;Mollicutes;;Acholeplasmatales;;Acholeplasmataceae;;Acholeplasma_g2;EF406813_s
Bacteria;;;Firmicutes;;Clostridia;;Clostridiales;;Lachnospiraceae;;EF603662_g;EF603662_s
Bacteria;;;Bacteroidetes;;Bacteroidia;;Bacteroidales;;Bacteroidaceae;;Bacteroides;Bacteroides sartorii
Bacteria;;;Bacteroidetes;;Bacteroidia;;Bacteroidales;;Prevotellaceae;;Prevotella;EU622763_s
Bacteria;;;Bacteroidetes;;Bacteroidia;;Bacteroidales;;EF602759_f;EF602759_g;EU791194_s
Bacteria;;;Firmicutes;;Clostridia;;Clostridiales;;Ruminococcaceae;;EU791177_g;EU791177_s
Bacteria;;;Bacteroidetes;;Bacteroidia;;Bacteroidales;;Porphyromonadaceae;;Parabacteroides;EF096000_s
Bacteria;;;Bacteroidetes;;Bacteroidia;;Bacteroidales;;EF602759_f;AY239469_g;EF603769_s
Bacteria;;;Firmicutes;;Clostridia;;Clostridiales;;Ruminococcaceae;;Oscillibacter;DQ815311_s
Bacteria;;;Proteobacteria;;Deltaproteobacteria;;Desulfovibrionales;;Desulfovibrionaceae;;DQ815907_g;HM124141_s
Bacteria;;;Firmicutes;;Clostridia;;Clostridiales;;Ruminococcaceae;;Oscillibacter;JQ085130_s
Bacteria;;;Bacteroidetes;;Bacteroidia;;Bacteroidales;;Rikenellaceae;;Alistipes;DQ815748_s
Bacteria;;;Firmicutes;;Clostridia;;Clostridiales;;Lachnospiraceae;;DQ815599_g;DQ815599_s
Bacteria;;;Bacteroidetes;;Bacteroidia;;Bacteroidales;;EF602759_f;HM124280_g;EF603706_s
Bacteria;;;Bacteroidetes;;Bacteroidia;;Bacteroidales;;EF602759_f;DQ815871_g;DQ815871_s
Bacteria;;;Bacteroidetes;;Bacteroidia;;Bacteroidales;;Bacteroidales_uc;;Bacteroidales_uc_g;Bacteroidales_uc_s
Bacteria;;;Bacteroidetes;;Bacteroidia;;Bacteroidales;;EF602759_f;EF602759_g;EF097615_s
Bacteria;;;Firmicutes;;Clostridia;;Clostridiales;;HM124151_f;EF406417_g;EF406417_s
Bacteria;;;TM7;;TM7_c;;TM7_o;;TM7_f;AJ400239_g;AJ400239_s
Bacteria;;;Bacteroidetes;;Bacteroidia;;Bacteroidales;;EF602759_f;HM124280_g;EF406830_s
Bacteria;;;Bacteroidetes;;Bacteroidia;;Bacteroidales;;EF602759_f;AY239469_g;AY239469_g_uc
Bacteria;;;Bacteroidetes;;Bacteroidia;;Bacteroidales;;EF602759_f;AB606322_g;AB606322_s
Bacteria;;;TM7;;TM7_c;;TM7_o;;TM7_f;AJ400239_g;DQ777900_s
Bacteria;;;Bacteroidetes;;Bacteroidia;;Bacteroidales;;EF602759_f;FJ880046_g;EF406536_s
Bacteria;;;Proteobacteria;;Alphaproteobacteria;;EU939387_o;;AB270041_f;AB270041_g;AB270041_s
Bacteria;;;Firmicutes;;Clostridia;;Clostridiales;;Lachnospiraceae;;AB626939_g;FJ881271_s
Bacteria;;;Bacteroidetes;;Bacteroidia;;Bacteroidales;;EF602759_f;HM124280_g;HM124280_g_uc
Bacteria;;;Tenericutes;;Mollicutes;;Mycoplasmatales;;Mycoplasmataceae_f1;;Mycoplasmataceae_f1_uc;Mycoplasmataceae_f1_uc_s
Bacteria;;;Bacteroidetes;;Bacteroidia;;Bacteroidales;;EF602759_f;DQ815871_g;EF603109_s
Bacteria;;;Firmicutes;;Clostridia;;Clostridiales;;Lachnospiraceae;;DQ815599_g;HQ740248_s
Bacteria;;;Bacteroidetes;;Bacteroidia;;Bacteroidales;;EF602759_f;DQ815871_g;EF406459_s
Bacteria;;;Firmicutes;;Clostridia;;Clostridiales;;Lachnospiraceae;;Lachnospiraceae_uc;Lachnospiraceae_uc_s
Bacteria;;;Bacteroidetes;;Bacteroidia;;Bacteroidales;;EF602759_f;EF406806_g;EF406817_s
Bacteria;;;Firmicutes;;Clostridia;;Clostridiales;;Lachnospiraceae;;AB626958_g;EF604622_s
Bacteria;;;Firmicutes;;Clostridia;;Clostridiales;;Ruminococcaceae;;AM277340_g;FJ879877_s
Bacteria;;;Bacteroidetes;;Bacteroidia;;Bacteroidales;;EF602759_f;EF602759_g;EU457676_s

E.

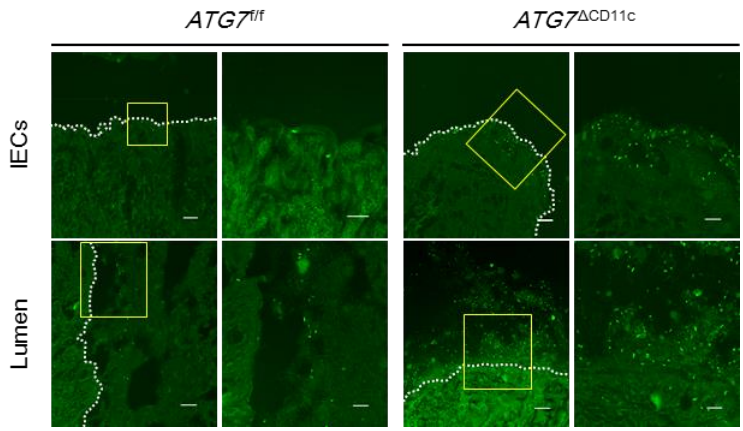

Figure 2.6. Pyrosequencing analysis in feces and confocal images of *Bacteroides acidifaciens*.

Pyrosequencing data were analyzed in terms of **(A)** phylum and **(B)** from class to genus level (n = 6). **(C).** The representative pie charts showing the proportion *B. acidifaciens* in feces detected by pyrosequencing analysis (n = 6). **(D).** Pie charts of bacterial composition in species levels of *Atg7*$^{f/f}$ and *Atg7*$^{\Delta CD11c}$ mice (n = 3), individually. The portion of *B. acidifaciens* and *B. sartorii* were indicated by red and blue arrow, respectively. The name of commensal bacteria was listed in top 50. **(E).** Increased numbers of *B. acidifaciens* in the intestinal epithelial cells (IECs) and lumen of colon of *Atg7*$^{f/f}$ and *Atg7*$^{\Delta CD11c}$ mice determined by fluorescence *in situ* hybridization (*FISH*) probe specified to *B. acidifaciens*. All data are presented as mean ± s.e.m. Statistical analyses were done with two-tailed paired *t*-test. *P<0.05.

II-3-7. Characterization of CD11c positive cells as phagocytes and antigen-presenting cells against *Bacteroides acidifaciens*.

To examine whether the expanded single commensal bacteria in *Atg7*$^{\Delta CD11c}$ mice was caused by deficiency of bacterial clearance through autophagy, I co-cultured CD11c positive cells of bone marrow-derived dendritic cells (BM-DCs) with *B. acidifaciens*. Interestingly, the number of *B. acidifaciens* inside BM-DCs at 24 hours after co-culture was significantly increased in *Atg7*$^{\Delta CD11c}$ mice, compared to that of control mice (Fig. 7A). Moreover, further analysis demonstrated that expanded *B. acidifaciens* in *Atg7*$^{\Delta CD11c}$ mice consequently affected to adaptive immune system, including elevated serum immunoglobulin G (IgG), IgA and fecal IgA specific for *B. acidifaciens*-derived antigens as well as increased co-stimulatory factors, such as CD40, CD80 and CD86 (Fig. 7B and Fig. 7C). Taken together, deleted function of autophagy in CD11c positive cells does not influence in both the capacity of antigen uptake and initiation of adaptive immunity.

A.

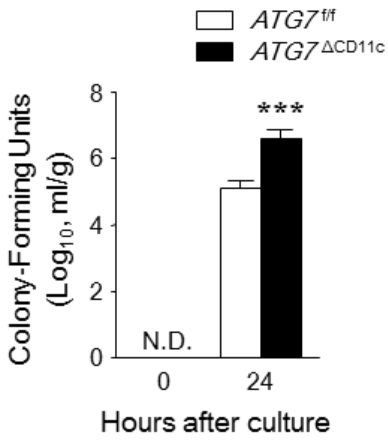
ATG7 f/f
ATG7 ΔCD11c
Colony-Forming Units
(Log10, ml/g)
8
6
4
2
0
***
N.D.
0
24
Hours after culture

B.

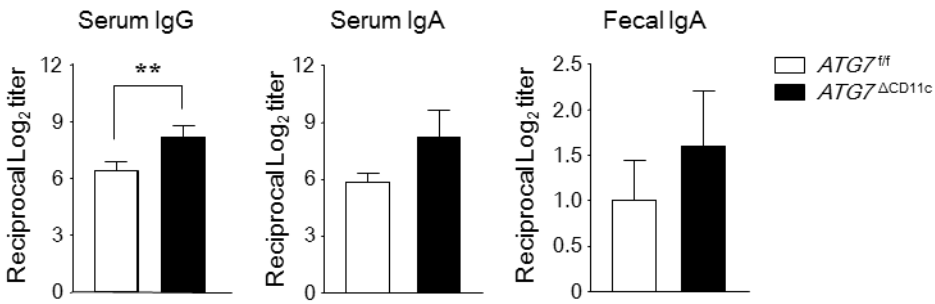
Serum IgG
Serum IgA
Fecal IgA
Reciprocal Log2 titer
12
9
6
3
0
**
2.5
2.0
1.5
1.0
0.5
ATG7 f/f
ATG7 ΔCD11c

C.

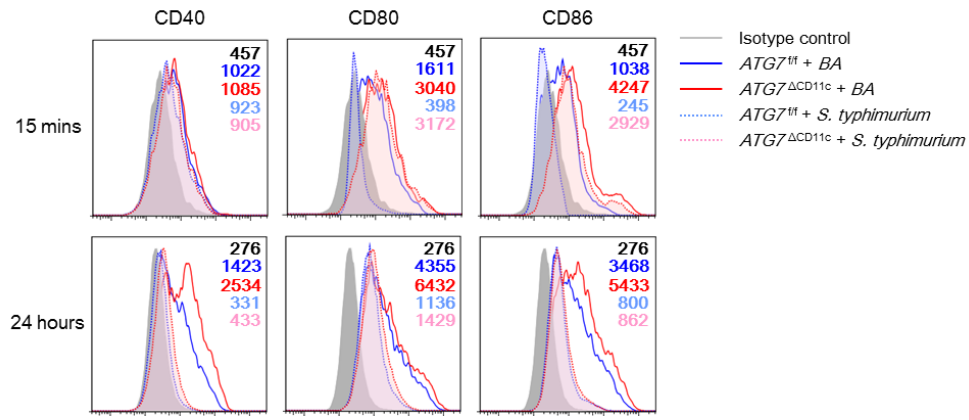
CD40
CD80
CD86
15 mins
24 hours
457
1022
1085
923
905
457
1611
3040
398
3172
457
1038
4247
245
2929
276
1423
2534
331
433
276
4355
6432
1136
1429
276
3468
5433
800
862
Isotype control
ATG7 f/f + BA
ATG7 ΔCD11c + BA
ATG7 f/f + S. typhimurium
ATG7 ΔCD11c + S. typhimurium

Figure 2.7. Colony forming units (CFUs) of *B. acidifaciens*, antibodies detection by Enzyme-linked immunosorbent assay (ELISA), and activation of co-stimulatory molecules by FACS analysis.

Lean phenotypes were originated from *B. acidifaciens* among gut commensal bacteria. **(A).** Colony-forming units (CFUs) of *B. acidifaciens* after 24 hours co-cultured with BM-DCs. **(B).** *B. acidifaciens*-specific antibodies responses were analyzed using serum and feces taken from $Atg7^{f/f}$ and $Atg7^{\Delta CD11c}$ mice by ELISA. **(C).** $CD11c^{+}$ cells differentiated from bone-marrows of $Atg7^{f/f}$ and $Atg7^{\Delta CD11c}$ mice were co-cultured with *B. acidifaciens* and *Salmonella typhimurium* as control, and then measured the expression levels of co-stimulatory molecules (i.e. CD40, CD80 and CD86) at 15 mins and 24 hours, respectively. All data are mean ± s.e.m. of at least two independent experiments. Statistical analyses were done with two-tailed paired *t*-test. **P<0.01 and ***P<0.001. N.D., not detected.

II-4. Discussion

Previous studies demonstrated that autophagy disruption would lead to insulin resistance and diabetes. For instance, mice deficient of *Atg7* in the pancreatic beta cells have significant defect on the insulin release and hyperglycemia (*26, 27*). In contrast, mice with skeletal muscle-specific deletion of *Atg7* showed decreased fat mass and diet-induced obesity, and protected from insulin resistance (*9*). Authors suggested mitochondrial dysfunction which provoked by autophagy disruption increased fibroblast growth factor 21 (Fgf21), a mitokine that contributes a strong effects on lipid mobilization. However, there are no reports about relationship between host lipid metabolisms and single commensal bacteria regulated by autophagy. I found mice with $CD11c^{+}$ cell specific autophagy deficiency revealed improved insulin sensitivity and expanded population of *Bacteroides acidifaciens*. On the other hands, while serum glucose levels were down regulated, high levels of insulin secretion were maintained in the $Atg7^{\Delta CD11c}$ mice. Therefore, I speculate that mitochondrial dysfunction by autophagy deficiency may improve insulin sensitivity but at the same time there might be uncontrolled insulin secretion by specific commensal bacteria.

B. acidifaciens were firstly isolated from the caecum of mice by Itoh K. et al (*23, 28*). These novel commensal bacteria were characterized anaerobic, gram-negative, good growth in bile acid and aesculin hydrolysis. Thereafter, their function was revealed by other group that *B. acidifaciens* possessing capacity to increase IL-6 and IL-10 production by enhancing expression of MHC class II and the co-stimulating molecules (i.e., CD80 and CD86) on antigen-presenting cells (*29*). In addition, *B. acidifaciens* is one of predominant commensal bacteria which responsible for promoting IgA Abs production in the large intestine specifically by inducing activation-induced cytidine deaminase expression (*30, 31*). Here, I noted another unique function that *B. acidifaciens* can modulate energy metabolisms and therefore applicable for therapeutic use for obesity and diabetes control.

Investigation of epidemiologic relationship between obesity and its causes revealed that environmental factors and host genetic background can influence the composition of gut commensal bacteria (*32*). The two phyla that consists the majority of gut commensal microbiota in the mammalian are the *Bacteroidetes* and the *Firmicutes*. Previous evidences in animal and human studies suggest that an increase ratio of *Firmicutes* to *Bacteroidetes* is making the gut microbiota more efficient to extract energy from the diet

and thereby can be one of causes for adiposity (*11*, *15*, *33*). In contrast, some studies described such alteration on phylum-level are too simple and insufficient to explain the mechanisms associated with adiposity and obesity (*34*, *35*). Those observations support our current finding that I could not find any changes in the proportion of *Firmicutes* and *Bacteroidetes* in feces of *Atg7*$^{\Delta CD11c}$ mice that are prone to lean compared to the littermate *Atg7*$^{f/f}$ mice (Fig. 6A). Instead, I found that specific species (i.e., *B. acidifaciens*) among *Bacteroidetes* phylum are largely expanded in the lean *Atg7*$^{\Delta CD11c}$ mice (Fig. 6C). Recent study revealed that cohousing obese mice with mice containing the lean twin′s microbiota prevented the body weight increase and obesity-associated metabolic phenotypes which correlated with invasion of specific members of *Bacteroides* such as *B. cellulosilyticus*, *B. uniformis*, *B. vulgatus*, *B. thetaiotaomicron*, and *B. caccae* (*16*). Furthermore, oral administration of *B. uniformis* CECT 7771 strain improved metabolic disorders and immunological dysfunction in HFD-induced obesity mice (*36*). In this study, I firstly identify *B. acidifaciens* which might be tightly regulated in steady-state condition by autophagy machinery of CD11c^{+} cells and might be associated with gut microbiota homeostasis for energy harvest.

There are two general cascades associated with weight loss; increased energy expenditure or reduced energy utilization/storage

efficiency. A NMR-based metabolic analysis revealed that there is clear segregation between *Atg7*$^{\Delta CD11c}$ and *Atg7*$^{f/f}$ mice (Fig. 4A). Loading plots shows SCFAs such as butyric acids, propionic acids and acetic acids are significantly lower and conversely lactate is higher in *Atg7*$^{\Delta CD11c}$ mice than those in *Atg7*$^{f/f}$ control mice (Fig. 4B). This profile of SCFAs is similar to the SPF mice fed with low-fiber diet (*37*). In this regards, caloric extraction from diet fiber is upregulated in the obese animal and human compared to the healthy control (*38*). Young mice administered subtherapeutic antibiotic therapy increased adiposity and revealed substantial increases in SCFAs in the caecal contents (*15*). Thus I assume that altered microbiota condition of *Atg7*$^{\Delta CD11c}$ mice seems to have poor caloric extraction propertied when compare to the control *Atg7*$^{f/f}$ mice. Given that SCFAs are good energy source for the host, the decrease of SCFAs levels may reduce energy supply and resulted in lean phenotype.

In summary, deletion of *autophagy-related gene 7* (*Atg7*) in CD11c^{+} cells alters commensal bacterial composition, especially expansion of *B. acidifaciens* belonging to *Bacteroides* genus. Current discovery of *B. acidifaciens* expanded in gut of *Atg7*$^{\Delta CD11c}$ mice suggests that commensal bacteria might be interlinked between autophagy deficiency and lean phenotypes. Although further studies are required to figure out whether *B.*

acidifaciens have a unique function to control host lipid metabolism, my finding suggest that a single commensal bacteria can be regulated by autophagy of CD11c positive cells.

II-5. References

1. **A. Kuma, M. Hatano, M. Matsui, A. Yamamoto, H. Nakaya, T. Yoshimori, Y. Ohsumi, T. Tokuhisa, N. Mizushima.** 2004. The role of autophagy during the early neonatal starvation period. *Nature* 432, 1032-1036.
2. **B. Levine, D. J. Klionsky.** 2004. Development by self-digestion: molecular mechanisms and biological functions of autophagy. *Developmental Cell* 6, 463-477.
3. **B. Levine, N. Mizushima, H. W. Virgin.** 2011. Autophagy in immunity and inflammation. *Nature* 469, 323-335.
4. **D. J. Klionsky.** 2010. The autophagy connection. *Developmental Cell* 19, 11-12.
5. **R. Singh, S. Kaushik, Y. Wang, Y. Xiang, I. Novak, M. Komatsu, K. Tanaka, A. M. Cuervo, M. J. Czaja.** 2009. Autophagy regulates lipid metabolism. *Nature* 458, 1131-1135.
6. **L. Yang, P. Li, S. Fu, E. S. Calay, G. S. Hotamisligil.** 2010. Defective hepatic autophagy in obesity promotes ER stress and causes insulin resistance. *Cell Metabolism* 11, 467-478.
7. **Y. Zhang, S. Goldman, R. Baerga, Y. Zhao, M. Komatsu, S. Jin.** 2009. Adipose-specific deletion of autophagy-related gene 7 (*atg7*) in mice reveals a role in adipogenesis. *Proceedings of the National Academy of Sciences of the United States of America* 106, 19860-19865.
8. **R. Singh, Y. Xiang, Y. Wang, K. Baikati, A. M. Cuervo, Y. K. Luu, Y. Tang, J. E. Pessin, G. J. Schwartz, M. J. Czaja.** 2009. Autophagy regulates adipose mass and differentiation in mice. *The Journal of Clinical Investigation* 119, 3329-3339.
9. **K. H. Kim, Y. T. Jeong, H. Oh, S. H. Kim, J. M. Cho, Y. N. Kim, S. S. Kim, H. Kim do, K. Y. Hur, H. K. Kim, T. Ko, J. Han, H. L. Kim, J. Kim, S. H. Back, M. Komatsu, H. Chen, D. C. Chan, M. Konishi, N. Itoh, C. S. Choi, M. S. Lee.** 2013. Autophagy deficiency leads to protection from obesity and insulin resistance by inducing Fgf21 as a mitokine. *Nature Medicine* 19, 83-92.
10. **N. M. Delzenne, A. M. Neyrinck, F. Backhed, P. D. Cani.** 2011. Targeting gut microbiota in obesity: effects of prebiotics and probiotics. *Nature Reviews Endocrinology* 7, 639-646.
11. **R. E. Ley, F. Backhed, P. Turnbaugh, C. A. Lozupone, R. D.**

Knight, J. I. Gordon. 2005. Obesity alters gut microbial ecology. *Proceedings of the National Academy of Sciences of the United States of America* 102, 11070-11075.

12. **R. E. Ley, P. J. Turnbaugh, S. Klein, J. I. Gordon.** 2006. Microbial ecology: human gut microbes associated with obesity. *Nature* 444, 1022-1023.
13. **P. J. Turnbaugh, R. E. Ley, M. A. Mahowald, V. Magrini, E. R. Mardis, J. I. Gordon.** 2006. An obesity-associated gut microbiome with increased capacity for energy harvest. *Nature* 444, 1027-1031.
14. **M. Vijay-Kumar, J. D. Aitken, F. A. Carvalho, T. C. Cullender, S. Mwangi, S. Srinivasan, S. V. Sitaraman, R. Knight, R. E. Ley, A. T. Gewirtz. 2010.** Metabolic syndrome and altered gut microbiota in mice lacking Toll-like receptor 5. *Science* 328, 228-231.
15. **I. Cho, S. Yamanishi, L. Cox, B. A. Methe, J. Zavadil, K. Li, Z. Gao, D. Mahana, K. Raju, I. Teitler, H. Li, A. V. Alekseyenko, M. J. Blaser.** 2012. Antibiotics in early life alter the murine colonic microbiome and adiposity. *Nature* 488, 621-626.
16. **V. K. Ridaura, J. J. Faith, F. E. Rey, J. Cheng, A. E. Duncan, A. L. Kau, N. W. Griffin, V. Lombard, B. Henrissat, J. R. Bain, M. J. Muehlbauer, O. Ilkayeva, C. F. Semenkovich, K. Funai, D. K. Hayashi, B. J. Lyle, M. C. Martini, L. K. Ursell, J. C. Clemente, W. Van Treuren, W. A. Walters, R. Knight, C. B. Newgard, A. C. Heath, J. I. Gordon.** 2013. Gut microbiota from twins discordant for obesity modulate metabolism in mice. *Science* 341, 1241214.
17. **F. Backhed, H. Ding, T. Wang, L. V. Hooper, G. Y. Koh, A. Nagy, C. F. Semenkovich, J. I. Gordon.** 2004. The gut microbiota as an environmental factor that regulates fat storage. *Proceedings of the National Academy of Sciences of the United States of America* 101, 15718-15723.
18. **H. V. Lin, A. Frassetto, E. J. Kowalik, Jr., A. R. Nawrocki, M. M. Lu, J. R. Kosinski, J. A. Hubert, D. Szeto, X. Yao, G. Forrest, D. J. Marsh.** 2012. Butyrate and propionate protect against diet-induced obesity and regulate gut hormones via free fatty acid receptor 3-independent mechanisms. *PLoS One* 7, e35240.
19. **Z. Gao, J. Yin, J. Zhang, R. E. Ward, R. J. Martin, M. Lefevre, W. T. Cefalu, J. Ye.** 2009. Butyrate improves insulin sensitivity and increases energy expenditure in mice. *Diabetes* 58, 1509-1517.
20. **I. Kimura, K. Ozawa, D. Inoue, T. Imamura, K. Kimura, T. Maeda, K. Terasawa, D. Kashihara, K. Hirano, T. Tani, T.**

Takahashi, S. Miyauchi, G. Shioi, H. Inoue, G. Tsujimoto. 2013. The gut microbiota suppresses insulin-mediated fat accumulation via the short-chain fatty acid receptor GPR43. *Nature Communications* 4, 1829.

21. **B. P. Willing, A. Vacharaksa, M. Croxen, T. Thanachayanont, B. B. Finlay.** 2011. Altering host resistance to infections through microbial transplantation. *PLoS One* 6, e26988.
22. **T. H. Sannasiddappa, A. Costabile, G. R. Gibson, S. R. Clarke.** 2011. The influence of *Staphylococcus aureus* on gut microbial ecology in an in vitro continuous culture human colonic model system. *PloS One* 6, e23227
23. **Y. Momose, S. H. Park, Y. Miyamoto, K. Itoh.** 2011. Design of species-specific oligonucleotide probes for the detection of Bacteroides and Parabacteroides by fluorescence in situ hybridization and their application to the analysis of mouse caecal *Bacteroides-Parabacteroides* microbiota. *Journal of Applied Microbiology* 111, 176-184.
24. **G. F. Sonnenberg, L. A. Monticelli, T. Alenghat, T. C. Fung, N. A. Hutnick, J. Kunisawa, N. Shibata, S. Grunberg, R. Sinha, A. M. Zahm, M. R. Tardif, T. Sathaliyawala, M. Kubota, D. L. Farber, R. G. Collman, A. Shaked, L. A. Fouser, D. B. Weiner, P. A. Tessier, J. R. Friedman, H. Kiyono, F. D. Bushman, K. M. Chang, D. Artis.** 2012. Innate lymphoid cells promote anatomical containment of lymphoid-resident commensal bacteria. *Science* 336, 1321-1325.
25. **Y. W. Lim, B. K. Kim, C. Kim, H. S. Jung, B. S. Kim, J. H. Lee, J. Chun.** 2010. Assessment of soil fungal communities using pyrosequencing. *Journal of Microbiology* 48, 284-289**.**
26. **C. Ebato, T. Uchida, M. Arakawa, M. Komatsu, T. Ueno, K. Komiya, K. Azuma, T. Hirose, K. Tanaka, E. Kominami, R. Kawamori, Y. Fujitani, H. Watada.** 2008. Autophagy is important in islet homeostasis and compensatory increase of beta cell mass in response to high-fat diet. *Cell Metabolism* 8, 325-332**.**
27. **H. S. Jung, K. W. Chung, J. Won Kim, J. Kim, M. Komatsu, K. Tanaka, Y. H. Nguyen, T. M. Kang, K. H. Yoon, J. W. Kim, Y. T. Jeong, M. S. Han, M. K. Lee, K. W. Kim, J. Shin, M. S. Lee.** 2008. Loss of autophagy diminishes pancreatic beta cell mass and function with resultant hyperglycemia. *Cell Metabolism* 8, 318-324.
28. **Y. Miyamoto, K. Itoh.** 2000. *Bacteroides acidifaciens* sp. isolated from the caecum of mice. *International Journal of Systematic and*

Evolutionary Microbiology 50 Pt 1, 145-148.

29. **M. Tsuda, A. Hosono, T. Yanagibashi, S. Hachimura, K. Hirayama, K. Itoh, K. Takahashi, S. Kaminogawa.** 2007. Prior stimulation of antigen-presenting cells with *Lactobacillus* regulates excessive antigen-specific cytokine responses in vitro when compared with *Bacteroides*. *Cytotechnology* 55, 89-101.
30. **T. Yanagibashi, A. Hosono, A. Oyama, M. Tsuda, S. Hachimura, Y. Takahashi, K. Itoh, K. Hirayama, K. Takahashi, S. Kaminogawa.** 2009. *Bacteroides* induce higher IgA production than *Lactobacillus* by increasing activation-induced cytidine deaminase expression in B cells in murine Peyer's patches. *Bioscience, Biotechnology, and Biochemistry* 73, 372-377.
31. **T. Yanagibashi, A. Hosono, A. Oyama, M. Tsuda, A. Suzuki, S. Hachimura, Y. Takahashi, Y. Momose, K. Itoh, K. Hirayama, K. Takahashi, S. Kaminogawa.** 2013. IgA production in the large intestine is modulated by a different mechanism than in the small intestine: *Bacteroides acidifaciens* promotes IgA production in the large intestine by inducing germinal center formation and increasing the number of IgA^+ B cells. *Immunobiology* 218, 645-651.
32. **A. Spor, O. Koren, R. Ley.** 2011. Unravelling the effects of the environment and host genotype on the gut microbiome. *Nature Reviews Microbiology* 9, 279-290.
33. **P. J. Turnbaugh, F. Backhed, L. Fulton, J. I. Gordon.** 2008. Diet-induced obesity is linked to marked but reversible alterations in the mouse distal gut microbiome. *Cell Host & Microbe* 3, 213-223.
34. **E. F. Murphy, P. D. Cotter, S. Healy, T. M. Marques, O. O'Sullivan, F. Fouhy, S. F. Clarke, P. W. O'Toole, E. M. Quigley, C. Stanton, P. R. Ross, R. M. O'Doherty, F. Shanahan. 2010.** Composition and energy harvesting capacity of the gut microbiota: relationship to diet, obesity and time in mouse models. *Gut* 59, 1635-1642.
35. **C. K. Fleissner, N. Huebel, M. M. Abd El-Bary, G. Loh, S. Klaus, M. Blaut.** 2010. Absence of intestinal microbiota does not protect mice from diet-induced obesity. *The British Journal of Nutrition* 104, 919-929.
36. **P. Gauffin Cano, A. Santacruz, A. Moya, Y. Sanz.** 2012. Bacteroides uniformis CECT 7771 ameliorates metabolic and immunological dysfunction in mice with high-fat-diet induced obesity. *PLoS One* 7, e41079.
37. **Y. Furusawa, Y. Obata, S. Fukuda, T. A. Endo, G. Nakato, D.**

Takahashi, Y. Nakanishi, C. Uetake, K. Kato, T. Kato, M. Takahashi, N. N. Fukuda, S. Murakami, E. Miyauchi, S. Hino, K. Atarashi, S. Onawa, Y. Fujimura, T. Lockett, J. M. Clarke, D. L. Topping, M. Tomita, S. Hori, O. Ohara, T. Morita, H. Koseki, J. Kikuchi, K. Honda, K. Hase, H. Ohno. 2013. Commensal microbe-derived butyrate induces the differentiation of colonic regulatory T cells. *Nature* 504, 446-450.

38. **H. Tilg, A. Kaser.** 2011. Gut microbiome, obesity, and metabolic dysfunction. *The Journal of Clinical Investigation* 121, 2126-2132.

Chapter III. Gut commensal *Bacteroides acidifaciens* improves insulin sensitivity and prevents obesity in mice

III-1. Introduction

Bacteroides is a Gram-negative, obligately anaerobe, motile or nonmotile, and non-endospore forming bacterium belonging to the Enterobacteriaceae family. *Bacteroides* is one of the subcategory of *Bacteroidetes* phylum (*1*). *Bacteroides* are primary fermenters that lead carbohydrates to enter the network of syntrophic links within gut microflora. *Bacteroides* degrade carbohydrates to their component monosaccharides, which are metabolized to produce phosphenolpyruvate (PEP) converted to fermentation end products such as succinate and acetate. These products can be changed to butyrate by *Firmicutes*, which in turn can be taken up by the host and increase mucus production (*2*).

Obesity is one of leading social issue worldwide due to potentials to cause type 2 diabetes, cardiovascular disorder, cancer, and asthma (*3*). Although therapeutic trials to obesity become more complicated due to diverse life styles and genetic polymorphisms, it is obvious that obesity is caused by energy imbalance (*4*). Therefore, lots of scientific efforts are attempting to find contributing environmental factors that influence on the energy balance.

Bile acids are the main organic materials forming bile juice, and

especially play a critical physiological role in the liver and gastrointestinal organ (*5*). Bile acids are classified into primary- and secondary bile acids depending on their places to be created. The primary bile acids are synthesized from cholesterol to cholic acid (CA) and chenodeoxycholic acid (CDCA) by a variety of enzymes in liver (*5*). The commensal bacteria deconjugate residues that increase the water solubility of bile acids, and produce secondary bile acids like deoxycholic acid (DCA), lithocholic acid (LCA), ursodeoxycholic acid (UDCA) (*6*, *7*). Once the fat is entered into the gastrointestinal tract, the stored bile is secreted into the small intestine inside. Bile acid of 95 % remained in the intestinal area immediately after the completion of the function as digestive enzymes are mostly reabsorbed by active transport in ileum of small intestine, and repeats enterohepatic circulation (*8*).

To clarify the function of *Bacteroides acidifaciens* expanded in *Atg7*$^{\Delta CD11c}$ mice showing lean phenotypes, I orally administrated these bacteria to C57BL/6 mice everyday. Remarkably, *B. acidifaciens*-fed mice were shown the amelioration of metabolic disorders through TGR5-PPARα signals. My results suggest that single strain of commensal bacteria can be used as therapeutic agents for modulating metabolic disorders such as obesity.

III-2. Materials and Methods

III-2-1. Ethics statement

All animal experiments were approved by the Institutional Animal Care and Use Committee of the Asan biomedical research center (Approval No: PN 2014-13-069). All experiment was performed under anesthesia with a mixture of ketamine (100 mg/kg) and xylazine (20 mg/kg), and all efforts were made to minimize suffering.

III-2-2. Mice and bacteria strains

C57BL/6 (B6) and *CD11c*^{cre} mice were purchased from Charles River Laboratories (Orient Bio Inc., Sungnam, Korea) and Jackson Laboratory (Bar Harbor, ME), respectively. *ATG7*$^{flox/flox}$ mice were kindly provided by Dr. Masaaki Komatsu (Tokyo Metroplitan Institue of Medical Science, Japan). All mice were maintained under specific pathogen-free conditions in the animal facility at the Asan biomedical research center (Seoul, Korea) where they received sterilized food and water *ad libitum*. *Bacteroides* (*B.*) *acidifaciens* (JCM10556) and *B. sartorii* (JCM17136) used in this study were purchased from Japan Collection of Microorganisms (JCM) at RIKEN BioResource Center.

III-2-3. Bacteria culture and administration

B. acidifaciens and *B. sartorii* were grown in peptone-yeast-glucose (PYG) broth at 37 ^{o}C for 48 hours anaerobically with BBL^{TM} GasPak 100^{TM} EZ gas generating container (Becton Dickinson, Sparks, MD). The bacteria were concentrated by centrifuging for 15 minutes at 5,000 g and resuspended with sterile PBS. For therapeutic studies, mice were orally administered *B. acidifaciens* (5×10^{10} CFU/ml) or *B. sartorii* (5×10^{10} CFU/ml) everyday for a period of 10 weeks. The actual bacterial dose given was confirmed by plating serial dilutions onto EG blood agar plates.

III-2-4. Magnetic resonance imaging (MRI) analysis

All MRI experiments were performed at 9.4 T / 160 mm by Agilent MRI scanner (Agilent Technologies, Santa Clara, CA) using a millipede-shaped volume radiofrequency coil. All animals were anesthetized through a mask by spontaneous inhalation of 1.5 ~ 2% isoflurane. Shimming was performed to minimize B0 inhomogeneity prior to MR scanning both automatically and manually. The axial T1-weighted (T1-WI) fast spin echo (FSE) images was used to cover both kidneys completely. The parameters of T1-WI image were TR = 1100 msec, kzero = 1, echo spacing (ESP) =

9.82 msec (effective TE = 48 msec), 48 segments, echo train length (ETL) = 4, 4 averages, matrix = 192 × 192, the field of view (FOV) = 25 × 30 mm, slice thickness = 1.0 mm; and total scan time = 3 min 33 sec, respectively. During MR scanning, external triggering was used to eliminate respiratory motion artifacts.

III-2-5. MRI data analysis

Image J software (US National Institutes of Health, Bethesda, MD; http://rsb.info.nih.gov/ij/) was used for segmentation and measurement of compartments for MR images. We chose two representative MRI sections at the center of kidney level and at the kidney low pole. Then, the regions of interest were manually drawn to encompass the entire abdomen in order to calculate the total abdominal area and to encompass the peritoneal cavity for calculation of a visceral fat area. Contours of the visceral fat area were then generated semi-automatically based on the threshold of signal intensity to select fatty tissue. If there was a non-fat component within the contours, we manually removed those components.

III-2-6. Fluorescence *in situ* hybridization (*FISH*) analysis

The localization of *B. acidifaciens* in the gut mucosa was detected by *FISH* method as previously described (*9*). In brief, the large intestines were isolated and fixed with 4 % formaldehyde and dehydrated with 15 % - and 30 % - sucrose in PBS consecutively. Then dehydrated tissues were embedded in OCT compound (Sakura Finetek, Tokyo, Japan), frozen, sliced into 5-μm sections, and dried thoroughly. Hybridization buffer containing 5 ng of oligonucleotide probe μl^{-1} [Bacid2 (5′-AACATGTTTCCACATTATT CAGG-3′)] was applied to the slide and incubated at 50 ^{o}C for 2 hours. Oligonucleotide probes labeled with FAM were synthesized by Bioneer Corporation (Daejeon, Korea). The slides were rinsed with washing buffer at 50 ^{o}C for 10 min. After mounting with PermaFluor (Thermo scientific, Fremont, CA), slides were viewed under a confocal laser microscope (Zeiss, Göttingen, Germany).

III-2-7. Histology

The visceral adipose tissues were washed with PBS and fixed in 4 % formaldehyde for 1 hour at 4 ^{o}C. Tissues were dehydrated by gradually soaking in alcohol and xylene and then embedded in paraffin. The paraffin-

embedded specimens were cut into 5-μm sections, stained with H&E, and viewed with a digital light microscope (Olympus, Tokyo, Japan).

III-2-8. Real-time PCR for tissues

Tissue RNA was extracted using TRIzol® (Invitrogen), and total RNA (0.5 μg) was reverse-transcribed into cDNA according to the manufacturer′s instructions. All signal mRNAs were normalized to GAPDH mRNA. Specific primer sets are listed in table 3.1. All reactions were performed in the same manner: 95 °C for 10 seconds, followed by 45 cycles of 95 °C for 15 seconds and 60℃ for 1 minute. The results were analyzed with real-time system AB 7900HT software (Life Technologies), and all values were normalized to the levels of GAPDH.

III-2-9. Analysis of metabolic parameters

Serum glucose, total cholesterol and triglyceride concentrations were determined using commercially available enzymatic assay kits (Asan Pharmacology, Seoul, Korea). Serum insulin levels were measured with an ultra-sensitive mouse insulin ELISA kit (Shibayagi, Gunma, Japan).

Table 3.1. List of specific primer sets used for real time-PCR

Target gene Symbol	Forward sequence	Reverse sequence
FasN	AGCACTGCCTTCGGTTCAGTC	AAGAGCTGTGGAGGCCACTTG
HSL	TCCTGGAACTAAGTGGACGCAAG	CAGACACACTCCTGCGCATAGAC
PEPCK	GTGTTTGTAGGAGCAGCCATGAGA	GCCAGGTATTTGCCGAAGTTGTAG
SCD1	TCGCCCCTACGACAAGAACA	GTAAGCCAGGCCCA
PPARγ	TGTCGGTTTCAGAAGTGCCTTG	TTCAGCTGGTCGATATCACTGGAG
PPARα	ACGCTCCCGACCCATCTTTAG	TCCATAAATCGGCACCAGGAA
PRDM16	CCTAGCCCTGAGCGATACTGTGA	ACAGACAATGGCTGGAATGGTG
PGC1α	CCGTAAATCTGCGGGATGATG	CAGTTTCGTTCGACCTGCGTAA
Cidea	CTGTCTCAATGTCAAAGCCACGA	TGTGCAGCATAGGACATAAACCTCA
GLUT4	CTGTAACTTCATTGTCGGCATGG	AGGCAGCTGAGATCTGGTCAAAC
TGR5	GGCCTGGAACTCTGTTATCG	GTCCCTCTTGGCTCTTCCTC
GAPDH	CTGGAGAAACCTGCCAAGTA	AGTGGGAGTTGCTGTTGAAG

III-2-10. Measurement of glucagon-like peptide-1 (GLP-1)

Blood samples were taken from control and *B. acidifaciens*-fed mice, and then centrifuged for 30 minutes at 1800 g at 4 ^{o}C. DPP4 inhibitor was added to separated serum, GLP-1 concentrations were determined using GLP-1 ELISA kit (Shibayagi, Gunma, Japan).

III-2-11. Measurement of dipeptidyl peptidase-4 (DPP-4)

The DPP-4 activity was performed as previously described (*10*). In brief, mice were orally administrated with 5 x 10^{10} CFU / ml of *B. acidifaciens*, its supernatents, and fresh growth medium after fasting for 6 hours, and then additionally administrated glucose 30 minutes later. After 15 min, the intestinal epithelial cells of ileum were taken from pre-treated mice, and washed with PBS to remove luminal contents. The minced tissues were spun down by centrifugation (8,000 rpm, 4 ^{o}C, 5 min), and then 50 μl of the supernatant is incubated with kit reagents for 2 hours at 37 ^{o}C using DPP-4 Glo protease assay (Promega, Madison, WI). Relative DPP-4 activity was converted into a percentage based on the values of media group.

III-2-12. Comprehensive laboratory animal monitoring system (CLAMS)

Individually, eleven- to twelve-week-old *B. acidifaciens*-fed mice and controls placed in CLAMS (Columbus Instruments, Columbus, OH) cages and monitored over a 5-day period. The hourly file displays all measurements for each parameter: volume of oxygen consumed (VO_2; ml/kg/h), volume of carbon dioxide produced (VCO_2; ml/kg/h), respiratory exchange ratio, heat (kcal/h), activity (XY total-, XY ambulatory-, and Z activity). The data were recorded during the 30 seconds sampling period.

III-2-13. Capillary electrophoresis time-of-flight mass spectrometry (CE-TOFMS) measurement

A quantitative analysis of charged metabolites by CE-TOFMS was performed as described previously with slight modification (*11*). Briefly, 10 mg of freeze-dried fecal samples were disrupted using 3 mm zirconia/silica beads (BioSpec Products, Bartlesville, OK) and homogenized with 400 µl MeOH containing 20 µM each of methionine sulfone (Wako, Osaka, Japan) for cations, MES (Dojindo, Kumamoto, Japan) and CSA (D-Camphol-10-sulfonic acid, Wako, Osaka, Japan) for anions as internal standards. Then, 200 µl of de-ionized water and 500 µl of chloroform were added. After

vigorous shaking using Shakemaster neo (Bio Medical Science, Tokyo, Japan) at 1,500 r.p.m. for 10 min, the solution was centrifuged at 4,600 so*g* for 15 min at 4 lution was centrifuged at 4 roductsads [BioSpec Profiltered through a Millipore 5,000 Da cutoff filter (Millipore, Billerica, MA)] to remove proteins. The filtrate was lyophilized and dissolved in 25 µl of water containing 200 µM each of 3-aminopyrrolidine (Sigma Aldrich, St. Louis, MO) and trimesate (Wako, Osaka, Japan) as reference compounds. All CE-TOFMS experiments were performed using an Agilent CE capillary electrophoresis system (Agilent Technologies, Santa Clara, CA), an Agilent G3250AA LC/ MSD TOF system, an Agilent 1100 series binary HPLC pump, and the G1603A Agilent CE-MS adapter and G1607A Agilent CE-ESI-MS sprayer kit. To identify peak annotation and quantification, the obtained data were processed using in-house software (MasterHands) (*12*).

III-2-14. Statistics

GraphPad Prism software (GraphPad, La Jolla, CA) was used for statistical analysis. Significant differences between two groups were analyzed with two-tailed paired *t*-test or Mann-Whitney *t*-test. Multiple groups were analyzed by two-way ANOVA followed by Bonferroni *post-hoc* test (*, $P < 0.05$; **, $P < 0.01$; ***, $P < 0.001$).

III-3. Results

III-3-1. The scheme of oral administration with *B. acidifaciens.*

To clarify whether expanded *B. acidifaciens* can regulate lipid metabolisms, I obtained *B. acidifaciens* from RIKEN (JCM10556), cultured for large volume, and fed to naïve B6 mice. In order to determine optimal condition for administration, quantification of *B. acidifaciens* were examined in colon tissue and feces of mice fed with *B. acidifaciens* (5×10^{10} CFU/ml) using *FISH* analysis. The numerous *B. acidifaciens* were detected in lumen and tip of colon epithelium cells at 1 day following oral administration (Fig. 1A) and disappeared thereafter (data not shown). In addition, *B. acidifaciens* were recovered in feces at peak of 2 days after oral feeding, and rapidly disappeared (Fig. 1B). Therefore, I concluded the scheme of oral administration with *B. acidifaciens* (5×10^{10} CFU/ml, everyday)

A.

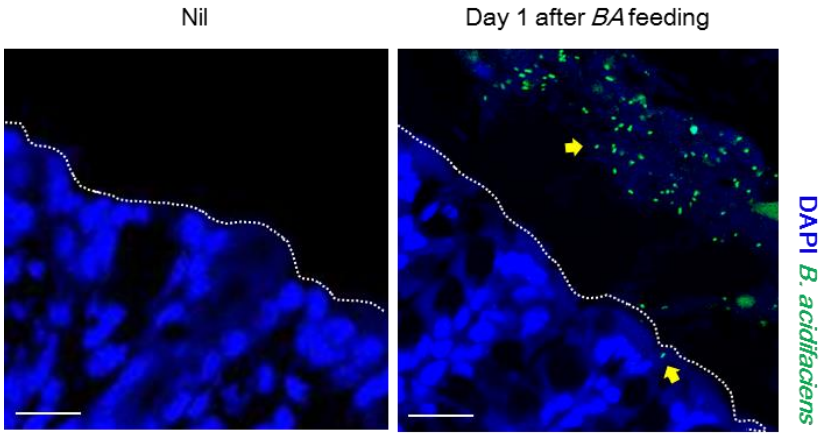
Nil
Day 1 after *BA* feeding
DAPI *B. acidifaciens*

B.

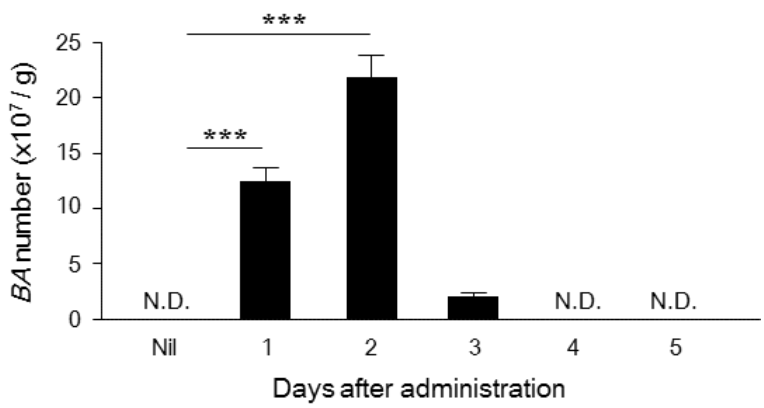
***
***
25
20
15
10
5
0
BA number (x10^7 / g)
N.D.
N.D.
N.D.
Nil
1
2
3
4
5
Days after administration

Figure 3.1. Confocal images of *B. acidifaciens* in colon and feces.

B. acidifaciens (*BA*) can temporarily reside in colon. Colon tissue and feces were obtained at nil, 1, 2, 3, 4, and 5 days after oral administration of *B. acidifaciens* (5 x 10^{10} CFU/ml), and then stained with *B. acidifaciens*-specific *FISH* probes. **(A).** Representative confocal images of *B. acidifaciens* (yellow arrow). **(B).** Quantification of *B. acidifaciens* in fecal extract at indicated time point. Numbers of *B. acidifaciens* were counted at least 20 regions per slide. Data are mean ± s.e.m. of three independent experiments. Statistical analyses were done with two-way ANOVA with Bonferroni *post-hoc* test. ***P<0.001. N.D., not detected.

III-3-2. Oral administration of *B. acidifaciens* leads to lean phenotypes in NCD- or HFD-fed B6 mice.

Wild-type B6 mice fed with *B. acidifaciens* for 10 weeks were shown reduced body weight and fat mass while similar levels of food intake between groups fed normal-chow diet (NCD) or high-fat diet (HFD) were detected (Fig. 2A-C). In contrast, *B. sartorri*-fed mice used as control anaerobic strain were not shown any loss of body weight (Fig. 2D). In addition, the size of a single adipocyte in epididymal adipose tissues taken from *B. acidifaciens*- and HFD-fed B6 mice was significantly smaller than that of PBS-fed HFD-fed mice (Fig. 2E). Collectively, long-term administration with *B. acidifaciens* promotes energy expenditure and consequently causes dominant lean phenotypes in diet-induced obesity mice.

A.

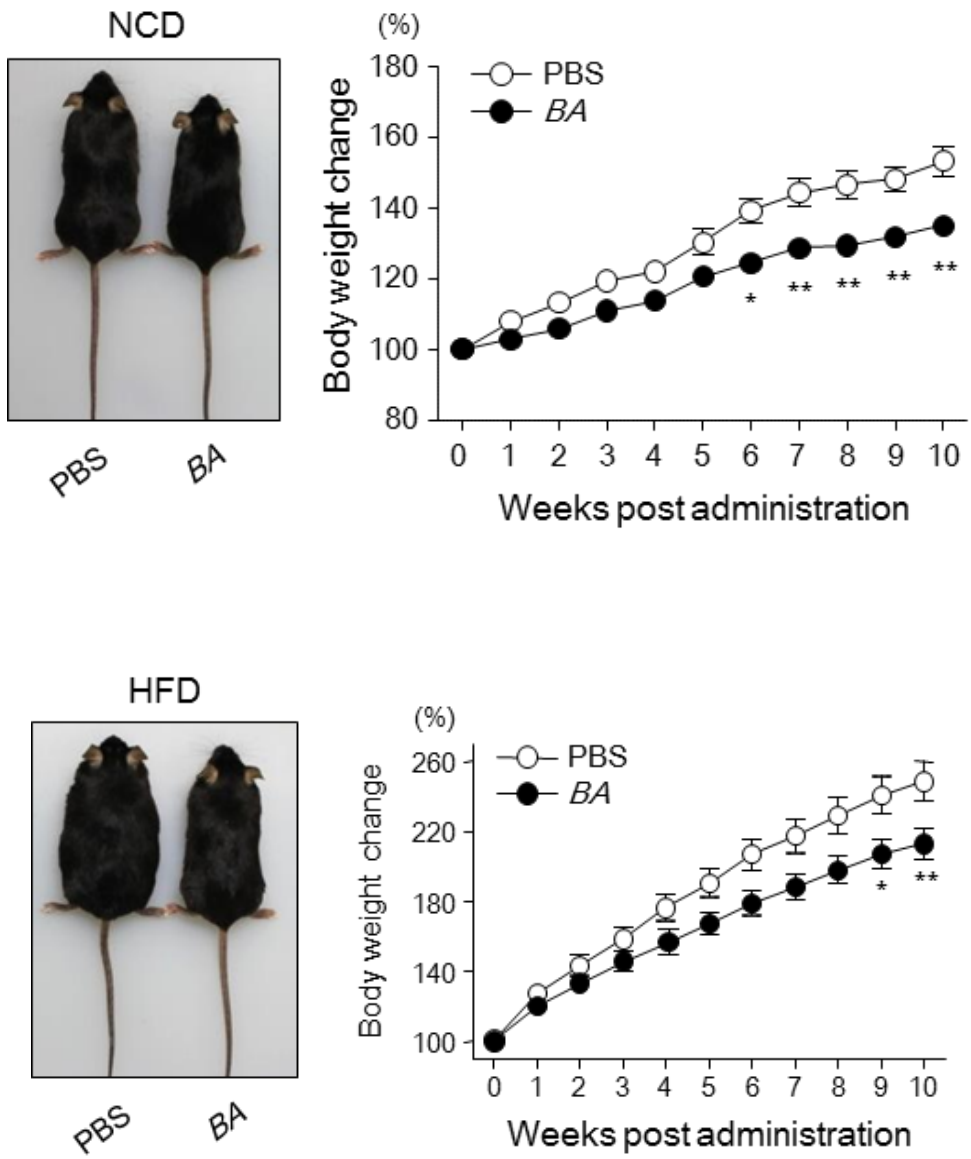
NCD
PBS
BA
(%)
Body weight change
PBS
BA
Weeks post administration
HFD
PBS
BA
(%)
Body weight change
PBS
BA
Weeks post administration

B.

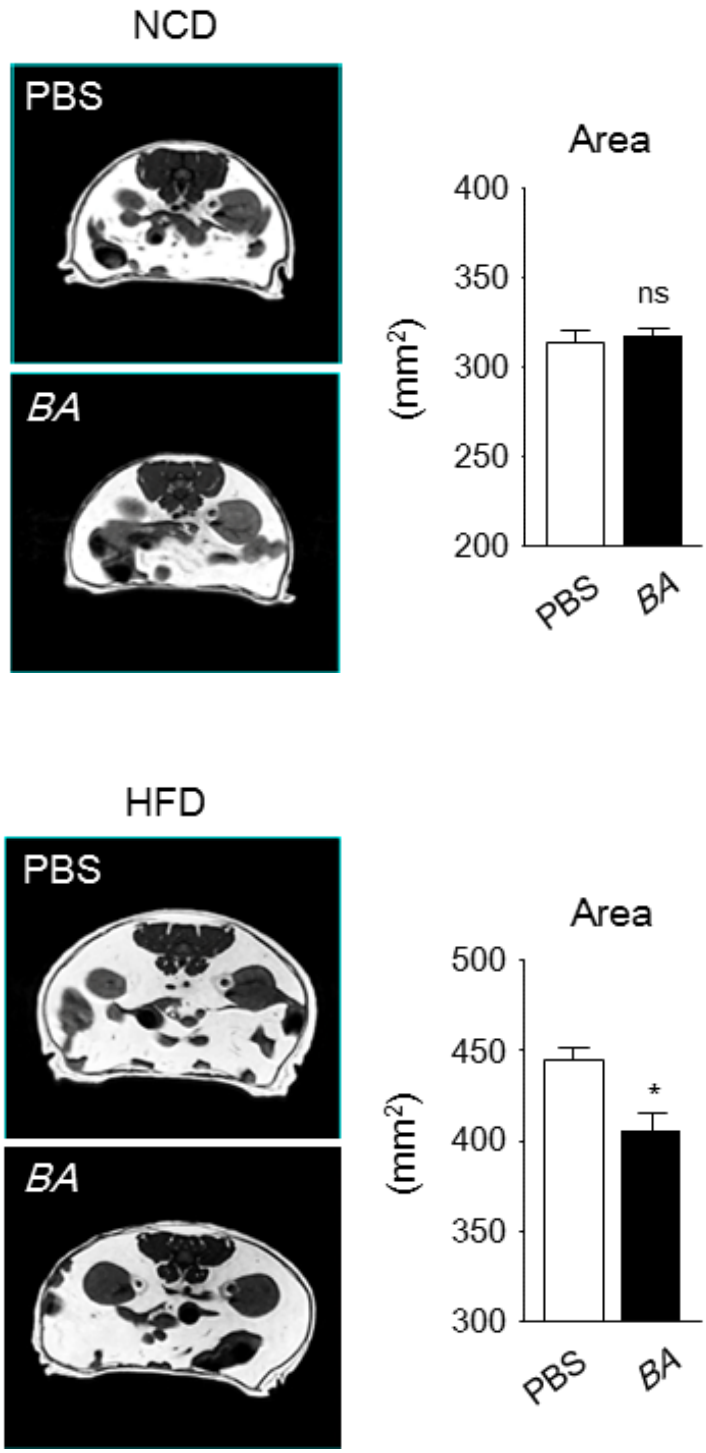
NCD
PBS
BA
Area
400
350
300
250
200
(mm²)
ns
PBS
BA
HFD
PBS
BA
Area
500
450
400
350
300
(mm²)
*
PBS
BA

C.

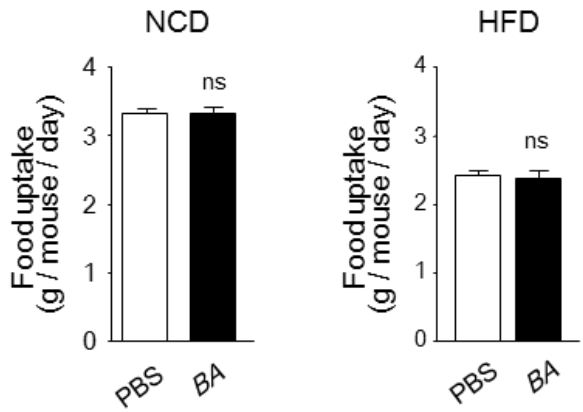
NCD
HFD
Food uptake
(g / mouse / day)
4
3
2
1
0
ns
ns
PBS
BA
PBS
BA

D.

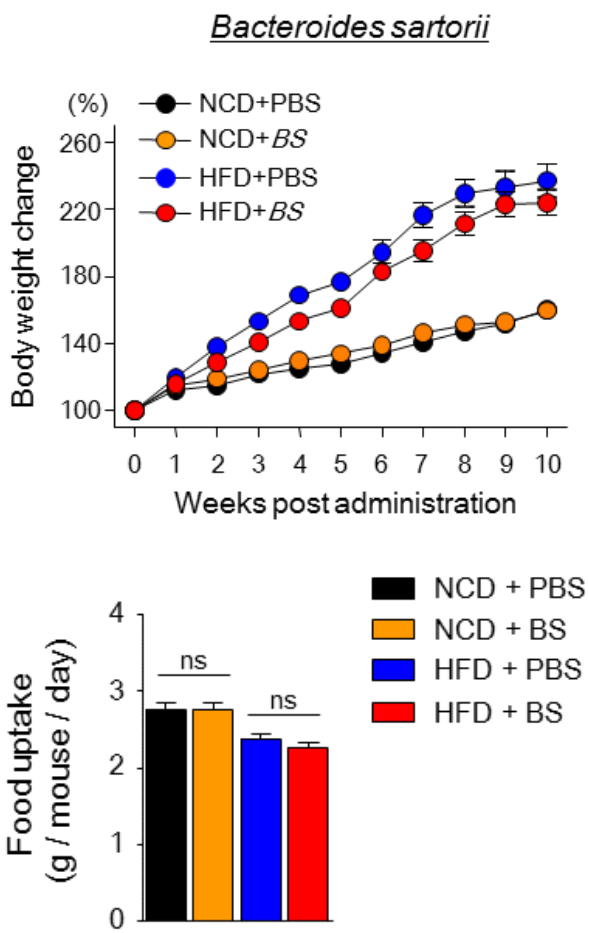
Bacteroides sartorii
(%)
NCD+PBS
NCD+BS
HFD+PBS
HFD+BS
Body weight change
260
220
180
140
100
0 1 2 3 4 5 6 7 8 9 10
Weeks post administration
NCD + PBS
NCD + BS
HFD + PBS
HFD + BS
Food uptake
(g / mouse / day)
4
3
2
1
0
ns
ns

E.

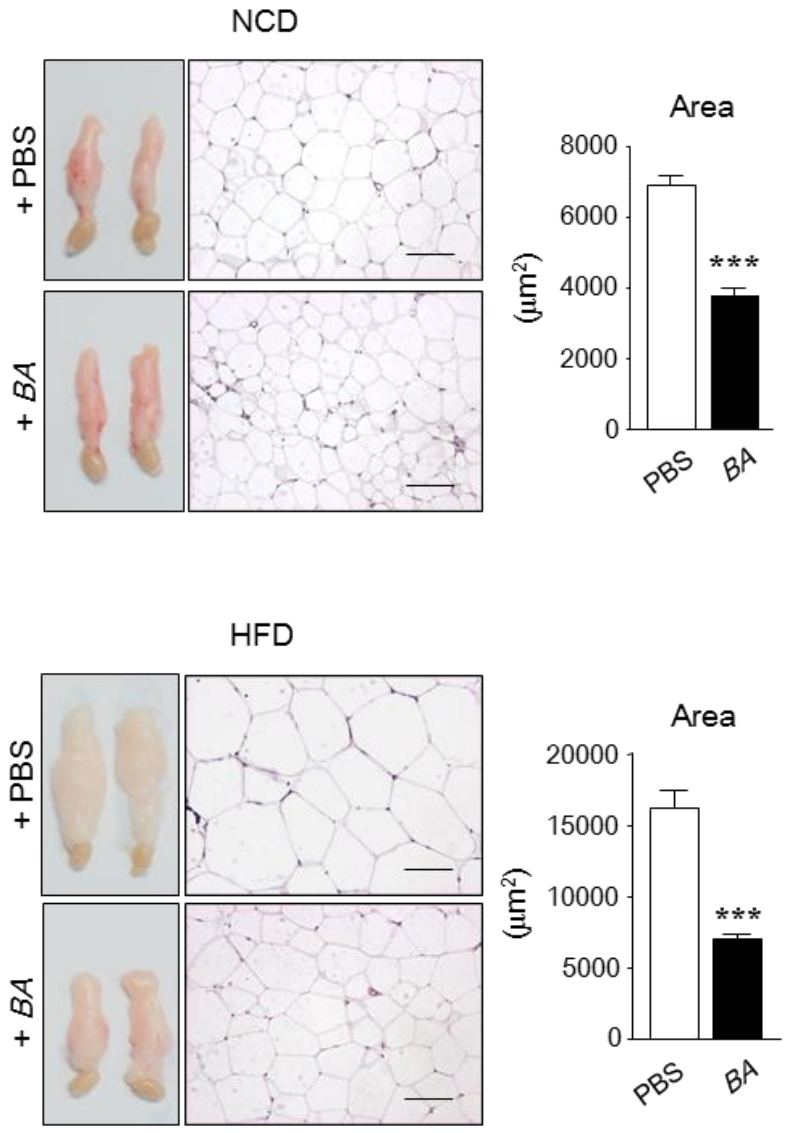
NCD
+ PBS
+ BA
Area
8000
6000
4000
2000
0
(μm²)
***
PBS
BA
HFD
+ PBS
+ BA
Area
20000
15000
10000
5000
0
(μm²)
***
PBS
BA

Figure 3.2. Representative photos, magnetic resonance imaging (MRI) analysis, and body / fat weight, and histologic analysis of adipose tissues. Effective functions of *B. acidifaciens* (BA) to regulate body weight and fat mass in diet-induced obesity mice. **(A).** Representative photos of PBS- and *B. acidifaciens*-fed B6 mice (left panel) and the body weight of each group was monitored for 10 weeks (right panel) during NCD (upper) and HFD (bottom). *B. acidifaciens* were orally administered ($5x10^{10}$ CFU/ml) everyday. **(B).** MRI analysis was examined with PBS- and *B. acidifaciens*-fed B6 mice. **(C).** Food intakes were checked everyday during *B. acidifaciens* feeding period. **(D**; upper panel**).** Monitoring of body weight for 10 weeks following oral administration of *B. sartorii* (5×10^{10} CFU/ml, everyday). **(D**; bottom panel**).** The food intakes were checked during oral feeding with PBS or *B. sartorii.* **(E).** Histological changes of adipose tissues (left panel) and size of adipocytes (right panel) of PBS- and *B. acidifaciens*-fed B6 mice. Scale bars = 50 μm. All data are presented as mean ± s.e.m. Statistical analyses were done with two-tailed paired *t*-test (**B, C**, and **E**) and two-way ANOVA with Bonferroni *post-hoc* test (**A** and **D**). *P<0.05, **P<0.01 and ***P<0.001. ns, not significant.

III-3-3. Increased insulin levels in serum and energy expenditure were detected in *B. acidifaciens*-fed B6 mice.

Of note, *B. acidifaciens*- and HFD-fed B6 mice were shown higher levels of insulin and lower levels of glucose than PBS- and HFD-fed B6 mice (Fig. 3A). Additionally, insulin resistance as determined by GTT and ITT was significantly improved in *B. acidifaciens*- and HFD-fed mice as compared to PBS- and HFD-fed mice (Fig. 3B). To further assess the energy expenditure, activity and substrate utilization, I next monitored mice fed with *B. acidifaciens* following individually housing in comprehensive laboratory animal monitoring system (CLAMS) cages for 5 days. Although groups of mice fed PBS or *B. acidifaciens* exhibited similar locomotor activity and respiratory exchange ratio (RER), HFD-B6 mice fed with *B. acidifaciens* revealed increased energy expenditure as compared to those mice fed PBS (Fig. 3C-E). Similar effects of oral *B. acidifaciens* were determined in the NCD-fed mice except energy expenditure (Fig. 3A-E). Collectively, long-term administration with *B. acidifaciens* promotes energy expenditure and consequently causes dominant lean phenotypes in diet-induced obesity mice.

A.

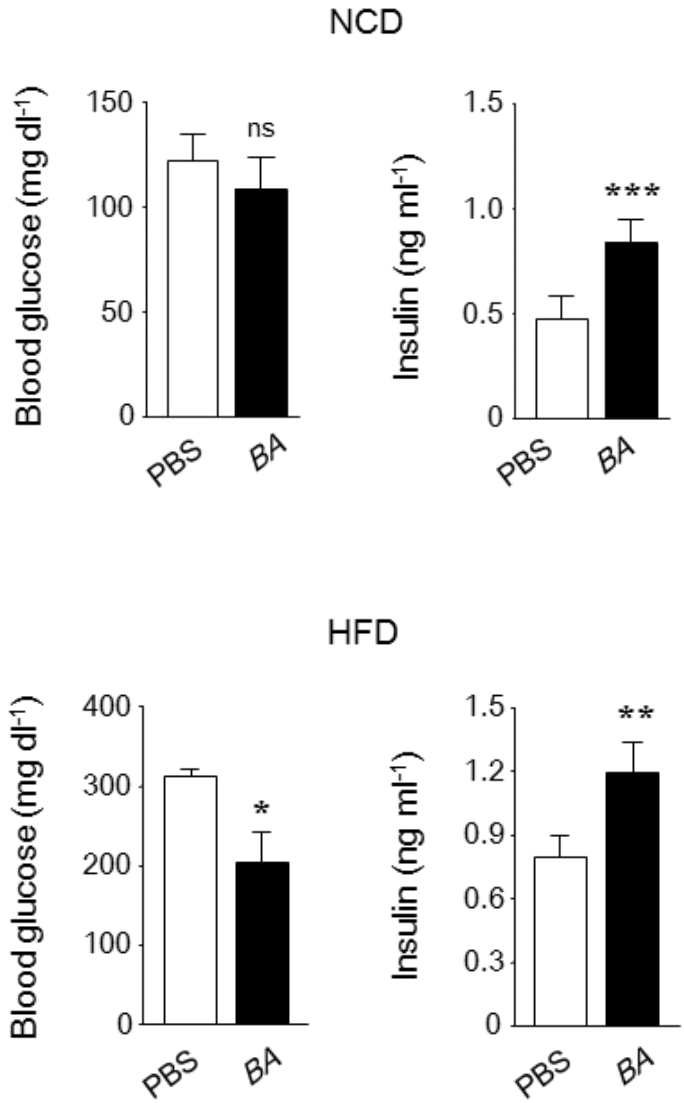
NCD
Blood glucose (mg dl-1)
150
100
50
0
ns
PBS
BA
Insulin (ng ml-1)
1.5
1.0
0.5
0
***
PBS
BA
HFD
Blood glucose (mg dl-1)
400
300
200
100
0
*
PBS
BA
Insulin (ng ml-1)
1.5
1.2
0.9
0.6
0.3
0
**
PBS
BA

B.

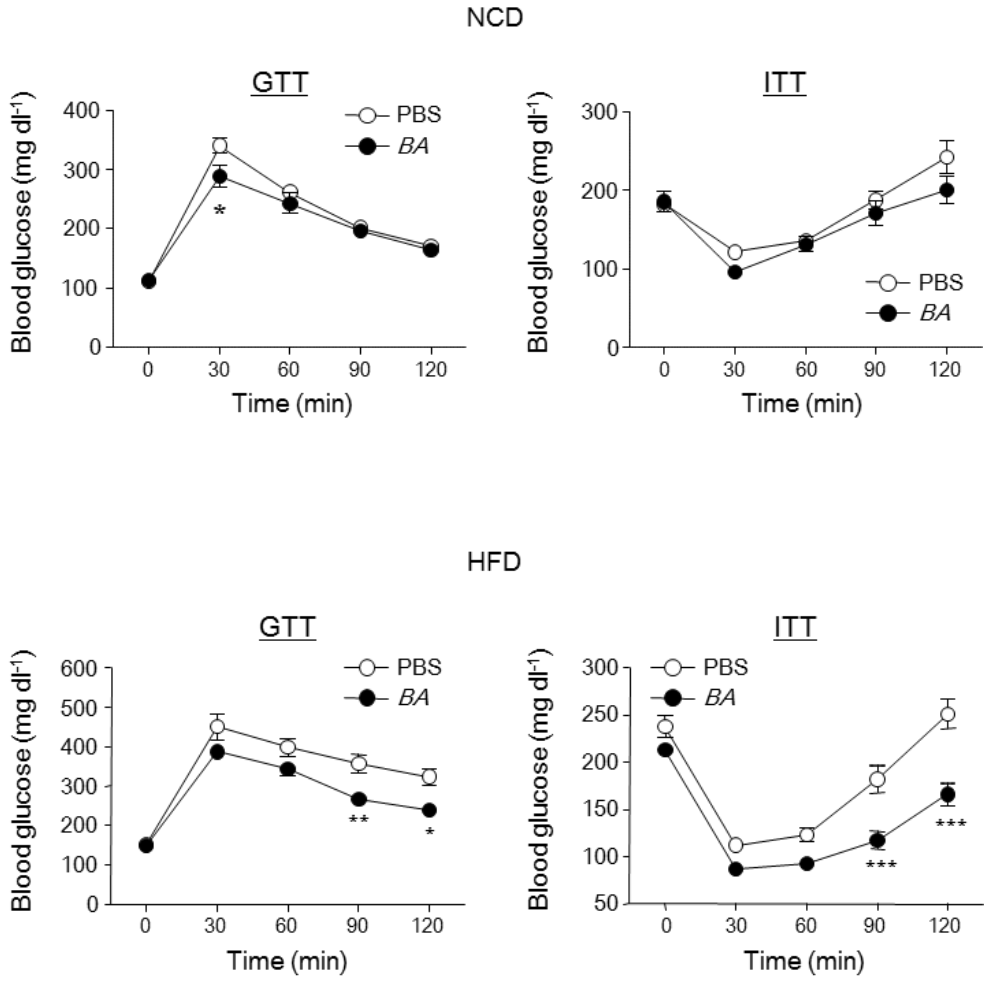
NCD
GTT
ITT
PBS
BA
Blood glucose (mg dl-1)
Time (min)
0
30
60
90
120
*
HFD
**
***

C.

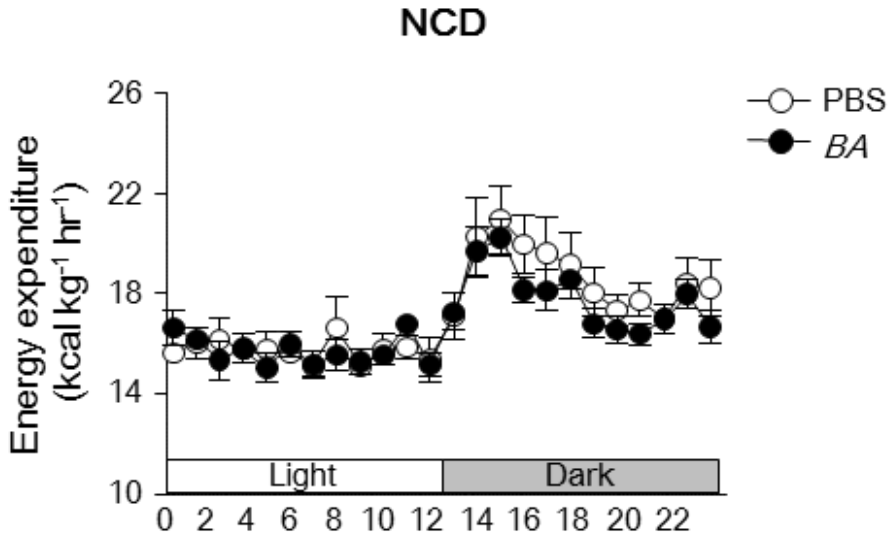
NCD
Energy expenditure (kcal kg-1 hr-1)
26
22
18
14
10
Light
Dark
0 2 4 6 8 10 12 14 16 18 20 22
PBS
BA

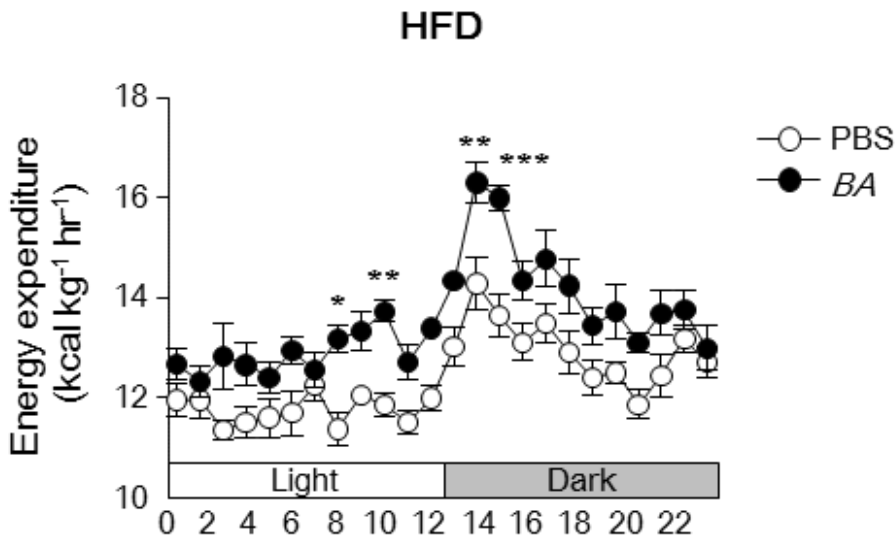
HFD
Energy expenditure (kcal kg-1 hr-1)
18
16
14
12
10
*
**
**
***
Light
Dark
0 2 4 6 8 10 12 14 16 18 20 22
PBS
BA

D.

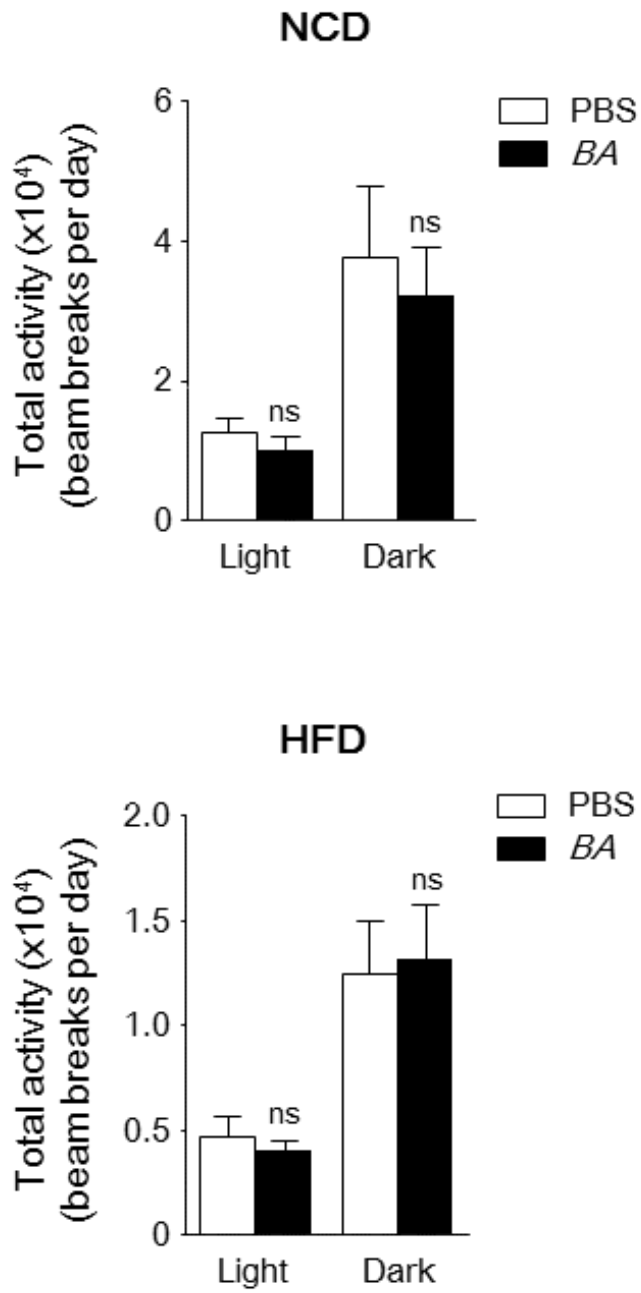
NCD
Total activity (x10⁴)
(beam breaks per day)
6
4
2
0
PBS
BA
ns
ns
Light
Dark
HFD
Total activity (x10⁴)
(beam breaks per day)
2.0
1.5
1.0
0.5
0
PBS
BA
ns
ns
Light
Dark

E.

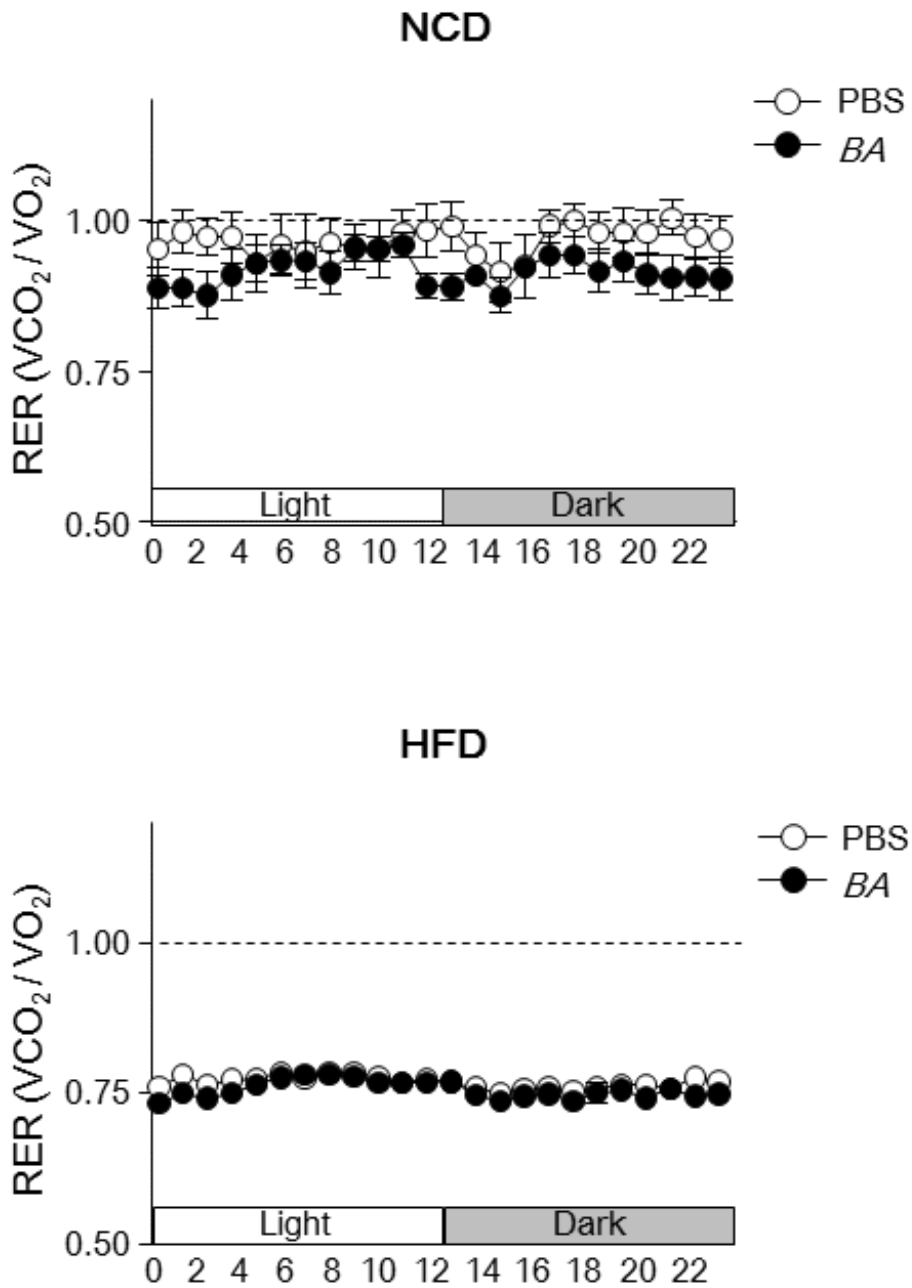
NCD
PBS
BA
RER (VCO2 / VO2)
1.00
0.75
0.50
Light
Dark
0 2 4 6 8 10 12 14 16 18 20 22
HFD
PBS
BA
RER (VCO2 / VO2)
1.00
0.75
0.50
Light
Dark
0 2 4 6 8 10 12 14 16 18 20 22

Figure 3.3. Glucose / insulin levels, GTT / ITT analysis, and comprehensive laboratory animal monitoring system (CLAMS) analysis.

(A). Levels of glucose and insulin in serum of PBS- and *B. acidifaciens*-fed B6 mice for 10 weeks everyday (n = 5). **(B).** GTT (left panel, n = 8-9) and ITT (right panel, n = 7-12) were analyzed using serum of PBS- and *B. acidifaciens*-fed B6 mice at the indicated time point after i.p. injection of glucose or insulin, respectively. **(C).** Energy expenditure of *B. acidifaciens*-administered B6 mice (n = 6). **(D).** Total activity in *B. acidifaciens*-administered B6 mice (n = 4). **(E).** RER of *B. acidifaciens*-administered B6 mice (n = 6). All data are presented as mean ± s.e.m. Statistical analyses were done with two-tailed paired *t*-test **(A)** and with two-way ANOVA with Bonferroni *post-hoc* test. *P<0.05, **P<0.01 and ***P<0.001. ns, not significant.

III-3-4. Mice having lean phenotypes exhibited enhanced peroxisome proliferator activated receptor (PPAR) α expression in their adipose tissues.

Because decreased body weight and fat mass were previously detected in *Atg7*$^{\Delta CD11c}$, FMT B6, and *B. acidifaciens*-fed B6 mice, I further analyzed gene expression levels related with lipid metabolisms in adipose tissue, liver, and small intestine. Of note, gene expressions related to lipid *β*-oxidation, especially PPARα, was significantly enhanced only in WAT (abdominal and subcutaneous) of *Atg7*$^{\Delta CD11c}$ mice as compared to *Atg7*$^{f/f}$ mice (Fig. 4A). No significant changes of this gene were seen in small intestine and liver (Fig. 4D-E). Consistent with these results, expression of PPARα was significantly upregulated in WAT (epididymal) of B6 mice transferred with fecal extracts of *Atg7*$^{\Delta CD11c}$ mice or fed with HFD and *B. acidifaciens* (Fig. 4B-C). Of interest, mRNA levels of PPARα in WAT of B6 mice were significantly enhanced 2 weeks after *B. acidifaciens* administration (Fig. 4F). We also assessed the expression levels of TGR5, a G-protein-coupled bile acid receptor that can stimulate energy expenditure through PPARα activation (*13, 14*). We found elevated TGR5 expression levels in adipose tissues following *B. acidifaciens* administration (Fig. 4G). These results suggest that lean phenotypes mediated by *B. acidifaciens*

might begin with lipid oxidation in adipose tissue through TGR5-PPARα activation.

A.

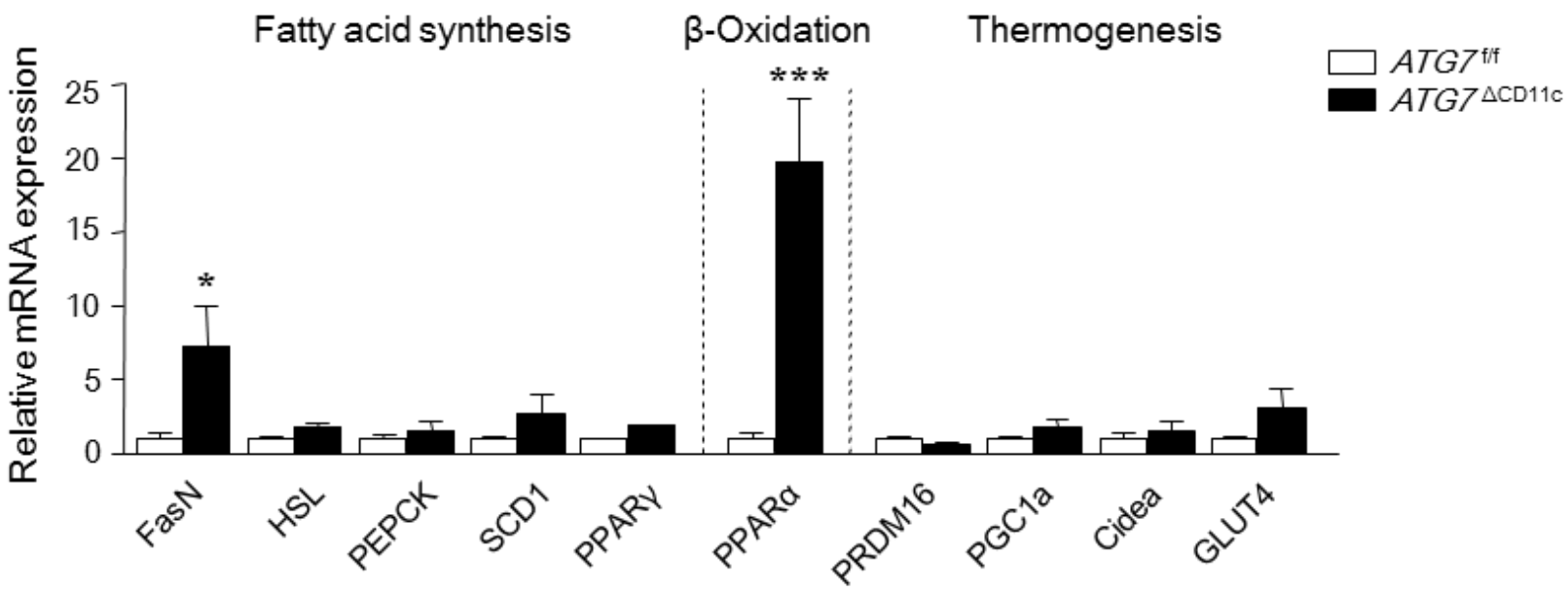
Fatty acid synthesis
β-Oxidation
Thermogenesis
ATG7 f/f
ATG7 ΔCD11c
Relative mRNA expression
25
20
15
10
5
0
*
***
FasN
HSL
PEPCK
SCD1
PPARγ
PPARα
PRDM16
PGC1a
Cidea
GLUT4

B.

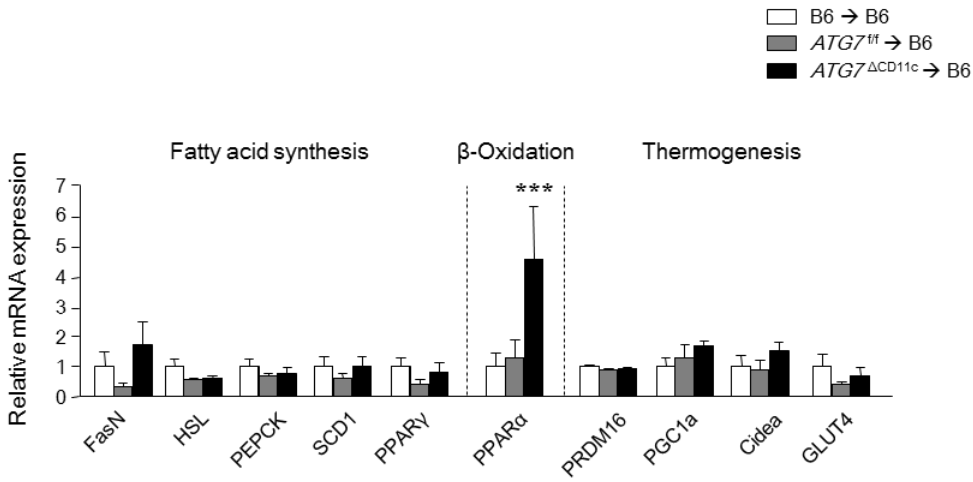
B6 → B6
ATG7f/f → B6
ATG7ΔCD11c → B6
Fatty acid synthesis
β-Oxidation
Thermogenesis
Relative mRNA expression
***
FasN
HSL
PEPCK
SCD1
PPARγ
PPARα
PRDM16
PGC1a
Cidea
GLUT4

C.

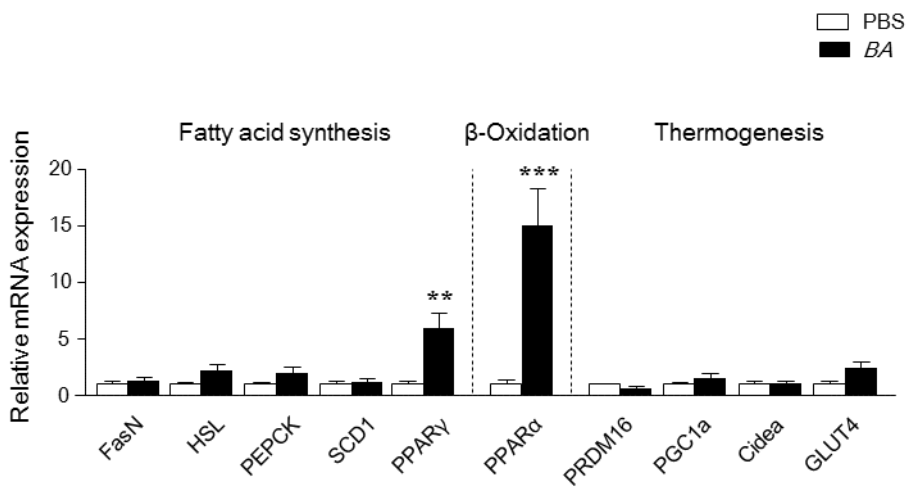
PBS
BA
Fatty acid synthesis
β-Oxidation
Thermogenesis
Relative mRNA expression
**
***
FasN
HSL
PEPCK
SCD1
PPARγ
PPARα
PRDM16
PGC1a
Cidea
GLUT4

D.

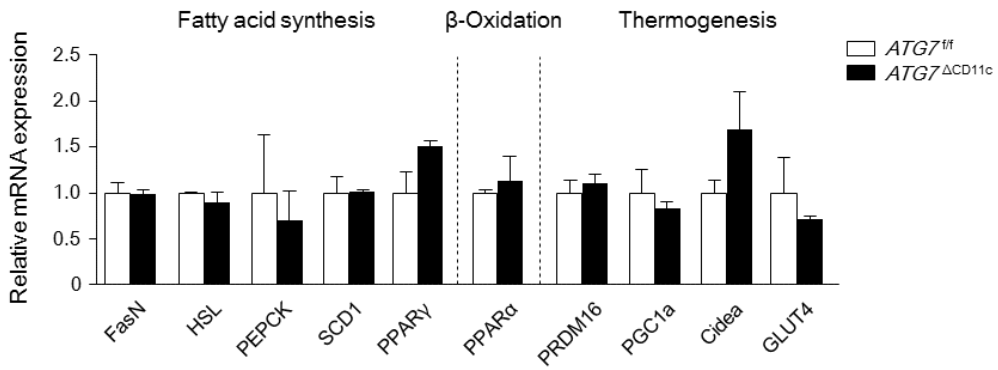
Fatty acid synthesis
β-Oxidation
Thermogenesis
Relative mRNA expression
2.5
2.0
1.5
1.0
0.5
0
ATG7 f/f
ATG7 ΔCD11c
FasN
HSL
PEPCK
SCD1
PPARγ
PPARα
PRDM16
PGC1a
Cidea
GLUT4

E.

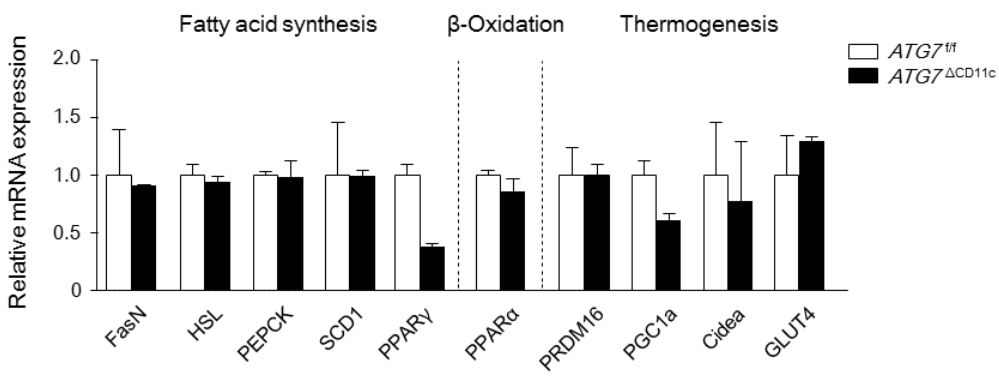
Fatty acid synthesis
β-Oxidation
Thermogenesis
Relative mRNA expression
2.0
1.5
1.0
0.5
0
ATG7 f/f
ATG7 ΔCD11c
FasN
HSL
PEPCK
SCD1
PPARγ
PPARα
PRDM16
PGC1a
Cidea
GLUT4

F.

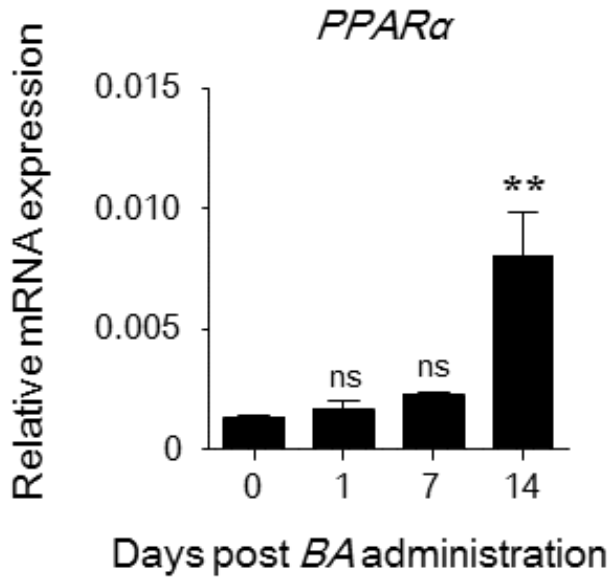
PPARα
Relative mRNA expression
0.015
0.010
0.005
0
ns
ns
**
0
1
7
14
Days post BA administration

G

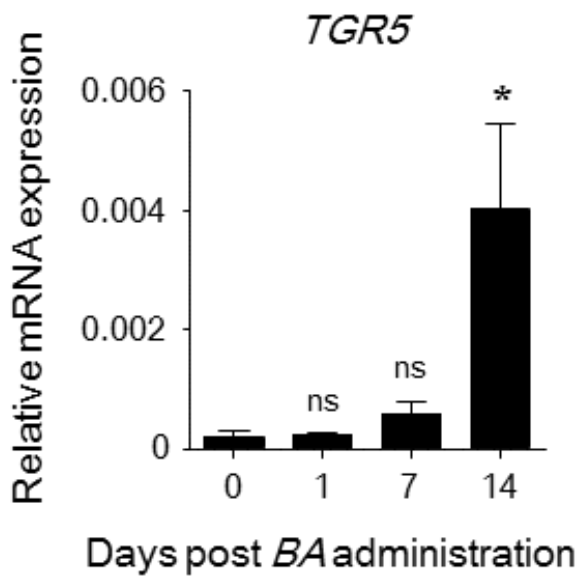
TGR5
Relative mRNA expression
0.006
0.004
0.002
0
ns
ns
*
0
1
7
14
Days post BA administration

Figure 3.4. mRNA expression levels of fatty acid synthesis, β-oxidation , and thermogenesis by RT-PCR.

B. acidifaciens (*BA*) promotes fat oxidation in the adipose tissues through PPARα activation. Expression level of mRNA genes related with fatty acid synthesis (FasN, HSL, PEPCK, SCD1, and PPARγ), β-oxidation (PPARα), and thermogenesis (PRDM16, PGC1a, Cidea, and GLUT4) were determined by real-time PCR using adipose tissues taken from $Atg7^{f/f}$ and $Atg7^{\Delta CD11c}$ mice (**A**), fecal microbiota transplanted mice (**B**), and *B. acidifaciens*-fed mice (**C**) at the end point of each experiments. The mRNA expression of equal candidates as above was measured in liver **(D)** and intestine **(E)**. Expression levels of PPARα **(F)** and TGR5 **(G)** in adipose tissue were analyzed by RT-PCR 1, 7, and 14 days after daily *BA* administration. All data are mean ± s.e.m of ≥2 independent experiments. Statistical analyses were done with two-way ANOVA with Bonferroni *post-hoc* test **(A-E)** and with Mann-Whitney *t*-test **(F** and **G)**. *P < 0.05, **P < 0.01, ***P<0.001; ns, not significant.

III-3-5. *B. acidifaciens* modulates GLP-1 production by regulating DPP-4 enzyme in small intestine.

In order to investigate the underlying mechanism of high levels of insulin secretion in *B. acidifaciens*-fed lean mice, I next studied the glucagon-like protein-1 (GLP-1) levels that could stimulate insulin release to blood (*15*). The GLP-1 levels in serum were dramatically enhanced following administration of *B. acidifaciens* in NCD- and HFD-fed mice (Fig. 5A). Of note, the levels of dipeptidyl peptidase-4 (DPP-4), a well-known enzyme responsible for the degradation of GLP-1 (*16*), was decreased in the small intestine ileum after oral administration of *B. acidifaciens* or culture supernatants (Fig. 5B). Previous studies suggested that bile acids play a pivotal role in glucose homeostasis by stimulating GLP-1 secretion through TGR5 activation (*17, 18*). I found significantly increased levels of cholate, salts of cholic acid (CA), and taurine deconjugated from primary bile acid in feces of B6 mice fed with *B. acidifaciens* for 10 weeks but no significant loss of cholesterol (Fig. 5C-D). These results indicate that *B. acidifaciens* and/or their metabolites may reduce DPP-4 enzyme activity and subsequently result in GLP-1 activation, improving insulin sensitivity and glucose tolerance.

A.

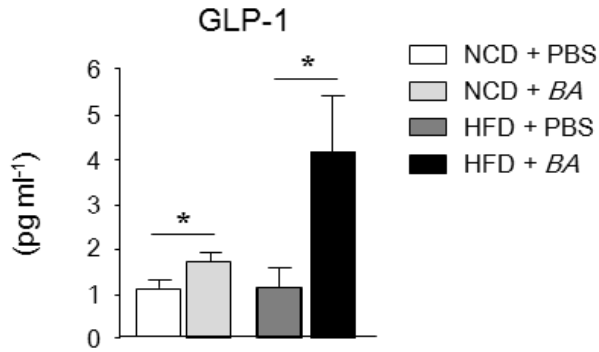
GLP-1
(pg ml-1)
0
1
2
3
4
5
6
*
*
NCD + PBS
NCD + BA
HFD + PBS
HFD + BA

B.

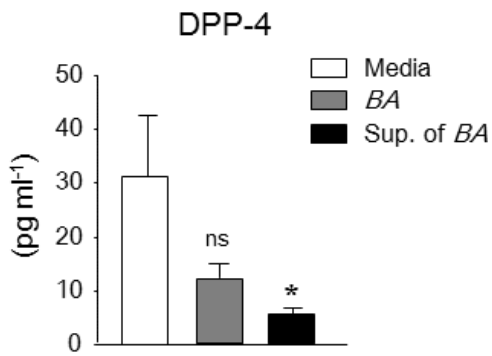
DPP-4
(pg ml-1)
0
10
20
30
40
50
ns
*
Media
BA
Sup. of BA

C.

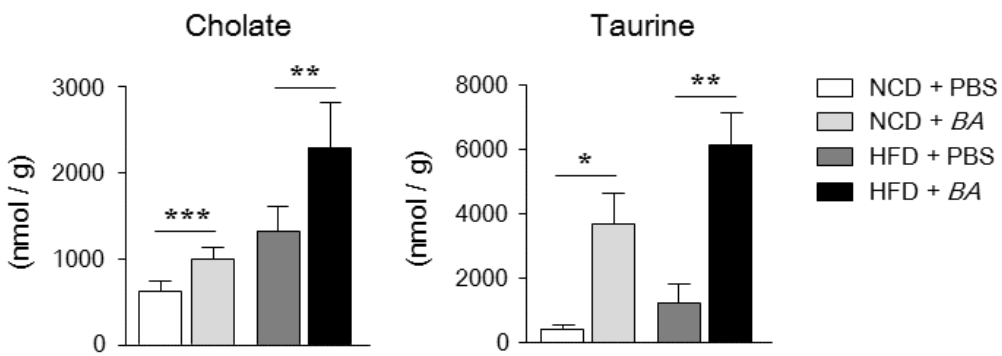
Cholate
(nmol / g)
0
1000
2000
3000
***
**
Taurine
(nmol / g)
0
2000
4000
6000
8000
*
**
NCD + PBS
NCD + BA
HFD + PBS
HFD + BA

D.

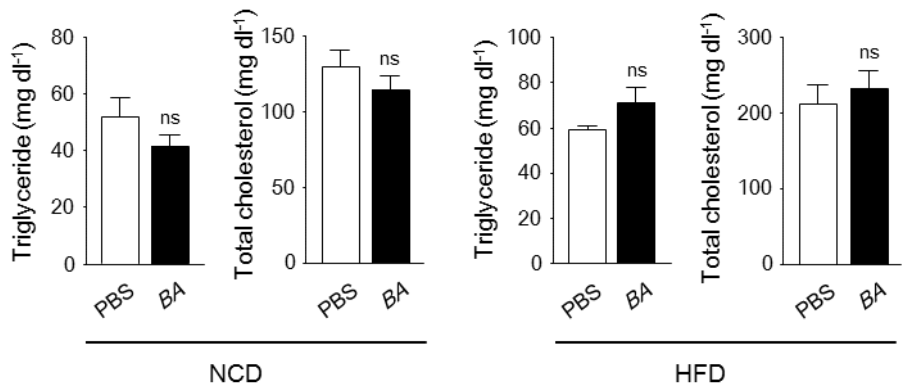

Figure 3.5. *B. acidifaciens* (BA) can regulate intestinal dipeptidal peptidase-4 (DPP-4) secretion and subsequently induce glucagon-like peptide 1 (GLP-1) production in B6 mice.

Active GLP-1 **(A)** in serum of PBS- and BA-fed mice (normal chow diet, NCD; high-fat diet, HFD; n = 5). **(B).** At 1 hour after BA administration or supernatant of BA culture or medium alone into naïve B6 mice, DPP-4 levels in the small intestine were detected by luminescent assay. **(C).** Quantification of cholate and taurine in feces of PBS- and BA-fed mice (n = 5) by capillary electrophoresis-mass spectrometry. Concentrations of serum triglycerides and total cholesterol were analyzed using enzymatic assay kits in BA-fed mice **(D**; n = 5**)**. All data are mean ± s.e.m of ≥2 independent experiments. Statistical analyses were done with two-tailed paired *t*-test. *P < 0.05, **P < 0.01, ***P<0.001; ns, not significant.

III-4. Discussion

Bacteroides (B.) acidifaciens were firstly isolated from the caecum of mice by Itoh K. et al (*9, 19*). These novel commensal bacteria were characterized anaerobic, gram-negative, good growth in bile acid and aesculin hydrolysis. Thereafter, their function was revealed by other group that *B. acidifaciens* possessing capacity to increase IL-6 and IL-10 production by enhancing expression of MHC class II and the co-stimulating molecules (i.e., CD80 and CD86) on antigen-presenting cells (*20*). In addition, *B. acidifaciens* is one of predominant commensal bacteria which responsible for promoting IgA Abs production in the large intestine specifically by inducing activation-induced cytidine deaminase expression (*1, 21*). Here, I noted another unique function that *B. acidifaciens* can modulate energy metabolisms and therefore applicable for therapeutic use for obesity and diabetes control.

PPARα is a nuclear receptor contributed on regulating several aspects of lipid metabolism (*22*). Previous studies have demonstrated that PPARα activation through its agonists resulted in reduced body weight by regulating satiety, and ameliorate obesity-derived inflammation in adipose tissue (*23, 24*). Although PPARα$^{-/-}$ mice fed HFD showed several obesity

phenotypes in terms of body weight, fat mass and fat droplets (*25*), the two major mechanisms for PPARα to regulate lipid metabolism are accounted for regulating fatty acids (FAs) cellular uptake or for stimulating FA oxidation (*26, 27*). In my studies, enhanced mRNA expression levels of PPARα were constantly detected only in adipose tissues obtained from *Atg7*$^{\Delta CD11c}$ mice, FMT mice, and *B. acidifaciens*-fed mice (Fig. 4), indicating that β-oxidation through PPARα signaling might be implicated as a mechanism for protection to obesity provoked by specific commensal bacteria *B. acidifaciens*.

The gastrointestinal tract is a locus of incretin hormone products such as glucagon-like peptide 1 (GLP-1) that stimulates insulin release and decreases blood glucose levels (*15*). The GLP-1 is inactivated by the enzyme dipeptidyl peptidase-4 (DPP-4) and thus DPP-4 inhibitor is a class of oral hypoglycemic (*16*). I found similar patterns of low glucose and high insulin levels in the serum of *Atg7*$^{\Delta CD11c}$ mice, FMT mice, and *B. acidifaciens*-fed mice (Fig. 3A, Fig. 5F of part II, and Fig. 3A). Notably, there are significantly decreased levels of DPP4 in ileum and increased levels of GLP-1 in the serum of *B. acidifaciens*-fed mice (Fig. 5A-B). It seems likely that unknown metabolites synthesized by *B. acidifaciens* or bacteria itself may directly interact with gut epithelial cells and inhibit DPP-

4 activation, and thereby increase circulating GLP-1.

In mice, cholic acid (CA), a primary bile acid, is secreted as a taurine-conjugated form from the gallbladder into the duodenum and then is deconjugated in the ileum by commensal bacteria (*28*). Recent studies have shown that the bile acid profiles in the small intestine, feces, and serum of conventionally raised mice is totally different from those of germ-free mice, suggesting that commensal bacteria can modulate gene expression levels related to bile acid synthesis, conjugation, and reabsorption (*7*). In the present study, significantly elevated levels of cholate and taurine were determined in feces (Fig. 5C) and their receptor TGR5 in adipose tissues (Fig. 4G) of B6 mice fed *B. acidifaciens*. Others have shown that administration of the TGR5 agonists CA and taurine result in significant improvement of body weight and fat mass in HFD-fed mice (*18, 29*). The authors suggest that the bile acid-TGR5-cAMP signaling pathways increase energy expenditure in adipose tissue and skeletal muscle. Thus, I propose that bile acids activated by *B. acidifaciens* serve as ligands for TGR5-mediated regulation of energy expenditure through PPARα activation.

In summary, expansion of *B. acidifaciens* leads to increased insulin production and β-oxidation, and finally to protect host from obesity. Although further studies are required to figure out the efficiency of *B.*

acidifaciens on diverse combination of genetic and environment factors, my finding suggest that a single commensal bacteria can be used as a potent "probiotics" for metabolic diseases such as diabetes and obesity.

III-5. References

1. **T. Yanagibashi, A. Hosono, A. Oyama, M. Tsuda, A. Suzuki, S. Hachimura, Y. Takahashi, Y. Momose, K. Itoh, K. Hirayama, K. Takahashi, S. Kaminogawa.** 2013. IgA production in the large intestine is modulated by a different mechanism than in the small intestine: *Bacteroides acidifaciens* promotes IgA production in the large intestine by inducing germinal center formation and increasing the number of IgA^+ B cells. *Immunobiology* 218, 645-651.
2. **A. Spor, O. Koren, R. Ley.** 2011. Unravelling the effects of the environment and host genotype on the gut microbiome. *Nature Reviews. Microbiology* 9, 279-290.
3. **P. G. Kopelman.** 2000. Obesity as a medical problem. *Nature* 404, 635-643.
4. **X. Zhang, G. Zhang, H. Zhang, M. Karin, H. Bai, D. Cai.** 2008. Hypothalamic IKKbeta/NF-kappaB and ER stress link overnutrition to energy imbalance and obesity. *Cell* 135, 61-73.
5. **J. Y. Chiang.** 2009. Bile acids: regulation of synthesis. *Journal of Lipid Research* 50, 1955-1966.
6. **D. W. Russell.** 2009. Fifty years of advances in bile acid synthesis and metabolism. *Journal of Lipid Research* 50 Suppl, S120-125.
7. **S. I. Sayin, A. Wahlstrom, J. Felin, S. Jantti, H. U. Marschall, K. Bamberg, B. Angelin, T. Hyotylainen, M. Oresic, F. Backhed.** 2013. Gut microbiota regulates bile acid metabolism by reducing the levels of tauro-beta-muricholic acid, a naturally occurring FXR antagonist. *Cell Metabolism* 17, 225-235.
8. **J. Y. Chiang.** 2013. Bile acid metabolism and signaling. *Comprehensive Physiology* 3, 1191-1212.
9. **Y. Momose, S. H. Park, Y. Miyamoto, K. Itoh.** 2011. Design of species-specific oligonucleotide probes for the detection of *Bacteroides* and *Parabacteroides* by fluorescence in situ hybridization and their application to the analysis of mouse caecal *Bacteroides-Parabacteroides* microbiota. *Journal of Applied Microbiology* 111, 176-184.
10. **A. Waget, C. Cabou, M. Masseboeuf, P. Cattan, M. Armanet, M. Karaca, J. Castel, C. Garret, G. Payros, A. Maida, T. Sulpice, J. J. Holst, D. J. Drucker, C. Magnan, R. Burcelin.** 2011. Physiological and pharmacological mechanisms through which the

DPP-4 inhibitor sitagliptin regulates glycemia in mice. *Endocrinology* 152, 3018-3029.

11. **E. Mishima, S. Fukuda, H. Shima, A. Hirayama, Y. Akiyama, Y. Takeuchi, N. N. Fukuda, T. Suzuki, C. Suzuki, A. Yuri, K. Kikuchi, Y. Tomioka, S. Ito, T. Soga, T. Abe.** 2014. Alteration of the intestinal environment by lubiprostone is associated with amelioration of adenine-induced CKD. *Journal of the American Society of Nephrology* 10, 1681/ASN.2014060530.
12. **M. Sugimoto, D. T. Wong, A. Hirayama, T. Soga, M. Tomita.** 2010. Capillary electrophoresis mass spectrometry-based saliva metabolomics identified oral, breast and pancreatic cancer-specific profiles. *Metabolomics* 6, 78-95.
13. **M. Watanabe, S. M. Houten, C. Mataki, M. A. Christoffolete, B. W. Kim, H. Sato, N. Messaddeq, J. W. Harney, O. Ezaki, T. Kodama, K. Schoonjans, A. C. Bianco, J. Auwerx.** 2006. Bile acids induce energy expenditure by promoting intracellular thyroid hormone activation. *Nature* 439, 484-489.
14. **V. Stepanov, K. Stankov, M. Mikov.** 2013. The bile acid membrane receptor TGR5: a novel pharmacological target in metabolic, inflammatory and neoplastic disorders. *Journal of Receptor and Signal Transduction Research* 33, 213-223.
15. **D. J. Drucker, M. A. Nauck.** 2006. The incretin system: glucagon-like peptide-1 receptor agonists and dipeptidyl peptidase-4 inhibitors in type 2 diabetes. *Lancet* 368, 1696-1705.
16. **B. Ahren, O. Schmitz.** 2004. GLP-1 receptor agonists and DPP-4 inhibitors in the treatment of type 2 diabetes. *Hormone and Metabolic Research* 36, 867-876.
17. **S. Katsuma, A. Hirasawa, G. Tsujimoto.** 2005. Bile acids promote glucagon-like peptide-1 secretion through TGR5 in a murine enteroendocrine cell line STC-1. *Biochemical and Biophysical Research Communications* 329, 386-390.
18. **H. Sato, C. Genet, A. Strehle, C. Thomas, A. Lobstein, A. Wagner, C. Mioskowski, J. Auwerx, R. Saladin.** 2007. Anti-hyperglycemic activity of a TGR5 agonist isolated from Olea europaea. *Biochemical and Biophysical Research Communications* 362, 793-798.
19. **Y. Miyamoto, K. Itoh.** 2000. *Bacteroides acidifaciens sp.* nov., isolated from the caecum of mice. *International Journal of Systematic and Evolutionary Microbiology* 50 Pt 1, 145-148.
20. **M. Tsuda, A. Hosono, T. Yanagibashi, S. Hachimura, K.**

Hirayama, K. Itoh, K. Takahashi, S. Kaminogawa. 2007. Prior stimulation of antigen-presenting cells with *Lactobacillus* regulates excessive antigen-specific cytokine responses in vitro when compared with *Bacteroides*. *Cytotechnology* 55, 89-101.

21. **T. Yanagibashi, A. Hosono, A. Oyama, M. Tsuda, S. Hachimura, Y. Takahashi, K. Itoh, K. Hirayama, K. Takahashi, S. Kaminogawa.** 2009. *Bacteroides* induce higher IgA production than *Lactobacillus* by increasing activation-induced cytidine deaminase expression in B cells in murine Peyer's patches. *Bioscience, Biotechnology, and Biochemistry* 73, 372-377.
22. **P. Lefebvre, G. Chinetti, J. C. Fruchart, B. Staels.** 2006. Sorting out the roles of PPAR alpha in energy metabolism and vascular homeostasis. *The Journal of Clinical Investigation* 116, 571-580.
23. **J. Fu, S. Gaetani, F. Oveisi, J. Lo Verme, A. Serrano, F. Rodriguez De Fonseca, A. Rosengarth, H. Luecke, B. Di Giacomo, G. Tarzia, D. Piomelli.** 2003. Oleylethanolamide regulates feeding and body weight through activation of the nuclear receptor PPAR-alpha. *Nature* 425, 90-93.
24. **A. Tsuchida, T. Yamauchi, S. Takekawa, Y. Hada, Y. Ito, T. Maki, T. Kadowaki.** 2005. Peroxisome proliferator-activated receptor (PPAR)alpha activation increases adiponectin receptors and reduces obesity-related inflammation in adipose tissue: comparison of activation of PPARalpha, PPARgamma, and their combination. *Diabetes* 54, 3358-3370.
25. **B. H. Kim, Y. S. Won, E. Y. Kim, M. Yoon, K. T. Nam, G. T. Oh, D. Y. Kim.** 2003. Phenotype of peroxisome proliferator-activated receptor-alpha(PPARalpha)deficient mice on mixed background fed high fat diet. *Journal of Veterinary Science* 4, 239-244.
26. **K. Motojima, P. Passilly, J. M. Peters, F. J. Gonzalez, N. Latruffe.** 1998. Expression of putative fatty acid transporter genes are regulated by peroxisome proliferator-activated receptor alpha and gamma activators in a tissue- and inducer-specific manner. *The Journal of Biological Chemistry* 273, 16710-16714.
27. **C. Ribet, E. Montastier, C. Valle, V. Bezaire, A. Mazzucotelli, A. Mairal, N. Viguerie, D. Langin.** 2010. Peroxisome proliferator-activated receptor-alpha control of lipid and glucose metabolism in human white adipocytes. *Endocrinology* 151, 123-133.
28. **J. M. Ridlon, D. J. Kang, P. B. Hylemon.** 2006. Bile salt biotransformations by human intestinal bacteria. *Journal of Lipid Research* 47, 241-259.

29. **N. Tsuboyama-Kasaoka, C. Shozawa, K. Sano, Y. Kamei, S. Kasaoka, Y. Hosokawa, O. Ezaki.** 2006. Taurine (2-aminoethanesulfonic acid) deficiency creates a vicious circle promoting obesity. *Endocrinology* 147, 3276-3284.

Chapter IV. Overall conclusion

IV-1. Gut commensal *Bacteroides acidifaciens* expanded in *Atg7*$^{\Delta CD11c}$ mice improves insulin sensitivity and prevents obesity

I found lean phenotypes (i.e., reduced body weight and fat mass) in aged conditional knock-out mice (*Atg7*$^{\Delta CD11c}$) with CD11c^{+} cells with specific deletion of autophagy-related gene 7 when compared with littermate control mice (*Atg7*$^{f/f}$). Interestingly, body weight and fat mass were compensated in both *Atg7*$^{f/f}$ and *Atg7*$^{\Delta CD11c}$ mice through co-housing or fecal extracts transplantation, indicating that lean phenotypes might be mediated by commensal bacteria of *Atg7*$^{\Delta CD11c}$ mice. By pyrosequencing analysis, I found that *Bacteroides acidifaciens* were significantly increased (>5%) in feces of *Atg7*$^{\Delta CD11c}$ mice compared with those of control *Atg7*$^{f/f}$ mice. Taken together, these findings suggest that *B. acidifaciens* regulated by autophagy in CD11c^{+} cells could be a novel therapeutic agent related to obesity.

I further investigate a novel function of *B. acidifaciens* expanded in the gut of *Atg7*$^{\Delta CD11c}$ mice whether these single commensal bacteria can modulate host lipid metabolisms. I found B6 mice daily fed *B. acidifaciens* for 10 weeks were more likely to lose body weights and fat masses than a

group fed PBS, even though both groups were taken the same amount of food. Of note, predominant expression of PPARα was consistently found in the adipose tissues of *Atg7*$^{\Delta CD11c}$ mice, wild-type B6 mice transferred with fecal microbiota of *Atg7*$^{\Delta CD11c}$ mice, and *B. acidifaciens*-feeding wild-type B6 mice, not in liver and ileum. In addition, the expression of TGR5, well known as bile acid receptors, were also increased in adipose tissue by short-term treatment of *B. acidifaciens*, indicating that enhanced glucose homeostasis found in B6 mice fed with *B. acidifaciens* might be closely related with increased GLP-1 secretion through TGR5 activation. I also found elevated insulin levels following oral administration with *B. acidifaciens* were closely related to increased glucagon-like peptide 1 (GLP-1) and decreased dipeptidyl peptidase-4 (DPP-4). In addition, significantly increased levels of cholate and taurine were found in feces of B6 mice fed with *B. acidifaciens* for 10 weeks. Collectively, these finding suggest that *B. acidifaciens* could be a novel therapeutic agent related to obesity mediated by a TGR5-PPARα dependent pathway.

1. Lean phenotypes with reduced body weight and fat mass were detected in aged *Atg7*$^{\Delta CD11c}$ mice regardless gender. Other conditional knock-out mice such as *Atg7*$^{\Delta villin}$ and *Atg7*$^{\Delta M\Phi}$ mice were shown no difference on their body weight.

2. The levels of insulin in serum of *Atg7*$^{\Delta CD11c}$ mice were significantly elevated, even though *Atg7*$^{\Delta CD11c}$ mice have shown lower levels of serum glucose compare to that of *Atg7*$^{f/f}$ mice.

3. Body weight and fat mass of *Atg7*$^{f/f}$ and *Atg7*$^{\Delta CD11c}$ mice in co-housing cage were compensated. In addition, C57BL/6 mice fed with fecal extracts of *Atg7*$^{\Delta CD11c}$ mice for 18 weeks were shown significant loss of body weight compared to that of control group, indicating that commensal bacteria can be a ′transporter′ of host fat metabolism.

4. From Phylum to Genus level, the composition of commensal bacteria in feces was identical between *Atg7*$^{f/f}$ mice and *Atg7*$^{\Delta CD11c}$ mice. However, in the Species levels, *B. acidifaciens* were significantly expanded in the lumen and some of them are localized in the epithelial cells of the large intestine from *Atg7*$^{\Delta CD11c}$ mice.

5. B6 mice fed with *B. acidifaciens* for 10 weeks were shown significant body weight loss in normal-chow diet (17%) and in high-fat diet (43%) compared to that of B6 mice fed with PBS. In contrast, B6 mice fed with *B. sartorii*, as internal control strain which were included in same genus, were shown no effects on the body weight.

6. The increased levels of insulin and improved insulin sensitivity were detected in serum of B6 mice fed with *B. acidifaciens* which are consistant results from *Atg7*$^{\Delta CD11c}$ mice and B6 mice transferred with fecal extracts of *Atg7*$^{\Delta CD11c}$ mice. In addition, B6 mice fed with *B. acidifaciens* revealed highly enhanced energy expenditure in HFD condition, suggesting that *B. acidifaciens* may regulate host lipid metabolisms by activating the induction of fat consumption.

7. The expression levels of PPARα were significantly increased in adipose tissues of all mice shown lean phenotypes (*Atg7*$^{\Delta CD11c}$ mice, B6 mice transferred with fecal extracts of *Atg7*$^{\Delta CD11c}$ mice and fed with HFD and *B. acidifaciens*), indicating that lean phenotypes mediated by *B. acidifaciens* might begin with lipid oxidation in adipose tissue through PPARα activation.

8. ELISA analysis revealed that the levels of both glucagon-like peptide 1 (GLP-1) and dipeptidyl peptidase-4 (DPP-4) were closely connected with *B. acidifaciens* and/or their metabolites. On the other hand, the elevated levels of cholate and taurine were found in feces of B6 mice fed with *B. acidifaciens*. These results suggest that unknown metabolites synthesized by *B. acidifaciens* or bacteria itself may directly interact with gut epithelial cells to modulate gut

hormone and may plays a critical role of deconjugation of primary bile acids.

IV-2. Proposed models of 'lean bug' *B. acidifaciens* to protect host against insulin resistance and obesity

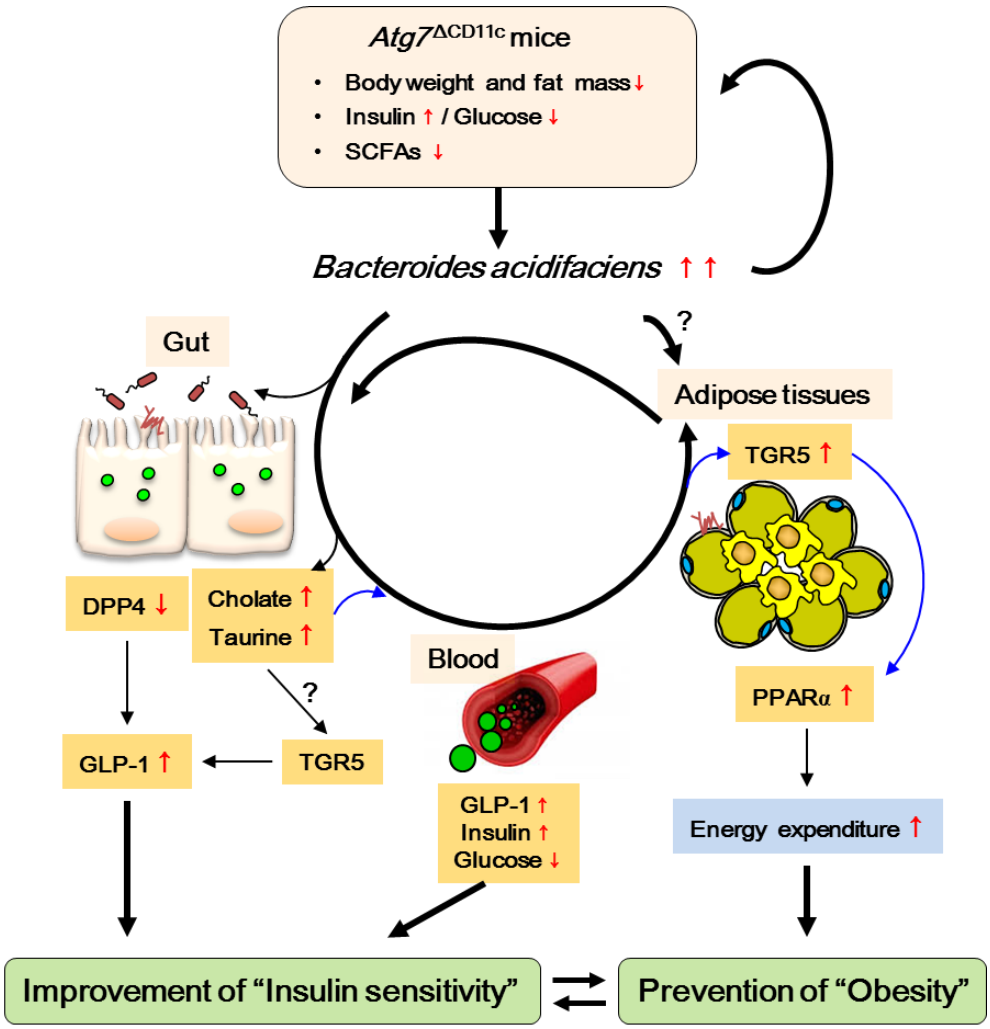

Figure 4.1.. The scheme of this study.

Specific gut commensal bacteria (i.e., *B. acidifaciens*) were expanded in *Atg7*$^{\Delta CD11c}$ mice with lean phenotypes. Administration of *B. acidifaciens* resulted in activation of fat oxidation through the bile acid-TGR5-PPARα axis in adipose tissues, which may lead to high energy expenditure. At the same time, *B. acidifaciens* activate DPP-4 in the gut and subsequently increase GLP-1, which may contribute to glucose homeostasis. Bile acids, cholate, and taurine may also contribute to GLP-1 activation through TGR5 and result in improved insulin sensitivity. Overall, *B. acidifaciens* may play a role in prevention of metabolic diseases such as diabetes and obesity.

국문 초록

장내 공생미생물은 대사물질을 조절하여 비만 및 당뇨병을 포함한 대사성 질환에 영향을 미치는 것으로 알려져 있다. 하지만 장내 미생물과 숙주의 지방 대사작용간의 구체적인 조절메커니즘 기전은 확실히 밝혀져 있지 않다. 본 연구에서 CD11c 세포 특이적으로 자가섭식 관련 유전자 (*Atg7*) 가 결손된 ($Atg7^{\Delta CD11c}$) 마우스에서 대조군 ($Atg7^{f/f}$ mice) 마우스에 비교하여 유의적으로 줄어든 체중과 지방량을 발견하였다. 흥미롭게도 저체중 및 저지방량을 보인 $Atg7^{\Delta CD11c}$ 마우스의 혈청 중 인슐린양이 증가하였고 이와 함께 혈당수치는 낮아져 있었으며 인슐린 저항성이 개선되었다. $Atg7^{f/f}$ 마우스와 $Atg7^{\Delta CD11c}$ 마우스를 한 케이지에서 함께 키우거나 서로의 분변추출액을 먹이는 실험을 통해 장내 미생물을 공유한 정상 마우스들이 유사한 저체중과 저지방량을 보인 점은 장내 미생물이 숙주의 지방대사와 밀접한 관련이 있음을 시사하였다. 파이로시퀀싱 분석을 통하여 마우스 장내미생물의 일종인 *Bacteroides acidifaciens* 가 $Atg7^{\Delta CD11c}$ 마우스의 분변 중에 대조군 마우스에 비해 현저히 증가 (5% 이상) 되어있는 것을 발견하였다. 그러나 같은 *Bacteroides* 속에 포함되는 *B. sartorii* 는 실험군과 대조군의 분변에서 비슷한

수준으로 검출되었다. 다음으로 파이로시퀀싱 분석에서 선정한 *B. acidifaciens* 의 숙주 대사조절 능력을 분석하기 위해 정상 마우스에 경구투여 하였다. *B. acidifaciens* 를 먹은 B6 마우스는 같은 양의 사료를 섭취하였음에도 불구하고, PBS 를 먹은 대조군에 비해서 체중과 지방량이 현저히 감소하였다. 이에 반해 *B. sartorii* 를 먹은 B6 마우스는 대조군과 유사한 체중 변화를 보였다, 이러한 *B. acidifaciens* 의 효과는 일반식과 고지방식을 먹인 마우스에서 동일하게 보였다. 글루코스와 인슐린 저항성 실험을 통해 *B. acidifaciens* 를 경구투여한 마우스 그룹에서 인슐린 감수성이 향상됨을 확인하였다. 저체중 표현 형질을 보인 $Atg7^{\Delta CD11c}$ 마우스, $Atg7^{\Delta CD11c}$ 마우스 분변 추출액을 먹인 B6 마우스, *B. acidifaciens* 를 먹인 B6 마우스들의 복부 지방조직에서 공통적으로 베타 산화작용을 통한 지방연소의 주요소로 알려진 PPAR 알파의 발현량이 유의적으로 증가되었다. 하지만 간이나 소장 조직에서의 PPAR 알파의 발현량에는 유의적인 변화가 관찰되지 않았다. CE-TOFMS 분석법을 통해 10 주간 *B. acidifaciens* 를 먹인 마우스의 분변에서 주담즙산인 콜레이트 양이 증가됨을 확인하였다. 추가적으로, 담즙산 관련 G 단백질 매개 수용체 TGR5 가 *B. acidifaciens* 를 단기간 먹인 마우스의 지방 조직에서 유의적으로 활성화되었고, 이는 *B.*

acidifaciens 의 투여가 지방조직의 담즙산-TGR5-PPAR 알파 축을 통한 지방 산화의 활성화를 이끌고, 나아가 높은 에너지 소비를 유도함을 시사하였다. 또한 *B. acidifaciens* 는 장내 디펩티딜 펩티다아제를 불활성시키고 글루코스 항상성에 기여하는 글루카곤 유사 펩타이드 1 을 순차적으로 증가시킨다. 이러한 결과는 장내미생물인 *B. acidifaciens* 가 비만 및 당뇨병과 같은 대사질환의 예방 및 치료에 능동적인 역할을 할 것이라고 시사하고 있다.

핵심어: 박테로이데스 아시디파시언스 (*Bacteroides acidifaciens*), 인슐린 감수성, PPAR 알파, 글루카곤 유사 펩타이드 1, 담즙산

학번: 2011-31031